

# **Hindcast Data on Winds, Waves, and Currents in Northern Gulf of Mexico in Hurricanes Katrina and Rita**



**Submitted to**  
**US Department of the Interior**  
**Minerals Management Service**  
**381 Elden Street, MS 4021**  
**Herndon, VA 20170**

**September 2006**

**oceanweather inc.**

5 River Road  
Cos Cob, CT, USA  
Tel: 203-661-3091  
Fax: 203-661-6809  
Email: [oceanwx@oceanweather.com](mailto:oceanwx@oceanweather.com)  
Web: [www.oceanweather.com](http://www.oceanweather.com)

*Front cover graphics courtesy MODIS-SSEC*

# TABLE OF CONTENTS

<b>1. PURPOSE .....</b>	<b>1</b>
<b>2. THE HINDCAST APPROACH .....</b>	<b>2</b>
2.1 Introduction.....	2
2.2 Wind Field Specification .....	5
2.3 Tropical Boundary Layer Model.....	6
2.4 Wave Model.....	8
2.5 ADCIRC Hydrodynamic Model.....	9
2.6 1-D Mixed Layer Current Profile Model.....	12
<b>3. METEOROLOGICAL CHARACTERISTICS OF HURRICANES</b>	
<b>KATRINA AND RITA .....</b>	<b>15</b>
3.1 Data Sources .....	15
3.2 General Storm Track/Wave Characteristics.....	16
<b>4. HINDCAST RESULTS .....</b>	<b>19</b>
4.1 Wind Field .....	19
4.2 Surface Waves .....	20
<b>5. VALIDATION.....</b>	<b>21</b>
5.1 NDBC Buoys.....	21
5.2 Coastal Hydrograph Trace .....	24
5.3 ADCP Deep Water Currents .....	24
<b>6. DELIVERABLES .....</b>	<b>25</b>
References .....	27
<b>APPENDIX A Storm Tracks .....</b>	<b>60</b>
Hurricane Katrina (2005_12) Track.....	61
Hurricane Rita (2005_18) Track .....	63
<b>APPENDIX B Hindcast Timeseries at NDBC Buoys/CMAN Stations.....</b>	<b>64</b>
<b>APPENDIX C Hindcast Wave Spectra at NDBC Buoys during Katrina ....</b>	<b>108</b>
<b>APPENDIX D Hindcast Wave Spectra at NDBC Buoys during Rita .....</b>	<b>139</b>
<b>APPENDIX E Wind, Wave, and Current Fields Definitions .....</b>	<b>165</b>
<b>APPENDIX F Wave Spectra Description.....</b>	<b>168</b>



## 1. PURPOSE

The purpose of this study is to develop a comprehensive, validated and reliable database of wind, sea state, and currents (vertically averaged in shallow water, mixed layer profile in deep water) associated with Hurricanes Katrina (2005) and Rita (2005) in the Northern Gulf of Mexico (GOM) through the implementation and application of advanced hindcast models. The models adopted have been previously applied and validated against historical GOM hurricanes and are also validated against the scant measured data acquired offshore in these two hurricanes. The objectives of this MMS supported project are analogous to comprehensive studies performed by Oceanweather Inc. (OWI) of Hurricane Andrew (1992) carried out in 1993-1994 (e.g. Puskar et al.1994), Hurricane Lili (2002) (Cardone et al. 2004) and Hurricane Ivan (2004) (Cox et al, 2005). The hindcast database is intended to satisfy the needs for wind, wave and current data for participants of the MMS (Minerals Management Service) programs assessing the impact of Katrina and Rita on the offshore industry.

Prior to this study, OWI responded to urgent industry needs for a preliminary assessment of the impact of Hurricanes Katrina and Rita by performing and distributing to several offshore operators an “emergency response” (ER) wind and wave hindcast (the output suite also included 2D shallow water currents and water levels made with a relatively simple 2-D hydrodynamic (HD) model. Those hindcasts utilized basically the same wind and wave hindcast technology as applied in the above noted Lili and Ivan hindcast studies, except that the databases tapped for specification of model inputs and validation of the hindcasts were essentially restricted to the databases available in real-time. This study differs from the ER hindcasts in the following ways: (1) it utilizes a larger base of measured wind, wave, surge and current data, including reanalyzed kinematic reanalyzed snapshots of the wind field produced by the NOAA National Hurricane Research Division (NHRD) with its HWnd system, both for specification of the model inputs and validation of model output; (2) it includes a more detailed reanalysis of the wind field; (3) particular attention is paid to provision of much higher resolution in shallow water and to the

inclusion of the storm perturbed water level in the shallow water wave hindcast; (4) more advanced and robust 1D and 2D ocean current models are applied.

## **2. THE HINDCAST APPROACH**

### **2.1 Introduction**

The hindcast approach as applied in this study consists of four basic steps. First, the evolution of the hurricane surface wind field is specified at hourly intervals in a process that requires considerable work by an experienced meteorologist to develop input parameters for a dynamical numerical model of the vortex boundary layer and to blend model solutions with kinematic analysis for use in areas where the numerical model solution is not sufficiently detailed. Second, the final wind fields are used to drive a proven hydrodynamic (HD) model to specify time variant water level anomalies (storm surge) and vertically integrated storm driven currents in shallow water. Third, the wind fields and the water level anomalies are used to drive the wave models adopted to the entire basin at high resolution and to two nested grids that resolve the coastal landfall areas at even higher resolution. Fourth, the wind fields are used to drive 1D current model at each grid point with water depth greater than 75 m. In this section we give concise descriptions of each of these processes, more extensive mathematical treatments are reserved to cited references.

OWI basically pioneered the application of the hindcast approach to GOM (Gulf of Mexico) tropical cyclones and have contributed significantly over the past 30 years to programs designed to understand, describe and model the surface marine meteorological characteristics of GOM hurricanes and the corresponding ocean response to the passage of hurricanes. The main impact of our work has been on practices of design of offshore structures in the GOM. The most notable programs include the so-called Analysis Phases of major measurement programs such as the Ocean Data Gathering Program (ODGP) for winds and waves (Cardone et al., 1976, Ward et al., 1979; Haring and Heideman, 1978), the Ocean Current Measurement Program (OCMP) for

continental shelf currents, the Ocean Test Structure (OTS) program for platform response, the Ocean Response to a Hurricane (ORTAH) program, which utilized air-dropped current meters to measure mixed layer storm driven currents, and the aforementioned Hurricane Andrew, Lili and Ivan studies. Our trilogy of GOM Joint Industry Projects (JIP) conducted in the early 1990s and known as GUMSHOE, WINX and GLOW have become established as the de-facto industry standard base of metocean design data in the northern GOM. Comparable studies have addressed the Bay of Campeche in the southwest GOM (Cardone and Ramos, 1997).

While much of the JIP work noted above has been proprietary to the industry sponsors, the underlying modeling and analysis methods have been documented and exposed to the scientific and engineering communities in the peer reviewed literature and in proceedings of major conferences (see also reference list attached) and the design data have been integrated into API updates. The OWI led JIP "Gulf of Mexico Storm Hindcast of Oceanographic Extremes" (GUMSHOE) served to update the ODGP study and provide more reliable extreme design data in shallow water. The ODGP utilized model grids of about  $1/3^{\text{rd}}$  degree spacing. This spacing was refined to about  $1/5^{\text{th}}$  degree in GUMSHOE,  $1/10^{\text{th}}$  degree for our Andrew hindcast and  $1/20^{\text{th}}$  degree for our Lili and Ivan hindcasts. ODGP and GUMSHOE included substantial hindcast model validation studies because wind, wave, surge and current measurements have been made in some notable historical Gulf of Mexico storms (Audrey, 1957; Bertha, 1957; Carla, 1961; Camille, 1969; Edith, 1971; Delia, 1973; Frederic, 1979; Danny, 1985; Juan 1985). These validation studies (e.g. Reece and Cardone, 1982) demonstrated the accuracy of our hindcast methods when applied to specify peak sea states (significant wave height) at an arbitrary site in a Gulf of Mexico hurricane (bias of less than 0.5 m, mean absolute error of less than 1.0 m and scatter index of 10-15%). More recently, the inner core of Lili passed over two NOAA data buoys (42001 and 42041) and excellent skill was achieved in our hindcasts not only at these buoys but in the far-field of the hurricane as well (Cardone et al., 2004). Similarly, Ivan's large size led to buoy measurements of extreme sea states in the inner core (42040) and up to 100 nm east and west of the track (e.g. 42001, 42003). Again, as found in the validation of our Lili hindcast, storm peak sea states of significant wave height (HS) and peak period (TP) were

specified with accuracy of 15% or better while more limited comparisons of measured and hindcast wave spectra also showed good agreement. A recently reported completely “blind” verification of the Ivan hindcast at the Matterhorn platform (Leverette et al., 2005) showed excellent agreement between the hindcast and measured time history of HS including specification of the peak HS within 10%, a margin comparable to the intrinsic sampling error of the measurement. Emergency response hindcasts of Katrina and Rita have also been carried to help major operators develop preliminary updated platform design criteria within the context of OWI’s update of GUMSHOE known as GOMOS-USA, and results of these emergency response hindcasts were made available to support the MMS contractors on the project of which this study is a part.

OWI continues to be active in hurricane wind and wave modeling, including participation in a NOPP (National Oceanographic Partnership Program) that consists of a 5-year program to develop a state-of-art hurricane forecasting system (Graber et al., 2006). OWI are also an active participant in the new U.S. Army Corps of Engineers sponsored 3-year MORPHOS (Modeling of Relevant Physics of Sediments in Three Dimensions) project and the National Academies Panel Interagency Performance Evaluation Task Force (IPET), whose mission is “to obtain the facts by collecting, analyzing, testing, and modeling data and information on the performance of the New Orleans hurricane protection system during Hurricane Katrina”.

With regard to modeling of ocean currents, unlike in its previous studies of Andrew and Lili, we do not in this study apply state-of-art 3D ocean models such as the Princeton Model (POM) and HYCOM. To date such efforts have met with very limited success and resulting current hindcasts have not been nearly as reliable as wave hindcasts in a quantitative sense. Rather in this study we focus on the two regimes that succumb to relatively simple 2D and 1D approaches. The first regime is in shallow water, say depths less than 75 m or so, in which the water column becomes well mixed, surface to bottom, and the current response may be modeled with a modern 2D HD model. In this study we have applied a US community HD model known as ADCIRC. In depths greater than 200 m, 1D analytical mixed layer models (e.g. Mellor-Durbin (1975) turbulence

closure model) have met with success in specifying the primary response of the upper layer (mixed layer) and we have applied this approach with success in recent studies. In this study we apply a newly recalibrated version of the model of Kantha and Clayson (1994).

## 2.2 Wind Field Specification

The method used in this study has been applied in over three-dozen studies involving almost all basins on the globe within which tropical cyclones can occur. The method starts from raw data whenever possible and includes an intensive reanalysis of traditional cyclone parameters such as track and intensity (in terms of pressure) and then develops new estimates of the more difficult storm parameters, such as the shape of the radial pressure profile and the ambient pressure field within which the cyclone is embedded. The time histories of all of these parameters are specified within the entire period to be hindcast. Storm track and storm parameters are then used to drive a numerical primitive equation model of the cyclone planetary boundary layer (PBL) to generate a complete picture of the time-varying wind field associated with the cyclone circulation itself. That solution is then compared to time histories of accurately measured surface winds (reduced to standard height) at available measurement sites, and if necessary the storm parameters are varied and the model iterated until good agreement is obtained between the modeled wind field and the discrete best-available wind observations available. An additional data source available in the GOM in recent years is provided by the NOAA HRD HWnd snapshots, which focus on the inner core wind structure. In general the PBL and HWnd approaches may be viewed as complementary so when both are available and considered reliable, the PBL solutions and the HWnd solutions are blended using OWI's IOKA (Interactive Objective Kinematic Analysis) system to provide a time and space continuous evolution of the inner core surface wind field. This resulting inner core tropical wind field is then blended into a basin-wide field, which incorporates both atmospheric modeled winds, in-situ measurements from buoys, CMAN stations, ship reports as well as satellite estimates of wind from altimeter and scatterometer instruments. The process is described in more detail in

Cox and Cardone (2000). A brief description of the PBL model is given below. The HWnd system is described by Powell et al. (1998).

### 2.3 Tropical Boundary Layer Model

This model, first developed into a practical tool in the Ocean Data Gathering Program (ODGP) (Cardone *et al.* 1976), can provide a fairly complete description of time-space evolution of the surface winds in the boundary layer of a tropical cyclone from the simple model parameters available in historical storms. The model is an application of a theoretical model of the horizontal airflow in the boundary layer of a moving vortex. That model solves, by numerical integration, the vertically averaged equations of motion that govern a boundary layer subject to horizontal and vertical shear stresses. The equations are resolved in a Cartesian coordinate system whose origin translates at constant velocity,  $V_f$ , with the storm center of the pressure field associated with the cyclone. Variations in storm intensity and motion are represented by a series of quasi-steady state solutions. The original theoretical formulation of the model is given by Chow (1971). A similar model was described more recently in the open literature by Shapiro (1983). The version of the model applied in this study is the result of two major upgrades, one described by Cardone *et al.*, (1992) and the second by Cardone *et al.* (1994) and Thompson and Cardone (1996). The first upgrade involved mainly replacement of the empirical scaling law by a similarity boundary layer formulation to link the surface drag, surface wind and the model vertically averaged velocity components. The second upgrade added spatial resolution and generalized the pressure field specification. A more complete description of the theoretical development of the model as upgraded is given by Thompson and Cardone (1996).

The model pressure field is described as the sum of an axially symmetric part and a large-scale pressure field of constant gradient. The symmetric part is described in terms of an exponential pressure profile, which has the following parameters:

$P_0$      minimum central pressure

- Pfar far-field pressure  
Rp scale radius of exponential pressure profile  
B profile peakedness parameter

B is an additional scaling parameter introduced by Graham and Hudson (1960) whose significance was discussed by Holland (1980). This analytical form is also used to explicitly model the storm pressure field for use in the hydrodynamic model.

The model is driven from parameters that are derived from data in historical meteorological records and the ambient pressure field. The entire wind field history is computed from knowledge of the variation of those parameters along the storm track by computing solutions, or so-called “snapshots,” on the nested grid as often as is necessary to describe different stages of intensity, and then interpolating the entire time history from the snapshots.

The model was validated originally against winds measured in several ODGP storms. It has since been applied to nearly every recent hurricane to affect the United States offshore area, to all major storms to affect the South China Sea since 1945, and to storms affecting many other foreign basins including the Northwest Shelf of Australia, Tasman Sea of New Zealand, Bay of Bengal, Arabian Sea and Caribbean Sea. Comparisons with over-water measurements from buoys and rigs support an accuracy specification of  $\pm 20$  degrees in direction and  $\pm 2$  meters/second in wind speed (1-hour average at 10-meter elevation). Many comparisons have been published (see e.g., Ross and Cardone, 1978; Cardone and Ross, 1979; Forristall *et al.*, 1977; 1978; Forristall 1980; Cardone *et al.*, 1992, Cardone and Grant, 1994).

As presently formulated, the wind model is free of arbitrary calibration constants, which might link the model to a particular storm type or region. For example, differences in latitude are handled properly in the primitive equation formulation through the Coriolis parameter. The variations in structure between tropical storm types manifest themselves basically in the characteristics of the pressure field of the vortex itself and of the surrounding region. The

interaction of a tropical cyclone and its environment, therefore, can be accounted for by a proper specification of the input parameters. The assignable parameters of the planetary boundary layer (PBL) formulation, namely planetary boundary layer depth and stability, and of the sea surface roughness formulation, can safely be taken from studies performed in the Gulf of Mexico, since tropical cyclones world-wide share a common set of thermodynamic and kinematic constraints.

## 2.4 Wave Model

OWI's standard UNIWAVE high-resolution full spectral wave hindcast model was used for all wave hindcasts. UNIWAVE incorporates deep water and shallow processes and the option to use either OWI's highly calibrated first generation source term physics (ODGP2) or third generation (3G) physics (OWI3G/DIA2). Extensive validations of OWI's wave models in long-term hindcast studies are given recently by Swail and Cox (2000) and Cox and Swail (2001). Details on the 3<sup>rd</sup> generation physics applied in UNIWAVE can be found in Khandekar *et al.* (1994). Third-generation physics was adopted for the hindcasts reported here. An interesting feature of this model is that it appears to be the first to incorporate a saturation surface drag formulation. That is, rather than retain the usual unlimited linear increase of the drag coefficient with increasing wind speed, OWI's model capped the drag coefficient at a value of  $2.2 \times 10^{-3}$  at a wind speed of about 30 m/s. Only recently have estimates of the 10-m surface marine drag coefficient in hurricanes in the field (Powell *et al.*, 2005) and in a wind-tunnel/wave-tank set up (Donelan *et al.*, 2005) "confirmed" that the drag coefficient saturates in hurricane inner core regimes.

Figures 1a-1c show the wave model grids adopted. The basin grid is of spacing .05 degrees in latitude and longitude. Bathymetry is specified from the IPET study of Katrina as described by the U.S. Army Corps of Engineers. Shallow water effects are included on the basin grid with static water depth. Two ultra-high resolution shallow water nests were developed to model the coastal regions in the areas of landfall of Katrina and Rita, each with spacing of .01 degrees, and within which the water level was considered time-variant and dependent on the ADCIRC HD

model output. This coupling of the HD and wave models has not been included in our studies of earlier storms.

## 2.5 ADCIRC Hydrodynamic Model

Hydrodynamic computations are performed using ADCIRC-2DDI, the depth-integrated option of a set of two- and three-dimensional fully nonlinear hydrodynamic codes (Luettich *et al.*, 1992). The model grid is shown in Figure 2 and was developed using the same bathymetry sources described in section 2.4. ADCIRC-2DDI uses the vertically averaged equations of mass and momentum conservation, subject to the hydrostatic pressure approximation. The two-dimensional, depth-integrated velocity field is appropriate to use for the tidal simulations performed herein due to the assumption that the vertical fluid velocities are negligible as compared to the horizontal fluid velocities of the tidal flow within the computational domain. For the applications presented in this report, the hybrid bottom friction formulation is used, baroclinic terms are neglected, and the advective and lateral diffusion/dispersion terms are employed, leading to the following set of balance laws in primitive, non-conservative form, expressed in a spherical coordinate system (Kolar *et al.*, 1994b):

$$(1) \quad \frac{\partial \zeta}{\partial t} + \frac{1}{R \cos \phi} \left[ \frac{\partial UH}{\partial \lambda} + \frac{\partial (VH \cos \phi)}{\partial \phi} \right] = 0$$

$$(2) \quad \frac{\partial U}{\partial t} + \frac{1}{R \cos \phi} U \frac{\partial U}{\partial \lambda} + \frac{1}{R} V \frac{\partial U}{\partial \phi} - \left( \frac{\tan \phi}{R} U + f \right) V =$$

$$- \frac{1}{R \cos \phi} \frac{\partial}{\partial \lambda} \left[ \frac{p_s}{\rho_0} + g(\zeta - \alpha \eta) \right] + \frac{1}{H} M_\lambda + \frac{\tau_{s\lambda}}{\rho_0 H} - \tau_* U$$

$$(3) \quad \frac{\partial V}{\partial t} + \frac{1}{R \cos \phi} U \frac{\partial V}{\partial \lambda} + \frac{1}{R} V \frac{\partial V}{\partial \phi} + \left( \frac{\tan \phi}{R} U + f \right) U =$$

$$- \frac{1}{R} \frac{\partial}{\partial \phi} \left[ \frac{p_s}{\rho_0} + g(\zeta - \alpha \eta) \right] + \frac{1}{H} M_\phi + \frac{\tau_{s\phi}}{\rho_0 H} - \tau_* V$$

where  $\lambda$ ,  $\phi$  = degrees longitude and latitude, respectively;  $U$ ,  $V$  = depth-integrated velocities in longitudinal and latitudinal directions, respectively;  $H$  = total height of the water column,  $h + \zeta$ ;  $h$  = bathymetric depth, relative to mean sea level;  $\zeta$  = free surface elevation, relative to mean sea level;  $R$  = radius of the Earth;  $f = 2\Omega \sin \phi$  = Coriolis parameter;  $\Omega$  = angular speed of the Earth;  $p_s$  = atmospheric pressure at the free surface;  $\rho_0$  = reference density of water;  $g$  = acceleration due to gravity;  $\alpha$  = Earth elasticity factor;  $M_\lambda = \frac{E_{h_2}}{R^2} \left[ \frac{1}{\cos^2 \phi} \frac{\partial^2 UH}{\partial \lambda^2} + \frac{\partial^2 UH}{\partial \phi^2} \right] =$  depth-integrated momentum dispersion, longitudinal direction;

$$M_\phi = \frac{E_{h_2}}{R^2} \left[ \frac{1}{\cos^2 \phi} \frac{\partial^2 VH}{\partial \lambda^2} + \frac{\partial^2 VH}{\partial \phi^2} \right] = \text{depth-integrated momentum dispersion, latitudinal}$$

direction;  $E_{h_2}$  = horizontal eddy viscosity;  $\tau_{s\lambda}$ ,  $\tau_{s\phi}$  = applied free surface stress in longitudinal and latitudinal directions, respectively;  $\tau_*$  = bottom stress; and  $\eta$  = Newtonian tide potential.

Solving the finite element discretization of the primitive, non-conservative form of the shallow water equations gives rise to numerical instabilities. Therefore, equations (1) - (3) are

reformulated into a generalized wave continuity equation (GWCE) to provide highly accurate, noise free, finite element based solutions to the shallow water equations (Lynch and Gray 1979; Kinnmark 1984). ADCIRC-2DDI solves the GWCE in conjunction with the primitive, non-conservative momentum equations using a Galerkin finite element method on linear, triangular elements in space and a finite difference method in time. Considerably more detailed presentations of ADCIRC-2DDI are given by Luetlich *et al.* (1992), Kolar *et al.* (1994b), and Westerink *et al.* (1994).

Frictional closure within the governing equations of ADCIRC-2DDI is achieved through the use of the hybrid bottom friction formulation, which employs the quadratic bottom friction equation and allows for the bottom friction coefficient to change with respect to bathymetric depth. In very shallow waters, the hybrid bottom friction formulation is useful particularly when wetting and drying of elements is implemented since this expression becomes highly dissipative as the water depth becomes small (Luetlich *et al.*, 1992). The quadratic bottom friction equation that is used within the hybrid bottom friction formulation is defined as:

$$(4) \quad \tau_* = \frac{C_f \sqrt{U^2 + V^2}}{H}$$

with the hybrid bottom friction formulation, the bottom friction coefficient is defined as:

$$(5) \quad C_f = C_{f_{\min}} \left[ 1 + \left( \frac{H_{break}}{H} \right)^\theta \right]^{\frac{\gamma}{\theta}}$$

where  $C_{f_{\min}}$  = minimum friction factor that is approached in deep water when the hybrid bottom friction function reverts to the quadratic bottom friction function;  $H_{break}$  = break depth to

determine if the hybrid bottom friction function will behave as a quadratic bottom friction function or increase with depth similar to a Manning's type bottom friction function;  $\theta$  = dimensionless parameter that determines how rapidly the hybrid bottom friction function approaches its upper and lower limits; and  $\gamma$  = dimensionless parameter that describes how quickly the friction factor increases as water depth decreases.

The zonal and meridional surface stress components are supplied by the familiar surface drag formulation as a function of the 10-meter average wind speed and direction. We use the 30-minute averaged wind speed, which is the only appropriate averaging interval to adopt for ocean response forcing though we have seen some applications in which winds referred to shorter averaging intervals have been used, no doubt in an attempt to indirectly scale up the wind stress. In addition while most ADCIRC modelers use the drag coefficient formulation of Large and Pond (1981) or similar linear law, capped or uncapped, we have found that since most of the surge is generated over the shallow shelf waters, where in a land falling hurricane situation the drag over equivalent deep water wind and wave regimes, we have scaled up the deep water drag coefficient by an appropriate factor.

## **2.6 1-D Mixed Layer Current Profile Model**

In deep water, currents near the peak of the storm are confined to a mixed layer near the surface. Two-dimensional storm surge models cannot describe such currents profiles. A 1-D vertical model can capture most of the processes that create the current profiles at the peak of the storm in deep water. They also give reasonably accurate surface current hindcasts for some time after the storm passes. These models are best suited to predicting mixed layer currents in water deeper than 100 m. One-dimensional models yield no information on currents below the mixed layer (200 m deep or less). For sites near coastlines, pressure gradients from the storm surge cause barotropic currents that are nearly constant with depth.

In this study we apply a model adapted by Forristall et al. (2006) for OWI's GOMOS project and the discussion below is extracted from a report prepared by Forristall to document the GOMOS application.

The critical factor in a one-dimensional current model is the parameterization of the turbulent stress. This stress is responsible for the downward mixing of momentum from surface wind stress. The Reynolds averaged equations of motion for turbulent flow give us more unknowns than equations. The higher moments in these equations must be parameterized. Mixed layer models of the ocean usually consist of a single conservation equation for the turbulence kinetic energy and a set of algebraic equations for the turbulence second moment quantities. Kantha and Clayson (2000) give a thorough discussion of these models.

The best known second moment closure model is due to Mellor and Yamada (1982). They chose tunable constants that helped the model match laboratory turbulent flows. That model has been successfully applied in many studies of the oceanic mixed layer. One drawback is that it appears to slightly underestimate mixing. That underestimation leads to predictions of sea surface temperatures that are warmer than observed temperatures. Kantha and Clayson (1994) developed a modified second order model with enhanced mixing. In the GOMOS study conducted prior to this project, tests of the Mellor and Yamada (1982) and Kantha and Clayson (1994) models against wind fields of Hurricane Katrina developed for the IPET project as validated against ADCP measurements at a platform located near the track of Hurricane Katrina led to the selection of the Kantha-Clayson formulation for this hindcast.

The most important input to turbulence closure models is the wind stress. The standard oceanic wind stress law is from Large and Pond (1981). The stress is given by:

$$(2.1) \quad \tau = \rho C_d U_{10}^2$$

where  $\rho$  is the density of the air,  $C_d$  is the drag coefficient and  $U_{10}$  is the wind speed at 10 m elevation. Large and Pond (1981) gave the drag coefficient as

$$(2.2) \quad 10^3 C_d = 0.44 + 0.063U_{10}$$

Powell et al. (2003) have recently presented compelling evidence that the drag coefficient does not continue growing at very high wind speeds. They do not propose a specific new drag law, but we can interpret their data as putting a cap of  $2.2 \times 10^{-3}$  on  $C_d$ . The cap takes effect for 10 m wind speeds greater than 27.9 m/sec. Imposition of this cap in the application of the Kantha Clayson model produced unbiased mixed layer currents in the study noted above.

The model is driven by time histories of wind speed and direction at each basin-grid point. The model is started from rest at the first time step in each storm. Wind speeds are very low in the early hours of the storms so the modeled currents grow smoothly from rest. No artificial inertial oscillations are created at the start of the storms.

The model also requires initial profiles of temperature and salinity. Those profiles were taken from the NODC World Ocean Atlas of 2001. This atlas gives the profiles on a one degree grid for each month of the year.

The 1-D model was run at all grid points with water depths of 75 m and deeper for a total of grid points.

### **3. METEOROLOGICAL CHARACTERISTICS OF HURRICANES KATRINA AND RITA**

#### **3.1 Data Sources**

Our analysis referred to the following data:

- Aircraft reconnaissance of Hurricane Katrina and Rita obtained from NOAA and U.S. Air Force hurricane hunter aircraft, including vortex messages as well as continuous flight level wind speed, direction, D-Value, air temperature.
- Gridded and image fields of marine surface wind composites from the Hurricane Research Division HWnd re-analysis of Katrina and Rita
- Synoptic observations from NOAA buoy and C-MAN stations
- Synoptic observations from coastal and land stations obtained from the GTS (Global Transmission System) in real time
- NOAA NHC/TPC advisories including intensity and position at 3-hourly intervals.
- NHC/TPC best track data
- NHC/TPC Tropical Storm Report
- Composite NWS radar imagery
- Loops of NOAA GOES visual, infrared and water vapor imagery
- NWS synoptic weather analysis charts
- NCEP model wind fields
- QUIKSCAT scatterometer winds
- TOPEX altimeter winds and waves
- ERS-2 altimeter winds and waves
- Aircraft tail radar Doppler wind speed images in Katrina
- Passive microwave images from the satellite mounted instruments AMSR-E, TRMM and SSMI

## 3.2 General Storm Track/Wave Characteristics

### **Katrina**

The evolution and impact of the costliest and one of the deadliest hurricanes to strike the U.S. is described in the NOAA NHC Tropical Cyclone Report on Hurricane which may be downloaded from the following site [http://www.nhc.noaa.gov/pdf/TCR-AL122005\\_Katrina.pdf](http://www.nhc.noaa.gov/pdf/TCR-AL122005_Katrina.pdf)

The full track and intensity history is given in Appendix A while Figure 3 shows the track in the GOM with respect to the NOAA NDBC buoy array. Katrina originated as a tropical depression that organized over the central Bahamas on August 24, and soon strengthened to a Category 1 hurricane on the Saffir-Simpson Hurricane Scale just a few hours before it entered South Florida during the evening August 25. Katrina briefly weakened to tropical storm intensity over South Florida but quickly regained minimal hurricane strength soon after it emerged into the GOM. Katrina's movement west then northwest in the GOM was accompanied by two separate bursts of intensification, the first late on August 26 which took Katrina to Cat. 3 intensity and the second late on the 27<sup>th</sup> and early the 28<sup>th</sup> which took Katrina to Cat. 5 intensity. These changes were accompanied by fairly typical structural changes in the size and degree of organization of the storm, particularly in the well monitored evolution of two distinct eye-wall replacement cycles, each of which was characterized by the formation of an outer eye wall near a radius of about 40 nm from the center and its contraction to between 15 nm and 20 nm from the center. The minimum central pressure attained by Katrina was 902 mb at about 1800 UTC August 28 with peak winds of 150 knots (this is the official NHC intensity expressed in terms of the maximum 1-minute average wind speed expected in one hour, or the so called "sustained wind"), when the center was located about 170 n mi southeast of the mouth of the Mississippi River. At maximum intensity, the radius of maximum wind was about 15 nm which is fairly large for a Cat. 5 hurricane. Rapid weakening of Katrina ensued over the subsequent 18 hours and Katrina, now moving almost due north, made its first Gulf landfall as a Cat. 3 hurricane at 1100 UTC

August 29. The pre-landfall weakening was accompanied by a radical change in wind structure as the inner eye-wall seen at maximum intensity collapsed as a new outer wind maximum formed, which instead of contracting maintained itself and thereby imparted a shelf-like structure to the radial distribution of wind speed, especially on the right side of the wind circulation. This transformation is revealed vividly in comparative aircraft tail Doppler radar wind speed cross section images contained in the NHC report noted above.

Unlike many recent hurricanes in the GOM, the center of Katrina did not pass directly over a NOAA data buoy but nevertheless, due to the large size of the circulation, significant wave heights (HS) exceeded 8 meters at buoys 42003, 42038 and 42039 and 15 meters at 42040. The highest single HS measurement at 42040 (located 64 n mi south of Dauphin Is.) of 16.9 m is stated by the NOAA NDBC to be the highest HS ever recorded by a NOAA buoy in a tropical cyclone. This measurement was made at 1100 UTC August 29 when the center of Katrina was located 73 n mi west of the buoy. Because of the stochastic nature of ocean surface waves, a single estimate of HS from say a 20-minute wave sample is subject to statistical sampling variability and a more reliable estimate of the peak HS is determined by running a 3-hour box-car filter through the hourly time series. This process yields a peak HS of 15.7 m with an associated peak spectral period of 13.7 sec.

The storm surge at the coast is, of course, of great interest because of the breach of the levees protecting New Orleans. The indications are that peak storm surge at the coast to the right of where the center crossed the coast was about 27 feet.

## **Rita**

Rita attained the fourth lowest central pressure on record for the Atlantic basin. As seen in Katrina, even though Rita reached rare Cat. 5 intensity in the GOM, it weakened to Cat. 3 before making landfall near the Sabine Pass along the Texas-Louisiana border. The storm evolution and

impact are described in the NOAA NHC Tropical Cyclone Report on Hurricane Rita which may be downloaded from the following site

[http://www.nhc.noaa.gov/pdf/TCR-AL182005\\_Rita.pdf](http://www.nhc.noaa.gov/pdf/TCR-AL182005_Rita.pdf)

The full track and intensity history is given in Appendix A while Figure 3 shows the track in the Gulf of Mexico with respect to the NOAA NDBC buoy array. Similar to Katrina, Rita can be traced to a complex evolution of disturbances in the Atlantic basin but not until the disturbance reached the central Bahamas at 0000 UTC September 18 was a tropical depression that was to become Rita first classified. Tropical storm intensity was attained about 18 hours later and by 1200 UTC September 20 Rita reached hurricane intensity at a position about 100 n mi east southeast of Key West, Fl. Another similarity between Rita and Katrina was the rapid intensification to Cat. 5 strength as the system passed westward over the deep-layered warm waters associated with the Loop Current. Rita maintained Cat. 5 strength for about 18 hours and during that time the peak intensity was logged by NHC at minimum central pressure of 897 mb and peak sustained wind speed of 155 knots. While the radius of maximum wind speed in Rita also exhibited temporal variability, the amplitude of the eye wall replacement cycle was smaller than seen in Katrina. with the radius generally confined to the range 20 n mi. to 10 n mi., with the smaller radius characterizing the most intense period of the storm history. However, the azimuth of the maximum wind speed in Rita seemed to exhibit more variability than usual such that while in an average sense the peak winds tended to lie to the right of the eye relative to storm heading, the actual bearing of the maximum wind speed varied in a rather regular fashion from the right rear to the left front quadrant with a periodicity of about 24-hours. Rita abruptly weakened to Cat. 4 intensity by 1800 UTC on September 22 and to Cat. 3 intensity by 1800 UTC September 23 at which time it was located about 140 n mi. southeast of Sabine Pass. The center made landfall at 0740 UTC September 24 with maximum sustained wind speeds of 100 knots in extreme southwestern Louisiana.

The center of Rita passed very near NOAA data buoy 42001 (25.8 N, 89.7W) at about 2300 UTC September 22. The sequence of continuous 10-minute averages of wind speed and direction

indicate that the left side of the eye wall wind maximum just barely passed over the buoy as indicated by the double maximum in the wind speed time history at the buoy. The peak 10-minute average wind speed was 88 knots and the peak 5-second gust was 119 knots. Since 42001 is a 10-meter discuss buoy with the anemometer mounted at the 10-meter elevation, these winds probably represent the true winds on the left side of the eye wall at this time. The maximum HS measured by the buoy was 11.63 m at 2100 UTC September 22, and the 3-hour box-car average centered on this time gives a more reliable peak HS of 10.63 m with associated peak period of 12.9 sec. The storm surge at the coast probably peaked in the 15 feet range along the coast to the east of where the eye made landfall (e.g. Cameron, LA).

## **4. HINDCAST RESULTS**

### **4.1 Wind Field**

In this study all winds are referred to the effective over-water 30-minute average winds at a height of 10 meters above sea level. Applying the following “gust” factors to the 30-minute average wind speed may derive wind speeds at shorter averaging intervals:

10-minute average	x 1.09
1-minute average	x 1.24
3-second gust	x 1.53

The maximum hindcast wind speeds in Katrina and Rita are shown in Figures 4 and 5 on the basin grid.. At the time of Cat. 5 strength, Katrina evidently generated higher peak winds and over a larger area than Rita. Peak wind speeds at maximum intensity in Katrina were in the range of 55 m/s to 60 m/s while Rita’s wind speeds peaked between 45 m/s and 50 m/s. This difference exemplifies the fact that storms with the same Saffir-Simpson Scale Number, same central pressure, and roughly comparable sizes and forward velocity in the same geographic area

can have significantly different maximum winds and consequent ocean response. The principle factor responsible for this natural variability is the shape of the radial pressure profile, effects of which are approximated by the B parameter of the exponential pressure profile, though storms may exhibit even more complex radial pressure and wind distributions, and may require double exponential representation of the radial pressure profile, as introduced by Thompson and Cardone (1996).

## 4.2 Surface Waves

The execution of the UNIWAVE hindcast model provides directly the two-dimensional wave spectrum at 15-minute intervals on the MMS Katrina and Rita model grids. Integrated properties of the spectrum are calculated from the 2-D spectrum at all Northern Gulf grid points and archived as part of the hindcast run. The maximum hindcast significant wave heights in Katrina and Rita are shown in Figures 6 and 7 for the basin grid and in Figures 8 and 9 for the Fine grids. The maximum sea state generated by a hurricane in the inner core region is a complex function of maximum wind speed, the radius of maximum wind, the peakedness of the radial wind profile and the storm forward speed. These factors were evidently highly tuned for maximum response in Katrina, as Figure 6 shows that the storm raised peak HS in the 16 m to 17 m range over most of its history from just north of 26° N to the deep waters just south of the MS Delta. In Rita, inner core HS peaked in the 14 m to 15 m range. However, in the deep water offshore development areas north of 26° N, both Rita and Katrina raised broad areas of extreme sea states. In both storms the mean cross track diameter of the 10 meter HS contour is about 275 n mi. with a trend to an even broader distribution in Katrina as the center approached its first landfall, no doubt a response of the wave field to the development of a shelf like structure to the wind field to the right of the center in the 24-hour pre-landfall period as noted in the last section.

### **4.3 Storm Surge and Shallow Water Currents**

The maximum storm surge specified on the ADCIRC nodal grid is shown in Figure 10 for Katrina and Figure 11 for Rita. The surge peaked at between 8 and 9 meters in Katrina and between 5 and 6 meters in Rita. The maximum hindcast vertically integrated current is shown in Figure 12 for Katrina and Figure 13 for Rita. There are no measurements of shallow water currents available but comparisons of hindcast simulated coastal hydrograph traces and measured traces are given in Section 5.

### **4.4 Deep Water Mixed Layer Current Profile**

The mixed layer model provides two representations of the profile. The first is the raw model generated output of the time history of the vertical profile of current speed and direction at 5 meter intervals between the free surface and the level of no motion. The second is a simplified profile represented in terms of the near surface current speed and direction, the depth of no motion and the current speed at a depth halfway between the surface and the depth of no motion. The simplified representation is usually sufficient for most engineering applications because the assumption of linear profile segments between the two nodes (i.e. surface to mid-depth of level of no motion and from the mid-depth to level of no motion) is typically consistent with the ability of the model to resolve the profile. The most important single predictive variable for most purposes is the maximum surface current speed and direction. The spatial pattern of maximum near surface current speed is shown in Figure 14 for Katrina and Figure 15 for Rita.

## **5. VALIDATION**

### **5.1 NDBC Buoys**

Validation of the wind and wave hindcast was performed against all available NDBC buoys in the Gulf of Mexico as listed in Table 1. Data were obtained from quality controlled

files available from the National Oceanographic Data Center and have undergone additional quality control procedure not possible in real-time. All wind speed have been adjusted for height and stability to a reference level of 10 meters and all data has been smoothed  $\pm 1$  hour with equal weighting to reduce sampling variability Figure 3 shows the locations of the buoys with respect to the storm tracks.

Appendix B gives plots that compare for each buoy and hindcast the time series of wind speed and wind direction, significant wave height, spectral peak wave period and vector mean wave direction (if available for the buoy) for each of the buoys. Difference statistics for these variables based on time series comparisons are given for each buoy in Table 2 for Katrina and Table 3 for Rita.

The buoy wind speed measurements can not be considered a priori to be unbiased in all cases. The 10-meter discuss buoys (#42001, #42002, #42003) have anemometers mounted at 10-meter elevation. The large buoy diameter and the high mounting of the anemometer imply that the buoy wind measurements are less likely to be affected by buoy motion and wave sheltering than measurements from the 3-meter discuss buoy (anemometer height 4-5 meters) which occupy all other NDBC sites in the GOM. Indeed, during the process of kinematic analysis of wind fields, OWI routinely assume that measured wind speeds from 3-meter discuss buoys begin to exhibit a negative bias at wind speeds above about 20 m/s as HS exceeds 5 m, and may be biased low by as much as 20% in the most extreme sea states such as experienced at buoy 42040 at closest approach of Katrina. The time series plots (e.g. see the wind speed comparison plot for 420040 in Katrina in the Appendix) and wind difference statistics reported herein do not reflect sea state adjustments of the 3-meter discuss buoy wind speed. Similarly, plots and statistics for the wave comparisons at buoy 42007 do not incorporate the fact that the buoy broke from its moorings as the core of Katrina approached and while it drifted (probably into shallower and more protected waters than at its nominal location) it is not located at the model grid point used for the comparisons (as of the writing of this report, NDBC still have not released a trajectory for the buoy drift.)

Overall all buoys in Katrina, the bias in HS and TP average -07 cm and -0.63 sec respectively and the correlation coefficient in HS is .96. In Rita the HS bias is -0.02 cm and the TP bias is -0.68 sec. with correlation coefficient in HS of 0.98. The negative period bias appears to be a property of most 3G wave models. The scatter index for HS is 0.23 in Katrina and 0.25 in Rita, which are considered very skillful for comparisons of continuous time series. Comparisons of storm peaks of wind speed and HS are given in Figure 11. The scatter index on wind speed is within expected limits but the scatter index on HS (at 0.18) is larger than usually achieved reflecting the mainly the difficulty of modeling the unusually rapid changes in storm intensity and the dramatic structural changes in the wind field of these storms in the GOM. However, a more stable population of statistics emerges when OWI3G model hindcasts of a larger population of Gulf of Mexico hurricanes are considered. Jensen et al. (2006) report a bias of .03 m and scatter index of only 0.14 on HS in comparisons of OWI3G hindcasts of Hurricanes Camille (1969), Lili (2002), Ivan (2004), Dennis (2005), Katrina (2005) and Rita (2005) where peaks at buoys exceeded 3 m.

Wave spectra comparisons are given in Appendix C for all buoys that reported such spectra in each storm. These plots were made from the format F291 files available from NDBC. For each comparison, two plots are shown. The first is of the frequency spectrum (i.e. the spectral energy in each frequency band summed over all directions) and the second is of the mean wave direction in each frequency band as a function of frequency. No attempt to smooth the spectra was made.

It is well known that in a hurricane environment the directional spectrum is quite complicated as wave energy generated in one quadrant of the storm propagates radially away from the center and mixes with locally generated winds in other quadrants. The buoy spectra exhibit this behavior in the form a significant and systematic variation of wave direction with frequency particularly in the disparity between the mean wave direction at the spectral peak and the mean wave direction in the tail of spectrum (say at twice the peak frequency and beyond). The motion

of the storm, azimuthal rotation of the inner core wind maximum and steady rotation of the local wind vector all serve to impart considerable temporal variability as well. The plots in the Appendix indicate in general an uncanny ability of the hindcast to track this complex evolution of the directional wave spectrum in the buoy array surrounding Katrina and Rita.

## **5.2 Coastal Hydrograph Trace**

Table 4 gives the locations at which at least partial hydrograph traces were obtained in the two storms. Figure 16 shows the locations of the stations affected by Katrina. The comparisons of hindcast and measured hydrographic traces are given in Figure 17. Unfortunately most gages failed to capture the storm peaks. Figure 18 shows the locations of the stations affected by Rita. The comparisons of hindcast and measured hydrographic traces are given in Figure 19. Again, unfortunately most gages failed to capture the storm peaks

## **5.3 ADCP Deep Water Currents**

Forristall et al. (2006) review the history of the application of 1D mixed layer models, including the Kantha-Clayson formulation applied in this study. That 1D current profile model has been developed and calibrated by virtue of several past projects as well as new data collected in Katrina. Beginning in the 1980s, the Ocean Response to a Hurricane Joint Industry Project (ORTAH) JIP provided measured current profiles in several hurricanes. The measurements were made using expendable current profilers (AXCP) dropped from airplanes. These instruments record the instantaneous velocity as the instruments fall through the water. Thus the measurements include the large orbital velocities that are due to waves as well as the steady currents. The wave and current velocities were separated by fitting the data to a tri-linear current profile plus the orbital velocity of a regular wave. When the Kantha and Clayson model was applied to these datasets, the average error in current speed was found to be 0.04 m/sec with rms error of 0.34 m/sec. The LATEX project measured currents at several sites on the Texas and Louisiana continental shelf in August 1992 during the passage of Hurricane Andrew which

passed close to LATEX moorings 13 and 14. Mooring 13 was in about 200 m of water, with current meters at 10, 100 and 190 m below the surface. The peak current was under-estimated by about 40 cm/sec. The modeled currents do not reach 100 m depth during the storm passage, but the observations show no sign of storm influence during the storm peak on August 26 either.

Most recently, Norske Hydro collected current measurements at their Telemark site during Hurricane Katrina (mooring at 27.881° N, 88.992° W) with an upward looking 300 kHz ADCP looking upward and a 75 kHz ADCP looking downward. Hurricane Katrina passed approximately 30 nautical miles west of Telemark. Katrina produced very strong currents (up to 230 cm/s near the surface). It was in the attempt to simulate this response that it was found necessary to cap the drag coefficient at  $2.2 \times 10^{-3}$ , as noted in a previous section.

Figure 20 compares the measurements at selected depths with the model results at the same depth. Near the surface and down to 40 m depth, the model with a stress cap gives results that are slightly lower than the measurements. At 70 m depth, the measurements are intermittent. At 100 m depth, the measured currents are small. The Kantha and Clayson equations predict that hurricane generated currents penetrate deeper than observed. For most deep water engineering purposes, it is better to have the best agreement near the surface and the Kantha and Clayson equations with a drag coefficient cap performs there. The stress cap is not expected to disturb the good validation results seen in the previous cases noted above because the wind speeds in the hurricanes in the vicinity of the current measurements were lower than the threshold wind speed at which the drag coefficient cap becomes effective.

## 6. DELIVERABLES

Along with this report, digital data from this hindcast is made available on a companion DVD. The DVD contains wind, wave, and current results for all active grid points north of 26°N in the Gulf of Mexico (basin grid). Files are in ASCII. Figure 21 22 and 23 show the grid point

locations that constitute the archive which is restricted to active points with depths greater than 10 meters and North of 26N. ADCIRC output (water level and vertically integrated currents) have been merged with the wind/wave results at all basin and fine-scale model points. Output from the 1-D current model has been merged with the basin results for locations greater than 75 meters. Wind, wave, 2D and 1D current archive fields are described in Appendix E. Wave spectra (24 directions by 23 frequencies) were archived at a subset of the basin and fine scale grids. Formats are described in Appendix F.

## References

- Cardone, V. J., W. J. Pierson and E. G. Ward. 1976. Hindcasting the directional spectra of hurricane generated waves. *J. of Petrol. Technol.*, 28, 385-394.
- Cardone, V. J. and D. B. Ross, 1979. State-of-the-art wave prediction methods and data requirements. *Ocean Wave Climate* ed. M. D. Earle and A. Malahoff. Plenum Publishing Corp., 1979, 61-91.
- Cardone, V. J. and . Ramos. Wave, wind and current characteristics of Bay of Campeche. Offshore Technology Conference , Houston, TX 4-7 May, 1998. Paper OTC 8697, 143-155.
- Cardone, V. J., C.V. Greenwood and J. A. Greenwood. 1992. Unified program for the specification of tropical cyclone boundary layer winds over surfaces of specified roughness. Contract Rep. CERC 92-1, U.S. Army Engrs. Wtrwy. Experiment Station, Vicksburg, Miss.
- Cardone, V. J. and C. K. Grant. 1994. Southeast Asia meteorological and oceanographic hindcast study (SEAMOS). OSEA 94132. 10th Offshore Southeast Asia Conference, 6-9 December, 1994.
- Cardone, V. J. and V. R. Swail. On surface wind and ocean wave coupling in severe marine extratropical cyclones. Symposium on the life cycles of extratropical cyclones. 27 June-1 July, 1994, Bergen, Norway.
- Cardone, V.J., A.T. Cox, K.A. Lisaeter and D.S. Szabo. Hindcast of Winds, Waves and Currents in Northern Gulf of Mexico in Hurricane Lili (2002). 2004 Offshore Technology Conference, May 2004, Houston, TX
- Chow, S. H., 1971. A study of the wind field in the planetary boundary layer of a moving tropical cyclone. Master of Science Thesis in Meteorology, School of Engineering and Science, New York University, New York, N.Y.
- Cox, A.T. and V.J. Cardone. Operational System for the Prediction of Tropical Cyclone Generated Winds and Waves. 6th International Workshop on Wave Hindcasting and Forecasting November 6-10, 2000, Monterey, California.
- Cox, A.T. and V.R. Swail. A Global Wave Hindcast over the Period 1958-1997: Validation and Climate Assessment. *JGR (Oceans)*, Vol. 106, No. C2, pp. 2313-2329, February 2001.
- Cox, A.T., V. Cardone, F. Counillon, and C. Szabo, 2005. Hindcast Study of Winds, Waves and Currents in Northern Gulf of Mexico in Hurricane Ivan, OTC 17736, Houston Texas, Offshore Technology Conference, May 2005.
- Donelan, M.A., B. K. Haus, N. Reul, W. J. Plant, M. Stiassnie, H. C. Graber, O.B. Brown and E.S. Saltzman, 2004. On the limiting aerodynamic roughness of the ocean in very strong winds. *Gephys. Res. Ltrrs.*, Vol. 31, L18306.
- Forristall, G.Z., R. C. Hamilton and V. J. Cardone, 1977. Continental shelf currents in tropical storm Delia: observations and theory. *J. of Phys. Oceanog.* 7, 532-546.
- Forristall, G. Z., E. G. Ward, V. J. Cardone, and L. E. Borgman. 1978. The directional spectra and kinematics of surface waves in Tropical Storm Delia. *J. of Phys. Oceanog.*, 8, 888-909.
- Forristall, G. Z., 1980. A two-layer model for hurricane driven currents on an irregular grid. *J. Phys. Oceanog.*, 10, 9, 1417-1438.
- Forristall, G.Z. 2006. Personal communication, paper in progress.

- Graber, H.C., V.J. Cardone, R.E. Jensen, D.N. Slinn, S.C. Hagen, A.T. Cox, M.D. Powell, and C. Grassl, 2006 : "Coastal forecasts and storm surge predictions for tropical cyclones: A timely partnership program.", *Oceanography*, vol. 19 no. 1, pp.130-141
- Graham , H. E. and G. N. Hudson, 1960. Surface winds near the center of hurricanes (and other cyclones). National Hurricane Research Project Report No. 39. Washington, D.C. 200 pp.
- Haring R.E. and J.C. Heideman, 1978. Gulf of Mexico Rare Wave Return Periods. OTC 3230, 10th Annual Offshore Technology Conference, Houston, TX May 8-11 1978.
- Holland, G. J., 1980. An analytical model of the wind and pressure profiles in hurricanes. *Mon. Wea. Rev.* 1980, 108, 1212-1218.
- Jensen, R.E., V.J. Cardone and A.T. Cox, 2006: Performance of Third Generation Wave Models in Extreme Hurricanes. 9th International Wind and Wave Workshop, September 25-29, 2006, Victoria, B.C.
- Kantha, L.H., and C.A. Clayson (1994), An improved mixed layer model for geophysical applications, *J. Geophys. Res.*, 99, 25235-25266.
- Kantha, L.H., and C.A. Clayson (2000), *Small Scale Processes in Geophysical Fluid Flows*, Academic Press, San Diego, 888 pp.
- Khandekar, M. L., R. Lalbeharry and V. J. Cardone. 1994. The performance of the Canadian spectral ocean wave model (CSOWM) during the Grand Banks ERS-1 SAR wave spectra validation experiment. *Atmosphere-Oceans*, 32, 31-60.
- Kinnmark, I. (1985). "The shallow water wave equations: Formulation, analysis and application." *Lecture Notes in Engineering*, Springer-Verlag, 15, New York.
- Kolar, R. L., Gray, W. G., Westerink, J. J., and Luettich, R. A. Jr. (1994a). "Shallow water modeling in spherical coordinates: Equation formulation, numerical implementation, and application." *Journal of Hydraulic Research*, 32(1), 3–24.
- Kolar, R. L., Westerink, J. J., Cantekin, M. E., and Blain, C. A. (1994b). "Aspects of nonlinear simulations using shallow-water models based on the wave continuity equation." *Computers and Fluids*, 23(3), 523–538.
- Large, W.G., and S. Pond (1981), Open ocean momentum flux measurements in moderate to strong winds, *J. Phys. Oceanogr.*, 11, 324-336.
- Leverette, S., S. Bian, D. Taberner and C. Van-der-Linden, 2005. Matterhorn SeaStar Hurricane Ivan response. *Deep Ocean Technology*, Brazil, November, 2005.
- Luettich, R. A. Jr., Westerink, J. J., and Scheffner, N. W. (1992). "ADCIRC: An advanced three-dimensional circulation model for shelves, coasts and estuaries, I: Theory and methodology of ADCIRC-2DDI and ADCIRC-3DL." *DRP Tech. Rep. 1*, U.S. Army Corps of Engineers, Waterways Experiment Station, Vicksburg, Mississippi.
- Lynch, D. R., and Gray, W. G. (1979). "A wave equation model for finite element tidal computations." *Computers and Fluids*, 7, 207–228.
- Mellor, G.L., and P.A. Durbin (1975), The structure and dynamics of the ocean surface mixed layer, *J. Phys. Oceanogr.*, 5, 718-728.
- Mellor, G.L., and T. Yamada (1982), Development of a turbulence closure model for geophysical fluid problems, *Rev. Geophys. Space Phys.*, 20, 851-875.
- Powell, M. D., S. H. Houston, L. R. Amat, and N. Morisseau-Leroy, 1998: The HRD real-time hurricane wind analysis system. *J. Wind Engineer. and Indust. Aerodyn.* 77&78, 53-64

- Powell, M.D., Vickery, P.J., and Reinhold, T.A., 2003: Reduced drag coefficient for high wind speeds in tropical cyclones, *Nature*, Vol 422, 279-283.
- Puskar, F. J., R. K. Aggarwal, C. A. Cornell, F. Moses and C. Petruskas, 1994: A comparison of analytically predicted platform damage to actual platform damage during Hurricane Andrew. 26th Annual Offshore Technology Conference, Houston, TX, 2-5 May, 1994. OTC Paper 7473.
- Reece, A. M. and V. J. Cardone. 1982. Test of wave hindcast model results against measurements during four different meteorological systems. Offshore Technology Conference. OTC 4323, 269-.
- Ross, D. B. and V. J. Cardone, 1978. A comparison of parametric and spectral hurricane wave prediction products. *Turbulent Fluxes through the Sea Surface, Wave Dynamics, and Prediction*, A. Favre and K. Hasselmann, editors, 647-665.
- Shapiro, L. J., 1983. The asymmetric boundary layer flow under a translating hurricane. *J. of Atm. Sci.* 39 (February).
- Swail, V.R. and A.T. Cox. On the use of NCEP/NCAR Reanalysis Surface Marine Wind Fields for a Long Term North Atlantic Wave Hindcast *J. Atmo. Tech.* Vol. 17, No. 4, pp. 532-545, 2000.
- Thompson, E. F. and V. J. Cardone. 1996. Practical modeling of hurricane surface wind fields. *ASCE J. of Waterway, Port, Coastal and Ocean Engineering.* 122, 4, 195-205.
- Ward, E. G., L. E. Borgman, and V. J. Cardone, 1979. Statistics of hurricane waves in the Gulf of Mexico. *J. Petrol. Tech.* Ward, E. G., L. E. Borgman, and V. J. Cardone, 1979. Statistics of hurricane waves in the Gulf of Mexico. *J. Petrol. Tech.*
- Westerink, J. J., Muccino, J. C., and Luetich, R. A. Jr. (1991). "Tide and hurricane storm surge computations for the western North Atlantic and Gulf of Mexico." *Proceedings of the 2nd International Conference on Estuarine and Coastal Modeling*, ASCE, Tampa, Florida, 538-550.

**Table 1. Locations of NDBC buoy and CMAN stations**

Location	Latitude	Longitude	GridPoint	Latitude	Longitude	Depth
42001	25.84	-89.66	39379	25.85	-89.65	3218.0
42002	25.17	-94.42	34726	25.15	-94.40	3567.4
42003	26.01	-85.91	40389	26.00	-85.90	3232.9
42007	30.09	-88.77	60949	30.10	-88.75	15.8
42013	27.20	-82.90	47719	27.20	-82.90	21.3
42019	27.91	-95.36	51546	27.90	-95.35	130.5
42020	26.94	-96.70	45949	26.95	-96.70	91.1
42022	27.50	-83.70	49468	27.50	-83.70	48.1
42035	29.25	-94.41	58578	29.25	-94.40	15.3
42036	28.50	-84.52	55077	28.50	-84.50	49.5
42038	27.42	-92.58	48706	27.40	-92.60	915.3
42039	28.79	-86.02	56620	28.80	-86.00	268.3
42040	29.18	-88.21	58467	29.20	-88.20	296.1
42046	27.90	-94.00	51573	27.90	-94.00	158.9
42055	22.02	-94.05	14407	22.00	-94.05	3471.1
42362	27.80	-90.70	51067	27.80	-90.70	621.9
BURL1	28.91	-89.43	57056	28.90	-89.45	25.2
DPIA1	30.25	-88.07	61160	30.25	-88.05	5.9
FWYF1	25.59	-80.10	37949	25.60	-80.10	192.1
GDIL1	29.27	-89.96	58641	29.25	-89.95	4.4
KTNF1	29.82	-83.59	60513	29.80	-83.60	3.7
MLRF1	25.01	-80.38	33975	25.00	-80.40	91.4
SANF1	24.46	-81.88	30137	24.45	-81.90	100.9
SGOF1	29.41	-84.86	59311	29.40	-84.85	21.6
SMKF1	24.63	-81.11	31543	24.65	-81.10	25.9
SRST2	29.67	-94.05	60040	29.65	-94.05	5.4
VENF1	27.07	-82.45	46833	27.05	-82.45	10.0

---



---

Hindcast Data on Winds, Waves, and Currents in Northern Gulf of Mexico in Hurricanes Katrina and Rita

---



---

Table 2. Statistical comparison of NDBC buoys during Hurricane Katrina 2005.

	Station	Number of Pts	Mean Meas	Mean Hind	Diff (H-M)	RMS Error	Stnd Dev	Scat Index	Ratio	Corr Coeff
Wind Spd. (m/s)	42001	174	8.37	8.39	0.03	1.30	1.30	0.16	0.44	0.98
Wind Dir. (deg)	42001	174	30.44	18.96	-1.36	N/A	11.30	0.03	N/A	N/A
Sig Wave Ht (m)	42001	173	2.01	2.29	0.28	0.89	0.84	0.42	0.46	0.98
Wave Period (s)	42001	173	5.46	5.04	-0.42	0.90	0.80	0.15	0.33	0.91
Wave Dir (deg)	42001	172	358.82	43.26	-52.15	N/A	58.12	0.16	N/A	N/A
Wind Spd. (m/s)	42002	174	4.94	4.92	-0.02	1.06	1.06	0.21	0.48	0.89
Wind Dir. (deg)	42002	174	334.71	335.52	-0.16	N/A	8.19	0.02	N/A	N/A
Sig Wave Ht (m)	42002	174	1.01	1.15	0.14	0.63	0.62	0.61	0.45	0.91
Wave Period (s)	42002	174	4.72	4.50	-0.23	1.00	0.97	0.21	0.33	0.83
Wave Dir (deg)	42002	174	104.04	90.34	-20.25	N/A	37.73	0.10	N/A	N/A
Wind Spd. (m/s)	42003	103	10.50	10.34	-0.16	1.21	1.20	0.11	0.44	0.99
Wind Dir. (deg)	42003	103	47.64	41.00	-5.90	N/A	13.86	0.04	N/A	N/A
Sig Wave Ht (m)	42003	103	2.54	2.52	-0.02	0.58	0.58	0.23	0.49	0.98
Wave Period (s)	42003	103	5.54	4.86	-0.68	1.20	0.99	0.18	0.28	0.91
Wave Dir (deg)	42003	102	88.43	55.62	-36.13	N/A	38.94	0.11	N/A	N/A
Wind Spd. (m/s)	42007	174	8.58	8.78	0.20	2.38	2.37	0.28	0.45	0.96
Wind Dir. (deg)	42007	174	97.77	96.09	-2.62	N/A	11.74	0.03	N/A	N/A
Sig Wave Ht (m)	42007	146	1.51	1.60	0.09	1.14	1.14	0.76	0.21	0.82
Wave Period (s)	42007	146	5.19	4.60	-0.59	1.56	1.44	0.28	0.25	0.78
Wave Dir (deg)	42007	116	108.52	117.58	8.89	N/A	20.43	0.06	N/A	N/A
Wind Spd. (m/s)	42013	67	8.15	7.91	-0.24	1.73	1.72	0.21	0.30	0.90
Wind Dir. (deg)	42013	67	49.43	40.19	-8.41	N/A	30.70	0.09	N/A	N/A
Wind Spd. (m/s)	42019	174	4.54	4.20	-0.34	1.05	0.99	0.22	0.41	0.91
Wind Dir. (deg)	42019	174	101.15	100.31	-0.49	N/A	12.75	0.04	N/A	N/A
Sig Wave Ht (m)	42019	174	0.94	0.81	-0.13	0.25	0.21	0.23	0.30	0.98
Wave Period (s)	42019	174	4.97	4.14	-0.83	1.03	0.61	0.12	0.08	0.92
Wave Dir (deg)	42019	173	149.42	133.10	-17.34	N/A	41.97	0.12	N/A	N/A
Wind Spd. (m/s)	42020	174	4.67	4.00	-0.67	1.32	1.14	0.24	0.24	0.70
Wind Dir. (deg)	42020	174	129.56	128.36	-1.20	N/A	11.92	0.03	N/A	N/A
Sig Wave Ht (m)	42020	171	0.90	0.90	0.01	0.42	0.42	0.47	0.47	0.91
Wave Period (s)	42020	171	5.25	4.79	-0.46	1.00	0.89	0.17	0.26	0.91
Wave Dir (deg)	42020	169	129.19	119.85	-8.10	N/A	27.76	0.08	N/A	N/A
Wind Spd. (m/s)	42035	174	4.32	3.85	-0.48	1.34	1.26	0.29	0.36	0.90

---

Hindcast Data on Winds, Waves, and Currents in Northern Gulf of Mexico in Hurricanes Katrina and Rita

---

Wind Dir. (deg)	42035	174	75.74	75.22	-0.69	N/A	8.93	0.02	N/A	N/A
Sig Wave Ht (m)	42035	167	0.71	0.39	-0.32	0.48	0.35	0.50	0.10	0.96
Wave Period (s)	42035	167	4.88	3.63	-1.25	1.50	0.83	0.17	0.02	0.82
Wave Dir (deg)	42035	166	156.75	152.46	-7.26	N/A	41.50	0.12	N/A	N/A
Wind Spd. (m/s)	42036	174	9.61	9.33	-0.28	1.15	1.11	0.12	0.47	0.96
Wind Dir. (deg)	42036	174	96.65	96.94	0.40	N/A	5.41	0.02	N/A	N/A
Sig Wave Ht (m)	42036	168	2.48	2.13	-0.35	0.47	0.32	0.13	0.13	0.98
Wave Period (s)	42036	168	5.71	5.07	-0.63	0.81	0.50	0.09	0.04	0.96
Wave Dir (deg)	42036	167	121.52	123.16	-3.79	N/A	35.95	0.10	N/A	N/A
Wind Spd. (m/s)	42038	172	6.02	5.94	-0.07	0.98	0.98	0.16	0.50	0.97
Wind Dir. (deg)	42038	172	343.72	341.70	-0.19	N/A	10.87	0.03	N/A	N/A
Sig Wave Ht (m)	42038	174	1.58	1.41	-0.17	0.37	0.33	0.21	0.24	0.99
Wave Period (s)	42038	174	5.16	4.46	-0.70	0.98	0.69	0.13	0.21	0.93
Wind Spd. (m/s)	42039	174	9.76	10.00	0.24	1.49	1.47	0.15	0.64	0.96
Wind Dir. (deg)	42039	174	103.35	103.00	-0.16	N/A	4.04	0.01	N/A	N/A
Sig Wave Ht (m)	42039	163	3.05	2.76	-0.29	0.60	0.52	0.17	0.31	0.98
Wave Period (s)	42039	163	6.06	5.41	-0.65	0.87	0.58	0.10	0.10	0.95
Wave Dir (deg)	42039	162	156.95	119.20	-29.41	N/A	27.30	0.08	N/A	N/A
Wind Spd. (m/s)	42040	174	9.48	10.24	0.76	1.90	1.74	0.18	0.71	0.98
Wind Dir. (deg)	42040	174	92.51	94.26	1.45	N/A	6.42	0.02	N/A	N/A
Sig Wave Ht (m)	42040	172	3.10	2.96	-0.14	0.54	0.52	0.17	0.30	0.99
Wave Period (s)	42040	172	6.00	5.27	-0.72	0.85	0.44	0.07	0.01	0.98
Wave Dir (deg)	42040	171	137.41	117.08	-14.98	N/A	40.04	0.11	N/A	N/A
Wind Spd. (m/s)	42046	109	4.20	4.74	0.54	1.04	0.89	0.21	0.72	0.95
Wind Dir. (deg)	42046	109	61.88	66.23	5.42	N/A	32.69	0.09	N/A	N/A
Wind Spd. (m/s)	42055	174	5.20	4.93	-0.26	1.46	1.43	0.28	0.40	0.69
Wind Dir. (deg)	42055	174	114.20	126.75	-0.52	N/A	7.54	0.02	N/A	N/A
Sig Wave Ht (m)	42055	172	1.03	1.14	0.11	0.35	0.33	0.33	0.62	0.96
Wave Period (s)	42055	172	5.11	4.68	-0.42	0.70	0.56	0.11	0.23	0.95
Wave Dir (deg)	42055	172	71.01	59.98	-17.46	N/A	38.70	0.11	N/A	N/A
Wind Spd. (m/s)	42362	85	4.65	4.54	-0.11	1.20	1.20	0.26	0.44	0.92
Wind Dir. (deg)	42362	85	40.50	38.78	13.96	N/A	51.21	0.14	N/A	N/A
Wind Spd. (m/s)	BURL1	125	7.48	7.98	0.50	1.27	1.17	0.16	0.64	0.98
Wind Dir. (deg)	BURL1	125	71.59	53.88	-14.85	N/A	42.67	0.12	N/A	N/A
Wind Spd. (m/s)	DP1A1	172	7.91	8.54	0.62	1.73	1.62	0.20	0.66	0.97

---



---

## Hindcast Data on Winds, Waves, and Currents in Northern Gulf of Mexico in Hurricanes Katrina and Rita

---



---

Wind Dir. (deg)	DPIA1	172	79.79	92.60	8.41	N/A	37.29	0.10	N/A	N/A
Wind Spd. (m/s)	FWYF1	172	8.74	7.54	-1.20	2.06	1.67	0.19	0.17	0.95
Wind Dir. (deg)	FWYF1	172	148.46	134.67	5.77	N/A	27.58	0.08	N/A	N/A
Wind Spd. (m/s)	GDIL1	129	6.59	7.74	1.15	2.05	1.70	0.26	0.67	0.98
Wind Dir. (deg)	GDIL1	129	54.40	51.40	-4.64	N/A	40.90	0.11	N/A	N/A
Wind Spd. (m/s)	KTNF1	172	5.12	6.29	1.17	2.75	2.48	0.48	0.71	0.50
Wind Dir. (deg)	KTNF1	172	85.86	96.59	8.03	N/A	24.91	0.07	N/A	N/A
Wind Spd. (m/s)	MLRF1	171	8.08	7.60	-0.48	1.74	1.67	0.21	0.32	0.96
Wind Dir. (deg)	MLRF1	171	176.55	137.75	-4.23	N/A	41.00	0.11	N/A	N/A
Wind Spd. (m/s)	SANF1	172	9.23	8.90	-0.33	1.43	1.39	0.15	0.41	0.98
Wind Dir. (deg)	SANF1	172	168.41	144.67	-2.06	N/A	19.67	0.05	N/A	N/A
Wind Spd. (m/s)	SGOF1	173	9.34	8.69	-0.65	1.74	1.61	0.17	0.39	0.91
Wind Dir. (deg)	SGOF1	173	96.02	95.10	-2.48	N/A	16.74	0.05	N/A	N/A
Wind Spd. (m/s)	SMKF1	166	8.75	8.37	-0.38	1.69	1.65	0.19	0.36	0.96
Wind Dir. (deg)	SMKF1	166	165.71	141.63	-5.86	N/A	26.23	0.07	N/A	N/A
Wind Spd. (m/s)	SRST2	173	3.55	3.55	0.01	1.73	1.73	0.49	0.44	0.64
Wind Dir. (deg)	SRST2	173	19.72	57.73	-6.91	N/A	58.55	0.16	N/A	N/A
Wind Spd. (m/s)	VENF1	173	5.97	7.67	1.70	3.31	2.85	0.48	0.70	0.44
Wind Dir. (deg)	VENF1	173	98.74	104.52	7.33	N/A	24.82	0.07	N/A	N/A
Wind Spd. (m/s)	Combined	4074	7.07	7.11	0.04	1.73	1.73	0.24	0.48	0.94
Wind Dir. (deg)	Combined	4074	91.39	88.51	-0.27	N/A	25.38	0.07	N/A	N/A
Sig Wave Ht (m)	Combined	1957	1.71	1.64	-0.07	0.60	0.59	0.35	0.34	0.96
Wave Period (s)	Combined	1957	5.33	4.70	-0.63	1.05	0.84	0.16	0.18	0.90
Wave Dir (deg)	Combined	1744	123.40	108.30	-16.90	N/A	40.98	0.11	N/A	N/A

Table 3. Statistical comparison of NDBC buoys during Hurricane Rita 2005.

	Station	Number of Pts	Mean Meas	Mean Hind	Diff (H-M)	RMS Error	Stnd Dev	Scat Index	Ratio	Corr Coeff
Wind Spd. (m/s)	42001	167	12.14	12.33	0.19	1.68	1.67	0.14	0.60	0.98
Wind Dir. (deg)	42001	167	85.39	81.88	-2.91	N/A	10.57	0.03	N/A	N/A
Sig Wave Ht (m)	42001	164	3.18	3.38	0.20	0.66	0.63	0.20	0.51	0.99
Wave Period (s)	42001	164	5.99	5.58	-0.41	0.80	0.69	0.11	0.30	0.94
Wave Dir (deg)	42001	164	72.46	88.21	-16.75	N/A	40.47	0.11	N/A	N/A
Wind Spd. (m/s)	42002	168	7.76	8.03	0.27	0.87	0.83	0.11	0.64	0.97
Wind Dir. (deg)	42002	168	45.88	47.91	-0.86	N/A	5.78	0.02	N/A	N/A
Sig Wave Ht (m)	42002	167	1.90	2.07	0.18	0.59	0.56	0.30	0.38	0.98
Wave Period (s)	42002	167	5.57	5.11	-0.46	0.58	0.36	0.07	0.17	0.99
Wave Dir (deg)	42002	167	84.95	61.83	-29.34	N/A	25.86	0.07	N/A	N/A
Wind Spd. (m/s)	42019	167	7.30	7.60	0.30	0.80	0.74	0.10	0.57	0.98
Wind Dir. (deg)	42019	167	54.86	55.37	0.14	N/A	10.44	0.03	N/A	N/A
Sig Wave Ht (m)	42019	166	1.77	1.68	-0.10	0.31	0.29	0.16	0.22	0.98
Wave Period (s)	42019	166	5.45	4.83	-0.62	0.75	0.42	0.08	0.03	0.98
Wave Dir (deg)	42019	166	112.54	95.60	-19.01	N/A	21.51	0.06	N/A	N/A
Wind Spd. (m/s)	42020	166	5.41	6.40	0.99	1.66	1.33	0.25	0.66	0.80
Wind Dir. (deg)	42020	166	48.37	50.66	1.52	N/A	9.95	0.03	N/A	N/A
Sig Wave Ht (m)	42020	160	1.60	1.42	-0.18	0.41	0.37	0.23	0.23	0.96
Wave Period (s)	42020	160	5.97	4.84	-1.13	1.39	0.80	0.13	0.00	0.98
Wave Dir (deg)	42020	158	112.21	90.97	-21.08	N/A	24.35	0.07	N/A	N/A
Wind Spd. (m/s)	42035	168	8.27	8.64	0.37	1.17	1.11	0.13	0.55	0.99
Wind Dir. (deg)	42035	168	105.49	77.56	-0.21	N/A	19.86	0.06	N/A	N/A
Sig Wave Ht (m)	42035	153	1.38	1.00	-0.38	0.58	0.44	0.32	0.09	0.95
Wave Period (s)	42035	153	5.40	4.14	-1.26	1.82	1.32	0.24	0.08	0.80
Wave Dir (deg)	42035	153	146.35	122.99	-20.91	N/A	29.94	0.08	N/A	N/A
Wind Spd. (m/s)	42036	168	8.49	8.49	0.00	0.63	0.63	0.07	0.51	0.99
Wind Dir. (deg)	42036	168	72.46	71.97	0.08	N/A	4.58	0.01	N/A	N/A
Sig Wave Ht (m)	42036	164	1.83	1.77	-0.06	0.25	0.24	0.13	0.37	0.98
Wave Period (s)	42036	164	5.19	4.76	-0.43	0.60	0.42	0.08	0.13	0.96
Wave Dir (deg)	42036	162	110.73	93.06	-0.38	N/A	41.80	0.12	N/A	N/A
Wind Spd. (m/s)	42038	20	4.60	4.53	-0.07	0.33	0.33	0.07	0.35	0.86
Wind Dir. (deg)	42038	20	102.41	106.16	3.94	N/A	5.83	0.02	N/A	N/A
Sig Wave Ht (m)	42038	20	0.50	0.22	-0.28	0.30	0.11	0.22	0.00	0.00
Wave Period (s)	42038	20	3.83	3.14	-0.69	0.77	0.34	0.09	0.10	0.17

---



---

## Hindcast Data on Winds, Waves, and Currents in Northern Gulf of Mexico in Hurricanes Katrina and Rita

---



---

Wind Spd. (m/s)	42039	168	8.81	8.87	0.06	0.63	0.63	0.07	0.45	0.99
Wind Dir. (deg)	42039	168	82.98	80.46	-1.02	N/A	7.37	0.02	N/A	N/A
Sig Wave Ht (m)	42039	168	2.13	2.08	-0.04	0.22	0.21	0.10	0.36	0.99
Wave Period (s)	42039	168	5.22	4.95	-0.26	0.44	0.35	0.07	0.27	0.99
Wave Dir (deg)	42039	168	166.72	93.18	-29.98	N/A	53.18	0.15	N/A	N/A
Wind Spd. (m/s)	42040	158	8.34	8.85	0.51	1.13	1.01	0.12	0.66	0.98
Wind Dir. (deg)	42040	158	75.46	74.79	2.03	N/A	11.65	0.03	N/A	N/A
Sig Wave Ht (m)	42040	141	2.67	2.53	-0.13	0.32	0.29	0.11	0.33	1.00
Wave Period (s)	42040	141	5.82	5.18	-0.64	0.91	0.65	0.11	0.04	0.95
Wave Dir (deg)	42040	139	123.76	96.18	-19.88	N/A	44.80	0.12	N/A	N/A
Wind Spd. (m/s)	42055	159	7.18	6.99	-0.19	0.92	0.90	0.12	0.43	0.91
Wind Dir. (deg)	42055	159	48.14	47.57	-2.26	N/A	5.01	0.01	N/A	N/A
Sig Wave Ht (m)	42055	159	1.67	1.84	0.17	0.47	0.44	0.26	0.55	0.97
Wave Period (s)	42055	159	5.85	5.23	-0.61	1.11	0.93	0.16	0.11	0.87
Wave Dir (deg)	42055	157	62.41	42.94	-19.27	N/A	11.03	0.03	N/A	N/A
Wind Spd. (m/s)	DPIA1	168	7.50	8.14	0.64	1.74	1.62	0.22	0.61	0.93
Wind Dir. (deg)	DPIA1	168	76.34	71.23	7.52	N/A	47.48	0.13	N/A	N/A
Wind Spd. (m/s)	FWYF1	168	9.47	9.14	-0.33	1.16	1.12	0.12	0.37	0.95
Wind Dir. (deg)	FWYF1	168	85.94	85.66	-0.25	N/A	9.48	0.03	N/A	N/A
Wind Spd. (m/s)	KTNF1	168	3.99	7.24	3.25	3.94	2.22	0.56	0.89	0.57
Wind Dir. (deg)	KTNF1	168	70.83	73.46	10.73	N/A	47.83	0.13	N/A	N/A
Wind Spd. (m/s)	MLRF1	168	9.91	9.67	-0.24	1.04	1.01	0.10	0.39	0.96
Wind Dir. (deg)	MLRF1	168	93.58	87.25	-6.35	N/A	9.42	0.03	N/A	N/A
Wind Spd. (m/s)	SANF1	70	10.05	10.61	0.56	1.02	0.85	0.08	0.71	0.99
Wind Dir. (deg)	SANF1	70	48.97	44.34	-4.51	N/A	11.08	0.03	N/A	N/A
Wind Spd. (m/s)	SGOF1	167	7.73	8.00	0.27	1.05	1.01	0.13	0.59	0.95
Wind Dir. (deg)	SGOF1	167	79.42	71.35	3.41	N/A	35.60	0.10	N/A	N/A
Wind Spd. (m/s)	SMKF1	168	10.10	9.93	-0.17	1.20	1.19	0.12	0.40	0.96
Wind Dir. (deg)	SMKF1	168	96.78	88.13	-8.73	N/A	13.79	0.04	N/A	N/A
Wind Spd. (m/s)	SRST2	168	7.58	8.55	0.97	2.41	2.21	0.29	0.60	0.96
Wind Dir. (deg)	SRST2	168	181.03	67.83	-17.17	N/A	41.92	0.12	N/A	N/A
Wind Spd. (m/s)	VENF1	168	4.71	8.85	4.14	4.65	2.13	0.45	0.99	0.70

---

## Hindcast Data on Winds, Waves, and Currents in Northern Gulf of Mexico in Hurricanes Katrina and Rita

---

Wind Dir. (deg)	VENF1	168	77.80	82.62	1.97	N/A	29.05	0.08	N/A	N/A
Wind Spd. (m/s)	Combined	2922	7.95	8.60	0.64	1.90	1.78	0.22	0.59	0.93
Wind Dir. (deg)	Combined	2922	77.93	74.38	-0.96	N/A	23.44	0.07	N/A	N/A
Sig Wave Ht (m)	Combined	1462	1.99	1.95	-0.04	0.45	0.45	0.22	0.34	0.97
Wave Period (s)	Combined	1462	5.58	4.94	-0.64	1.01	0.78	0.14	0.13	0.91
Wave Dir (deg)	Combined	1434	103.98	85.87	-19.73	N/A	35.00	0.10	N/A	N/A

**Table 4 NOS water level locations**

Storm	Station	ID	Latitude	Longitude
2005_12	Pascagoula River (NOAA)	PASM6	30.3669	-88.5633
	Petit Bois Island	BAY01	30.2144	-88.5056
	Biloxi, MS	8744117	30.4117	-88.9033
	Grand Isle, LA	8761724	29.2633	-89.9567
	Horn Island, MS	8742221	30.2383	-88.6667
	Waveland, MS	8747766	30.2817	-89.3667
2005_18	Galveston Bay Entrance, TX	8771341	29.3583	-94.7250
	Freeport, TX	8772440	28.9483	-95.3083
	Calcasieu Pass, LA	8768094	29.7650	-93.3433
	Galveston Pleasure Pier, TX	8771510	29.3100	-94.7933

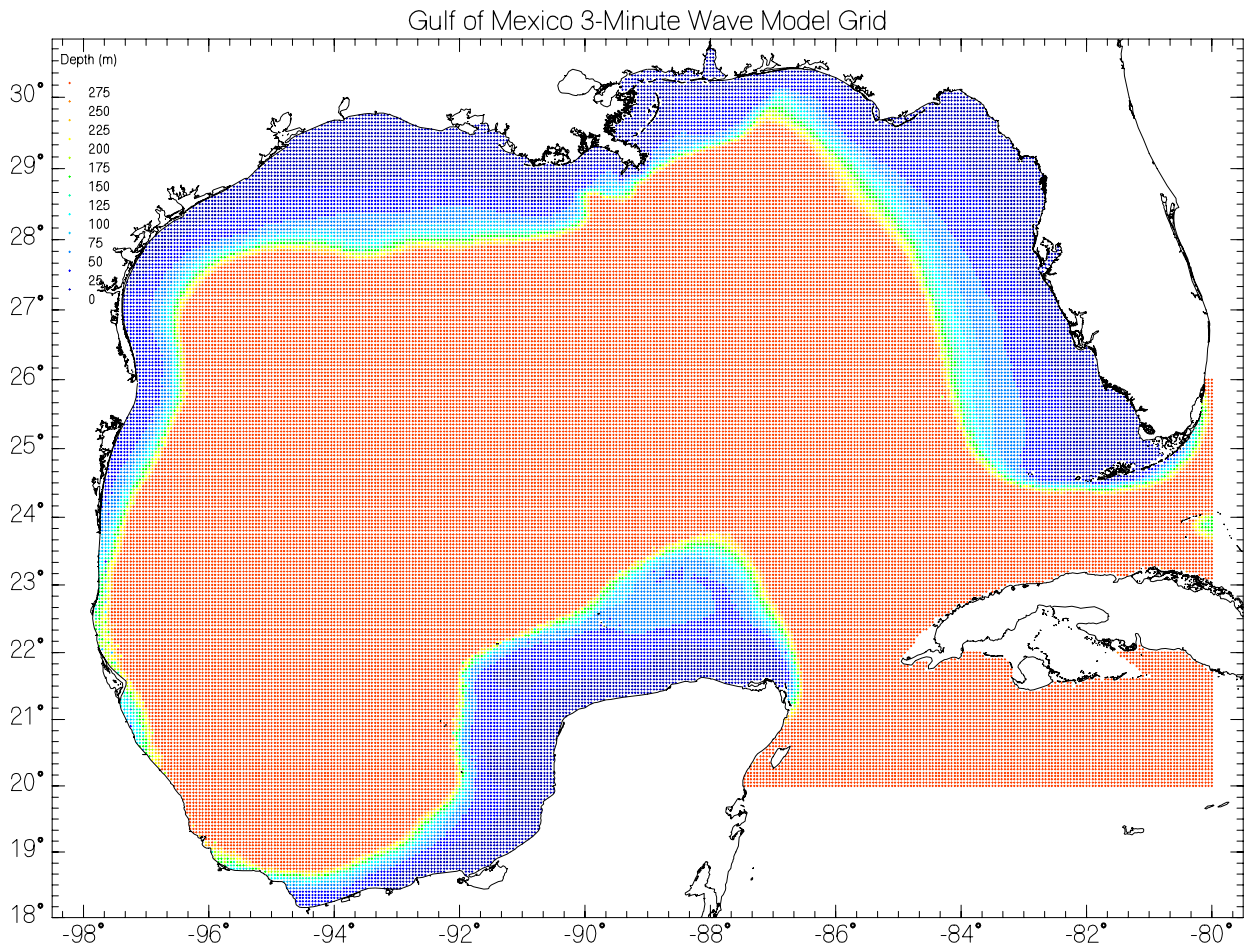


**Figure 1a** Wave model basin grid



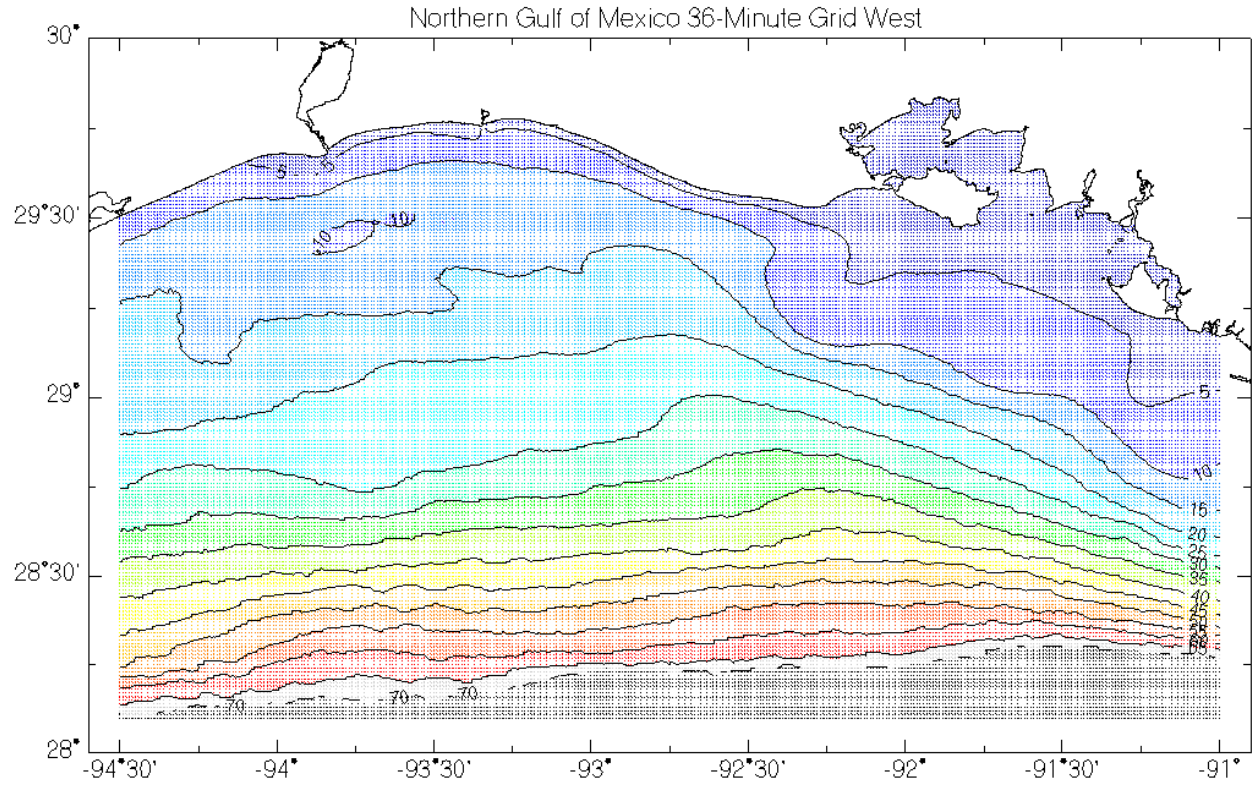


**Figure 1c Wave model fine mesh optimized for Rita**

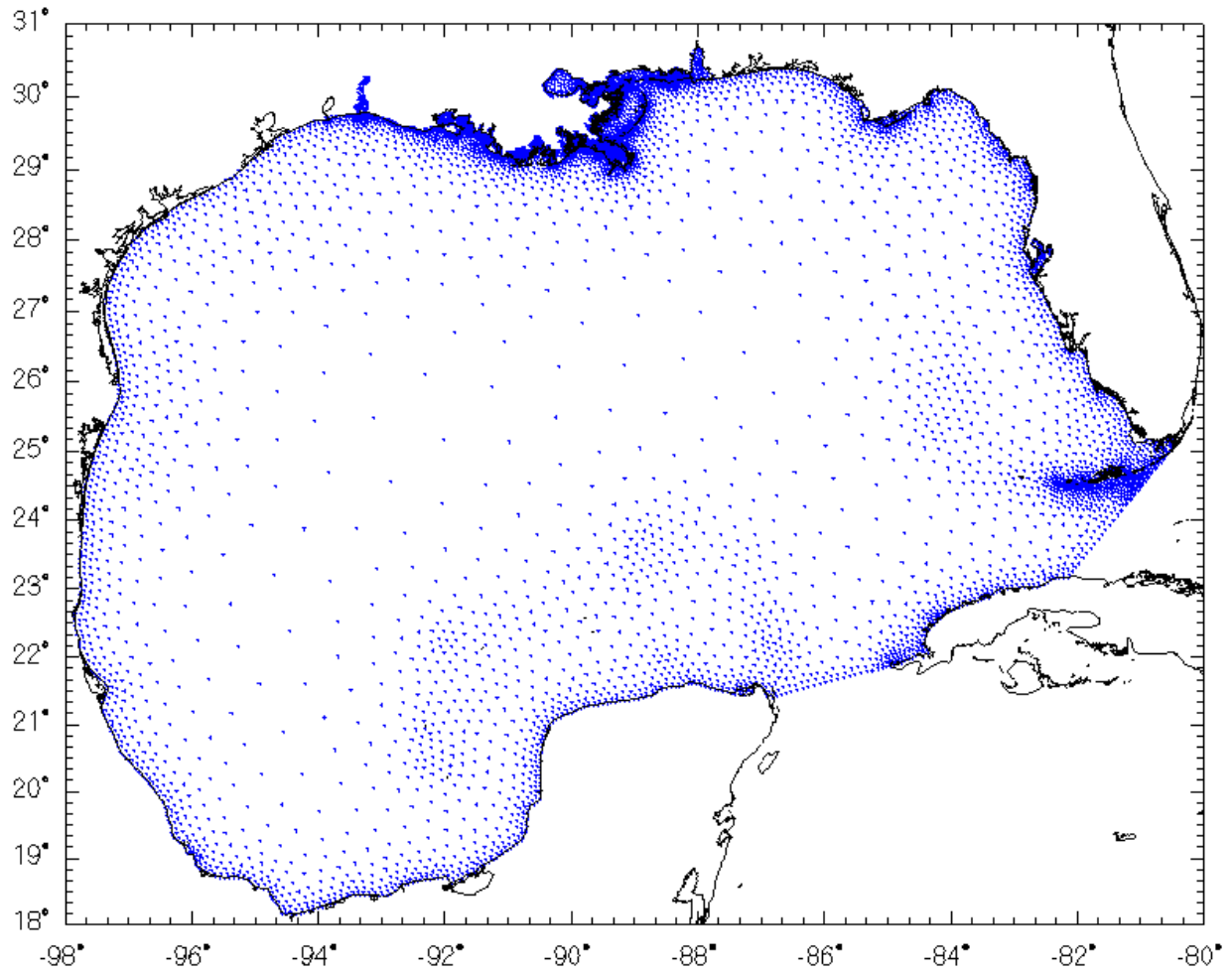


**Figure 2 ADCIRC grid**

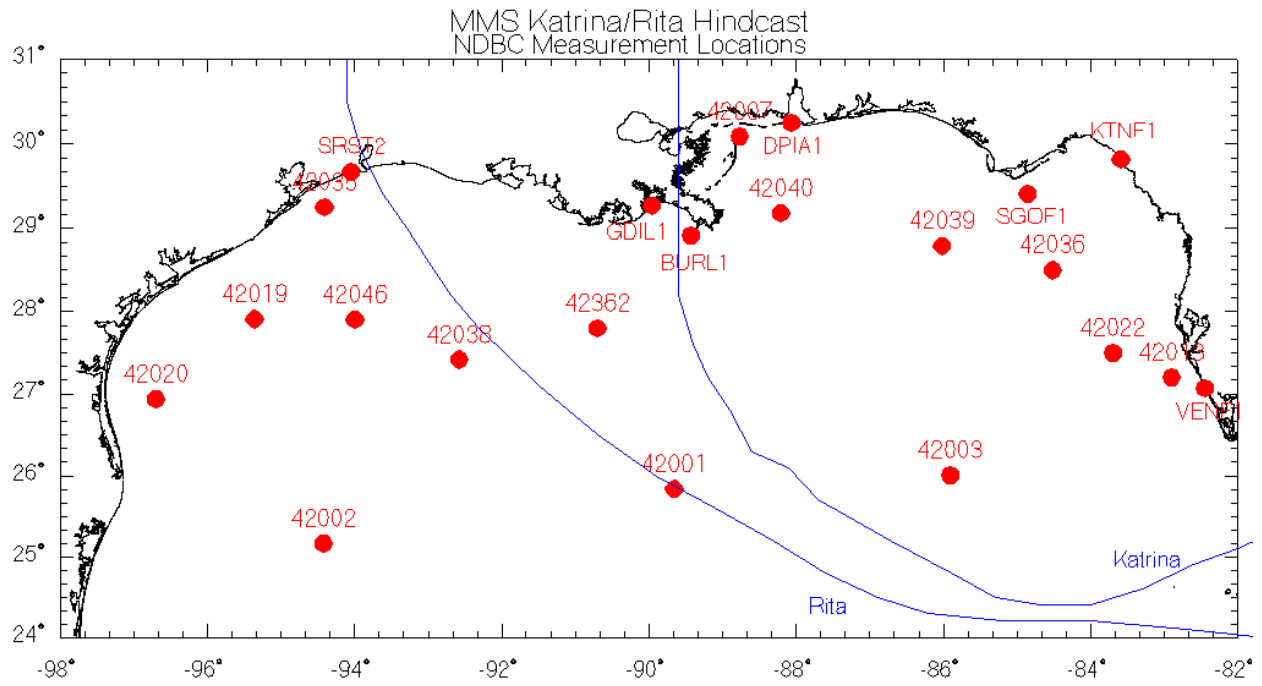
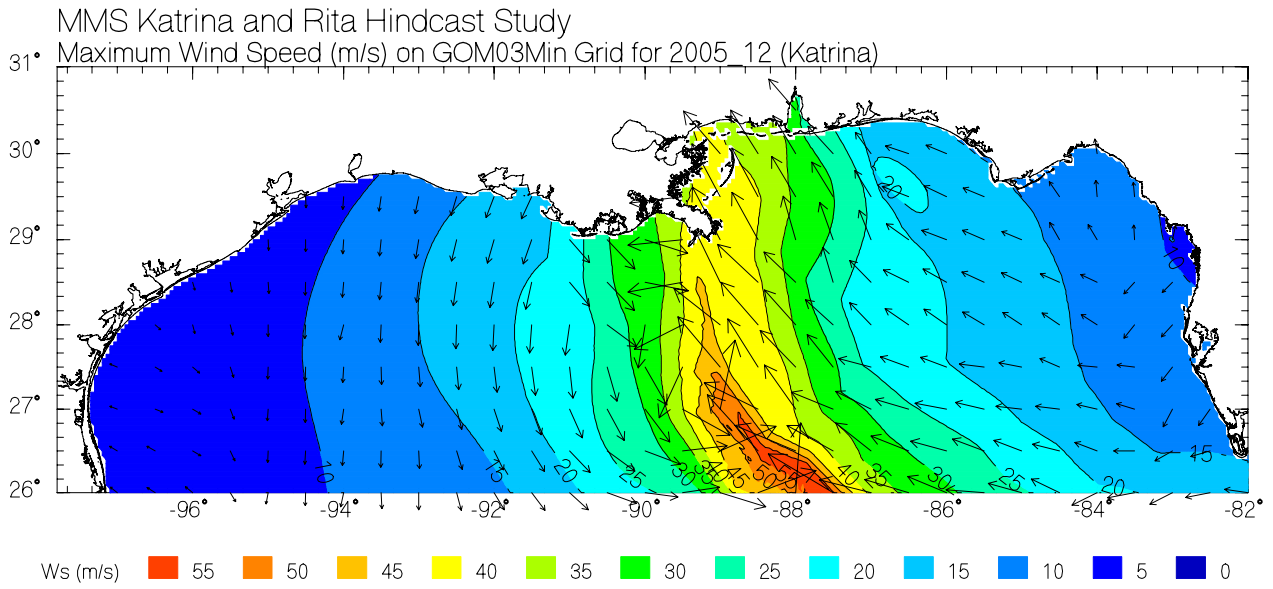
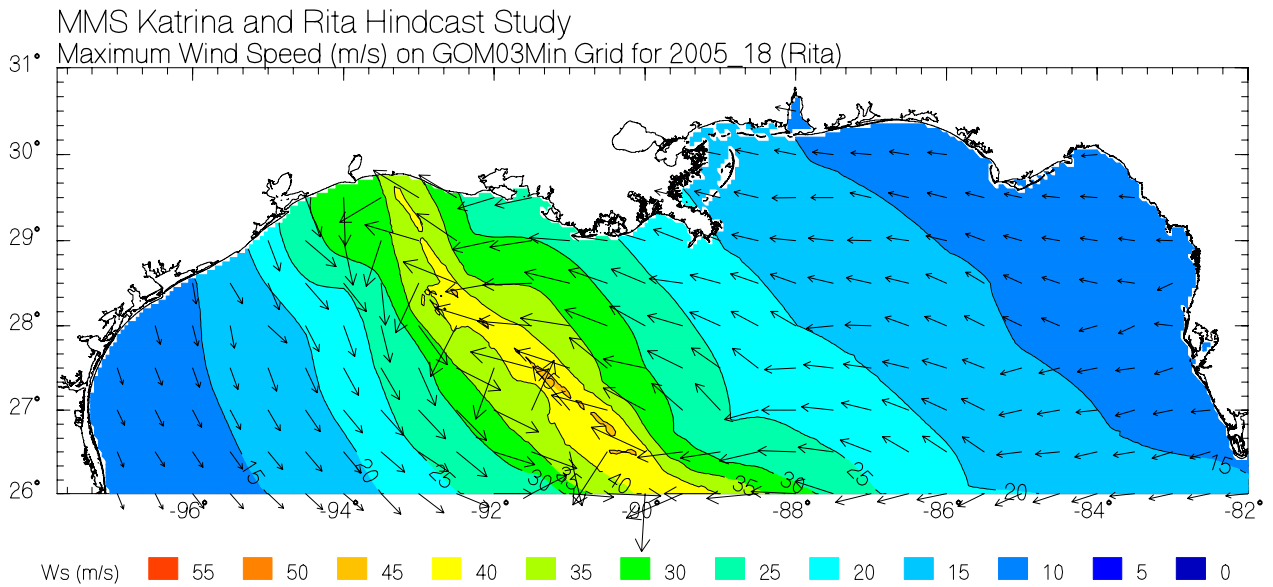


Figure 3 Tracks of Hurricane Katrina and Rita within the GOM with NDBC buoys shown



**Figure 4 Maximum wind speed (m/s, 10-meter, 30-minute) for Katrina**



**Figure 5 Maximum wind speed (m/s, 10-meter, 30-minute) for Rita**

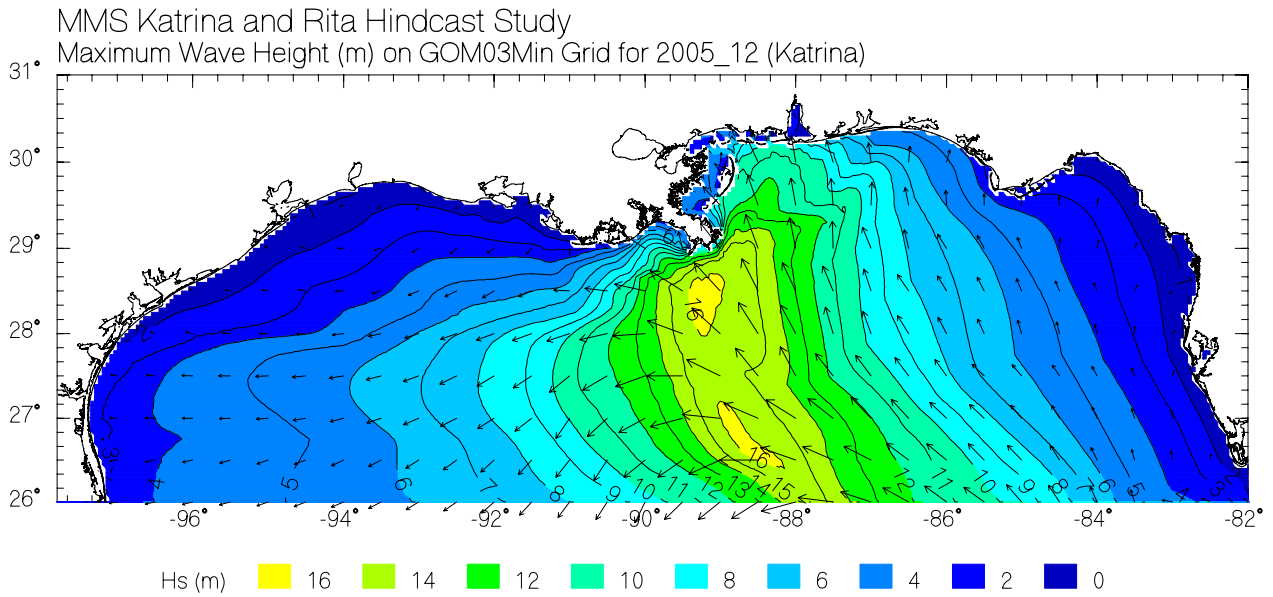


**Figure 6 Maximum hindcast significant wave height (m) for Katrina on basin grid**

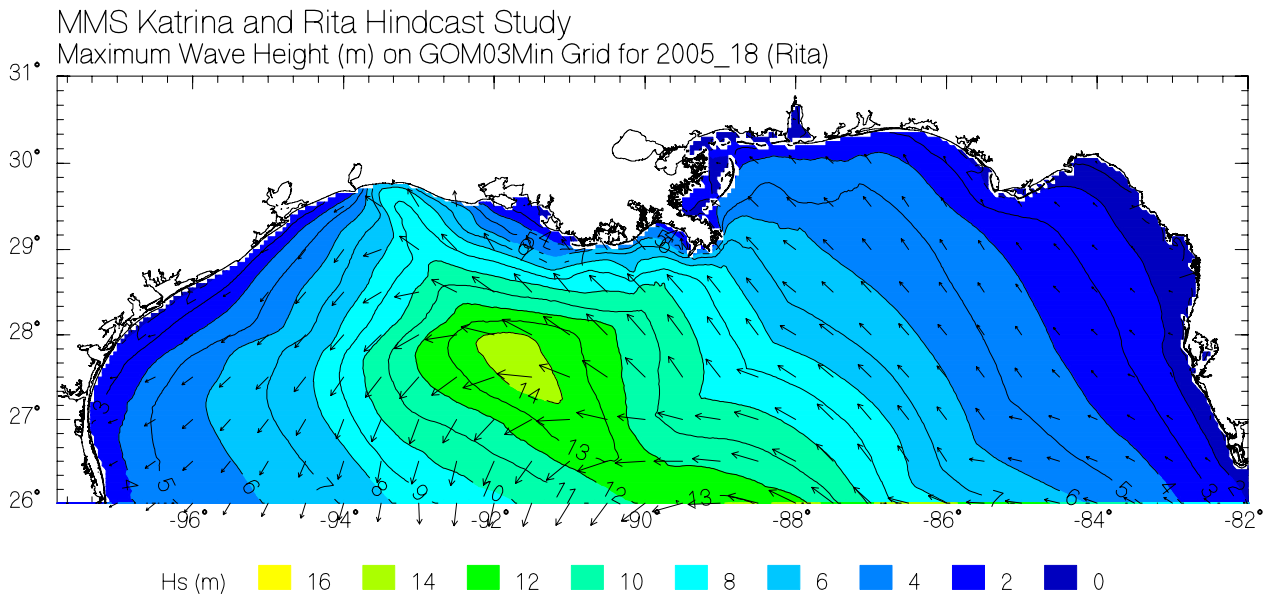


**Figure 7 Maximum hindcast significant wave height (m) for Rita on basin grid**

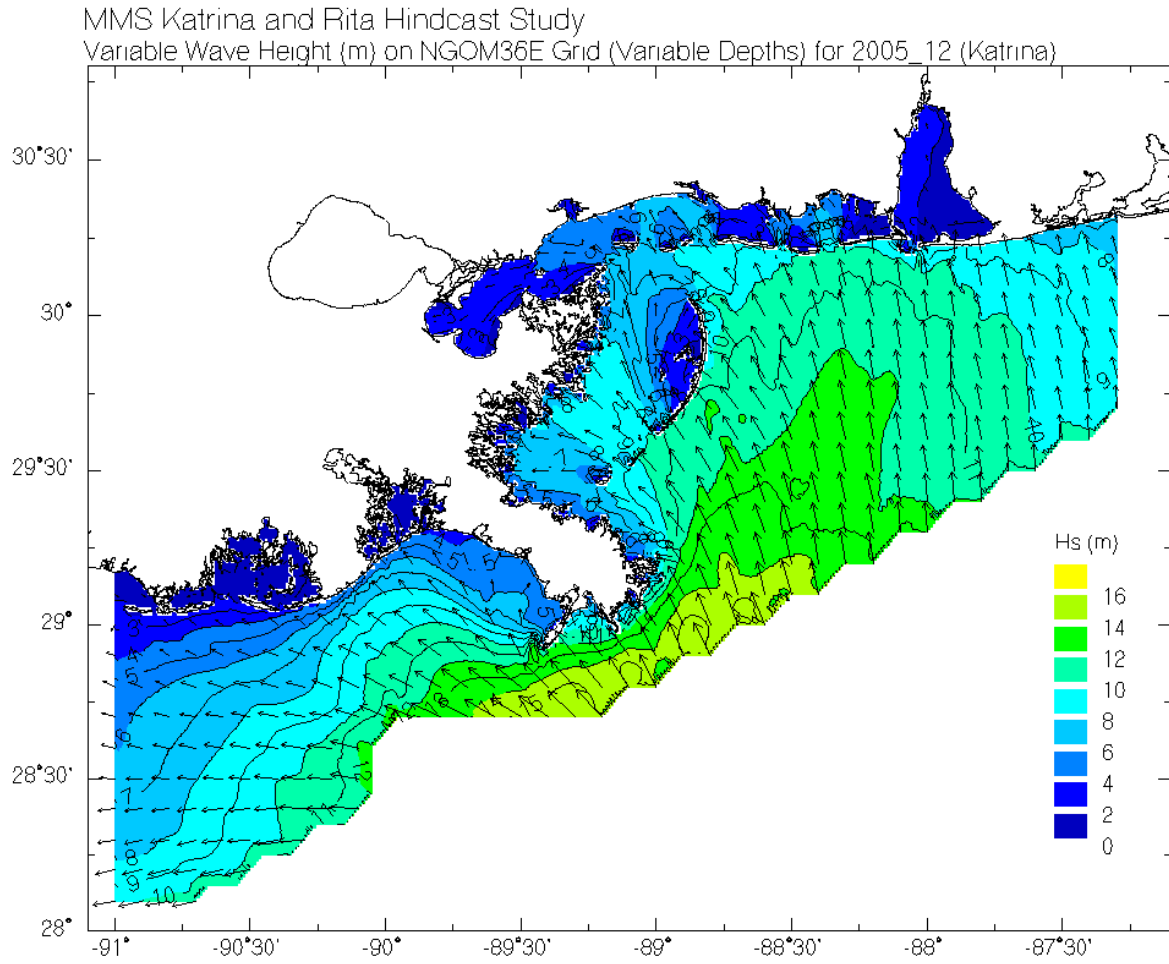


**Figure 8 Maximum hindcast significant wave height (m) for Katrina on fine grid**

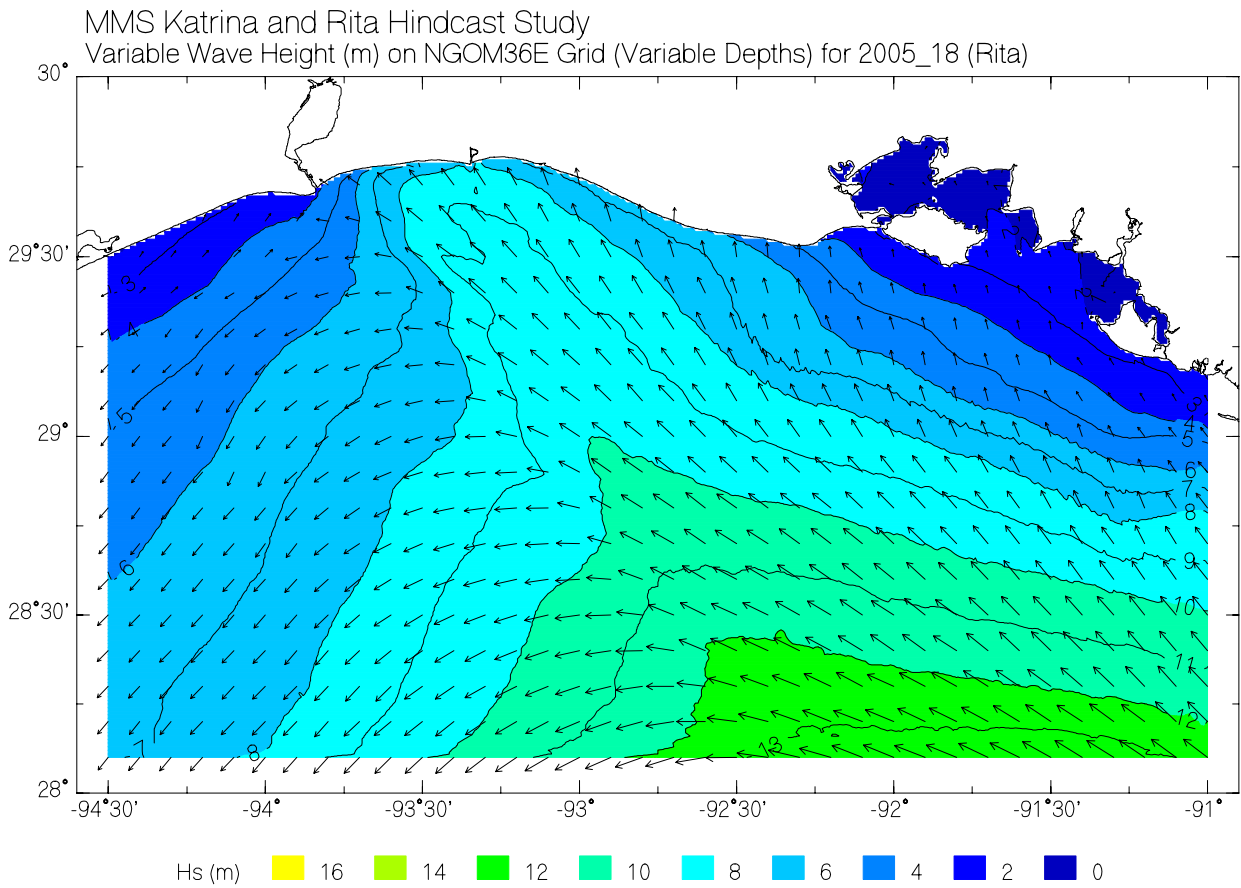


**Figure 9 Maximum hindcast significant wave height (m) for Rita on fine grid**

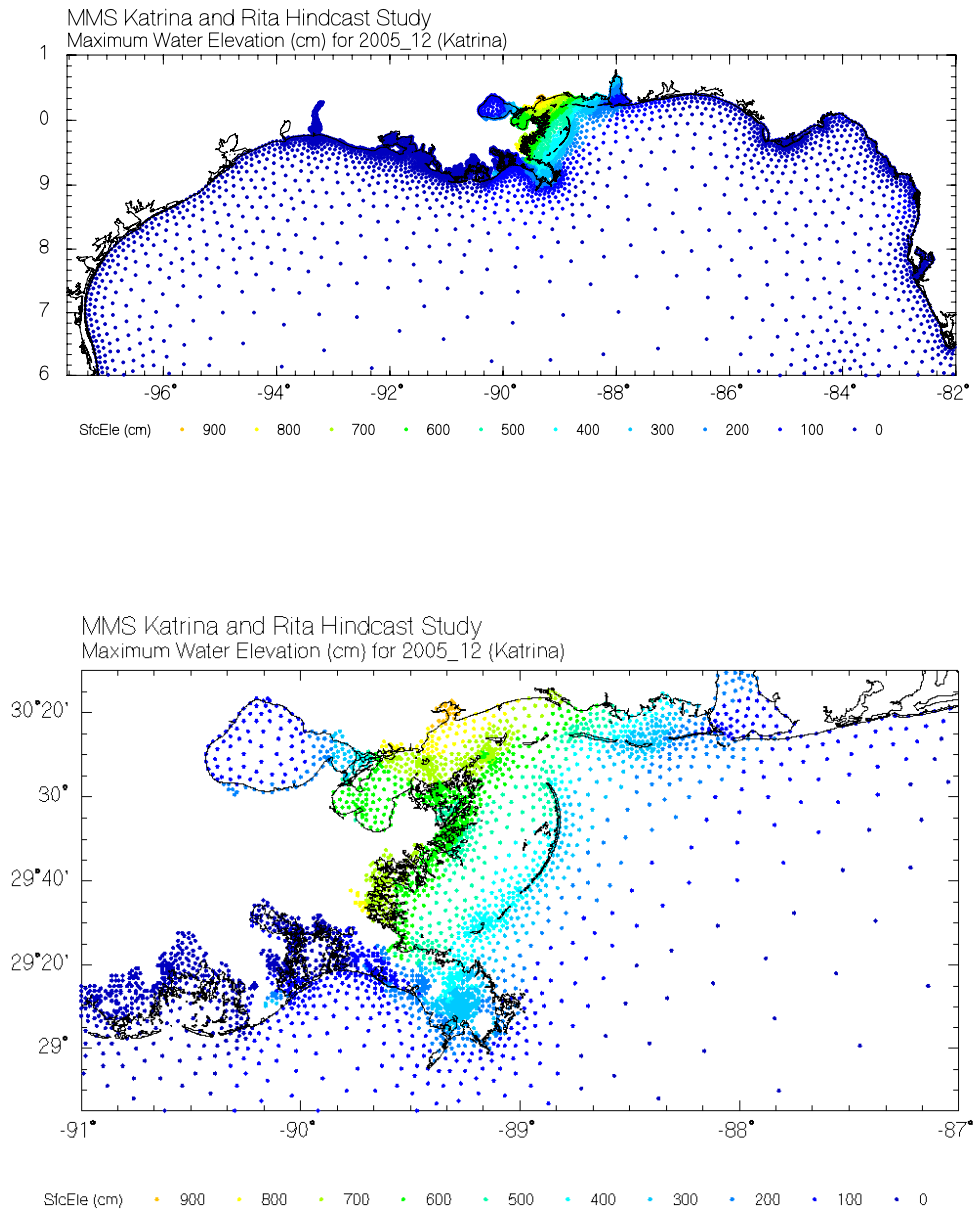


**Figure 10 Maximum water elevation (NGOM, top, landfall region, bottom) for Katrina**

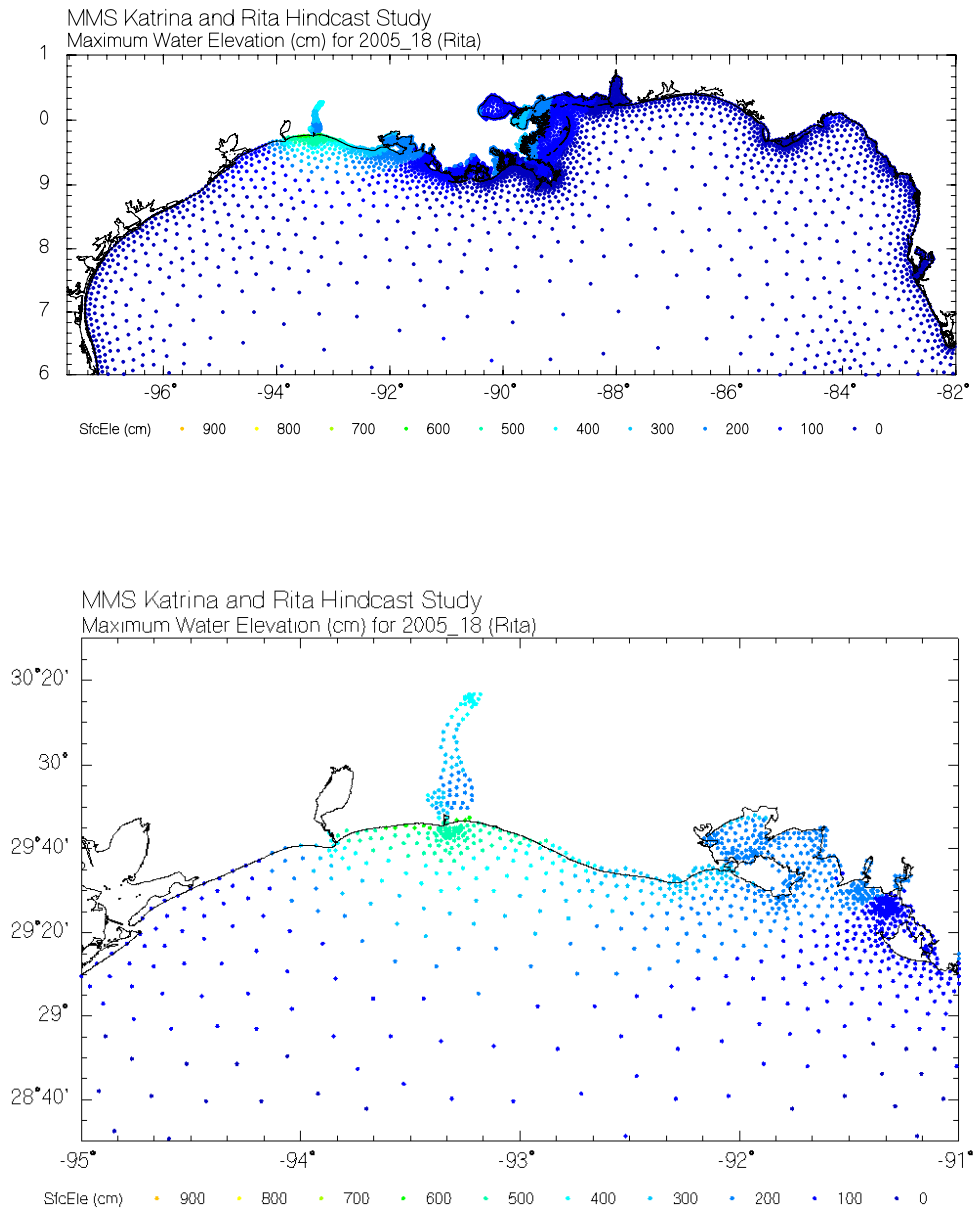
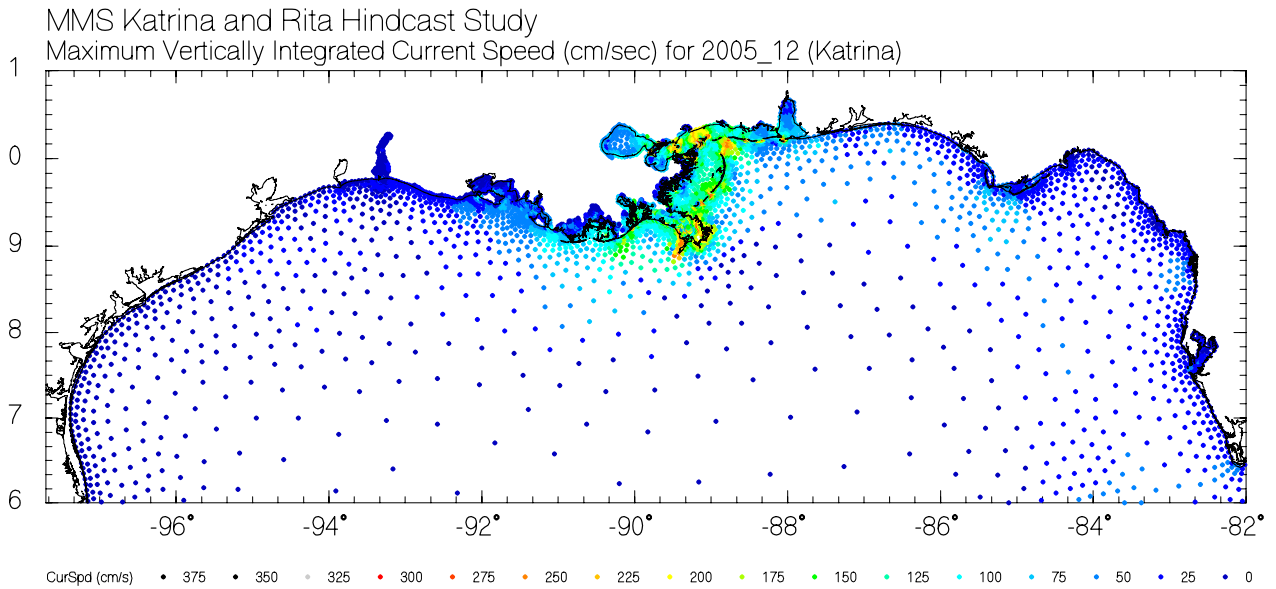
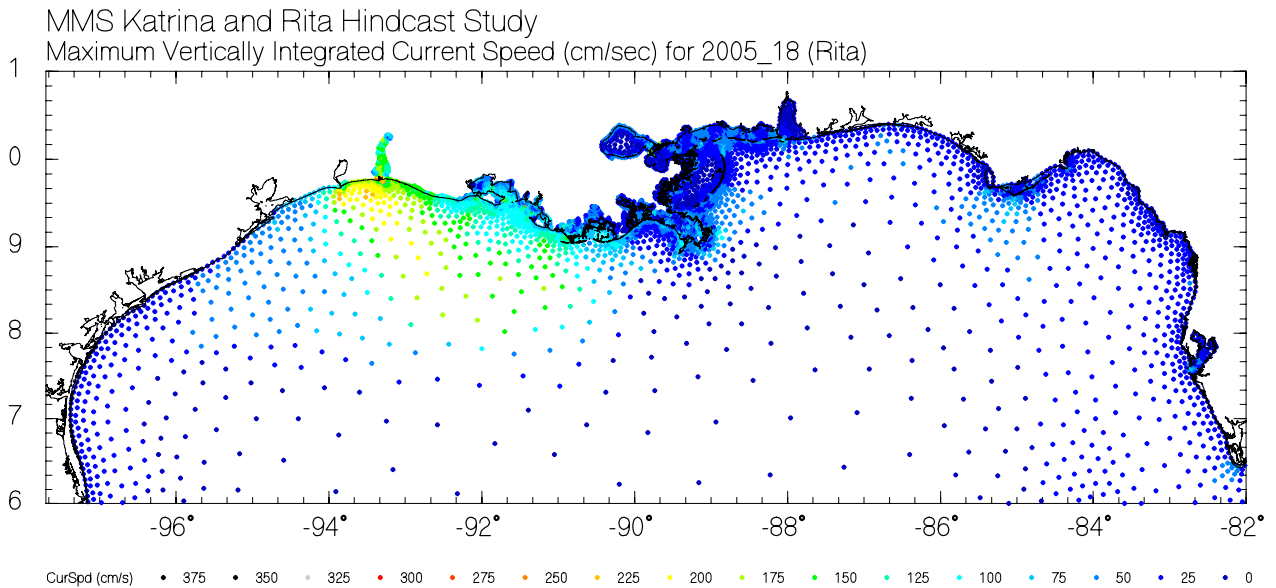


Figure 11 Maximum water elevation (NGOM, top, landfall region, bottom) for Rita



**Figure 12 Maximum 2-D vertically integrated currents (cm/s) for Katrina**



**Figure 13 Maximum 2-D vertically integrated currents (cm/s) for Rita**

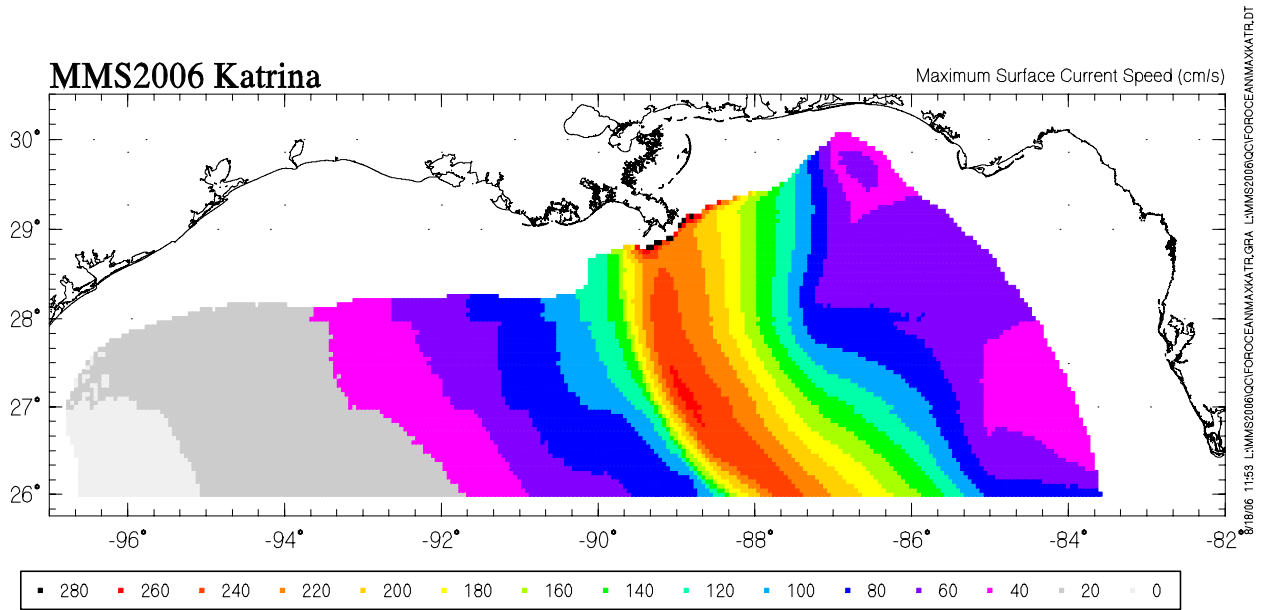


Figure 14 Maximum hindcast surface current speed (cm/s) for Katrina

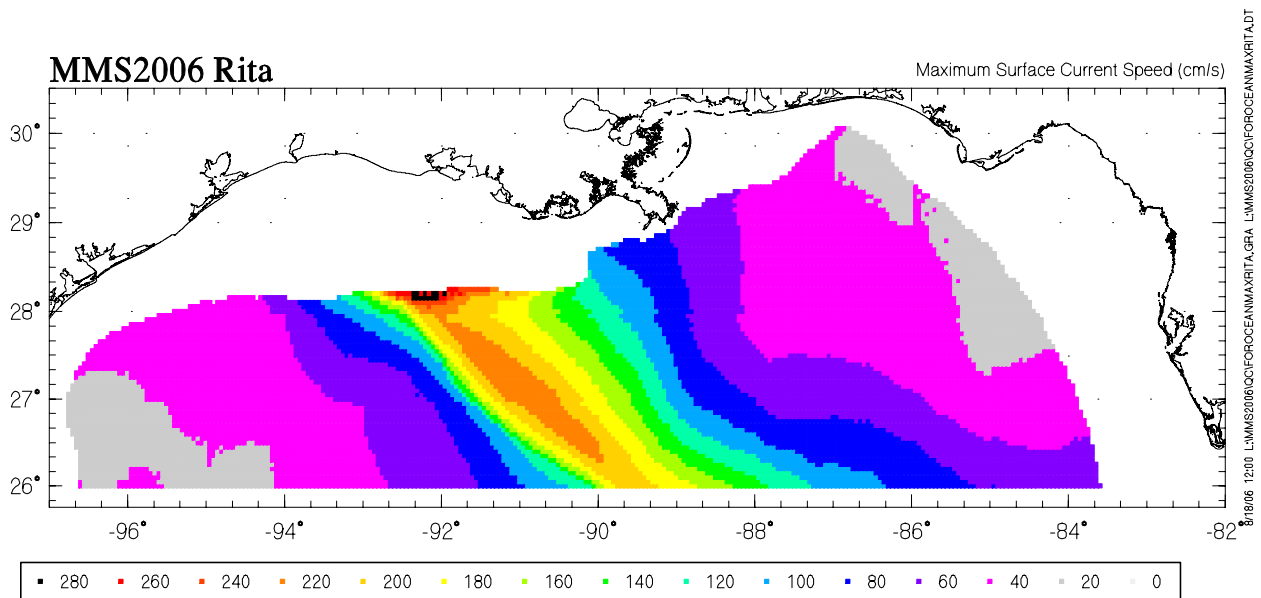
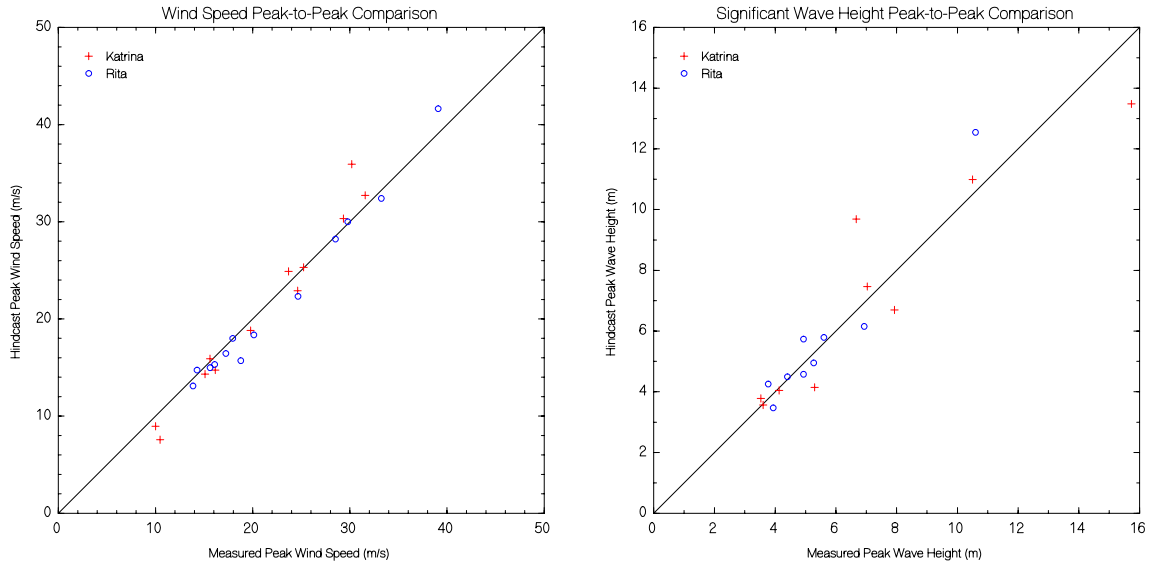


Figure 15 Maximum hindcast surface current speed (cm/s) for Rita



Variable	Avg Meas	Avg Hind	Diff (H-M)	Scatter Index
Wind Speed	21.6	21.3	-.29	8%
Wave Height	6.38	6.43	0.06	18%

Figure 16 Comparison of peak wind and waves during Katrina and Rita

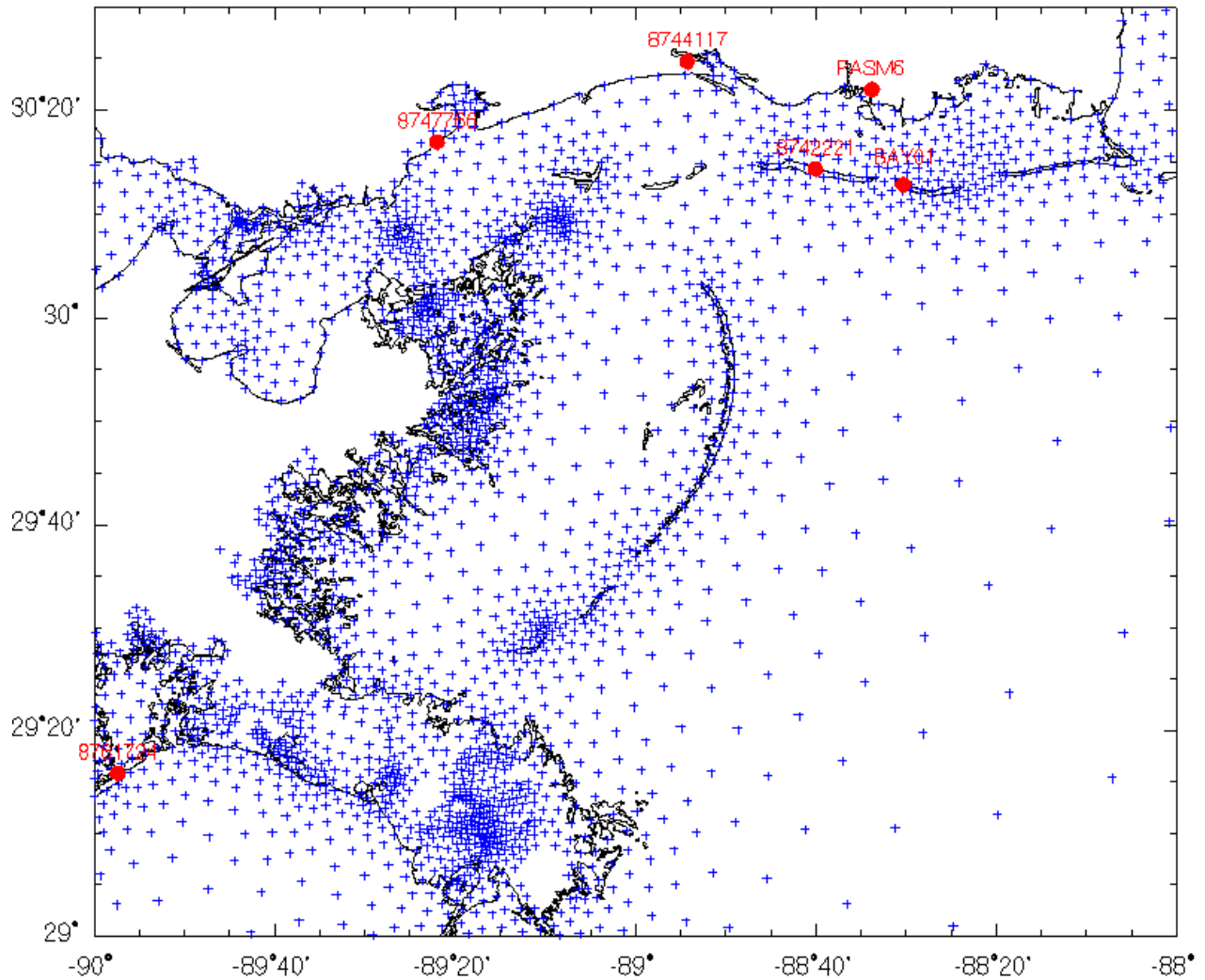


Figure 16 NOS verification sites in Katrina

# Hindcast Data on Winds, Waves, and Currents in Northern Gulf of Mexico in Hurricanes Katrina and Rita

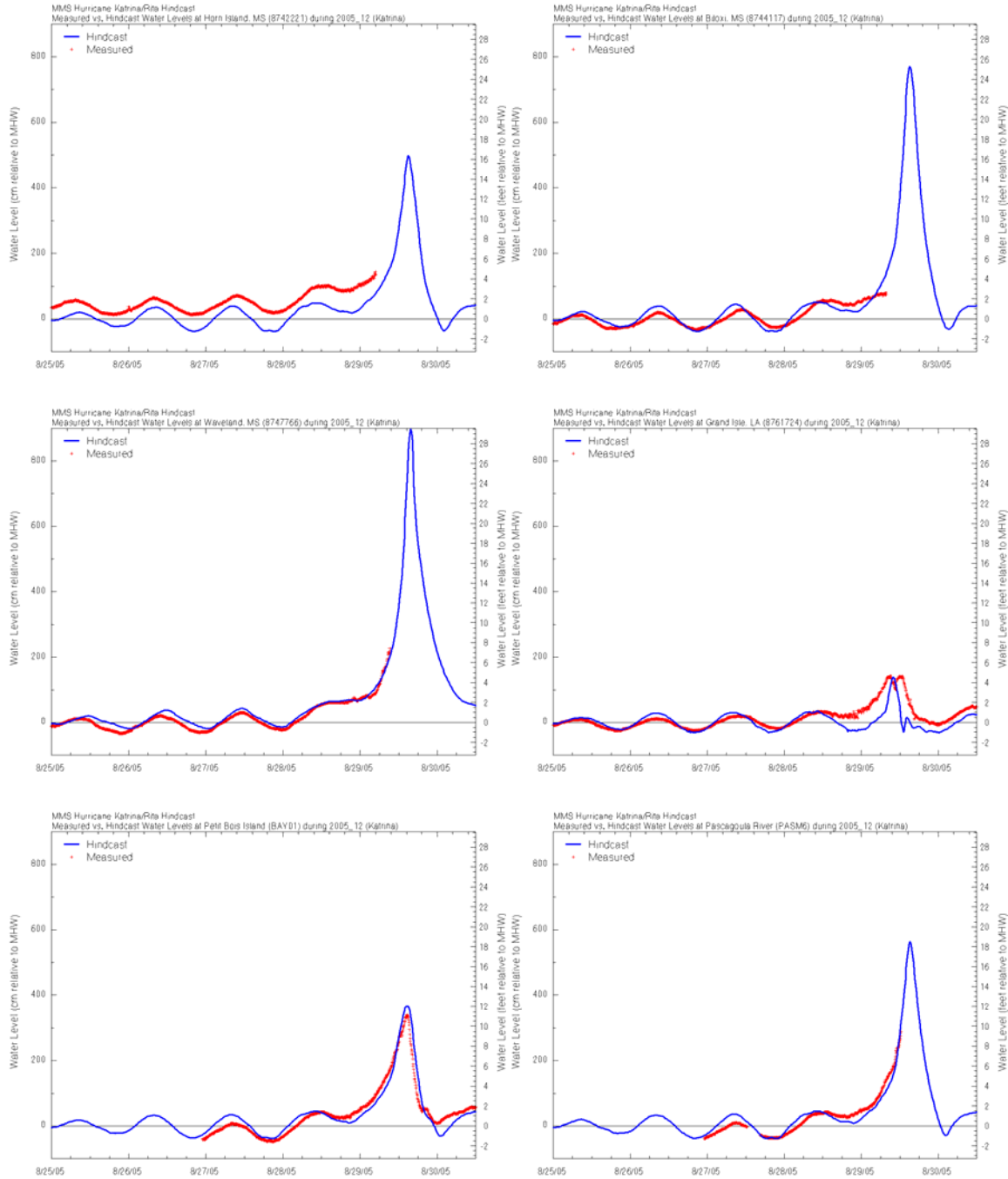


Figure 17 Predicted vs. measured water levels during Katrina

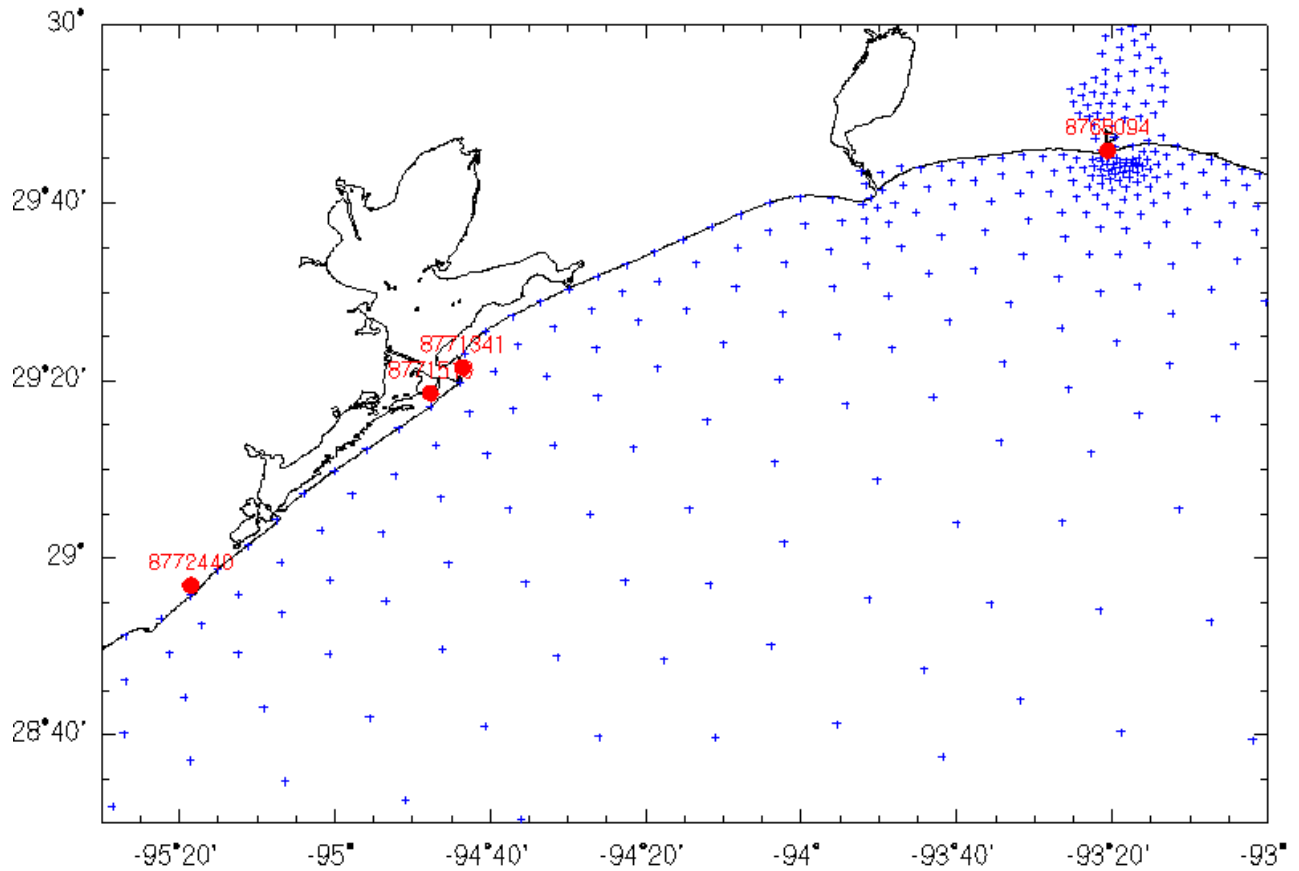
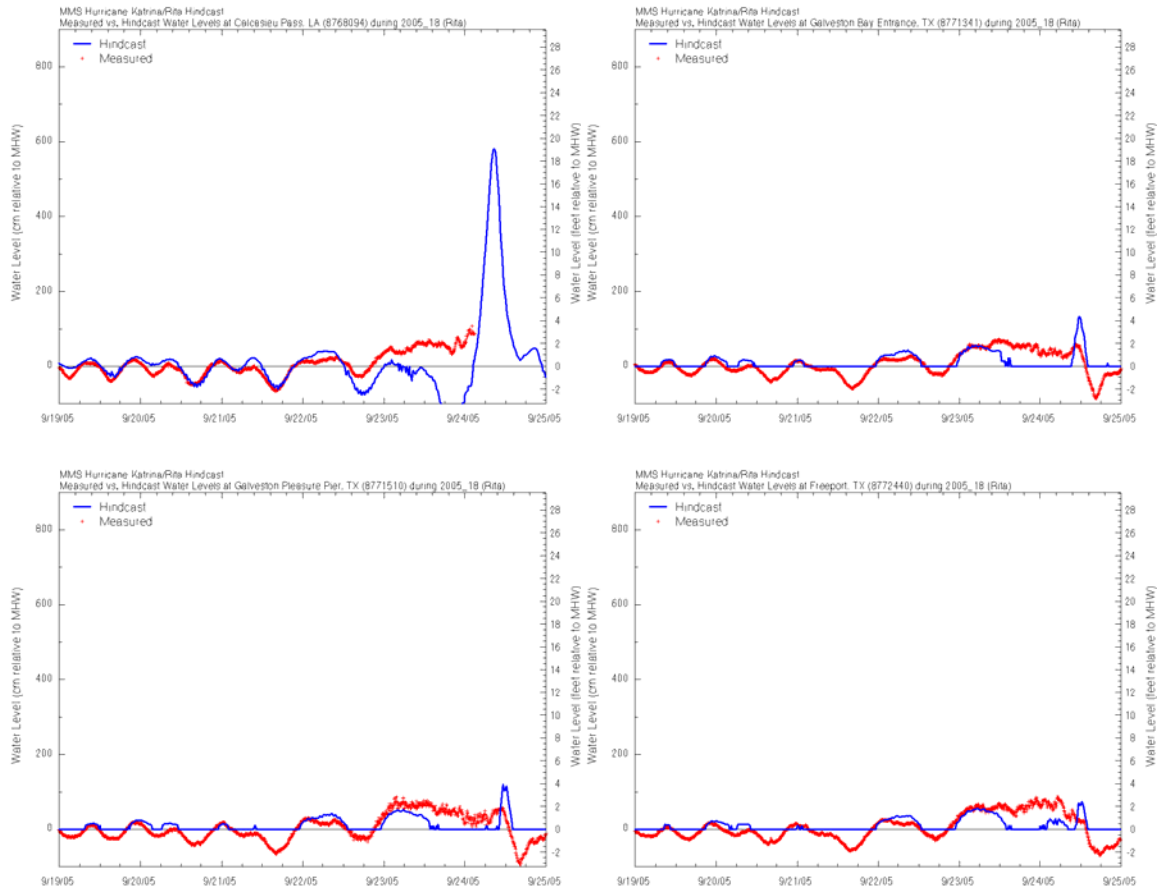


Figure 18 NOS verification sites during Rita

---

## Hindcast Data on Winds, Waves, and Currents in Northern Gulf of Mexico in Hurricanes Katrina and Rita

---



**Figure 19 Predicted vs. measured water levels during Rita**

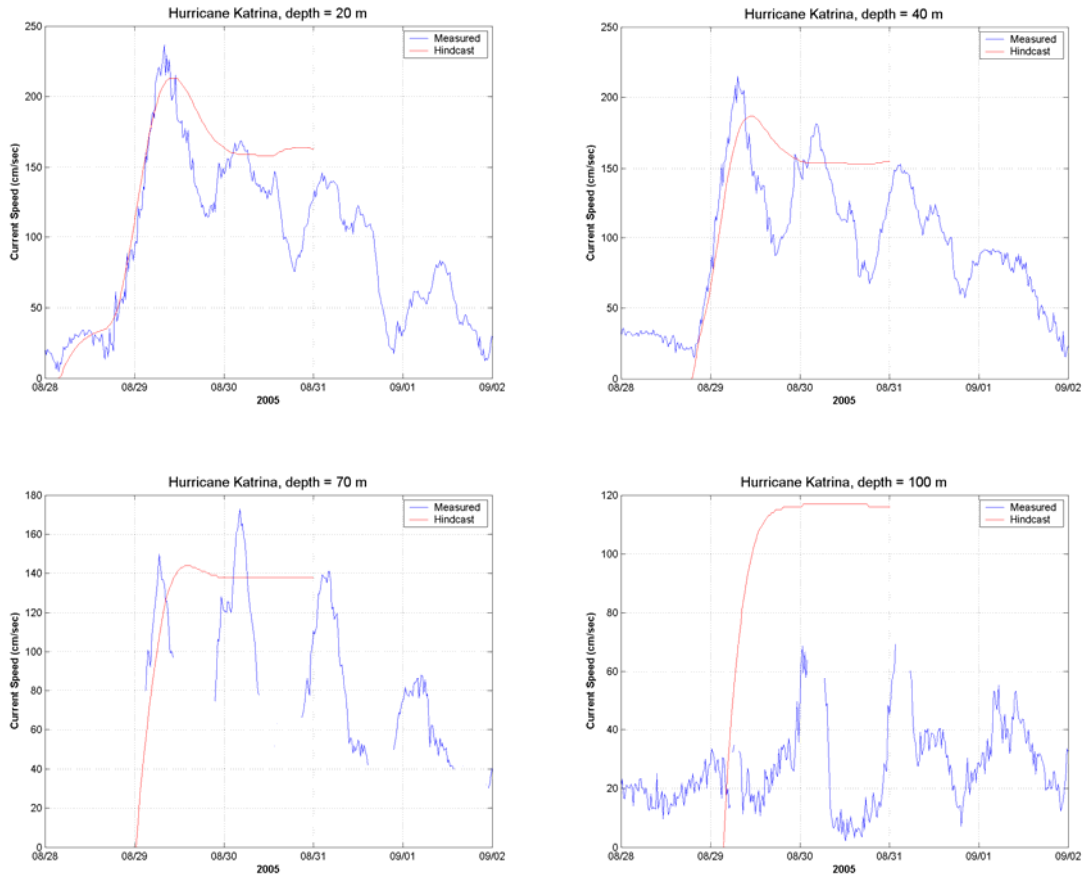


**Figure 20 Comparison of 1-D currents at ADCP at 4 depths**

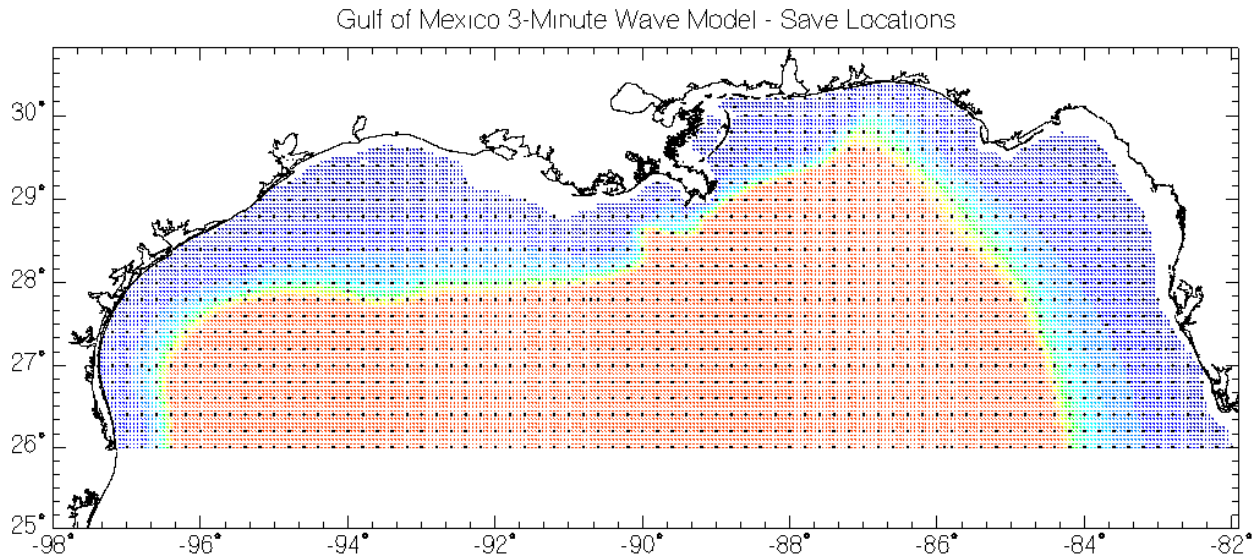


**Figure 21** Archive save locations for basin grid (spectra shown in black)

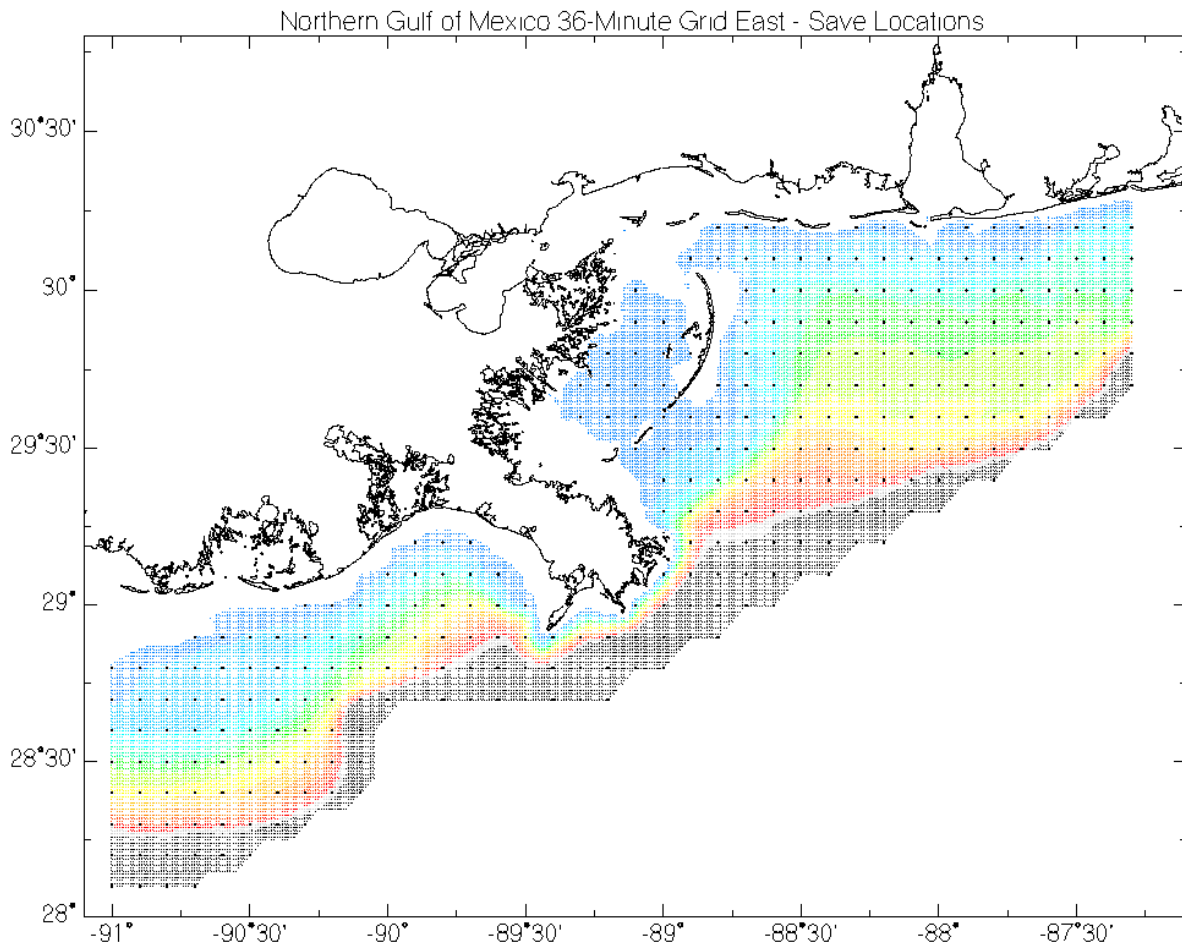


**Figure 22 Archive save locations for Katrina fine grid (spectra shown in black)**

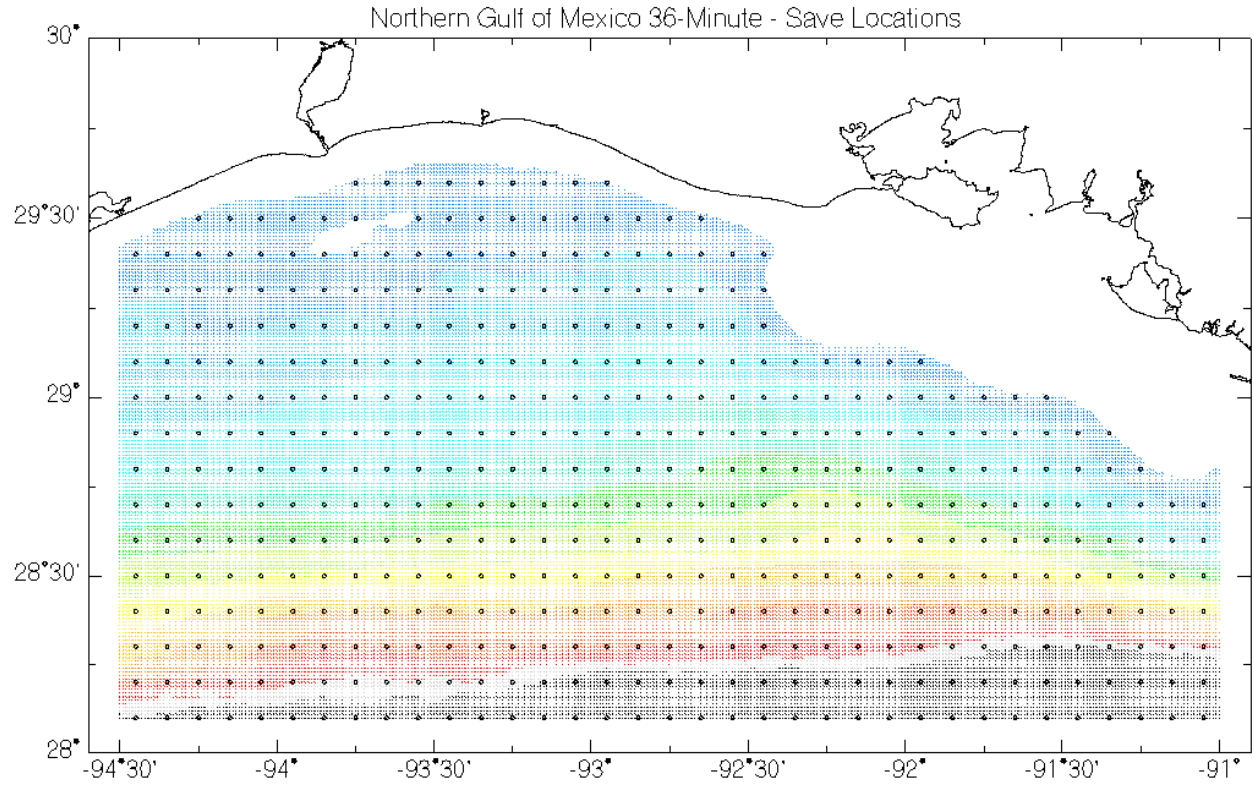


**Figure 23 Archive save locations for Rita fine grid (spectra shown in black)**

## **APPENDIX A Storm Tracks**

## Hurricane Katrina (2005\_12) Track

CYM	DHM	Latitude	Longitude	SLP (mb)
200508	231800	23.1	-75.1	1008
200508	240000	23.4	-75.7	1007
200508	240600	23.8	-76.2	1007
200508	241200	24.5	-76.5	1006
200508	241800	25.4	-76.9	1003
200508	250000	26	-77.7	1001
200508	250600	26.1	-78.4	1000
200508	251200	26.2	-79	992
200508	251800	26.2	-79.6	984
200508	260000	25.9	-80.3	985
200508	260600	25.4	-81.3	990
200508	261200	25.1	-82	980
200508	261800	24.9	-82.6	969
200508	270000	24.6	-83.3	965
200508	270600	24.4	-84	950
200508	271200	24.4	-84.7	949
200508	271800	24.5	-85.3	952
200508	280000	24.8	-85.9	942
200508	280600	25.2	-86.7	934
200508	281200	25.7	-87.7	910
200508	281500	26.1	-88.1	902
200508	281800	26.3	-88.6	902
200508	282100	26.8	-88.9	903
200508	290000	27.2	-89.2	904
200508	290300	27.6	-89.4	908
200508	290600	28.2	-89.6	910
200508	290900	28.8	-89.6	916
200508	291200	29.5	-89.6	922
200508	291500	30.2	-89.6	930
200508	291800	31.1	-89.6	955
200508	300000	32.6	-89.1	965
200508	300600	34.1	-88.6	978
200508	301200	35.6	-88	985

---

200508	301800	37	-87	990
200508	310000	38.6	-85.3	994
200508	310600	40.1	-82.9	996

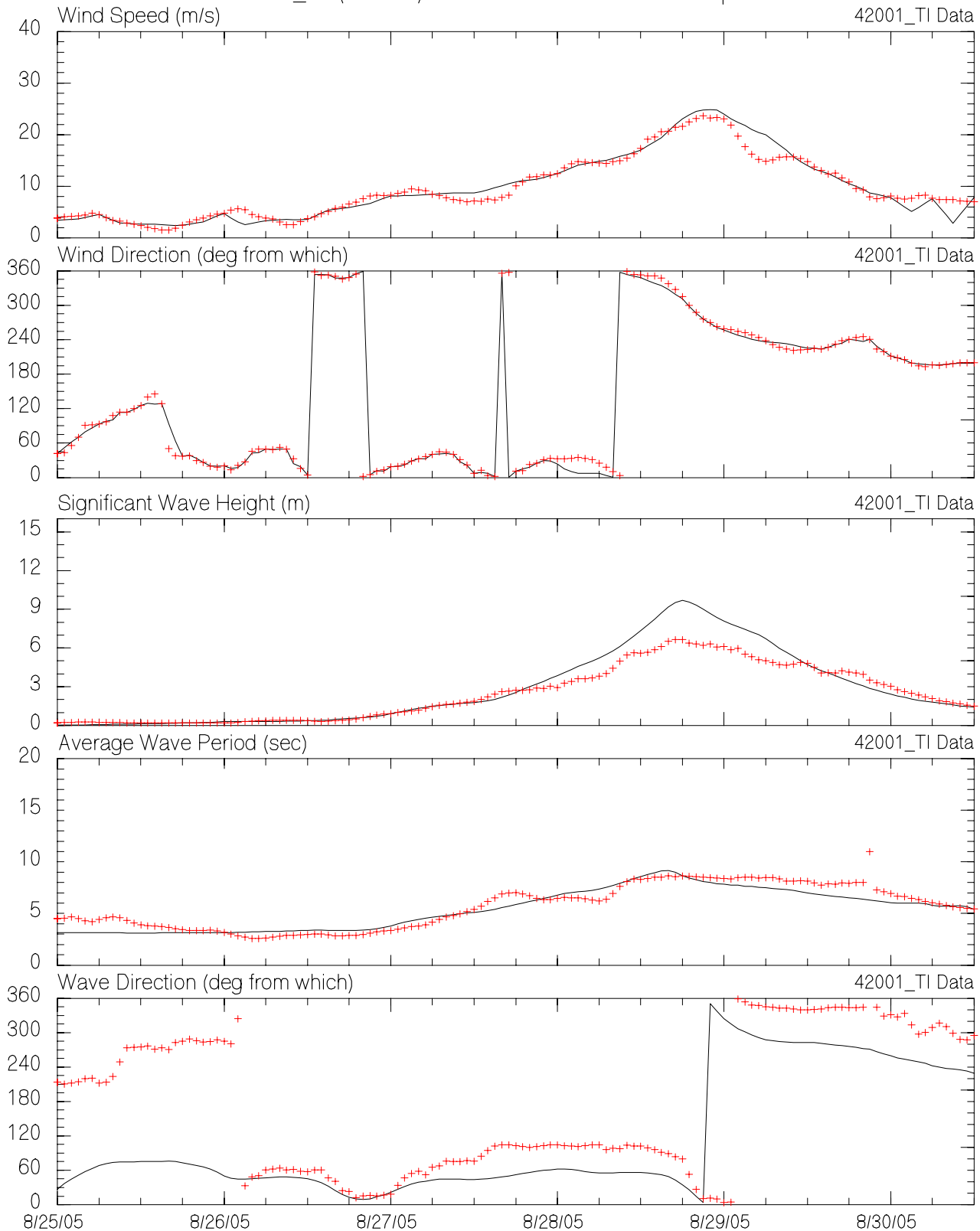
---

## Hurricane Rita (2005\_18) Track

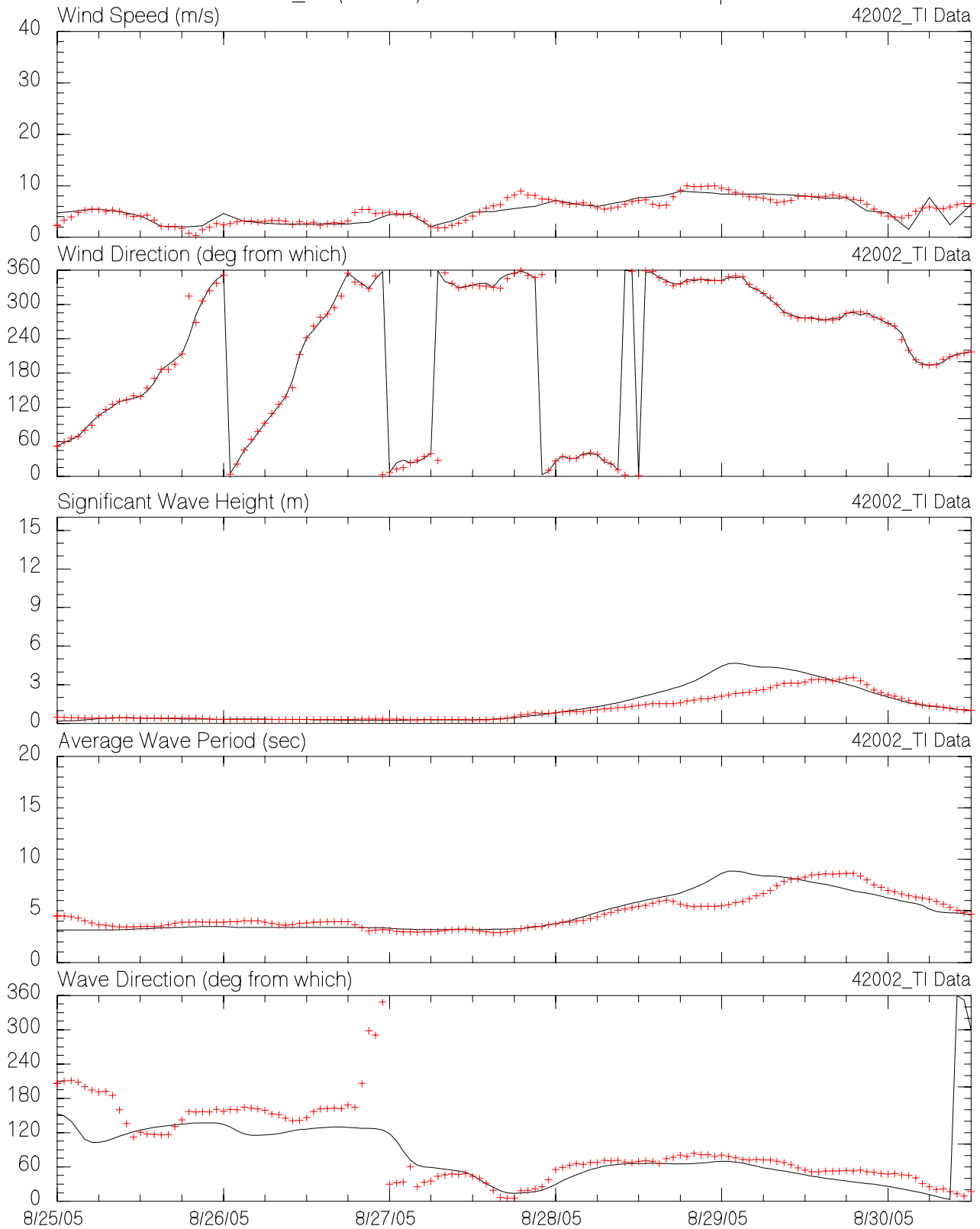
CYM	DHM	Latitude	Longitude	SLP (mb)
200509	180000	21.3	-69.9	1009
200509	180600	21.6	-70.7	1009
200509	181200	21.9	-71.5	1008
200509	181800	22.2	-72.3	1006
200509	190000	22.4	-73	1002
200509	190600	22.6	-73.8	999
200509	191200	22.8	-74.7	997
200509	191800	23.1	-75.9	993
200509	200000	23.3	-77.2	993
200509	200600	23.5	-78.8	991
200509	201200	23.7	-80.3	985
200509	201800	23.9	-81.6	976
200509	210000	24.1	-82.7	967
200509	210600	24.2	-84	960
200509	211200	24.2	-85.2	948
200509	211800	24.3	-86.2	920
200509	220000	24.5	-86.9	898
200509	220600	24.8	-87.6	898
200509	221200	25.2	-88.3	907
200509	221800	25.6	-89.1	914
200509	230000	26	-89.9	914
200509	230600	26.5	-90.7	924
200509	231200	27.1	-91.5	928
200509	231800	27.8	-92.3	930
200509	232100	28.2	-92.7	930
200509	240000	28.6	-93	930
200509	240300	29	-93.3	932
200509	240600	29.4	-93.6	937
200509	240900	29.9	-93.9	950
200509	241200	30.5	-94.1	960
200509	241800	31.6	-94.1	975
200509	250000	32.5	-94	983

## **APPENDIX B Hindcast Timeseries at NDBC Buoys/CMAN Stations**

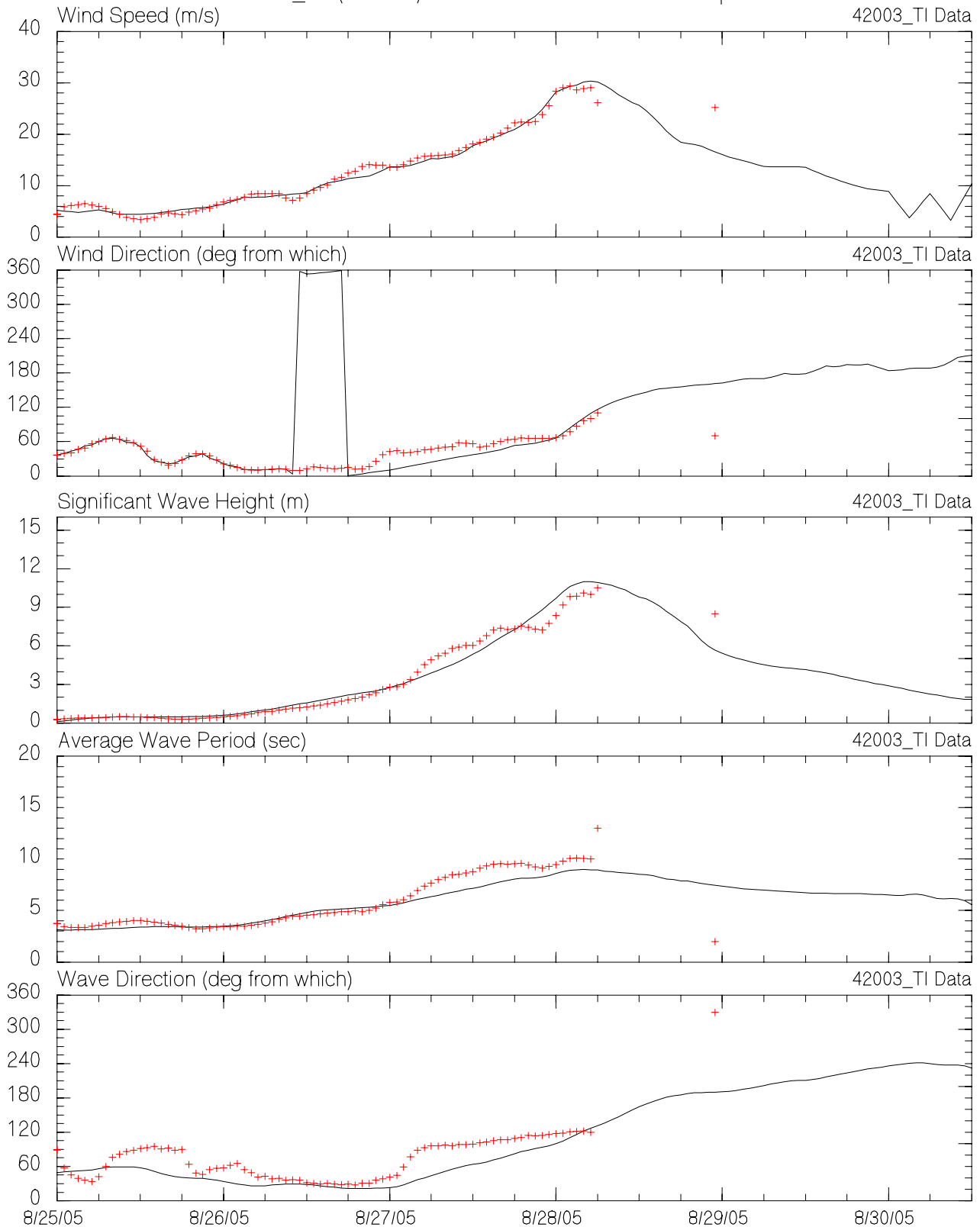
MMS Hurricane Katrina/Rita Hindcast  
Measured vs. Hindcast Winds and Waves at 42001  
2005\_12 (Katrina) GOM3Min Grid - Variable Depths



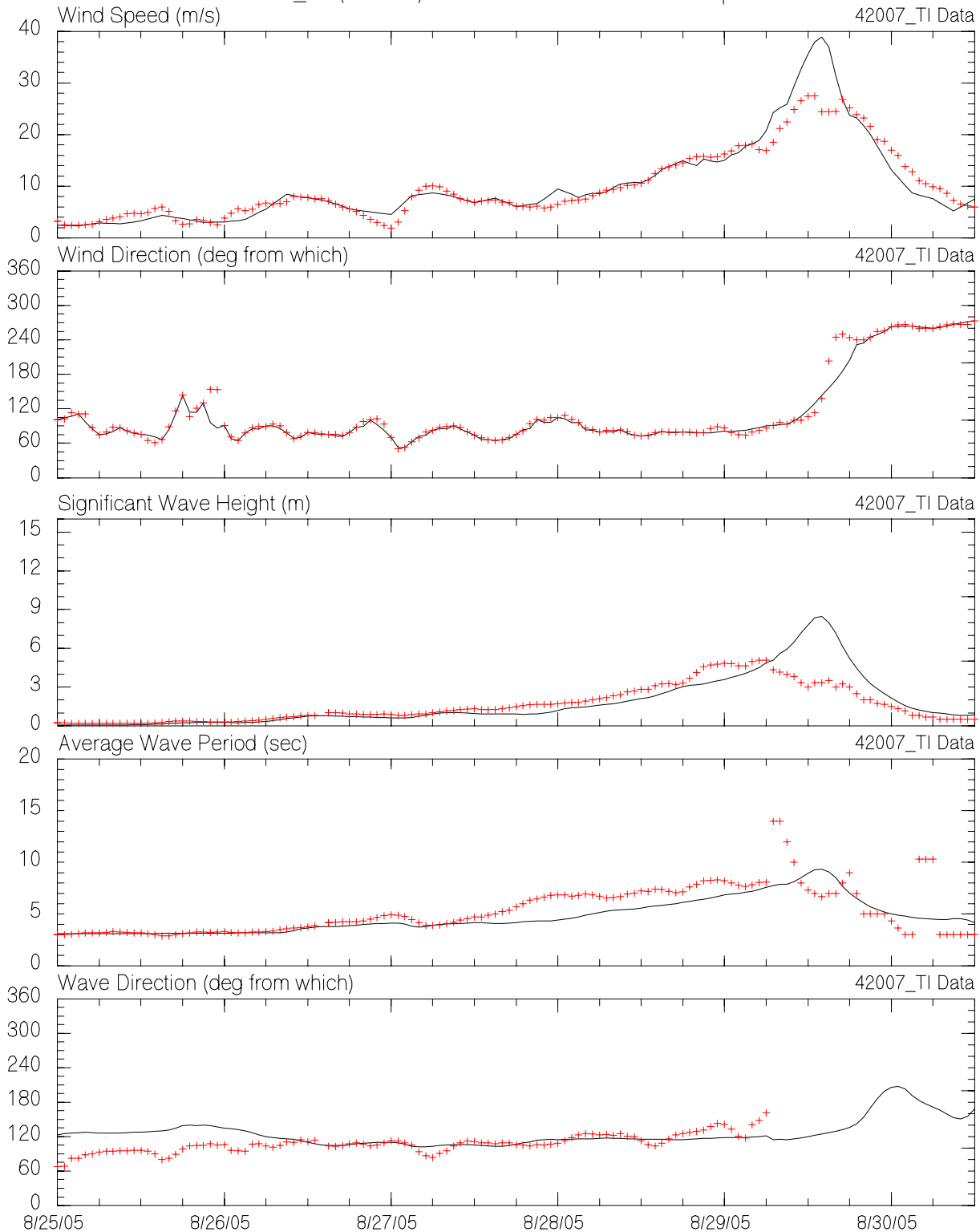
MMS Hurricane Katrina/Rita Hindcast  
Measured vs. Hindcast Winds and Waves at 42002  
2005\_12 (Katrina) GOM3Min Grid - Variable Depths



MMS Hurricane Katrina/Rita Hindcast  
Measured vs. Hindcast Winds and Waves at 42003  
2005\_12 (Katrina) GOM3Min Grid - Variable Depths

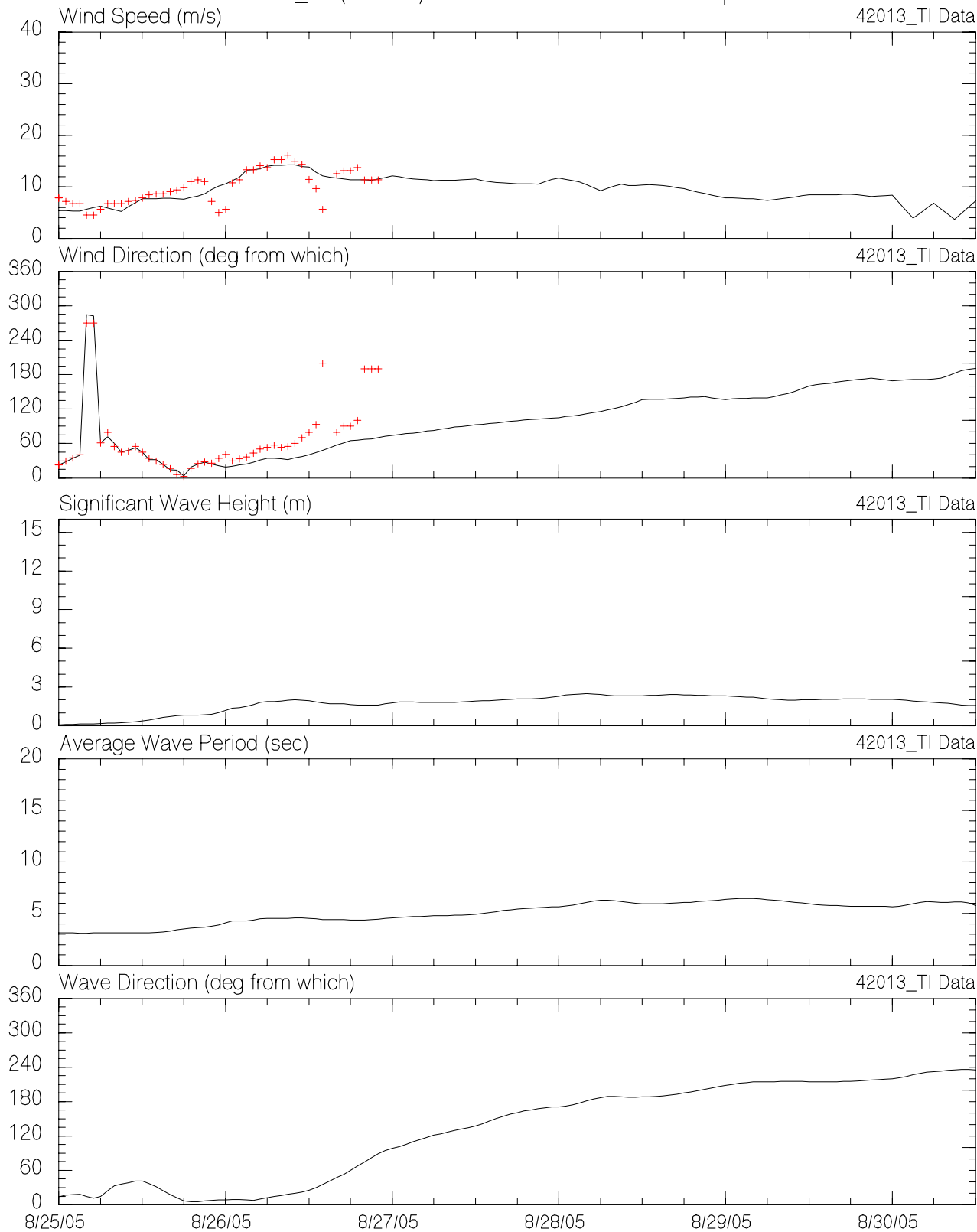


MMS Hurricane Katrina/Rita Hindcast  
Measured vs. Hindcast Winds and Waves at 42007  
2005\_12 (Katrina) GOM3Min Grid - Variable Depths

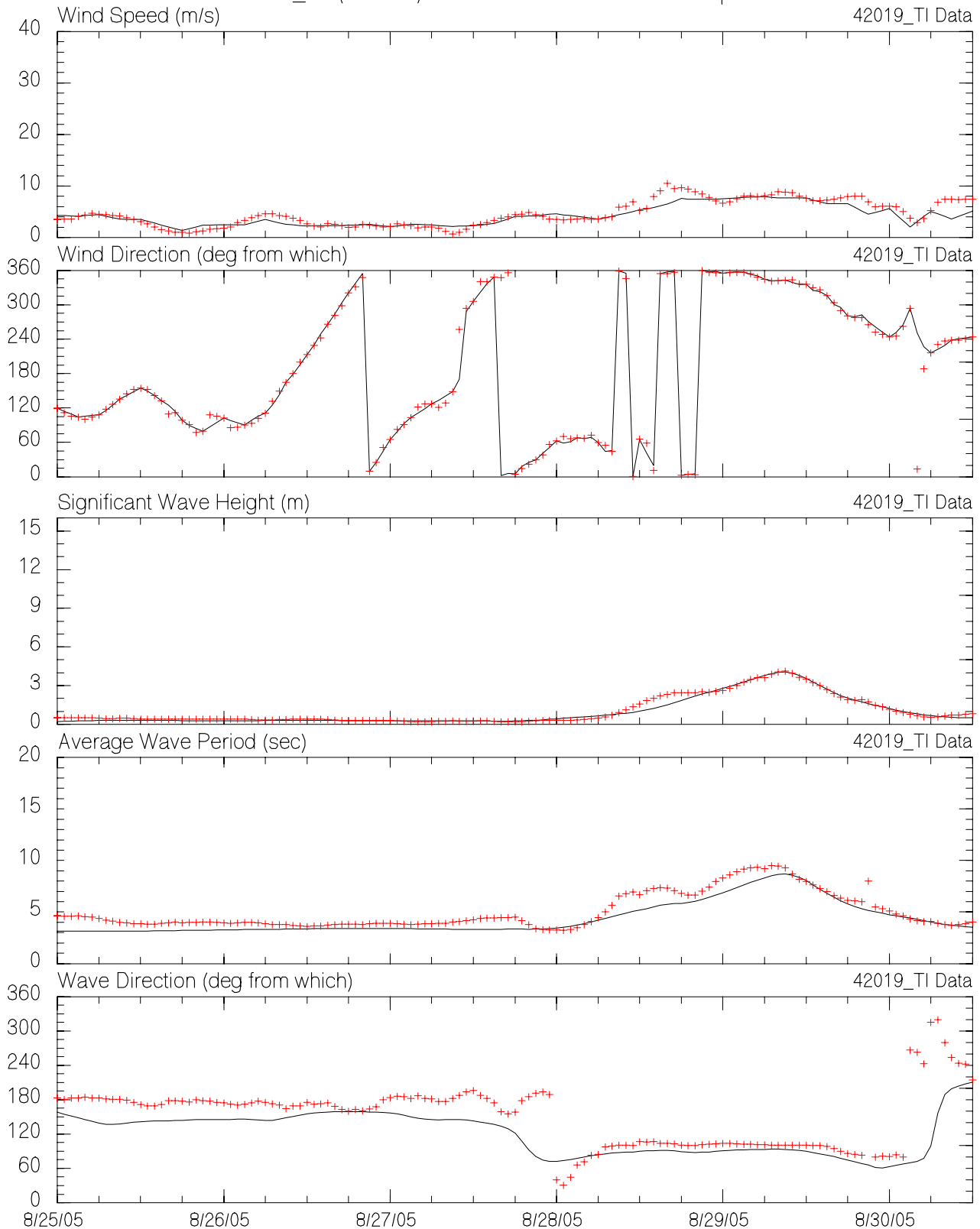


**Note: Buoy adrift on the 29th - position unknown**

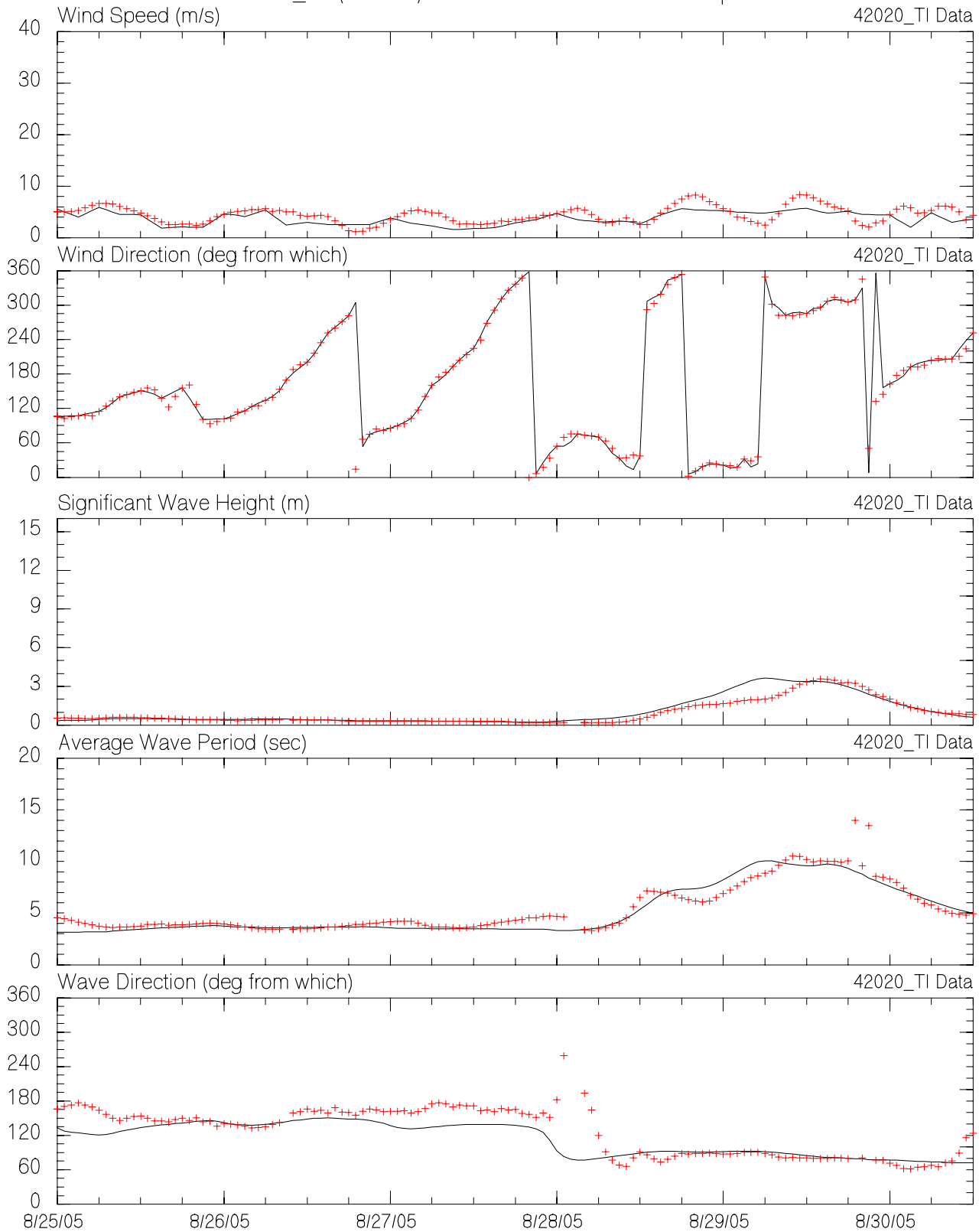
MMS Hurricane Katrina/Rita Hindcast  
Measured vs. Hindcast Winds and Waves at 42013  
2005\_12 (Katrina) GOM3Min Grid - Variable Depths



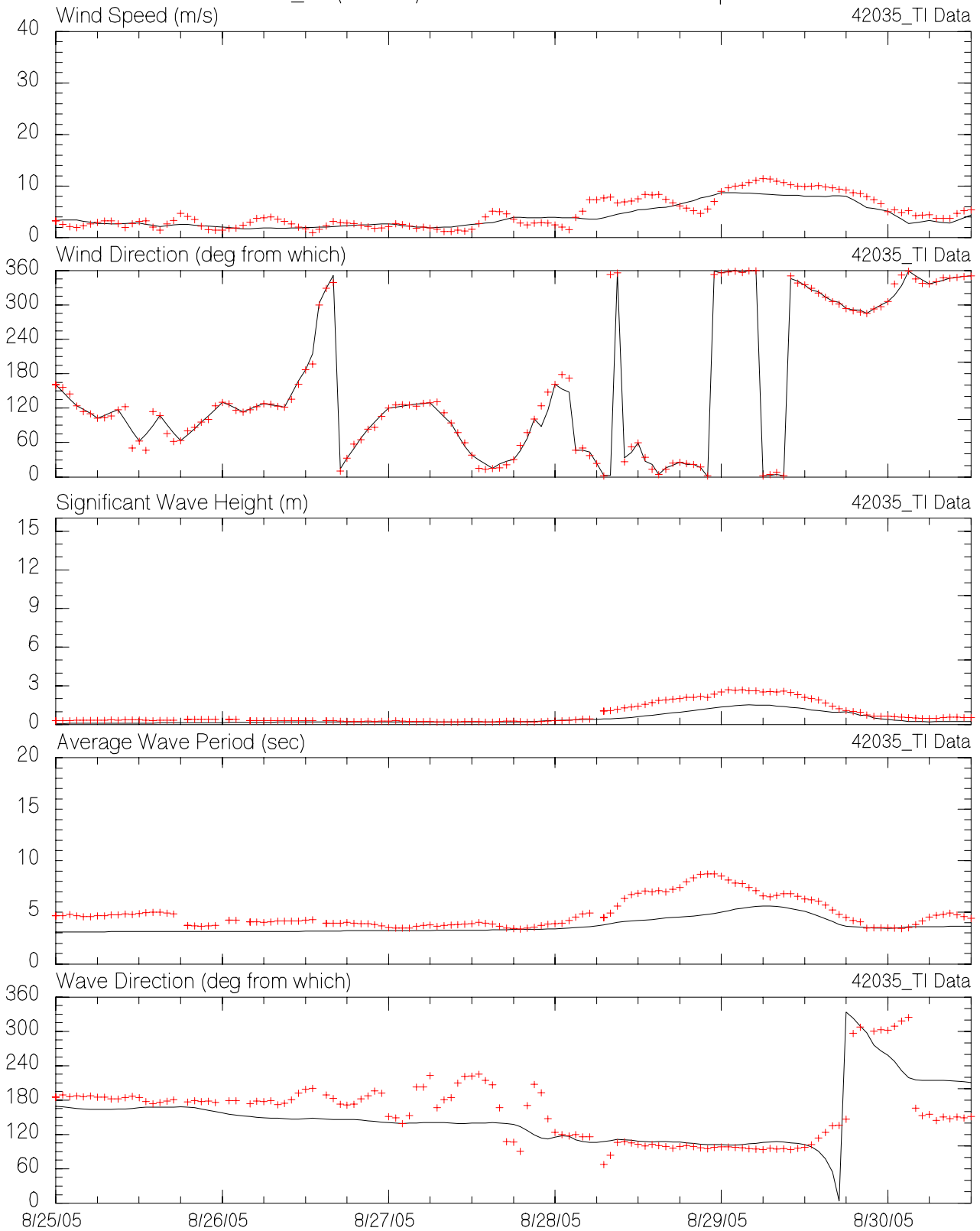
MMS Hurricane Katrina/Rita Hindcast  
Measured vs. Hindcast Winds and Waves at 42019  
2005\_12 (Katrina) GOM3Min Grid - Variable Depths



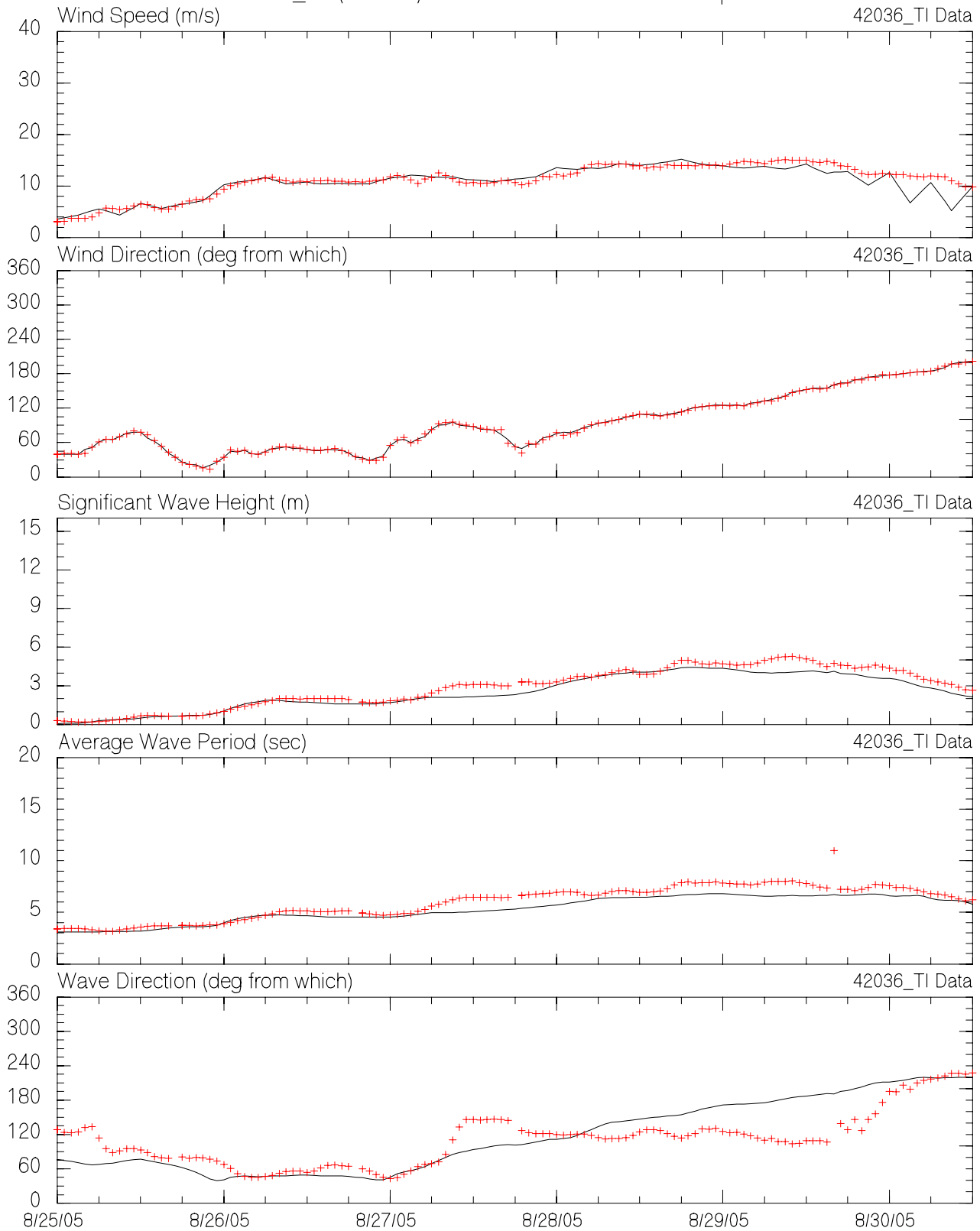
MMS Hurricane Katrina/Rita Hindcast  
Measured vs. Hindcast Winds and Waves at 42020  
2005\_12 (Katrina) GOM3Min Grid - Variable Depths



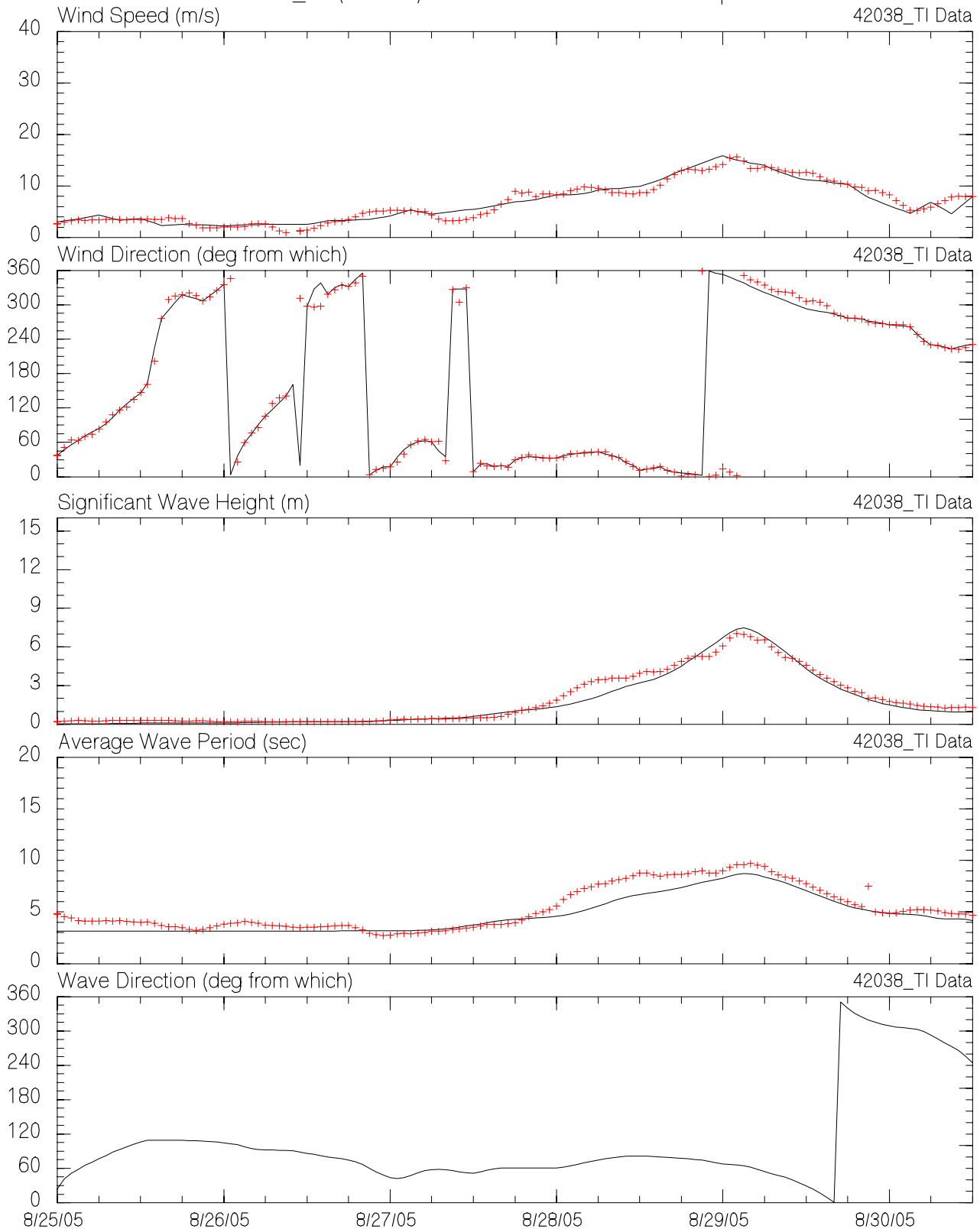
MMS Hurricane Katrina/Rita Hindcast  
Measured vs. Hindcast Winds and Waves at 42035  
2005\_12 (Katrina) GOM3Min Grid - Variable Depths



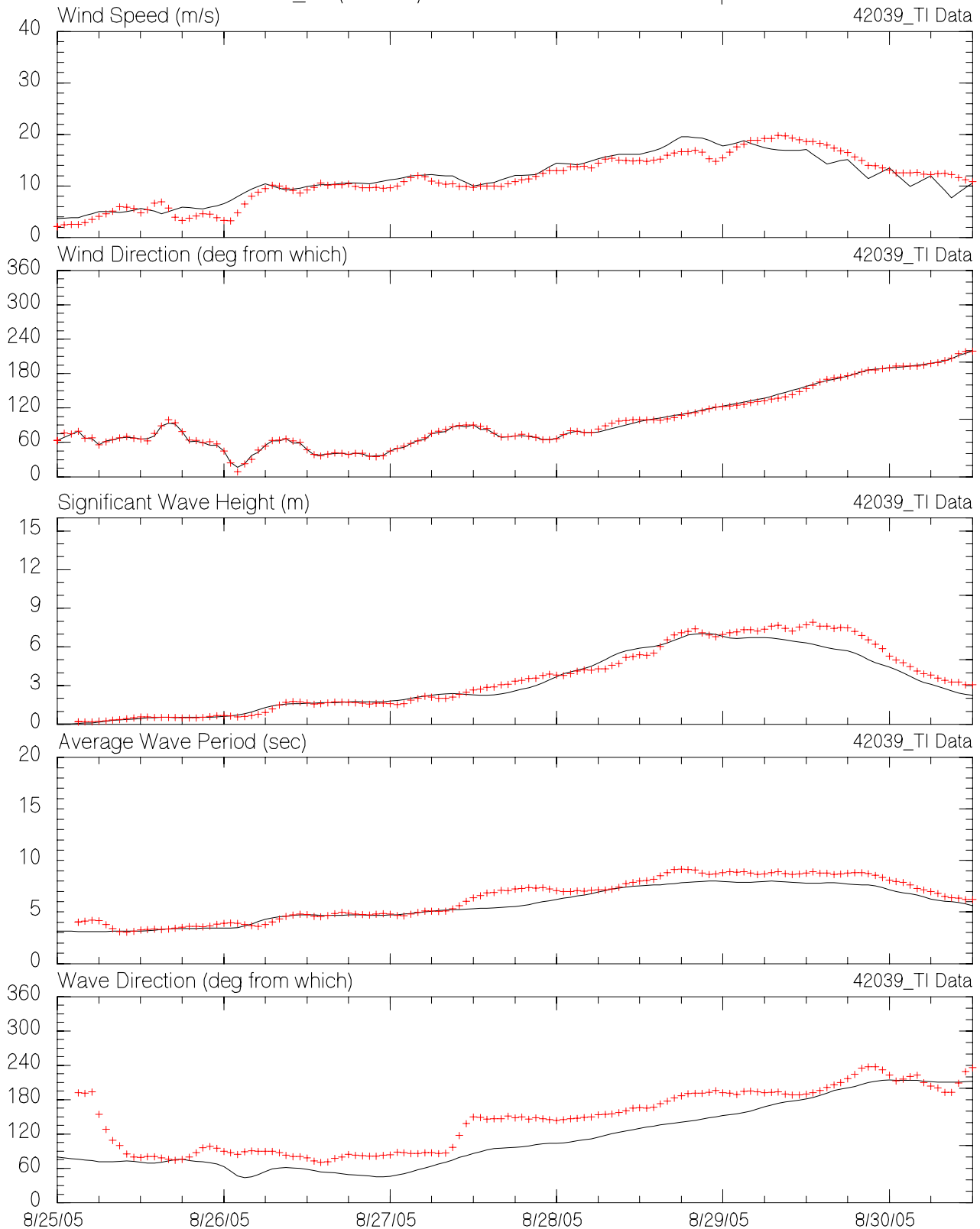
MMS Hurricane Katrina/Rita Hindcast  
Measured vs. Hindcast Winds and Waves at 42036  
2005\_12 (Katrina) GOM3Min Grid - Variable Depths



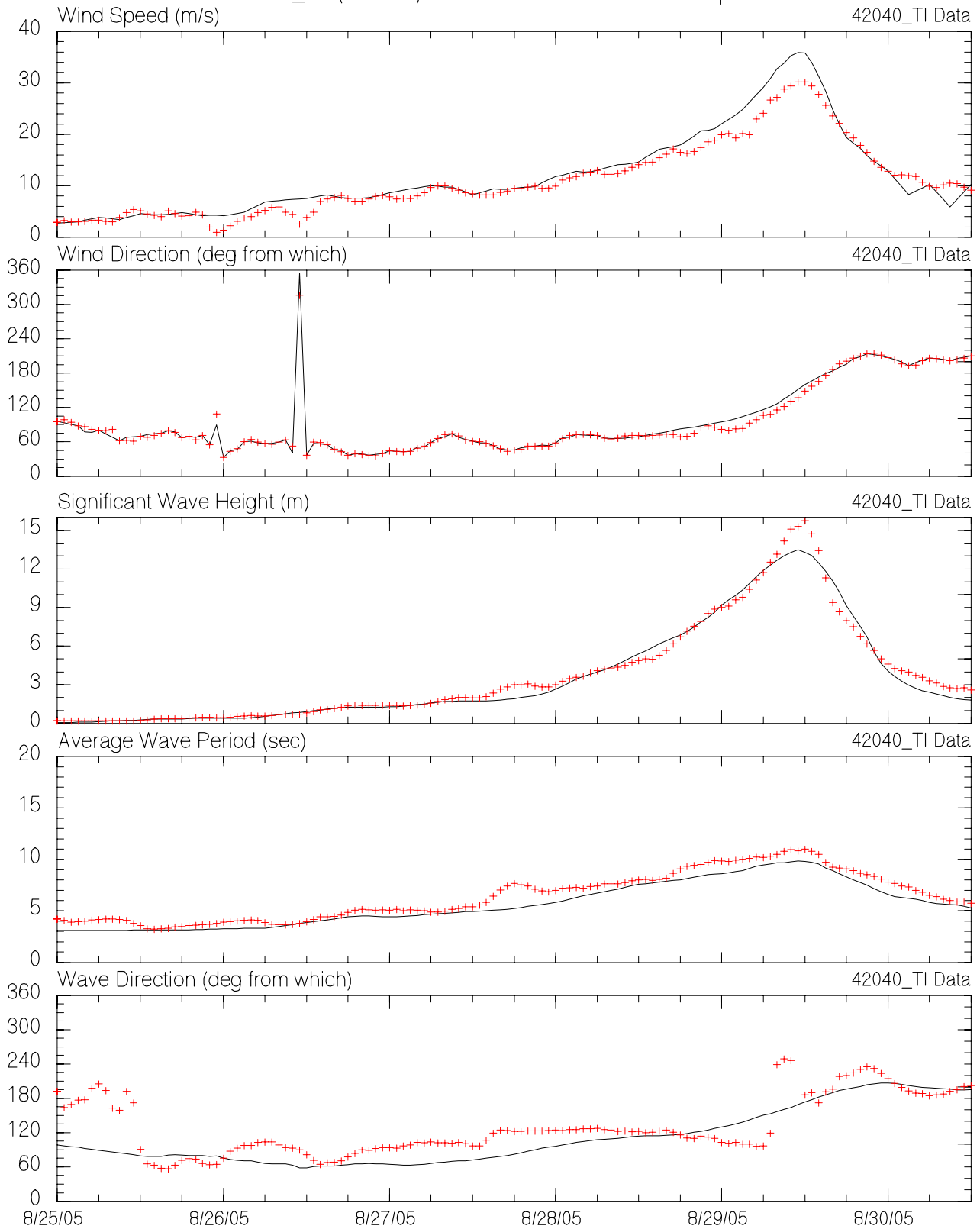
MMS Hurricane Katrina/Rita Hindcast  
Measured vs. Hindcast Winds and Waves at 42038  
2005\_12 (Katrina) GOM3Min Grid - Variable Depths



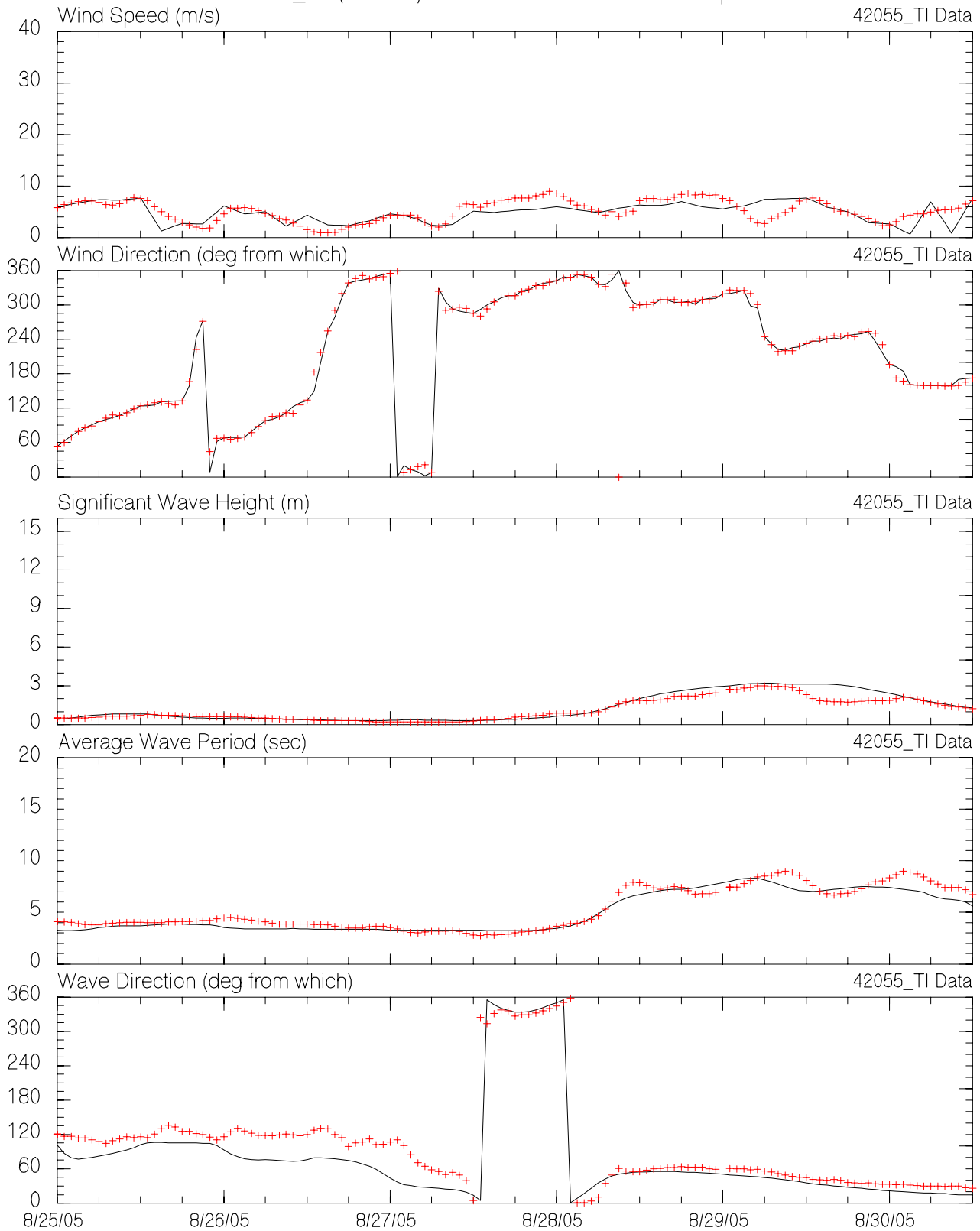
MMS Hurricane Katrina/Rita Hindcast  
Measured vs. Hindcast Winds and Waves at 42039  
2005\_12 (Katrina) GOM3Min Grid - Variable Depths



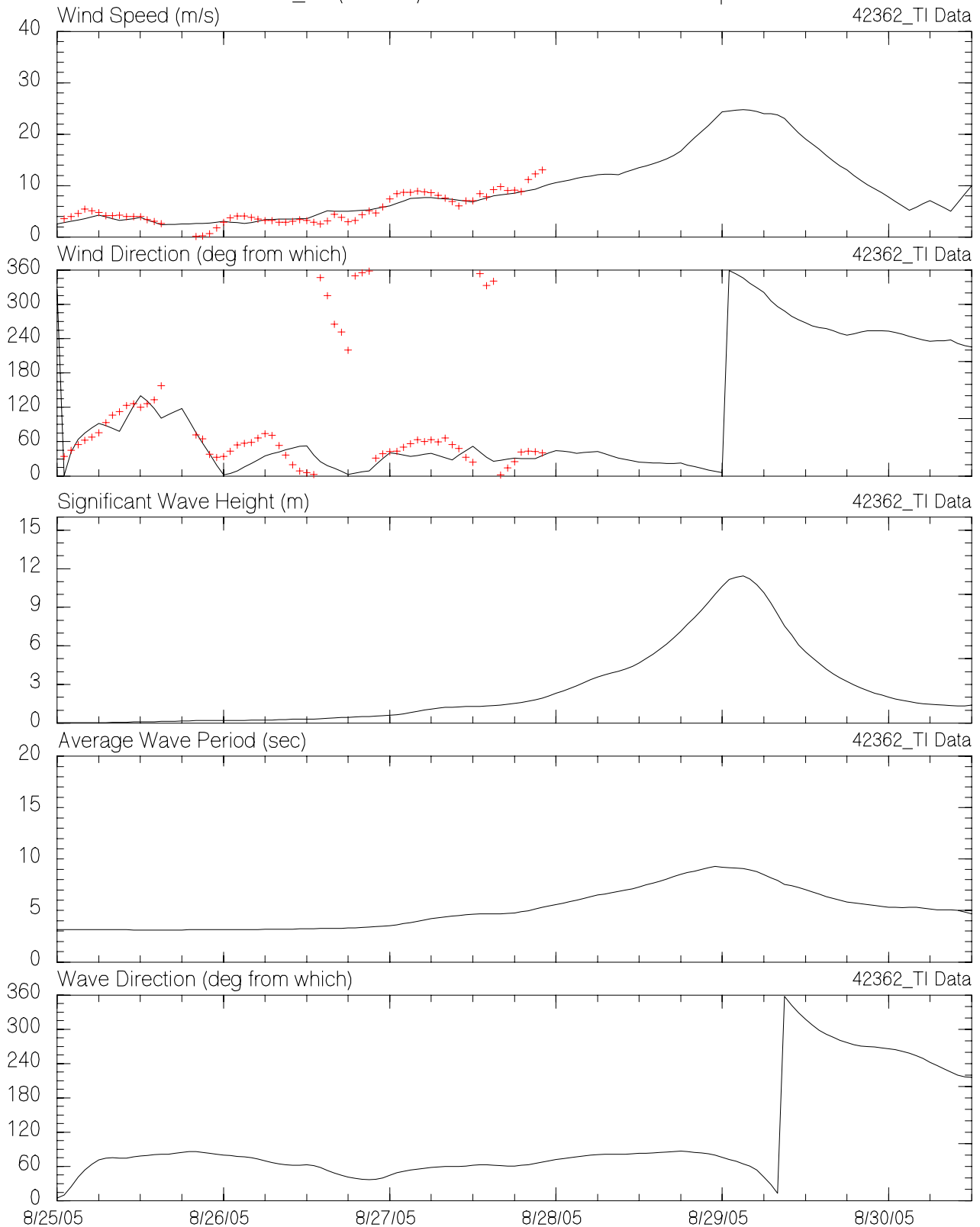
MMS Hurricane Katrina/Rita Hindcast  
Measured vs. Hindcast Winds and Waves at 42040  
2005\_12 (Katrina) GOM3Min Grid - Variable Depths



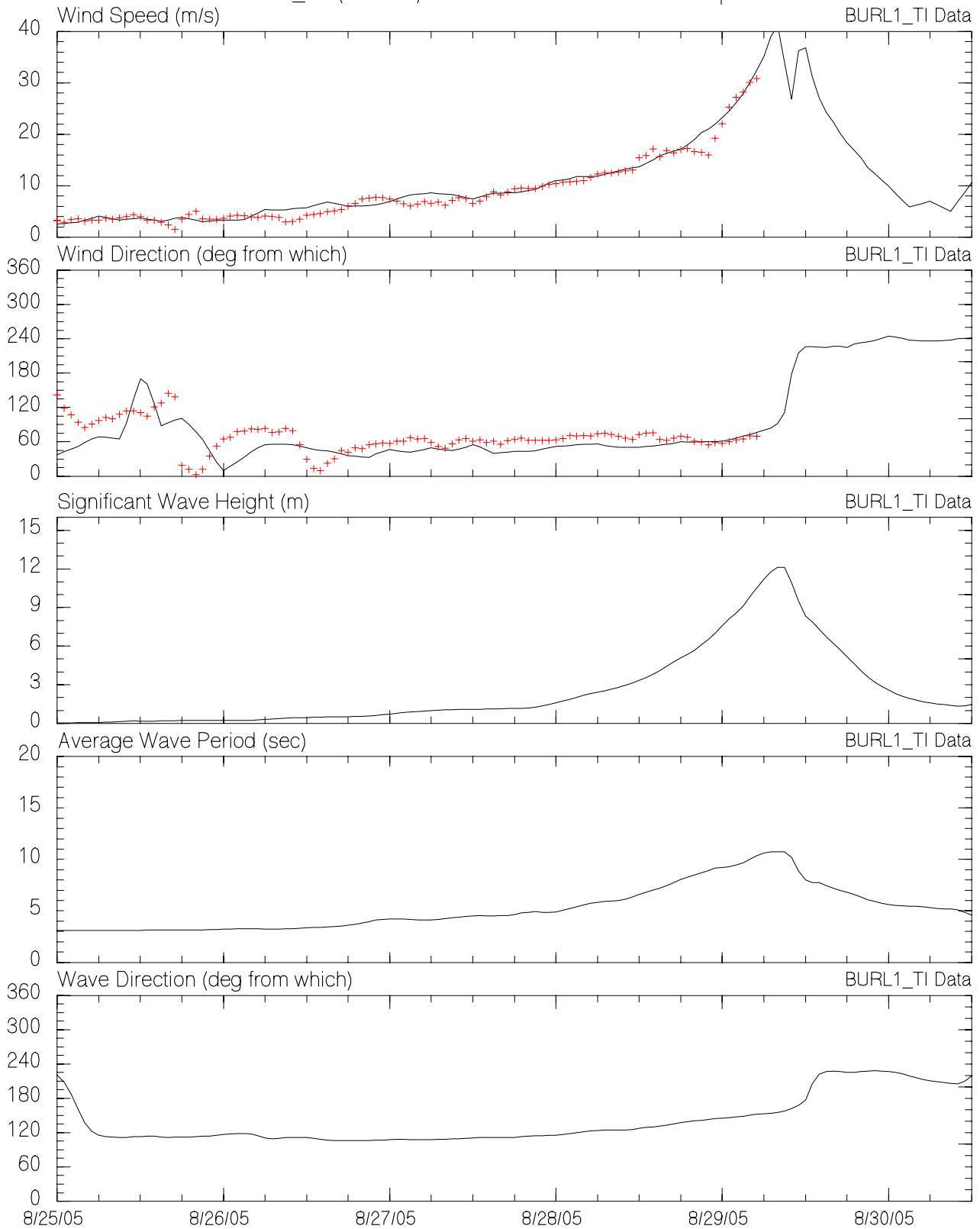
MMS Hurricane Katrina/Rita Hindcast  
Measured vs. Hindcast Winds and Waves at 42055  
2005\_12 (Katrina) GOM3Min Grid - Variable Depths



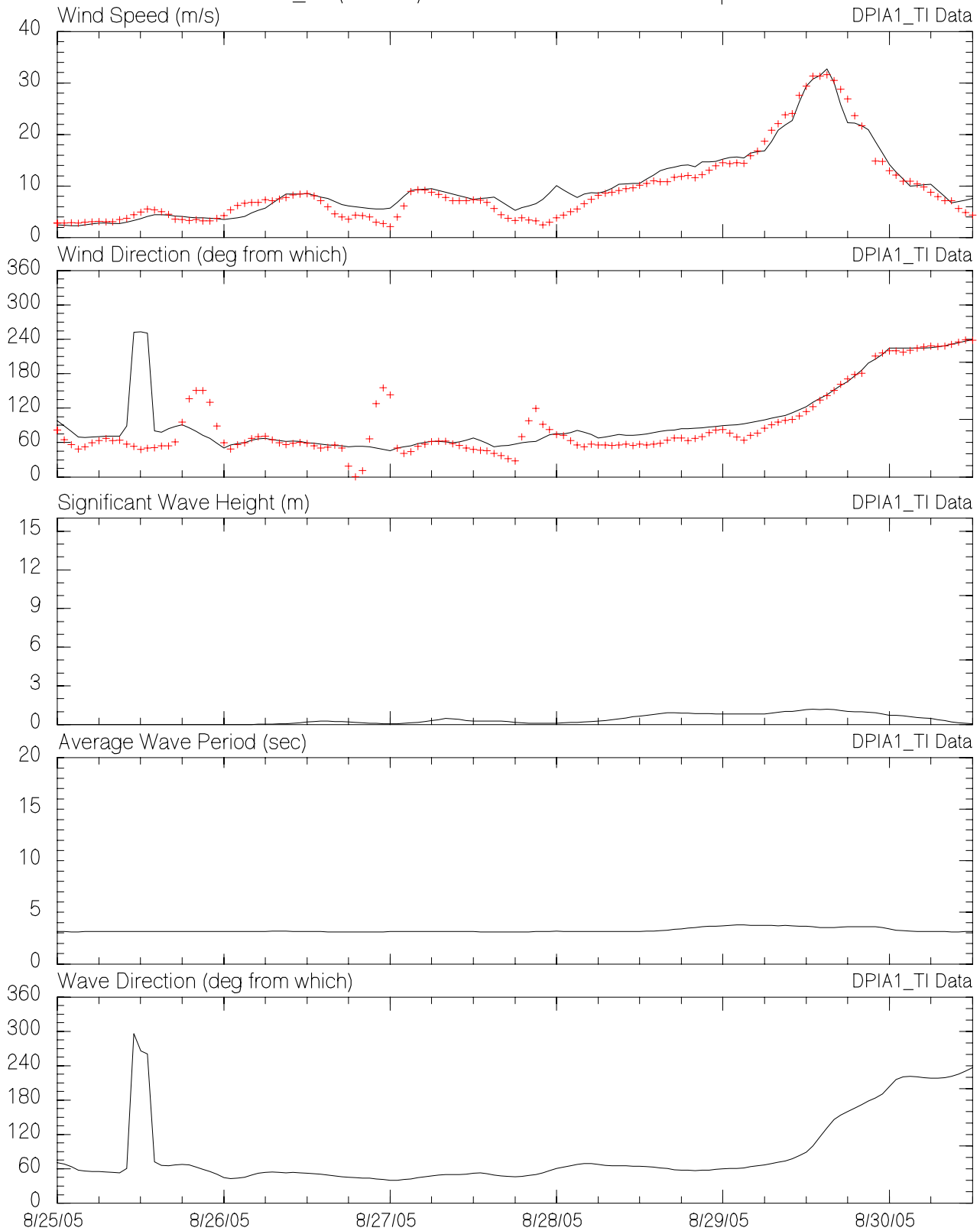
MMS Hurricane Katrina/Rita Hindcast  
Measured vs. Hindcast Winds and Waves at 42362  
2005\_12 (Katrina) GOM3Min Grid - Variable Depths



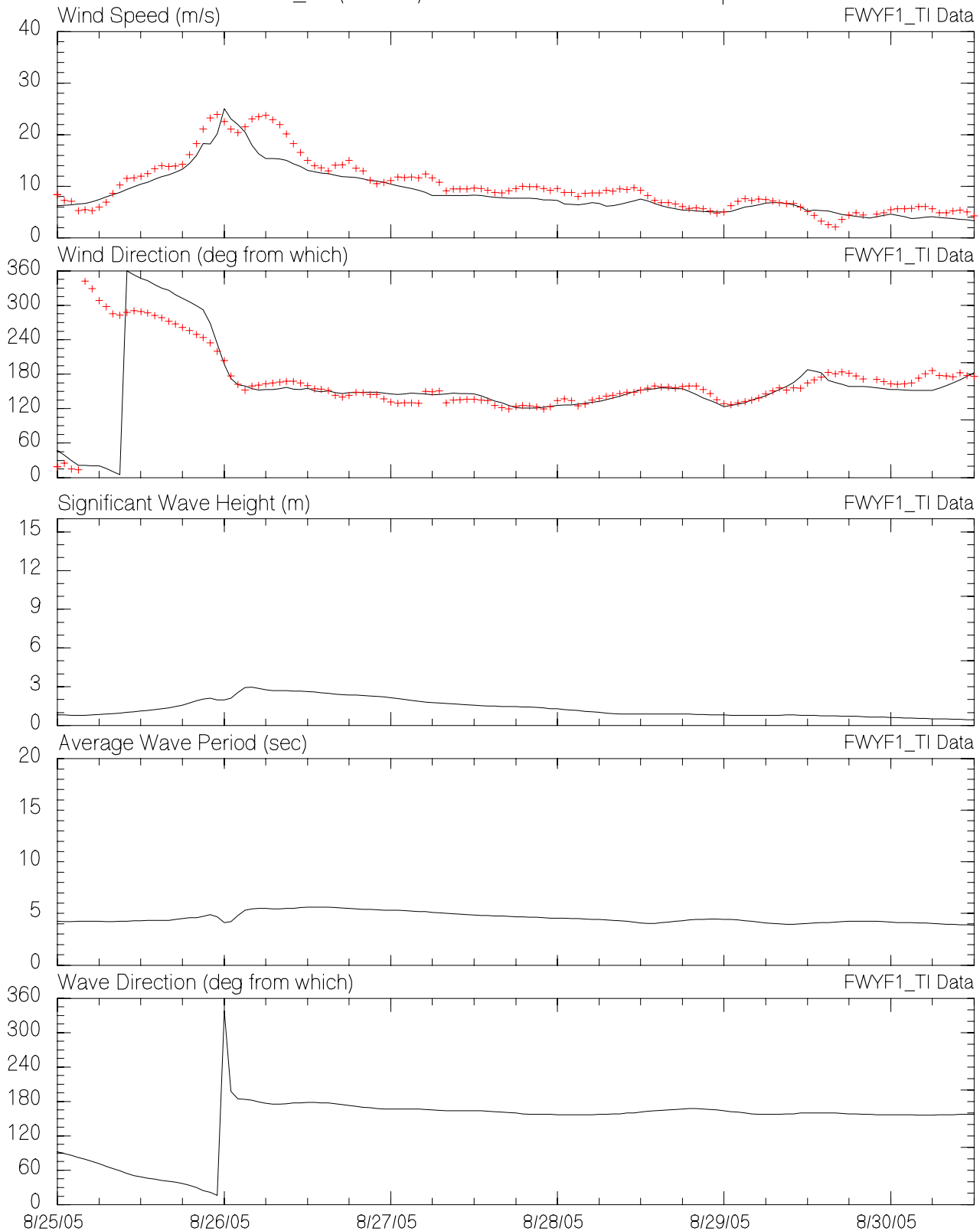
MMS Hurricane Katrina/Rita Hindcast  
Measured vs. Hindcast Winds and Waves at BURL1  
2005\_12 (Katrina) GOM3Min Grid - Variable Depths



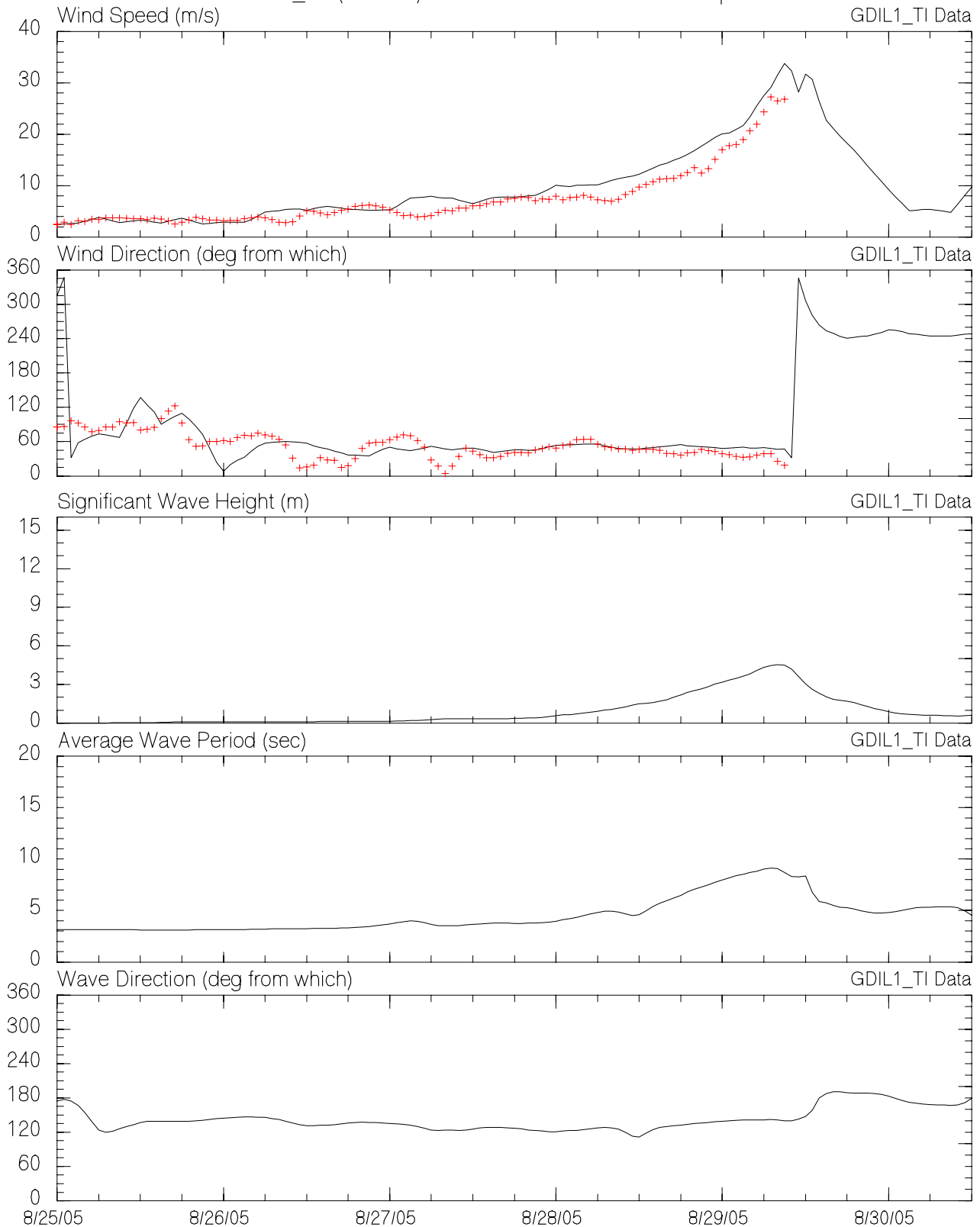
MMS Hurricane Katrina/Rita Hindcast  
Measured vs. Hindcast Winds and Waves at DPIA1  
2005\_12 (Katrina) GOM3Min Grid - Variable Depths



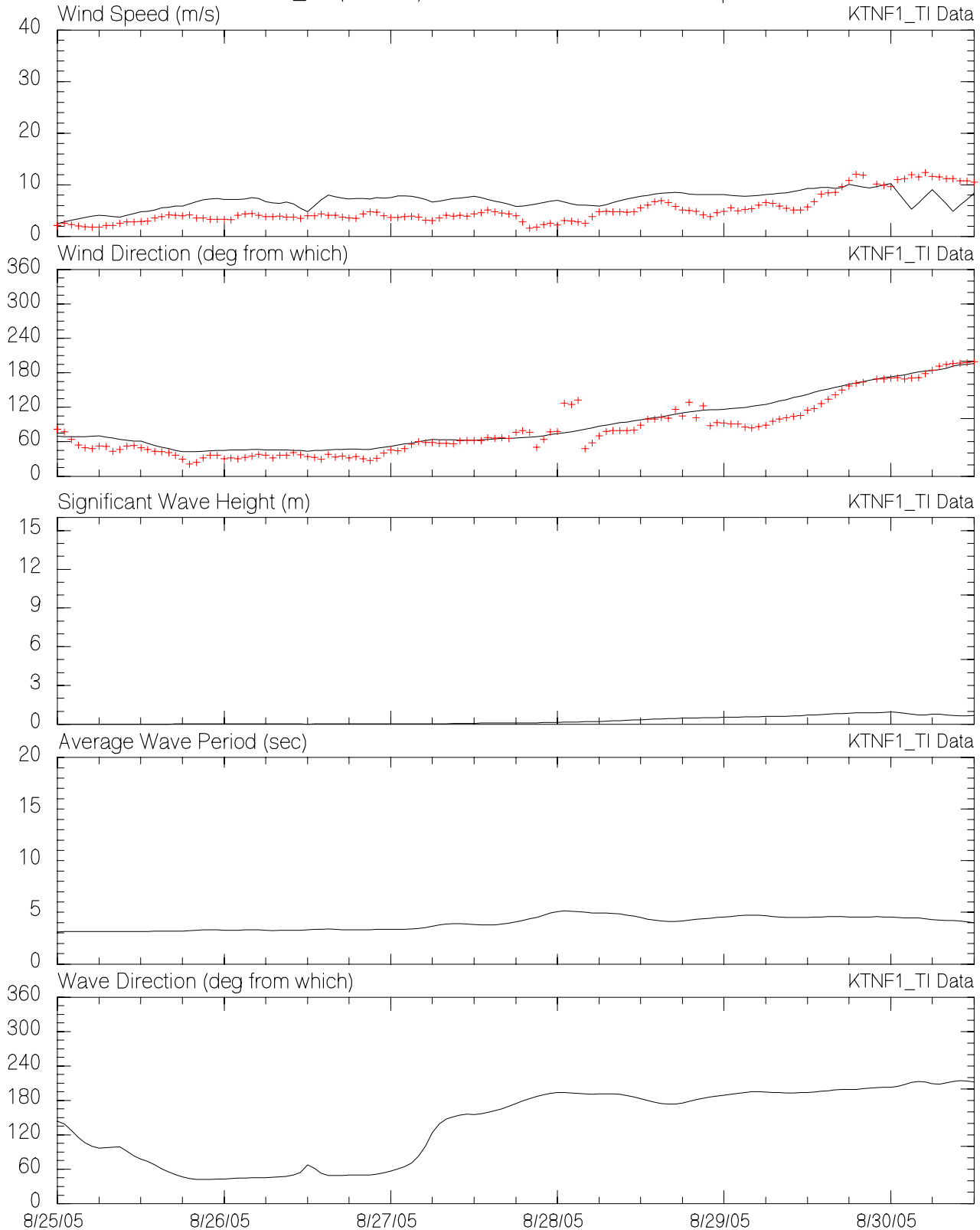
MMS Hurricane Katrina/Rita Hindcast  
Measured vs. Hindcast Winds and Waves at FWYF1  
2005\_12 (Katrina) GOM3Min Grid - Variable Depths



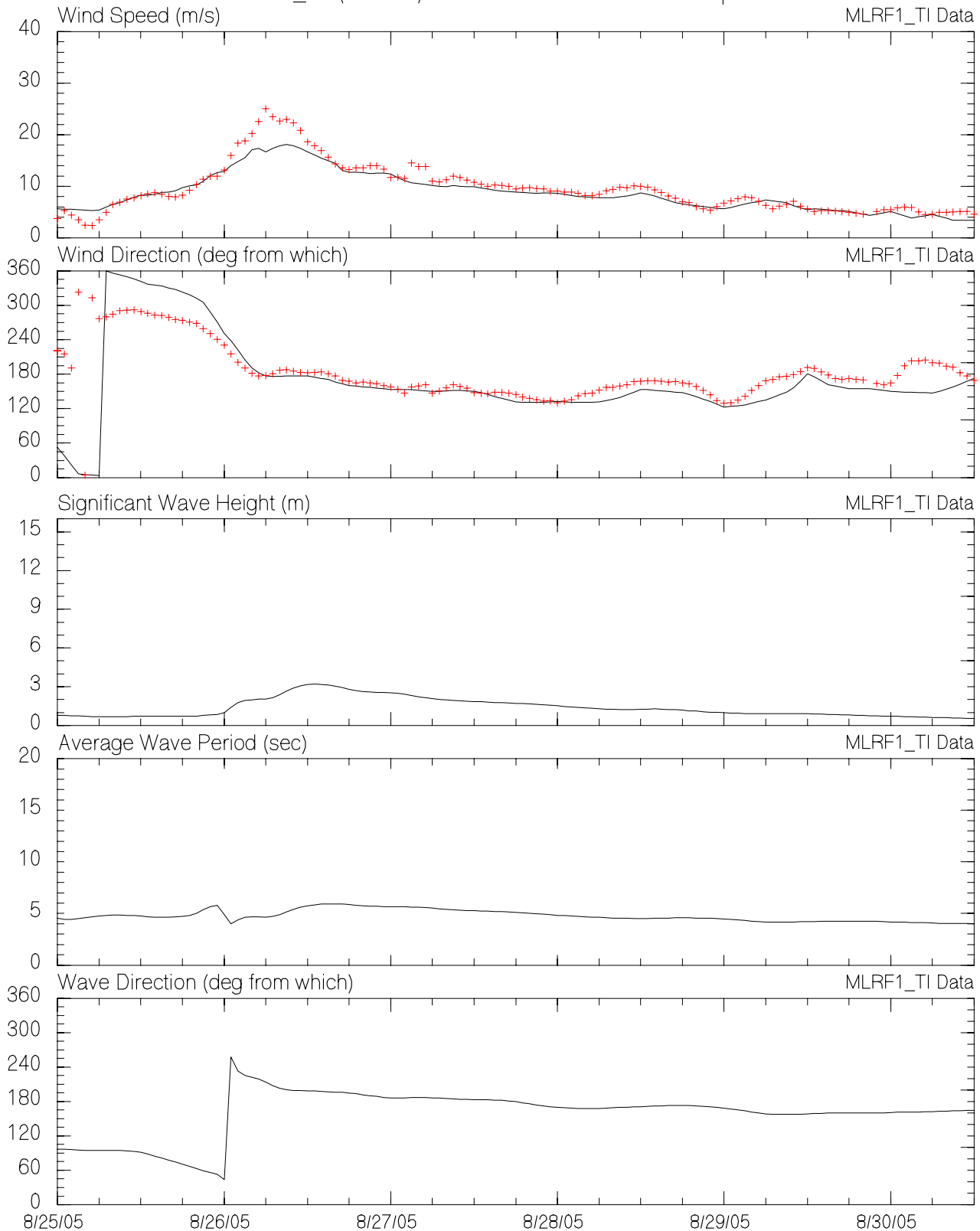
MMS Hurricane Katrina/Rita Hindcast  
Measured vs. Hindcast Winds and Waves at GDIL1  
2005\_12 (Katrina) GOM3Min Grid - Variable Depths



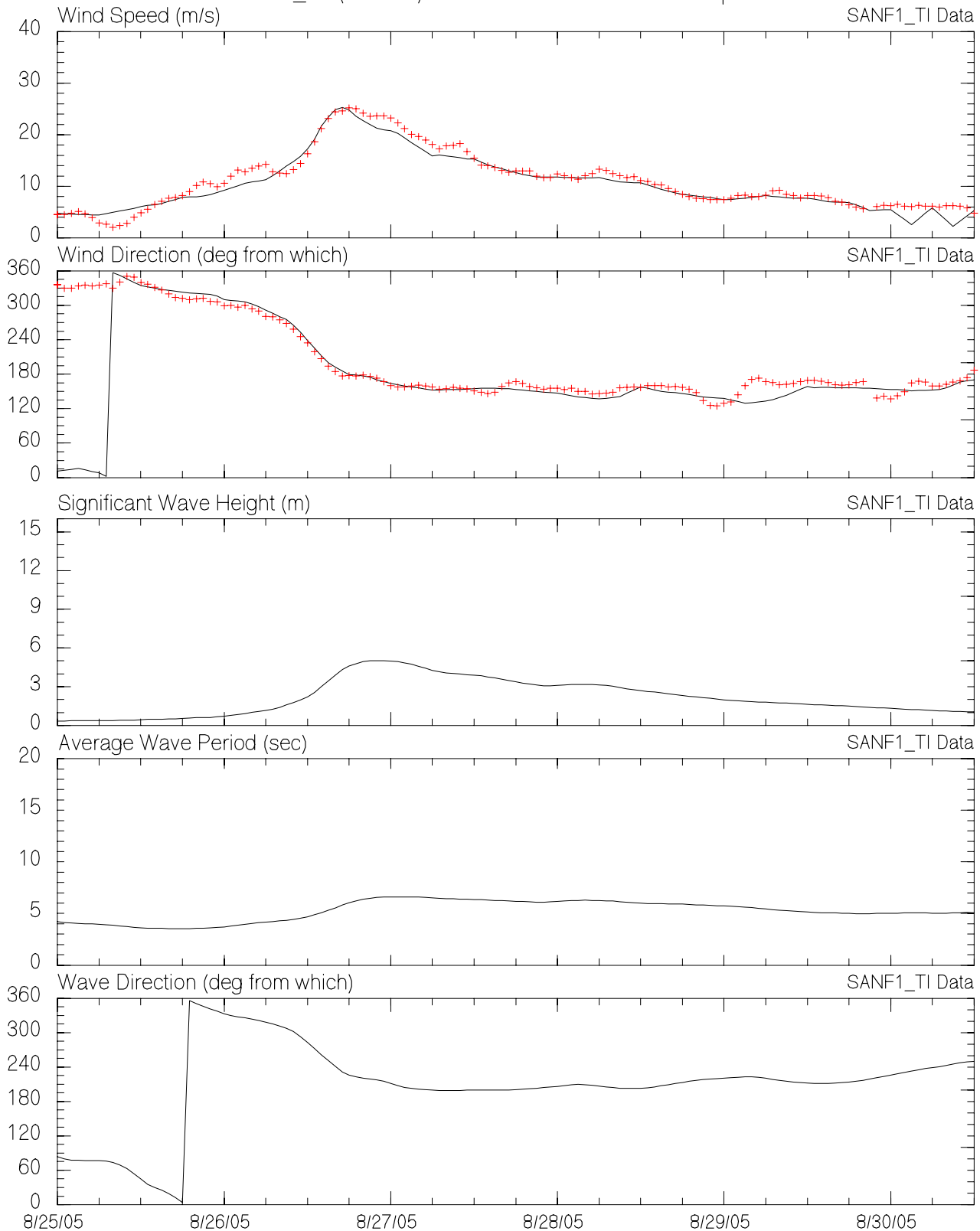
MMS Hurricane Katrina/Rita Hindcast  
Measured vs. Hindcast Winds and Waves at KTNF1  
2005\_12 (Katrina) GOM3Min Grid - Variable Depths



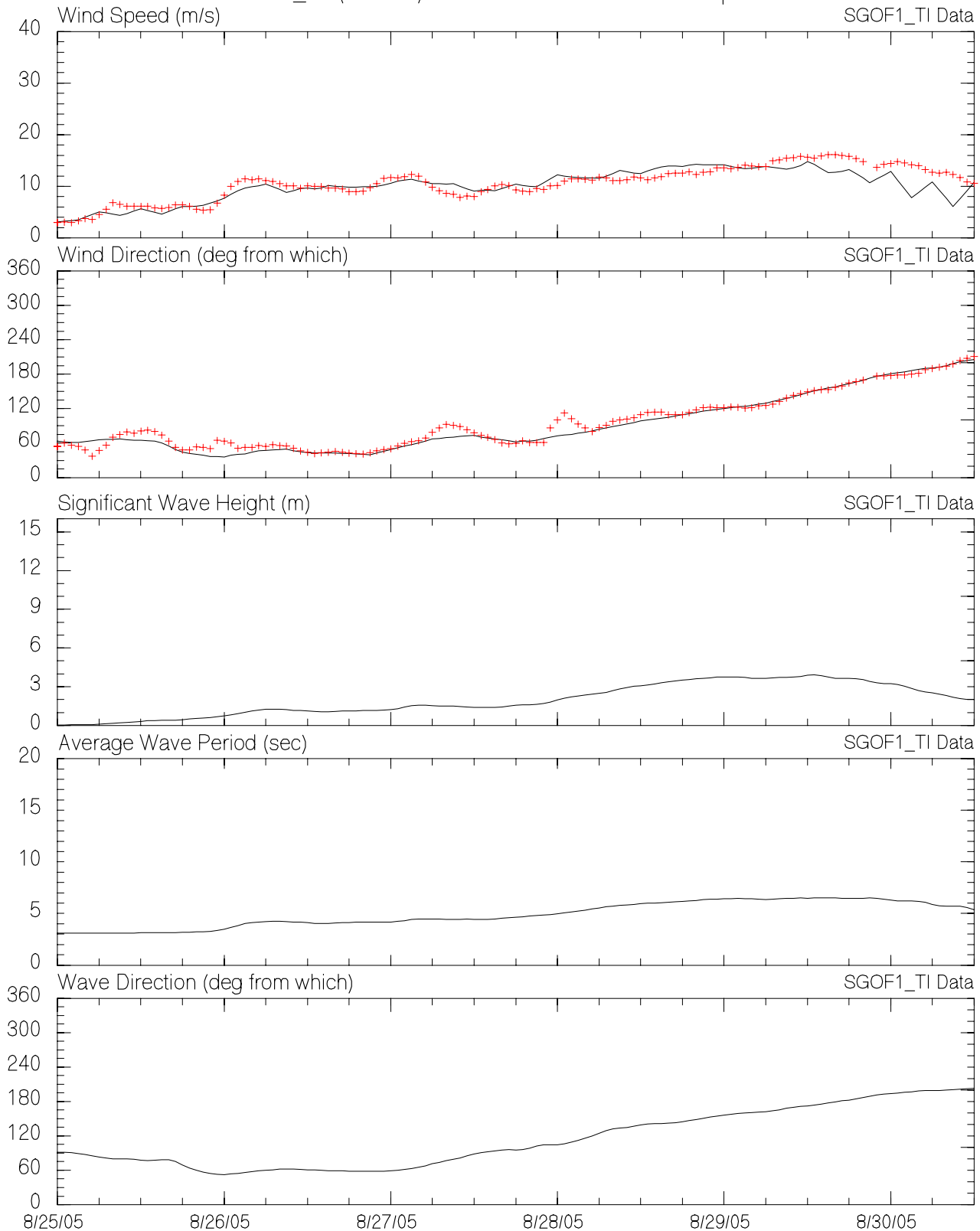
MMS Hurricane Katrina/Rita Hindcast  
Measured vs. Hindcast Winds and Waves at MLRF1  
2005\_12 (Katrina) GOM3Min Grid - Variable Depths



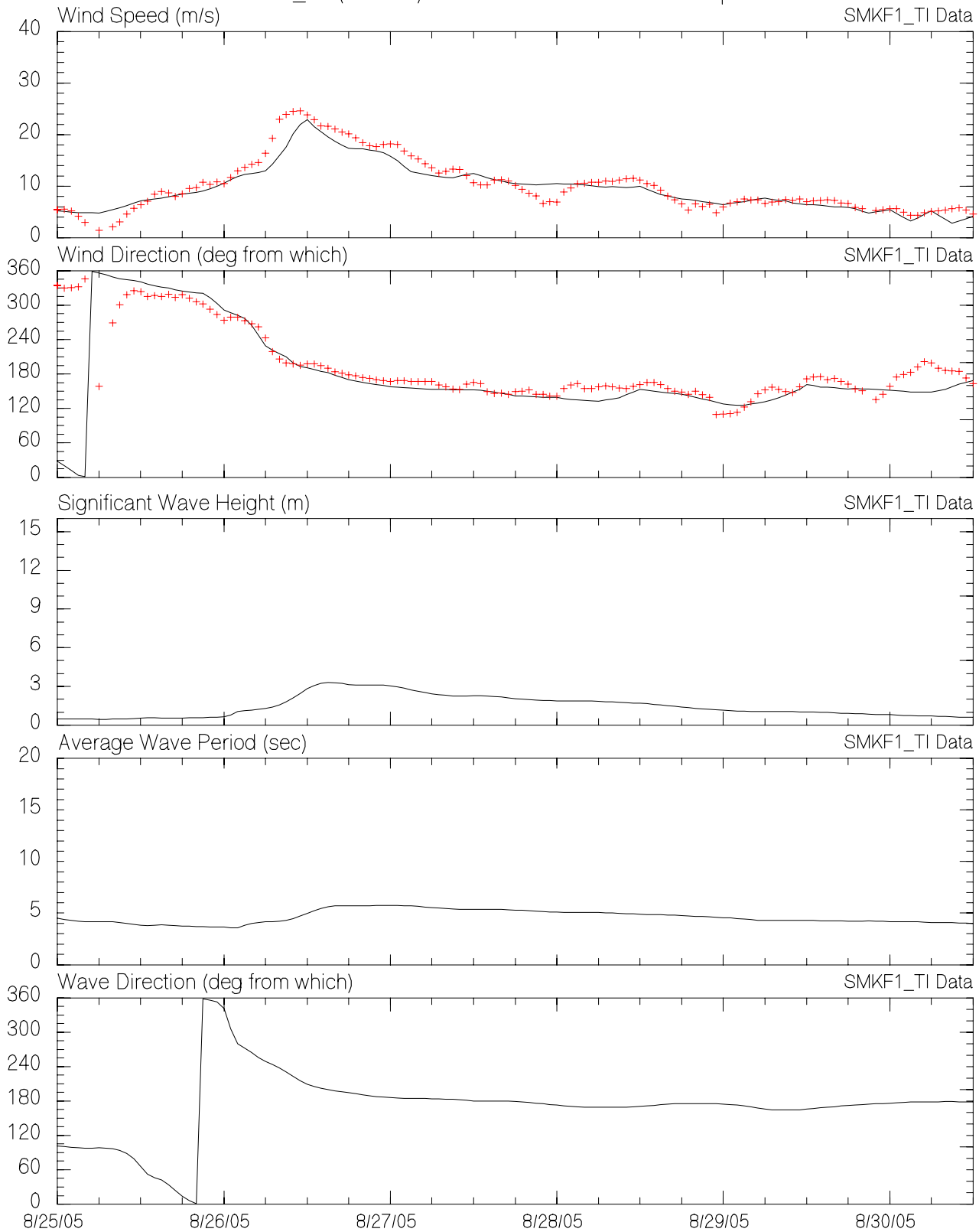
MMS Hurricane Katrina/Rita Hindcast  
Measured vs. Hindcast Winds and Waves at SANF1  
2005\_12 (Katrina) GOM3Min Grid - Variable Depths



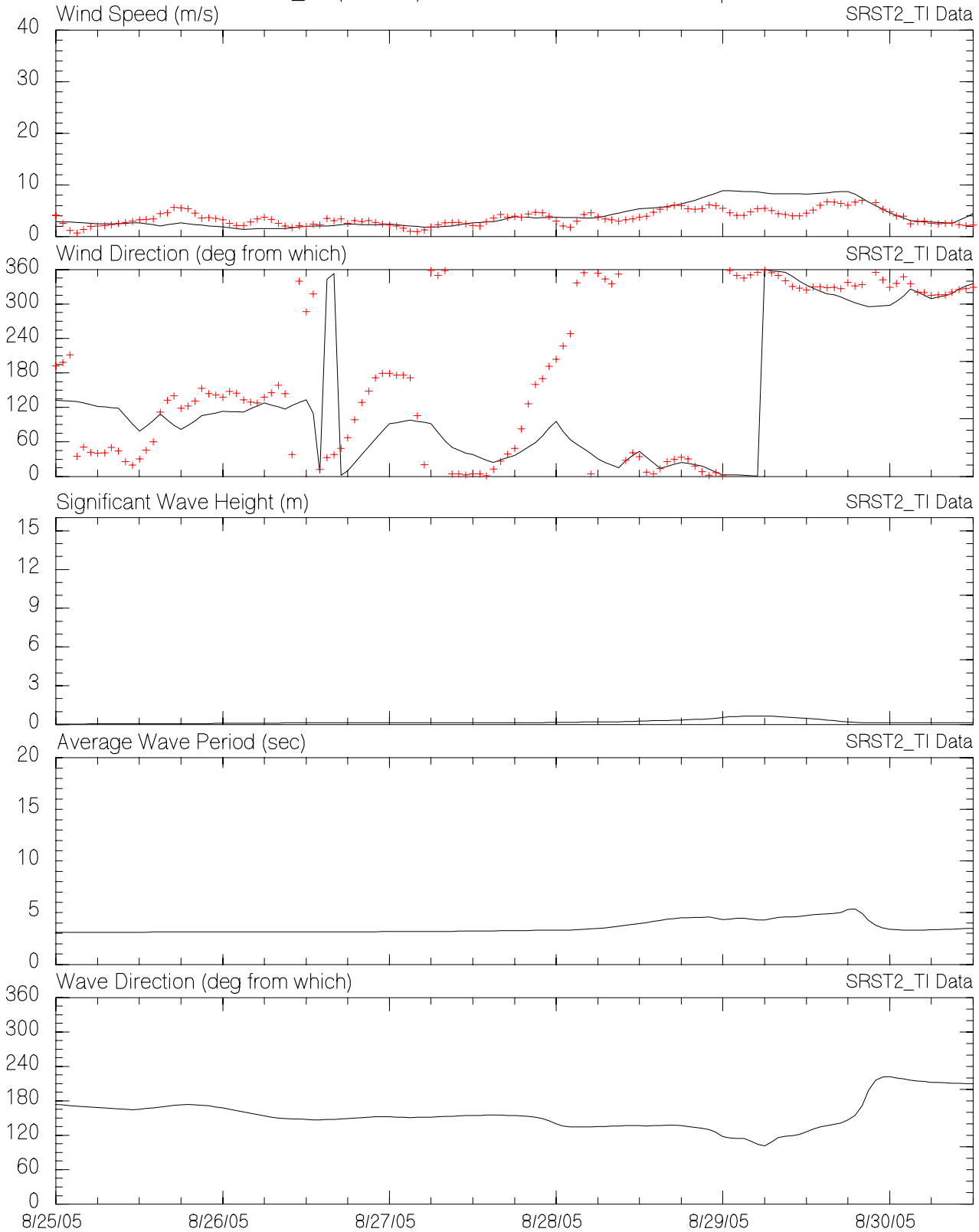
MMS Hurricane Katrina/Rita Hindcast  
Measured vs. Hindcast Winds and Waves at SGOF1  
2005\_12 (Katrina) GOM3Min Grid - Variable Depths



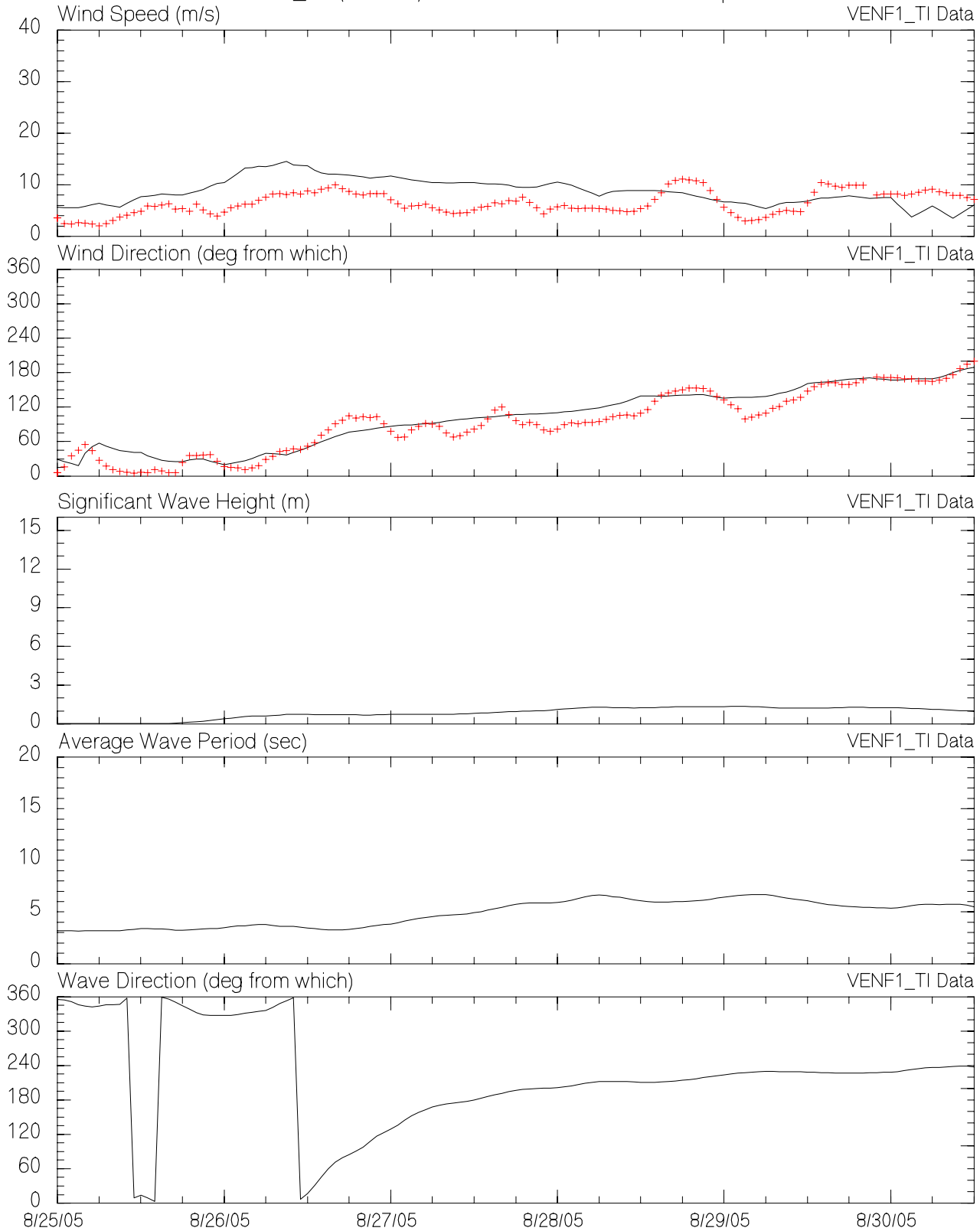
MMS Hurricane Katrina/Rita Hindcast  
Measured vs. Hindcast Winds and Waves at SMKF1  
2005\_12 (Katrina) GOM3Min Grid - Variable Depths



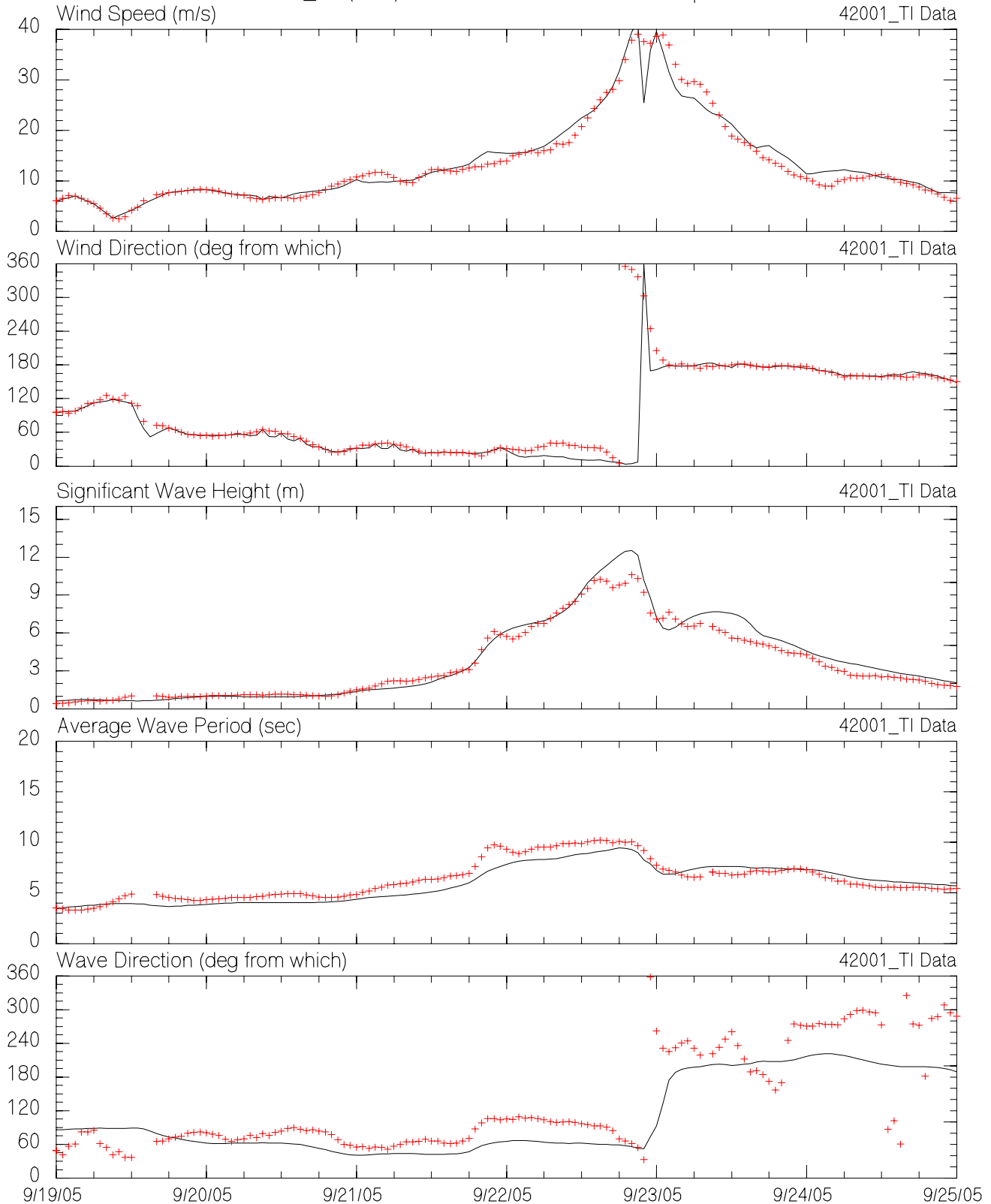
MMS Hurricane Katrina/Rita Hindcast  
Measured vs. Hindcast Winds and Waves at SRST2  
2005\_12 (Katrina) GOM3Min Grid - Variable Depths



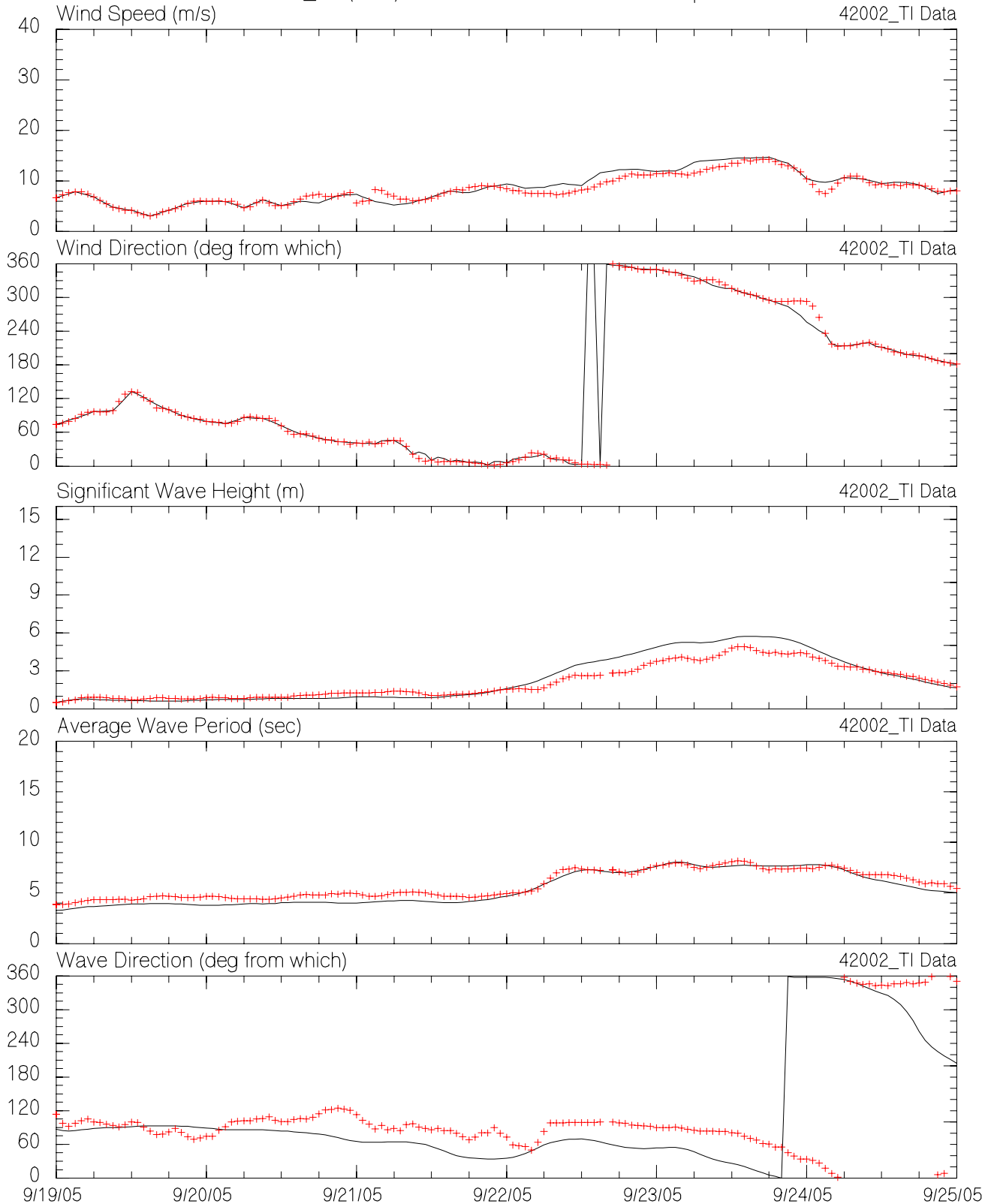
MMS Hurricane Katrina/Rita Hindcast  
Measured vs. Hindcast Winds and Waves at VENF1  
2005\_12 (Katrina) GOM3Min Grid - Variable Depths



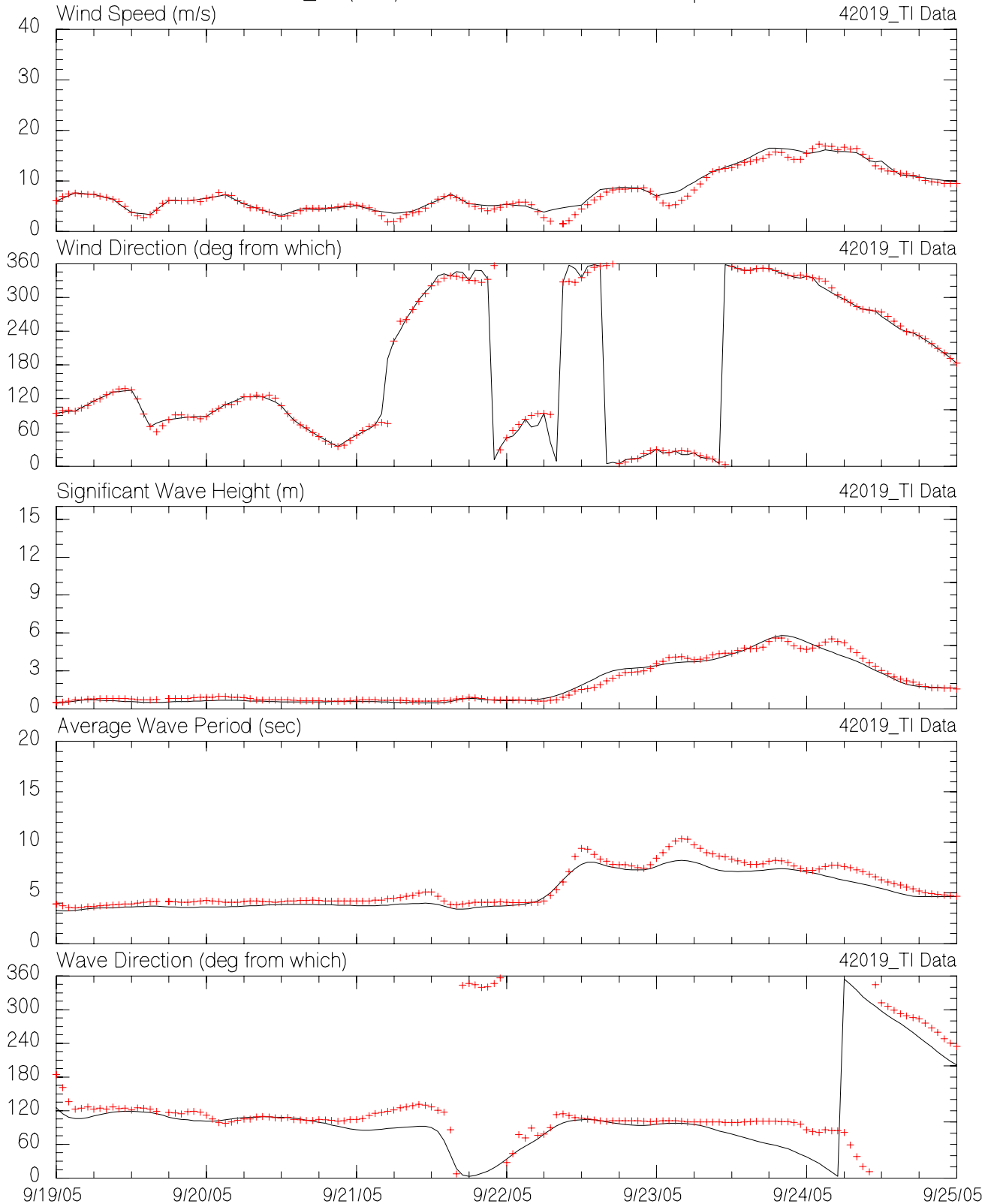
MMS Hurricane Katrina/Rita Hindcast  
Measured vs. Hindcast Winds and Waves at 42001  
2005\_18 (Rita) GOM3Min Grid - Variable Depths



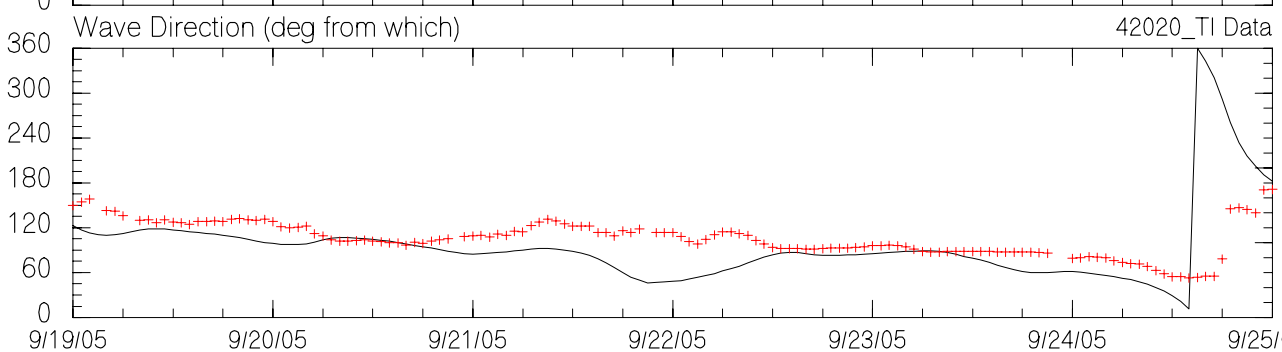
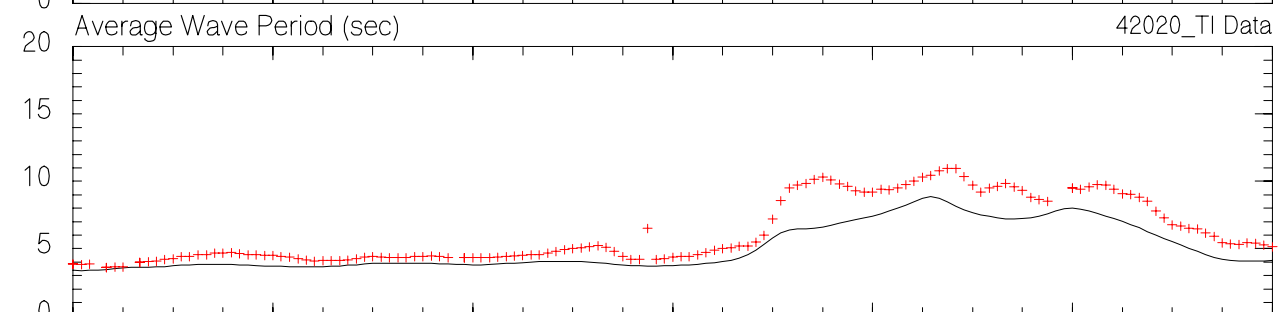
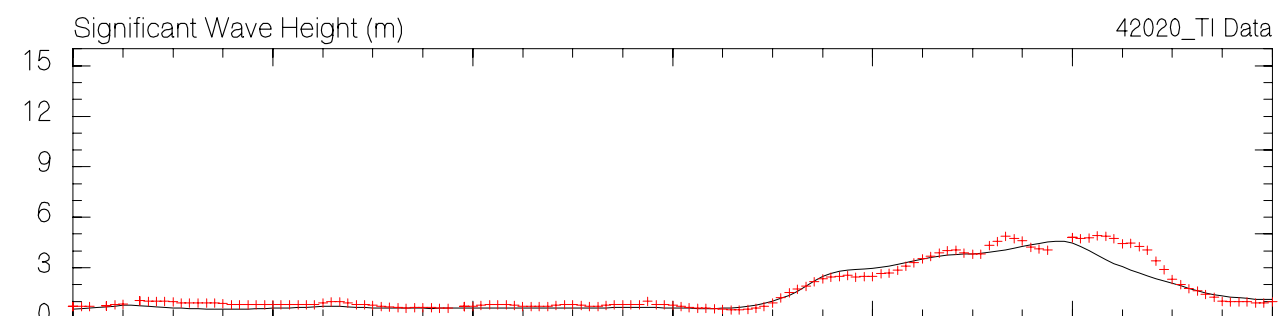
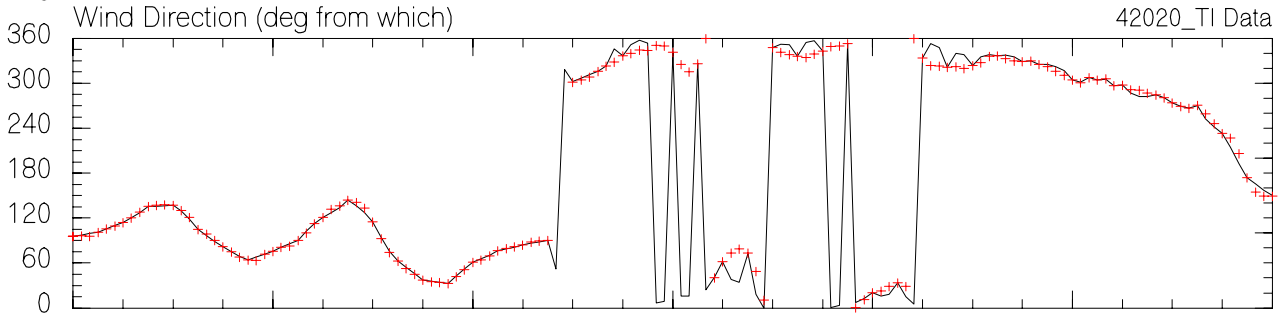
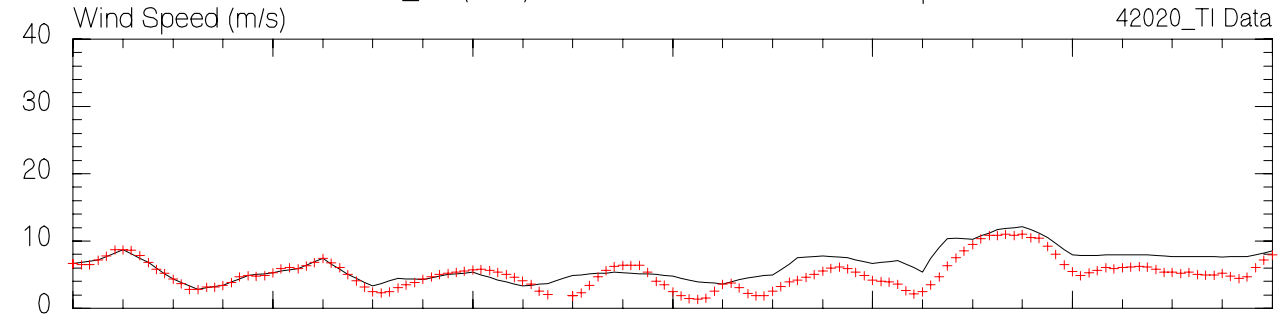
MMS Hurricane Katrina/Rita Hindcast  
Measured vs. Hindcast Winds and Waves at 42002  
2005\_18 (Rita) GOM3Min Grid - Variable Depths



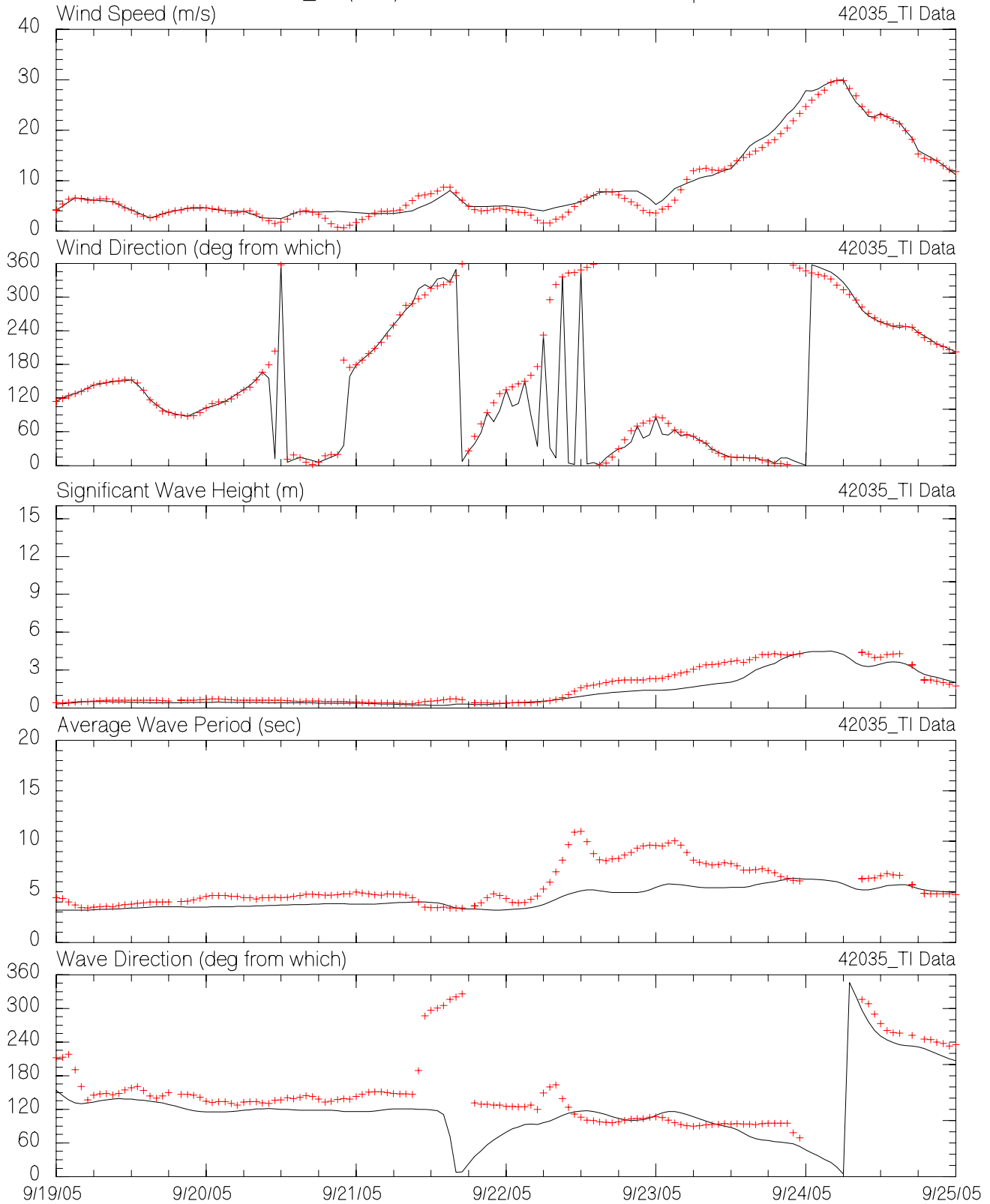
MMS Hurricane Katrina/Rita Hindcast  
Measured vs. Hindcast Winds and Waves at 42019  
2005\_18 (Rita) GOM3Min Grid - Variable Depths



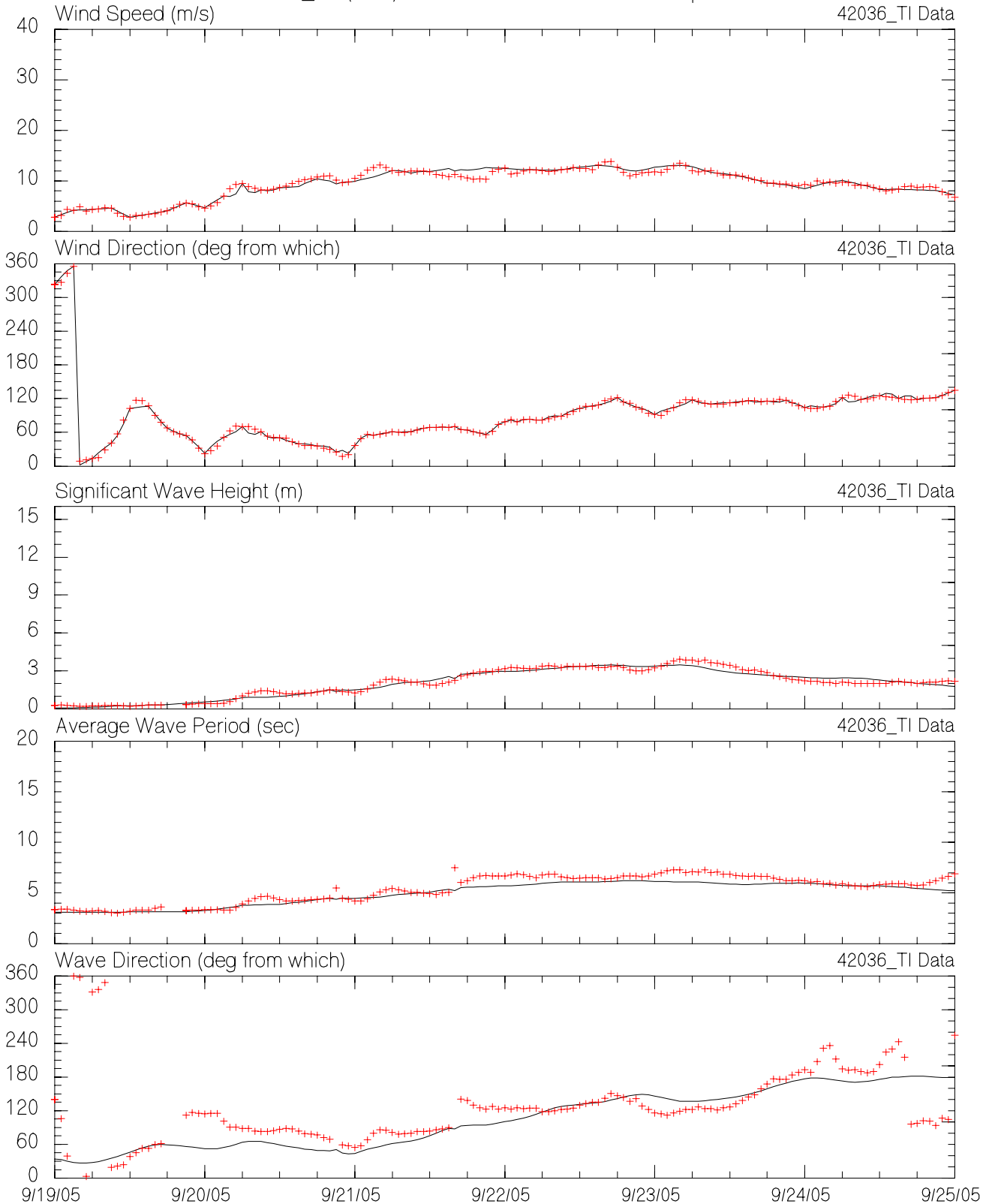
MMS Hurricane Katrina/Rita Hindcast  
Measured vs. Hindcast Winds and Waves at 42020  
2005\_18 (Rita) GOM3Min Grid - Variable Depths



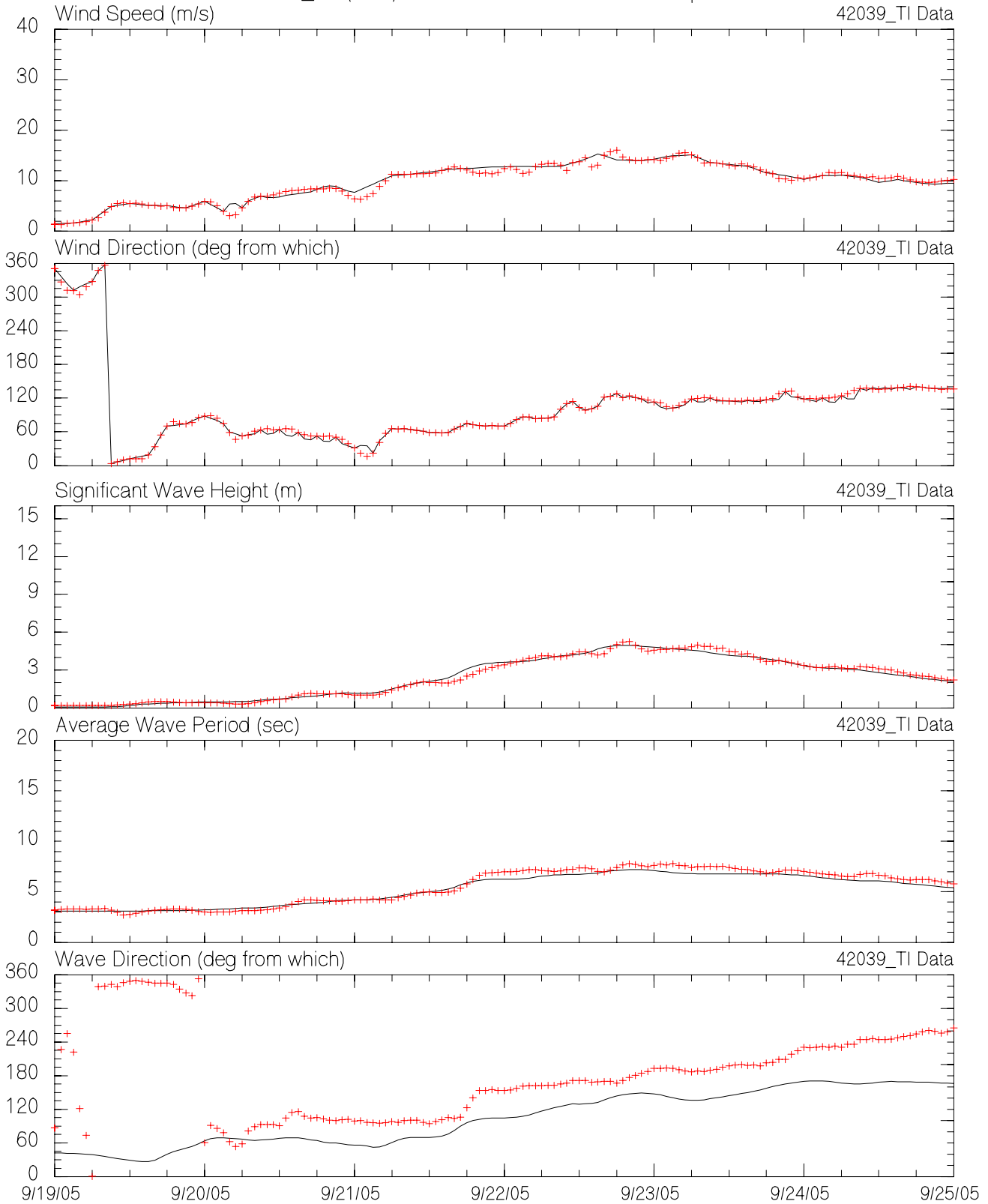
MMS Hurricane Katrina/Rita Hindcast  
Measured vs. Hindcast Winds and Waves at 42035  
2005\_18 (Rita) GOM3Min Grid - Variable Depths



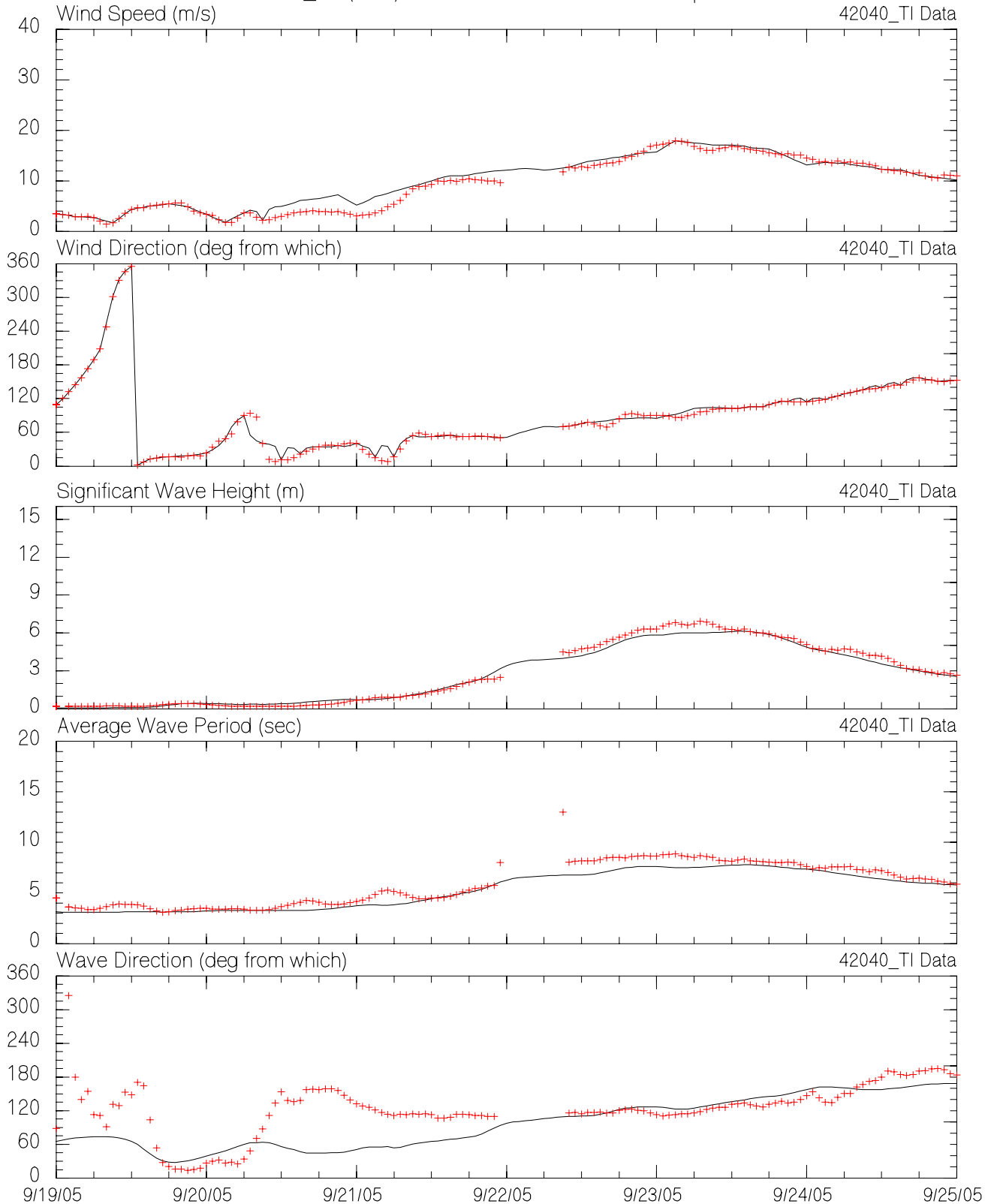
MMS Hurricane Katrina/Rita Hindcast  
Measured vs. Hindcast Winds and Waves at 42036  
2005\_18 (Rita) GOM3Min Grid - Variable Depths



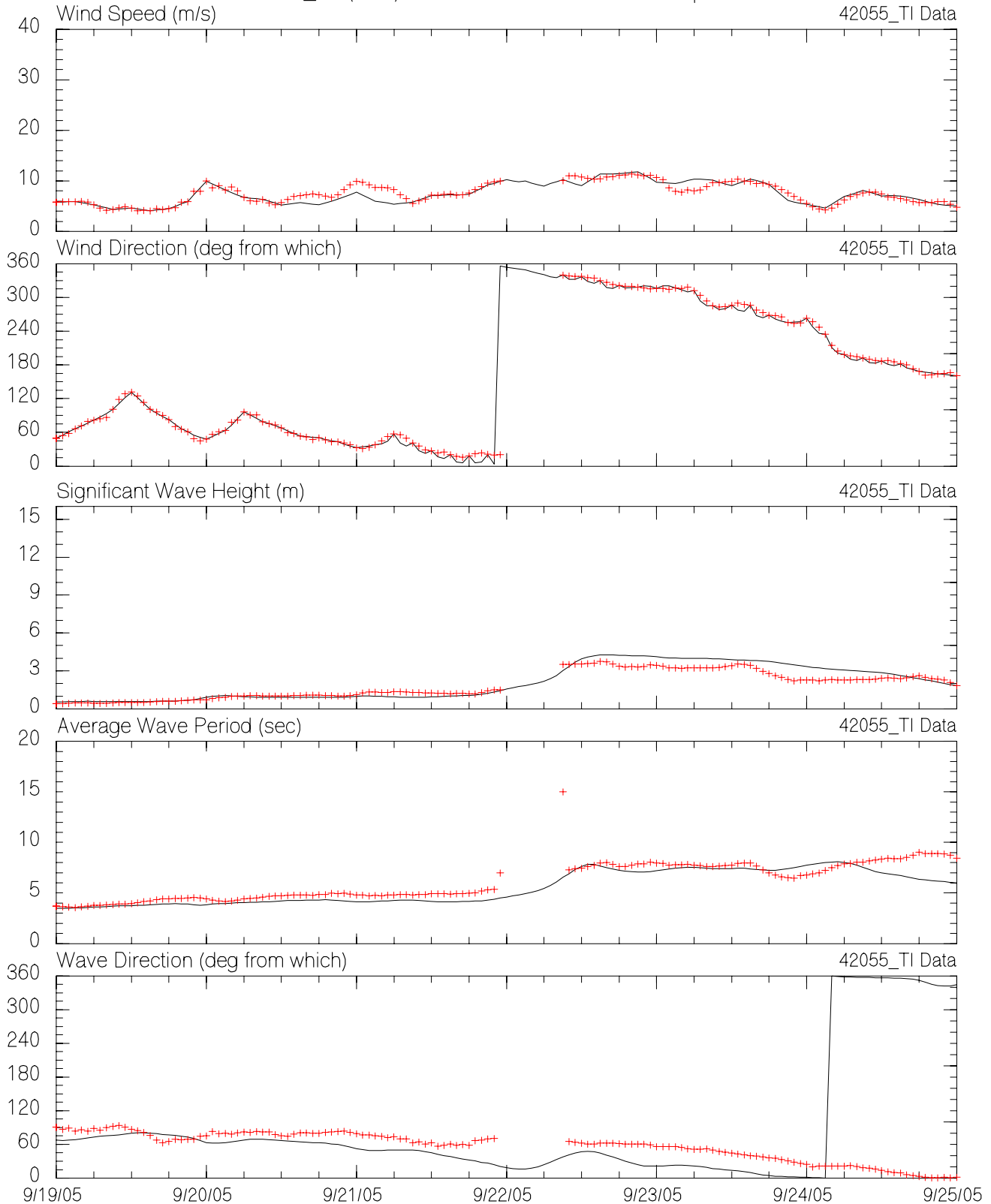
MMS Hurricane Katrina/Rita Hindcast  
Measured vs. Hindcast Winds and Waves at 42039  
2005\_18 (Rita) GOM3Min Grid - Variable Depths



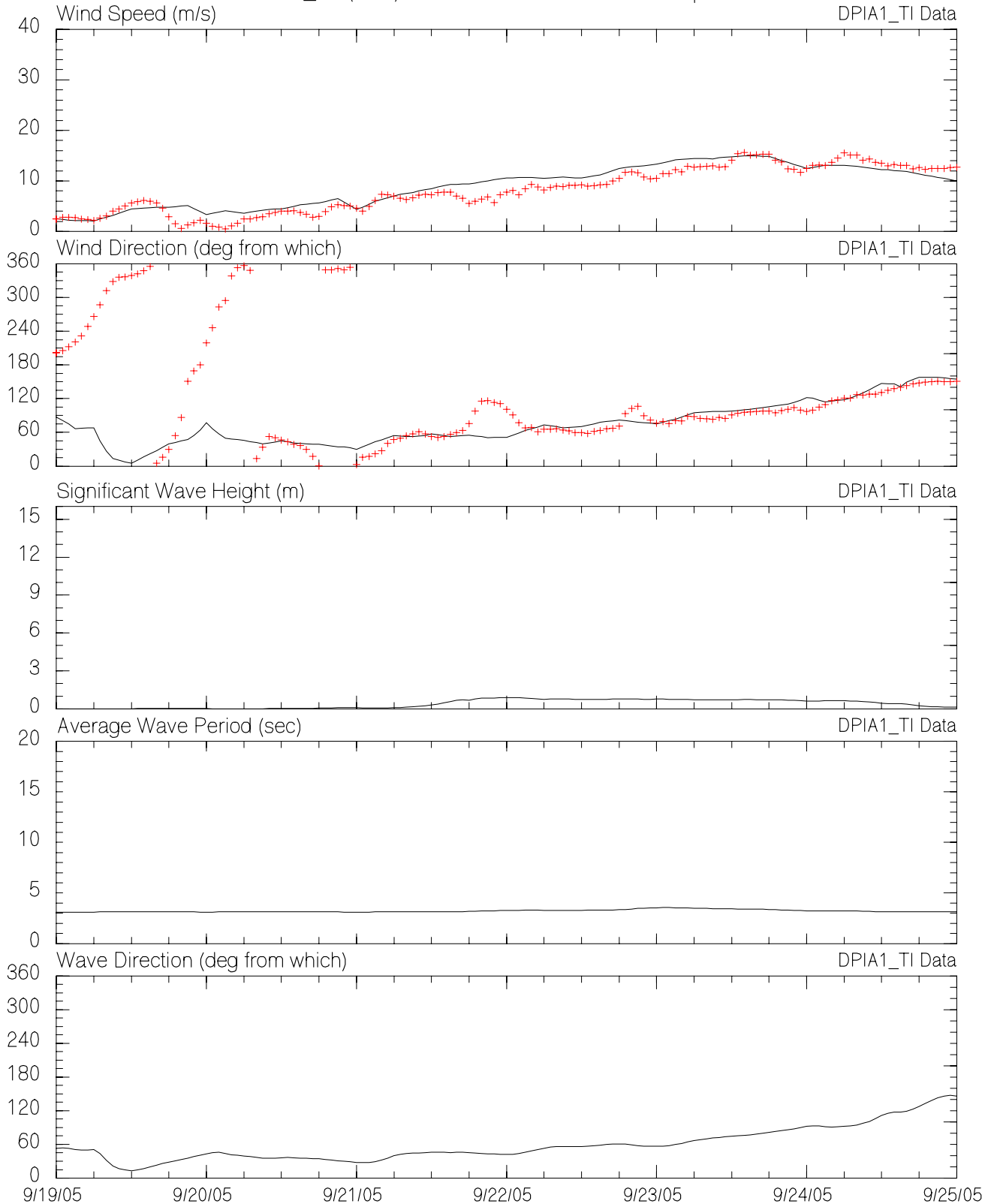
MMS Hurricane Katrina/Rita Hindcast  
Measured vs. Hindcast Winds and Waves at 42040  
2005\_18 (Rita) GOM3Min Grid - Variable Depths



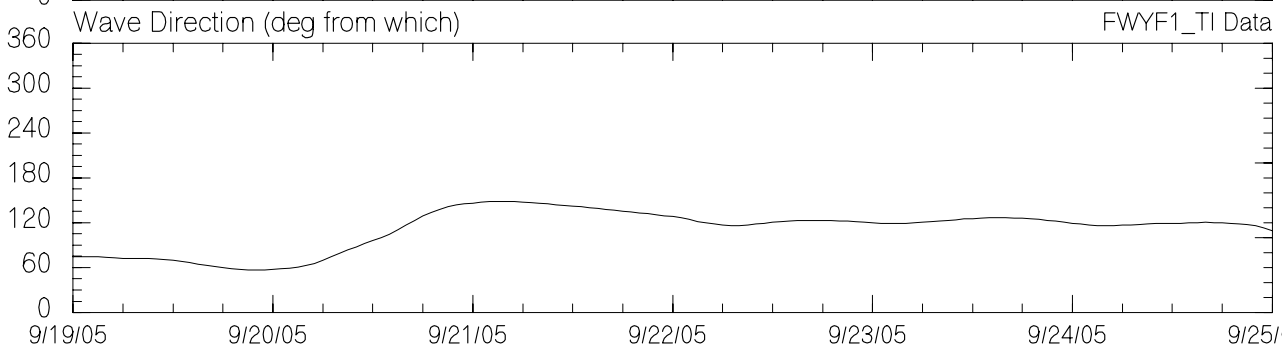
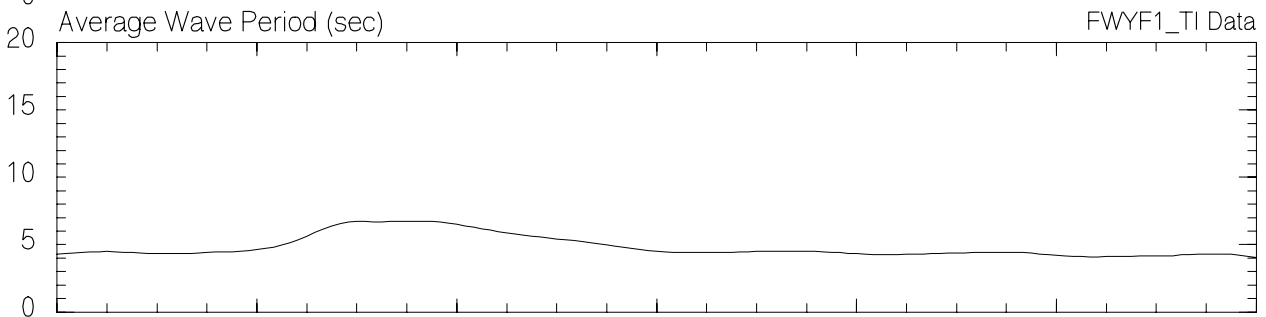
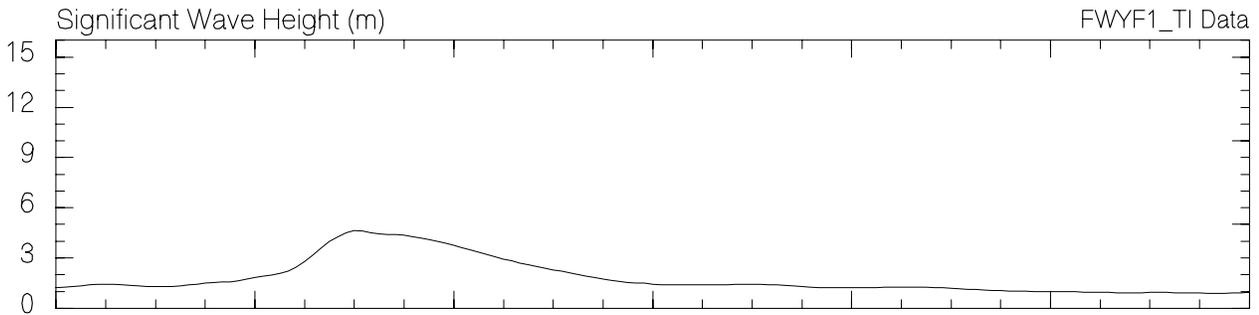
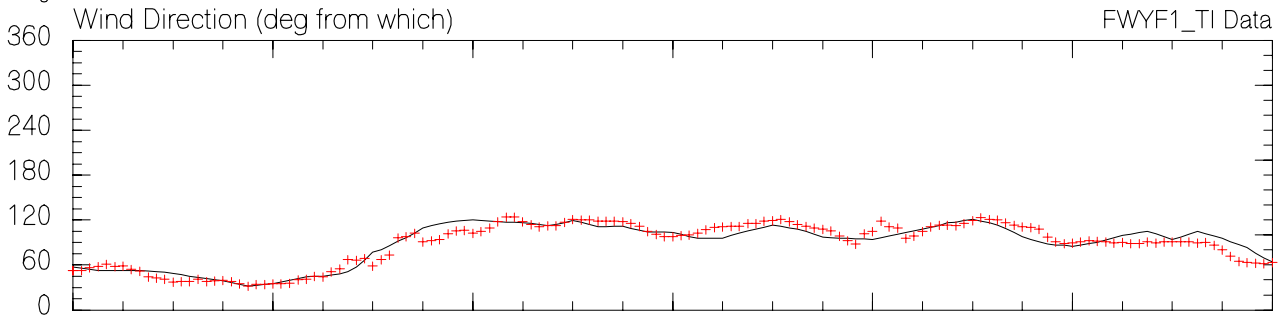
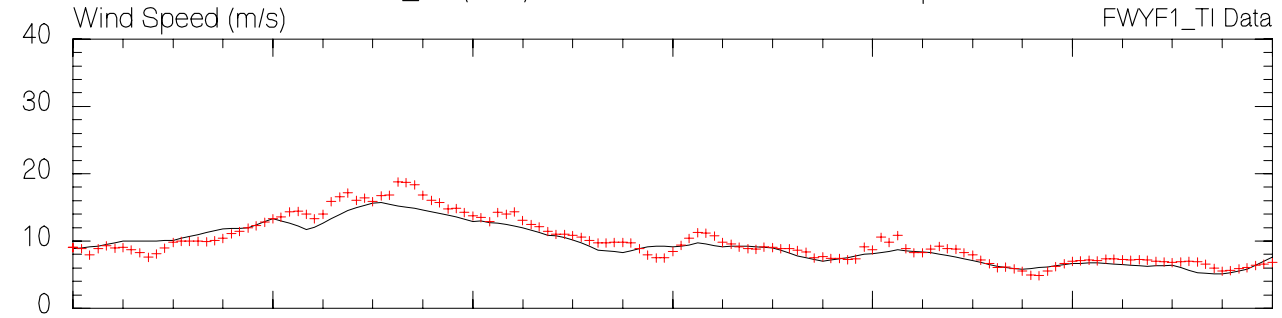
MMS Hurricane Katrina/Rita Hindcast  
Measured vs. Hindcast Winds and Waves at 42055  
2005\_18 (Rita) GOM3Min Grid - Variable Depths



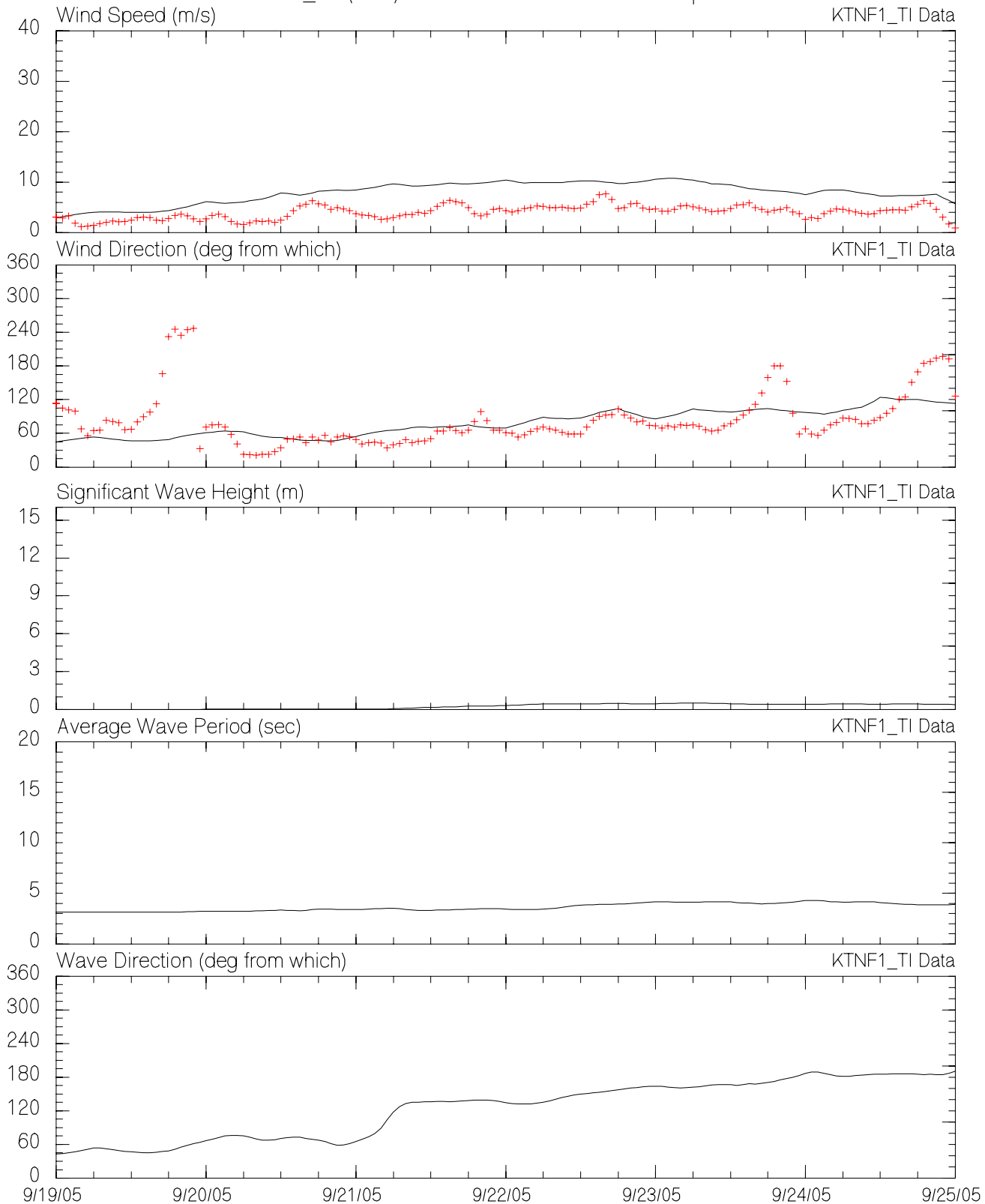
MMS Hurricane Katrina/Rita Hindcast  
Measured vs. Hindcast Winds and Waves at DPIA1  
2005\_18 (Rita) GOM3Min Grid - Variable Depths



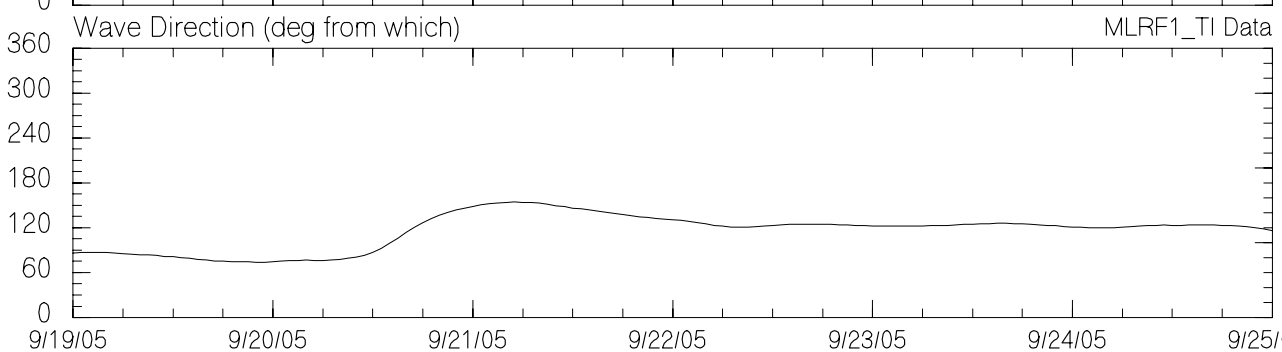
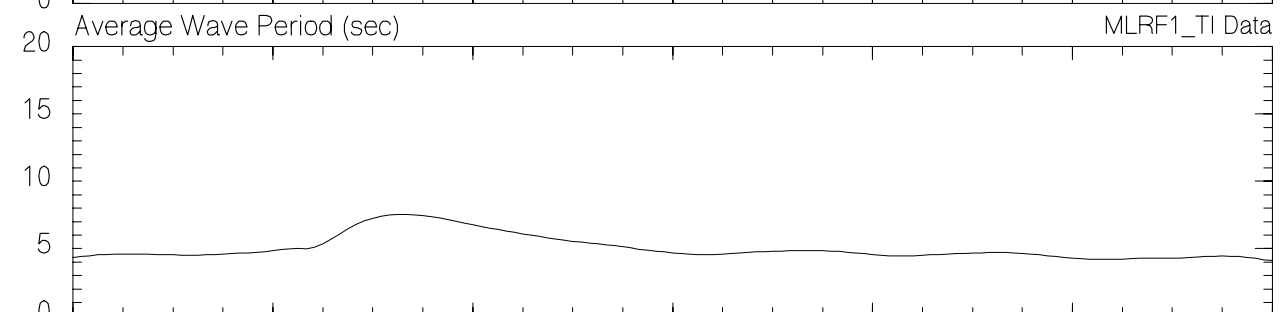
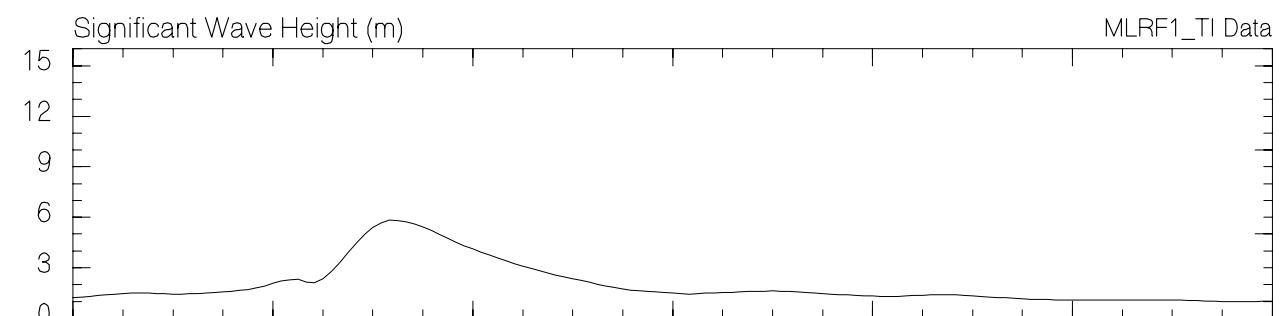
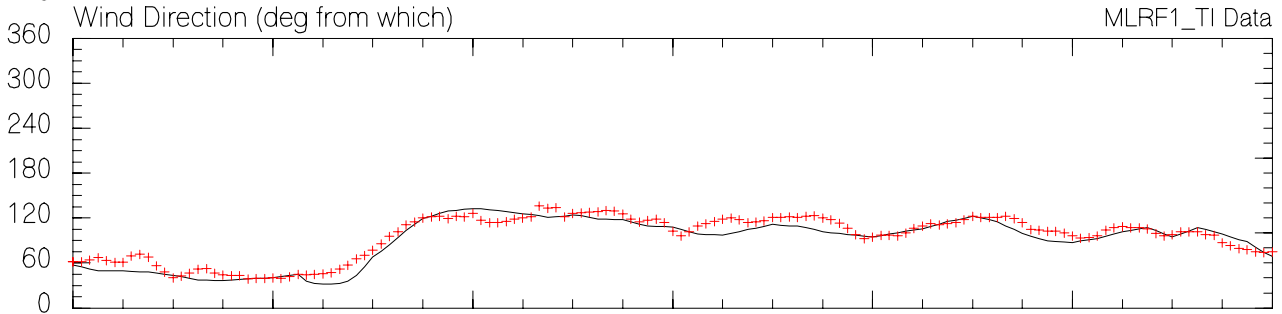
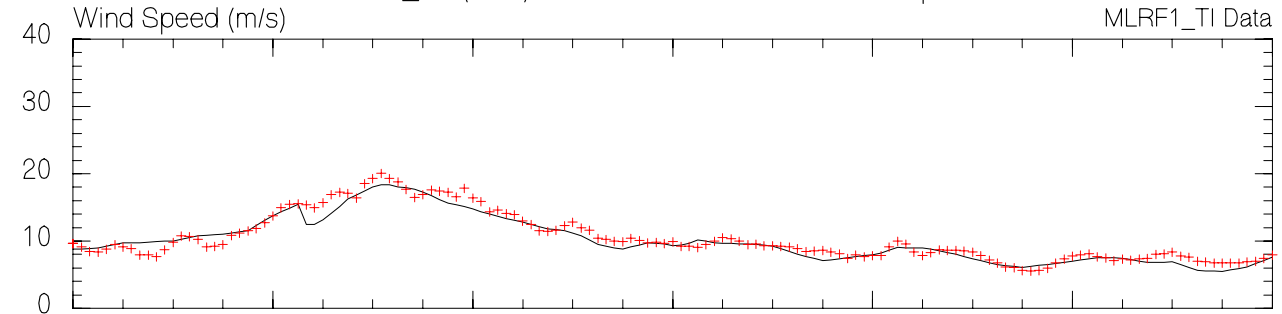
MMS Hurricane Katrina/Rita Hindcast  
Measured vs. Hindcast Winds and Waves at FWYF1  
2005\_18 (Rita) GOM3Min Grid - Variable Depths



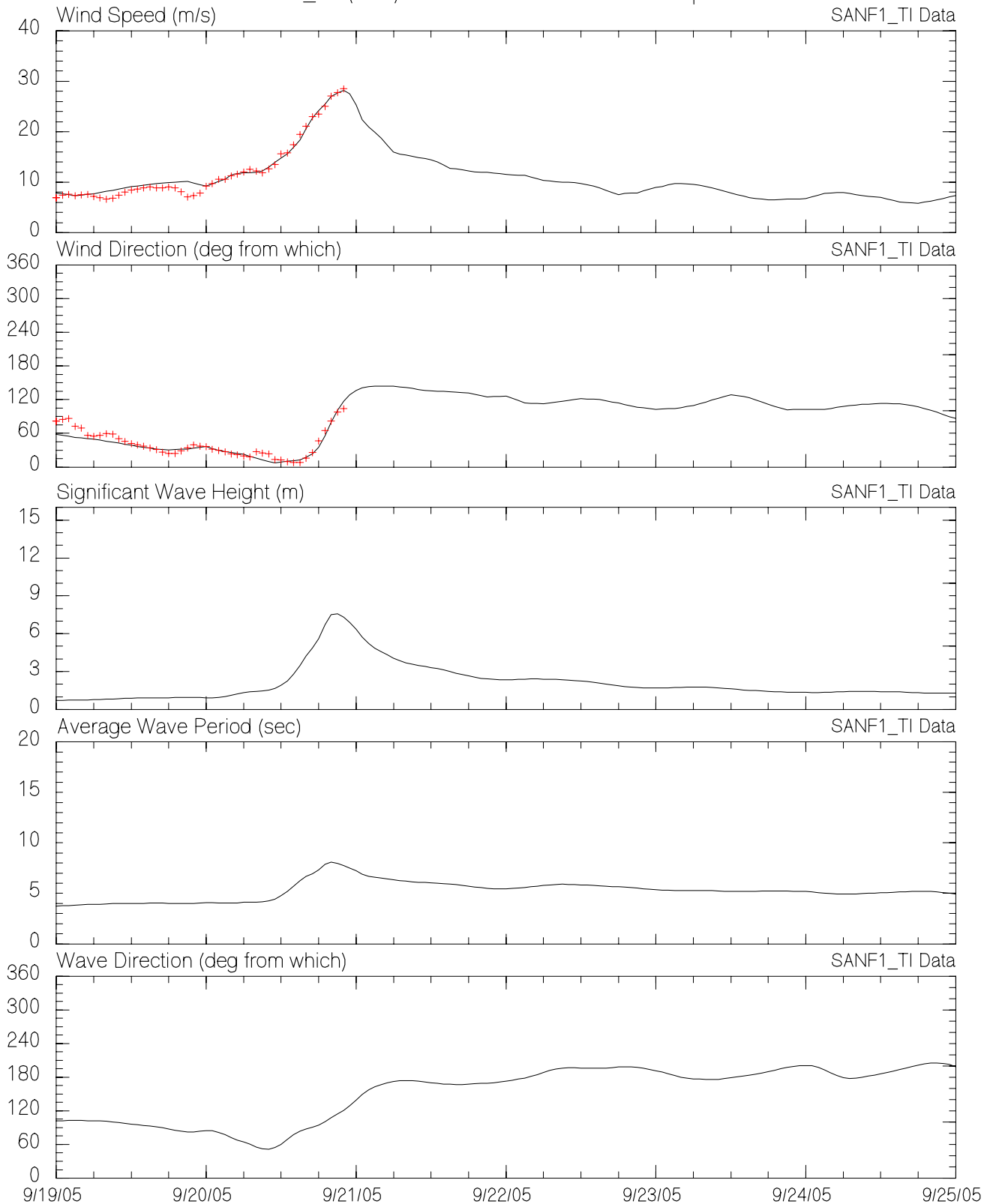
MMS Hurricane Katrina/Rita Hindcast  
Measured vs. Hindcast Winds and Waves at KTNF1  
2005\_18 (Rita) GOM3Min Grid - Variable Depths



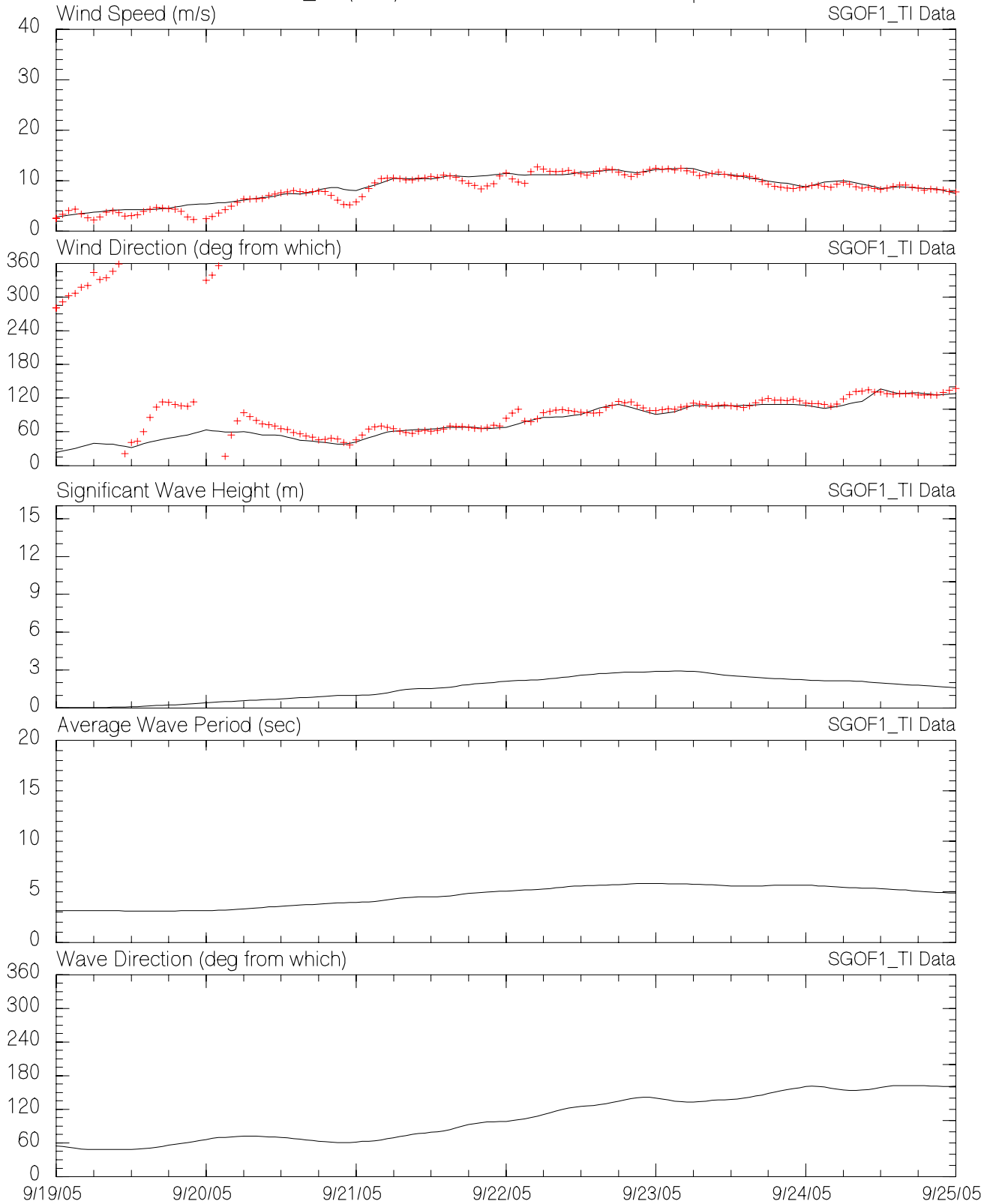
MMS Hurricane Katrina/Rita Hindcast  
Measured vs. Hindcast Winds and Waves at MLRF1  
2005\_18 (Rita) GOM3Min Grid - Variable Depths



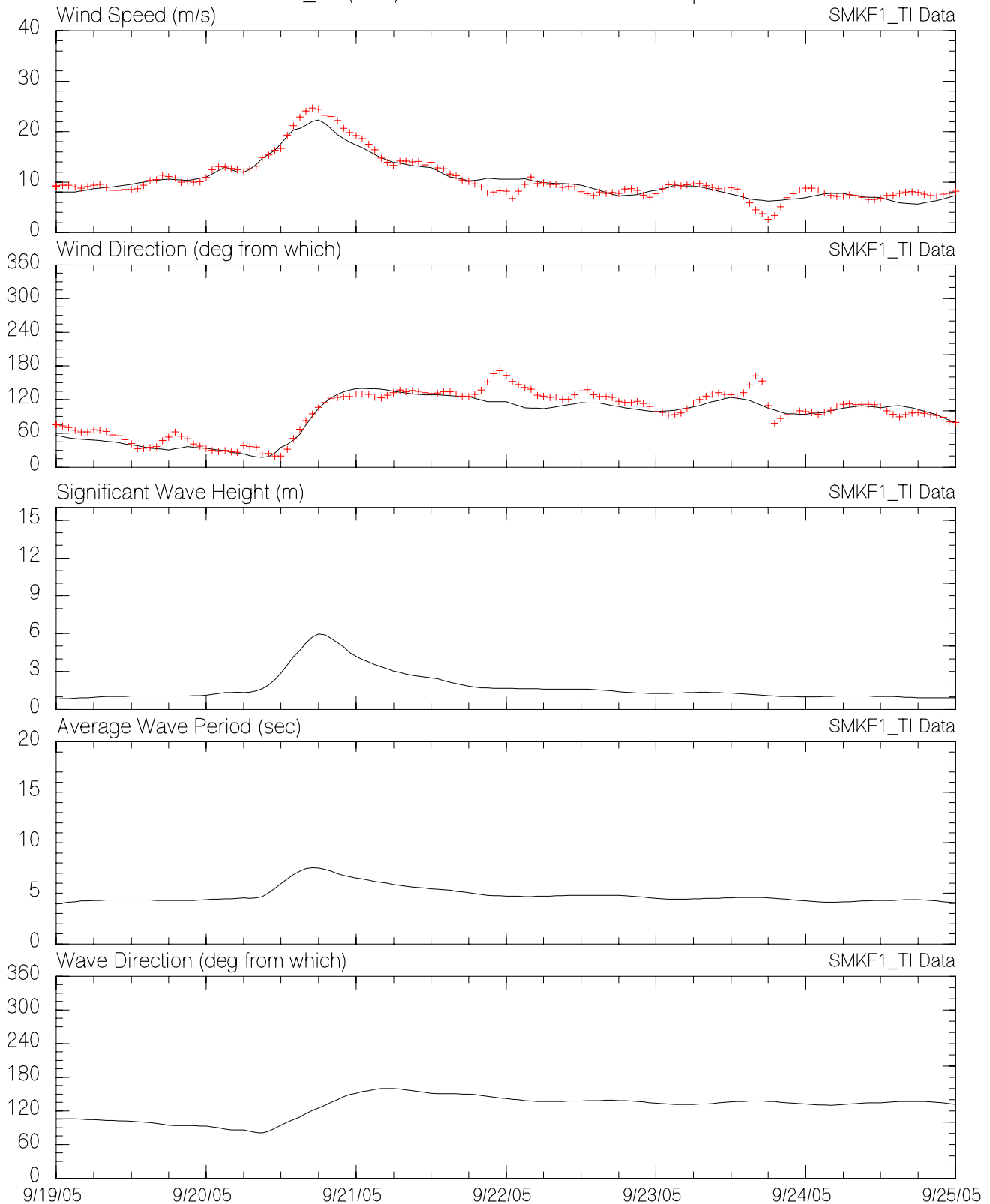
MMS Hurricane Katrina/Rita Hindcast  
Measured vs. Hindcast Winds and Waves at SANF1  
2005\_18 (Rita) GOM3Min Grid - Variable Depths



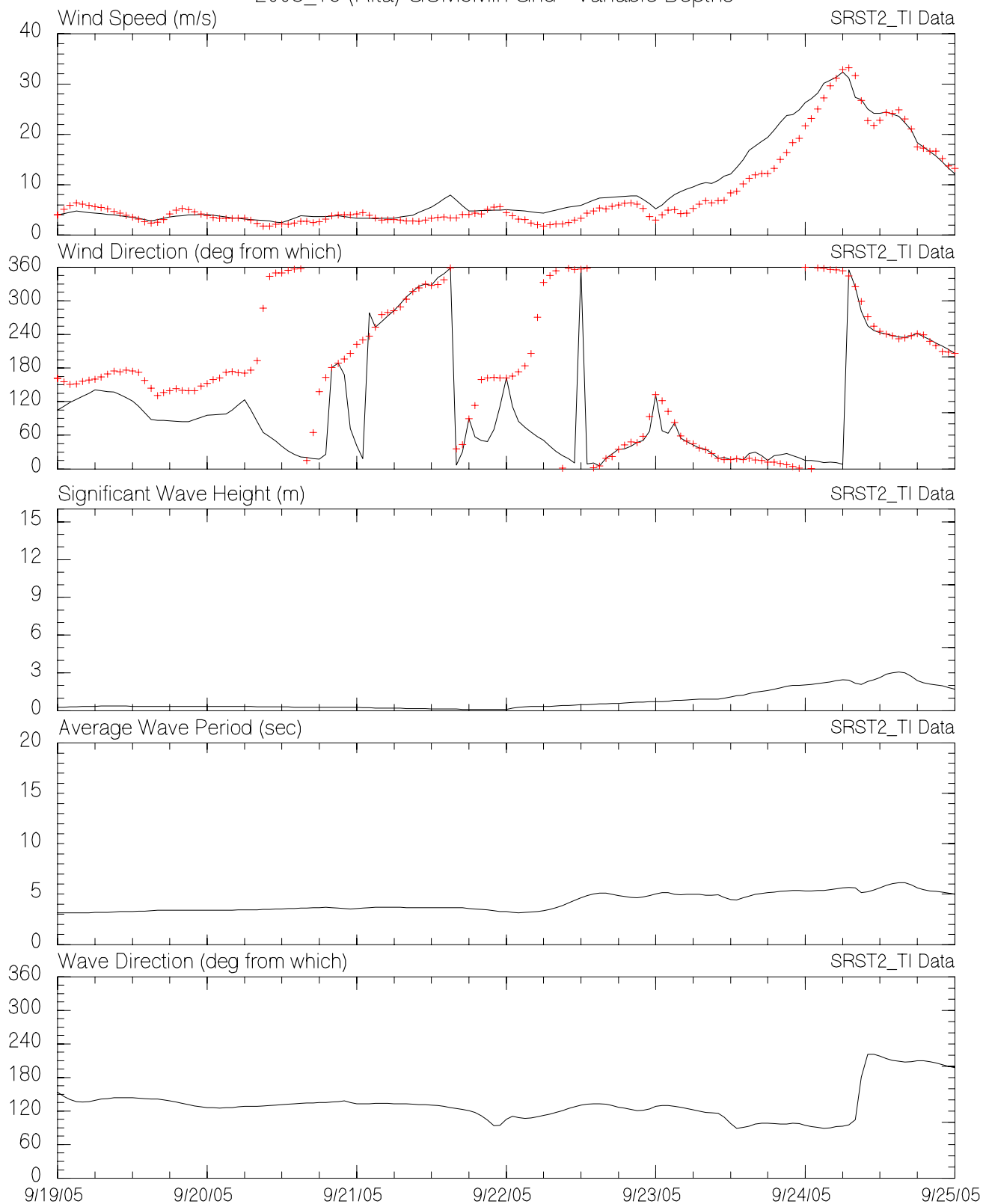
MMS Hurricane Katrina/Rita Hindcast  
Measured vs. Hindcast Winds and Waves at SGOF1  
2005\_18 (Rita) GOM3Min Grid - Variable Depths



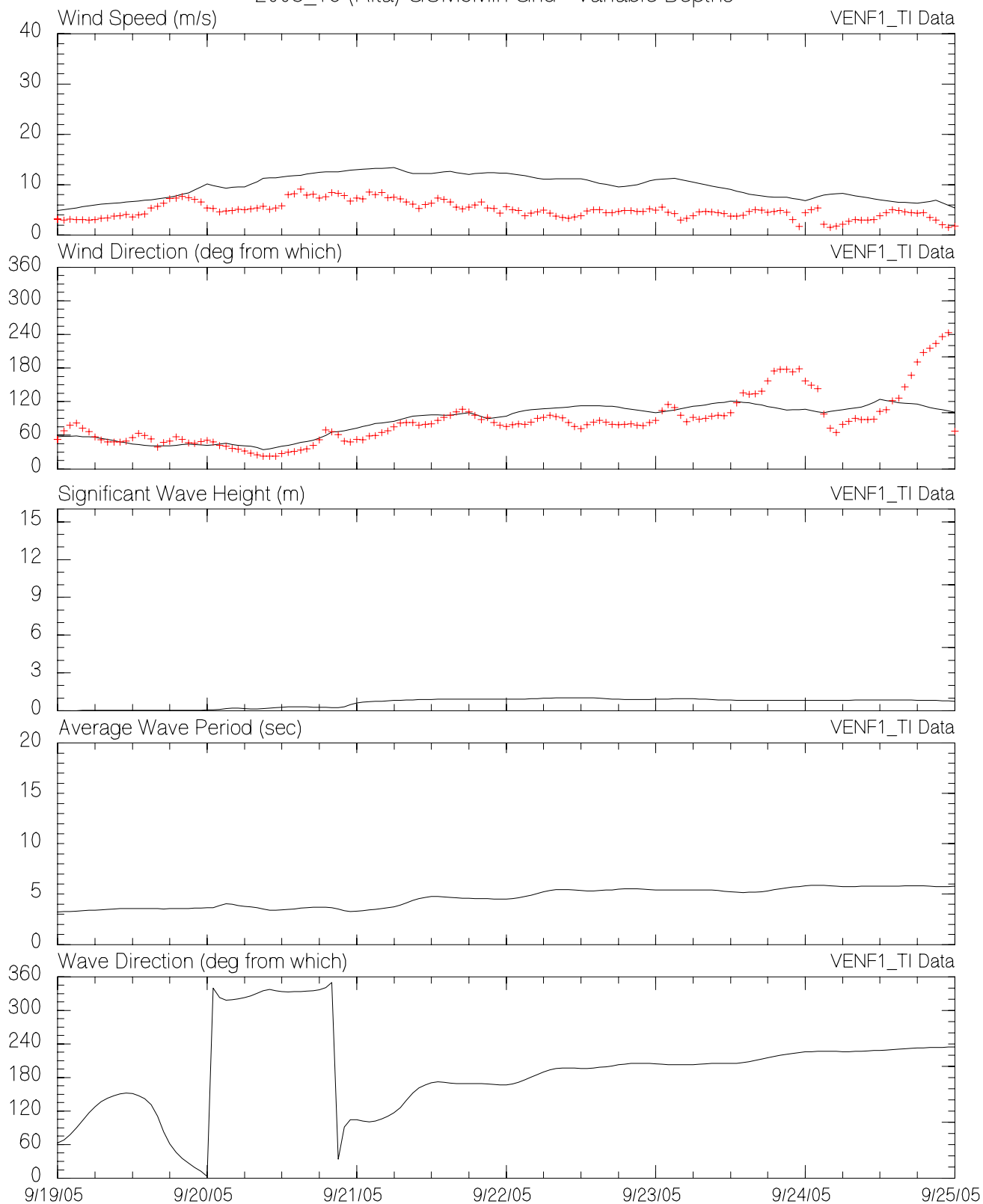
MMS Hurricane Katrina/Rita Hindcast  
Measured vs. Hindcast Winds and Waves at SMKF1  
2005\_18 (Rita) GOM3Min Grid - Variable Depths



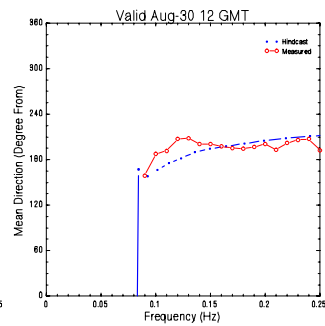
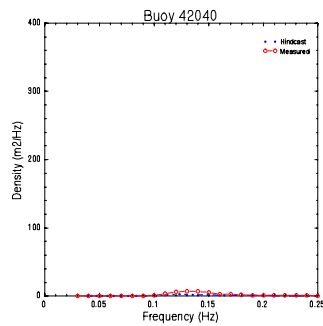
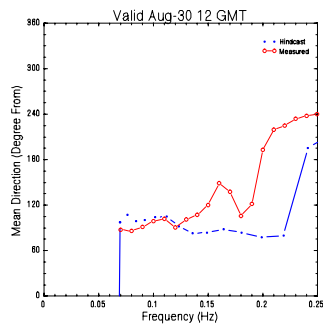
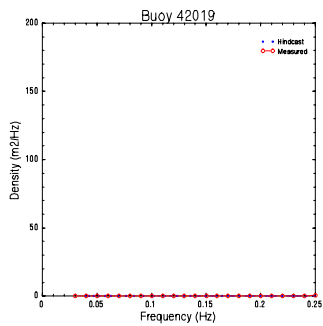
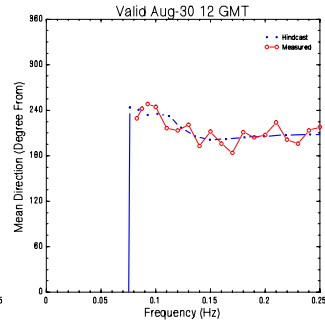
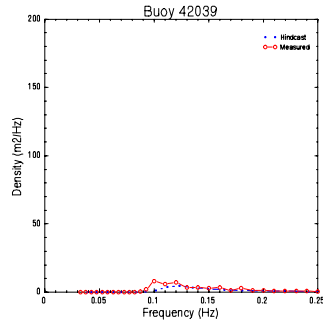
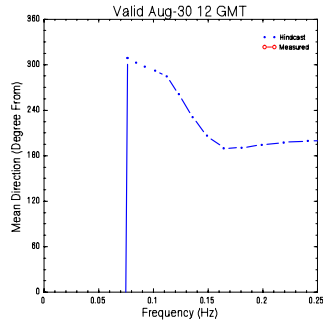
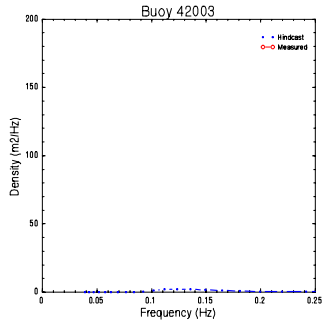
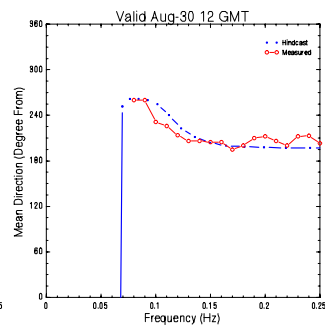
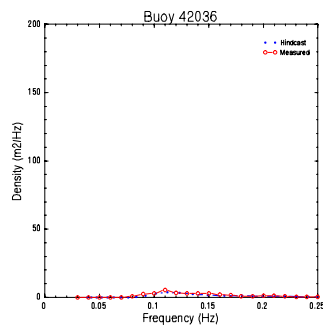
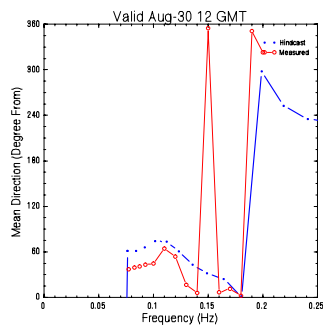
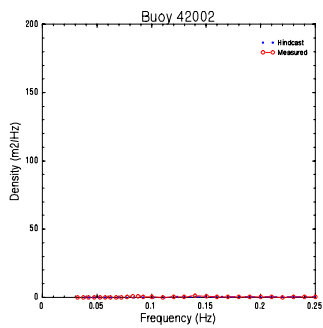
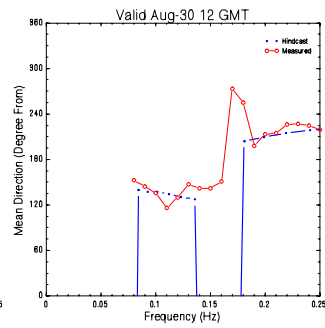
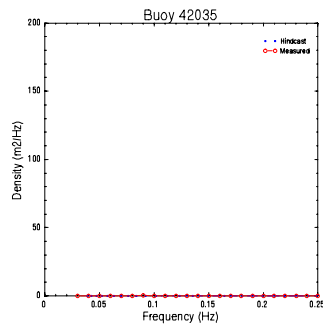
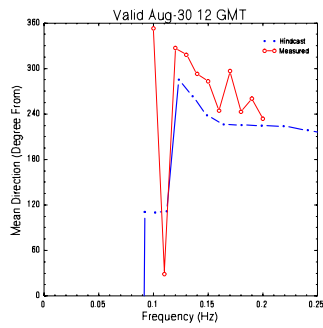
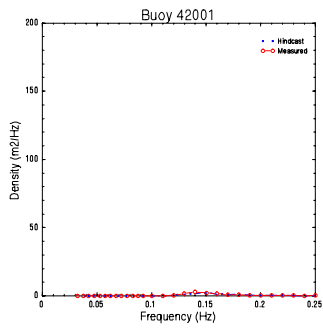
MMS Hurricane Katrina/Rita Hindcast  
Measured vs. Hindcast Winds and Waves at SRST2  
2005\_18 (Rita) GOM3Min Grid - Variable Depths

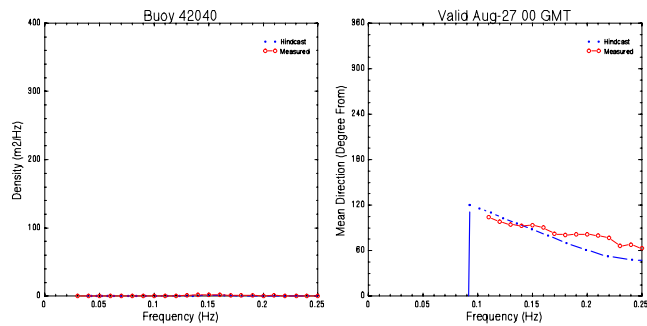
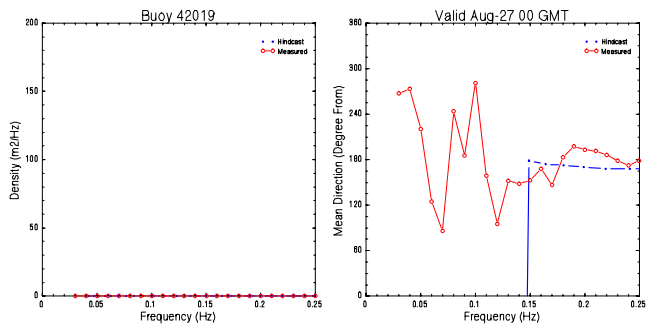
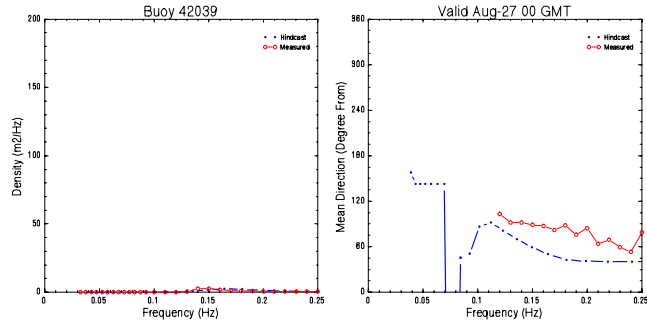
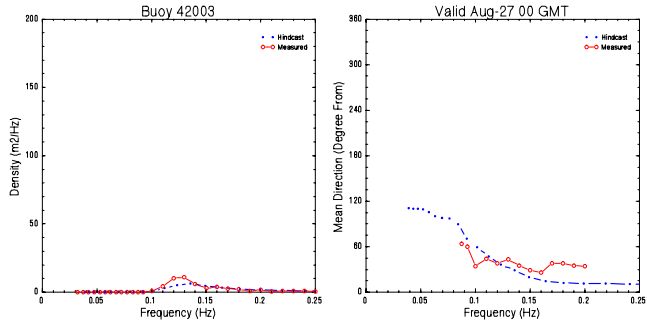
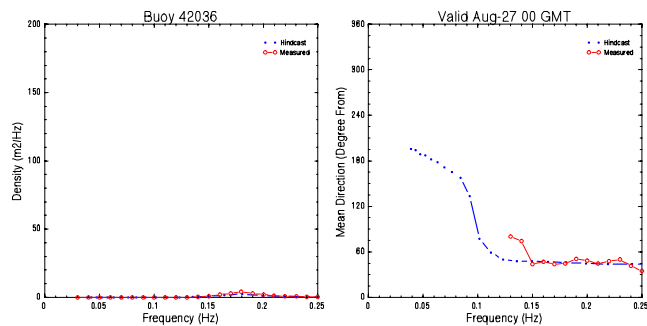
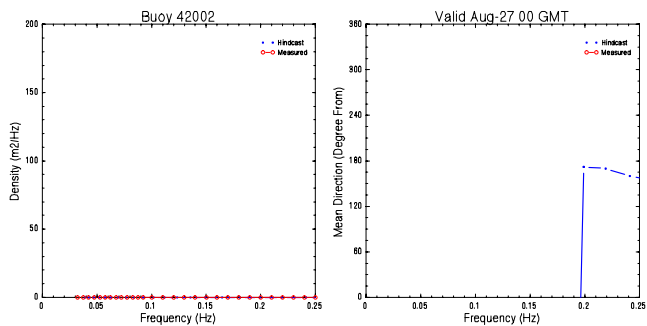
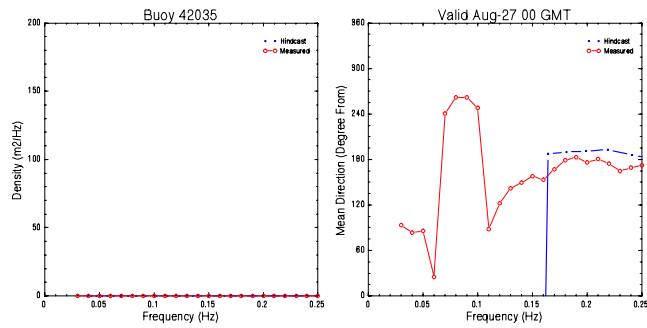
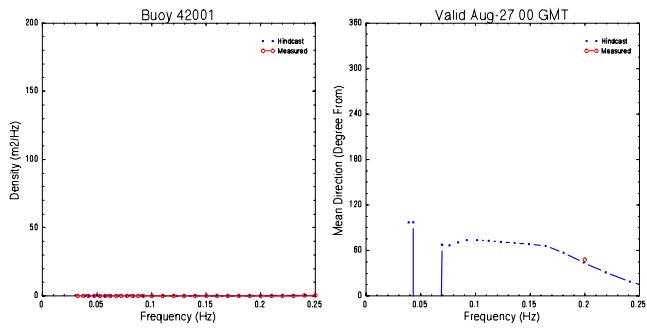


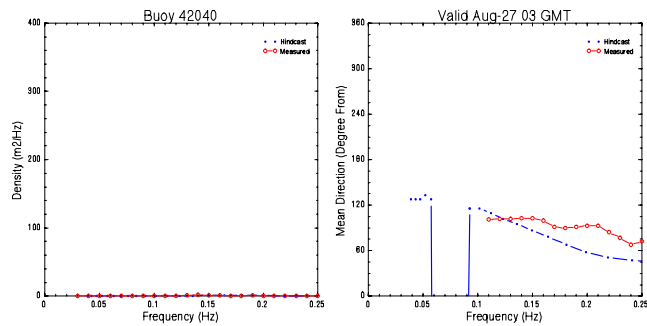
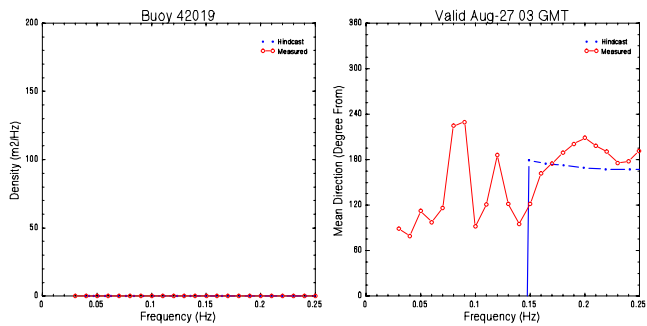
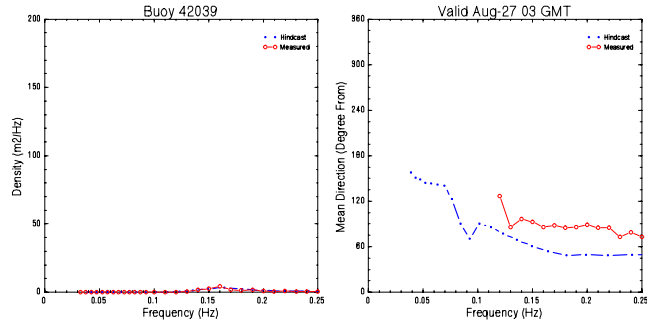
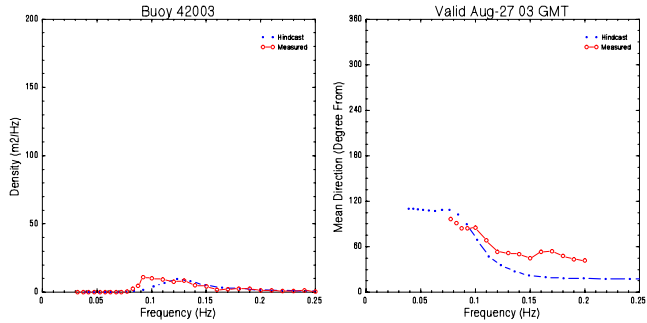
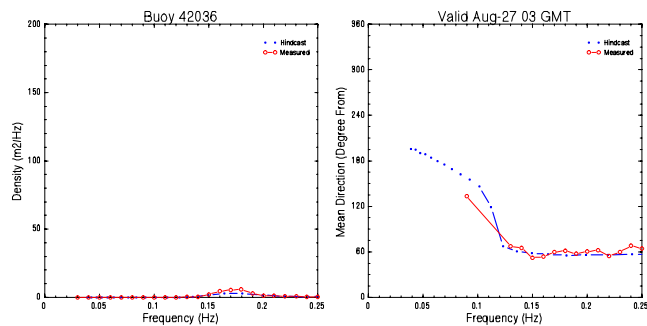
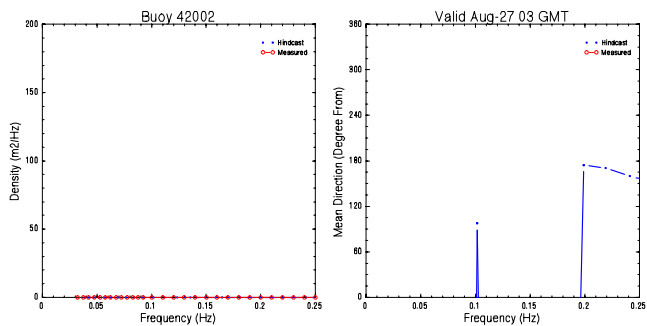
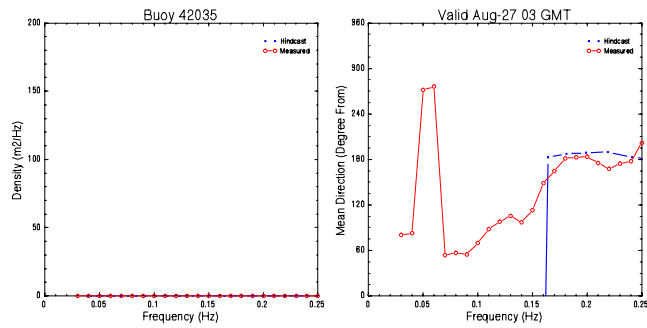
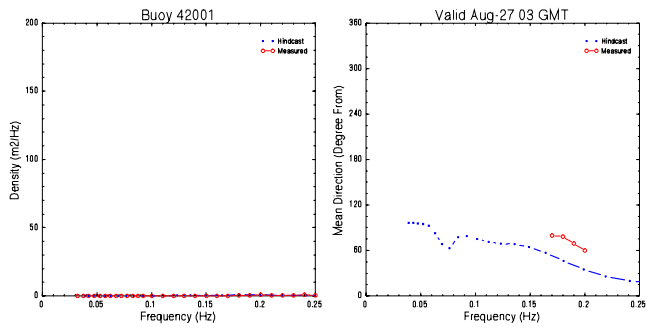
MMS Hurricane Katrina/Rita Hindcast  
Measured vs. Hindcast Winds and Waves at VENF1  
2005\_18 (Rita) GOM3Min Grid - Variable Depths



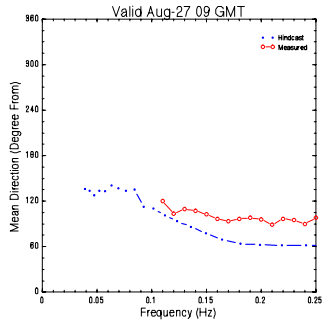
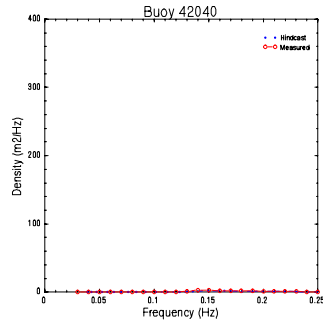
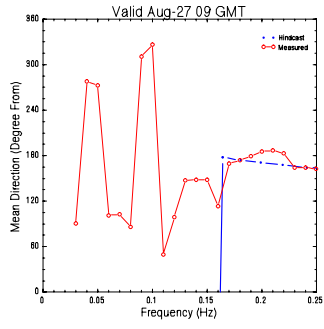
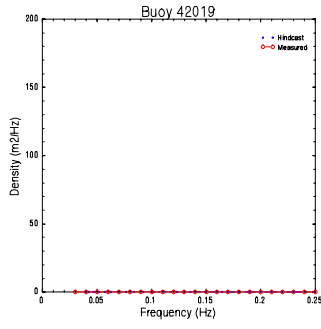
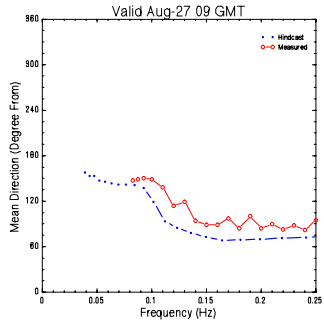
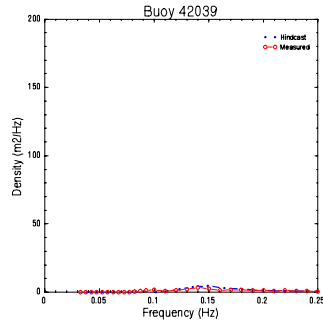
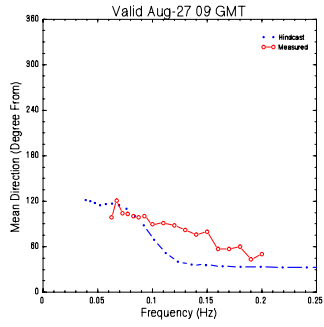
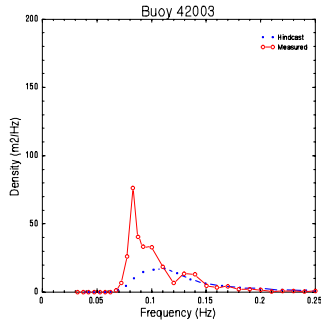
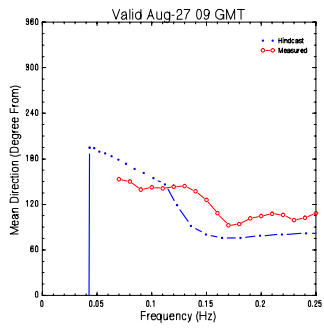
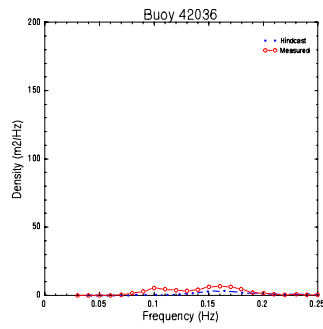
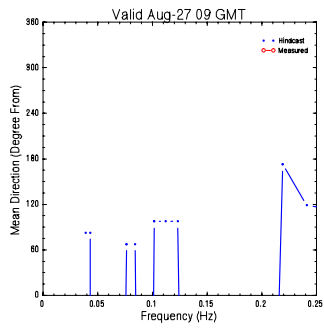
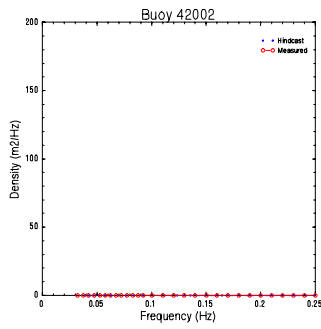
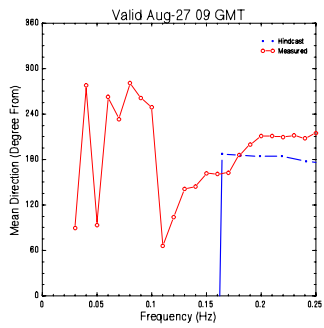
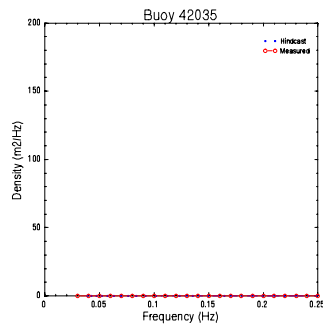
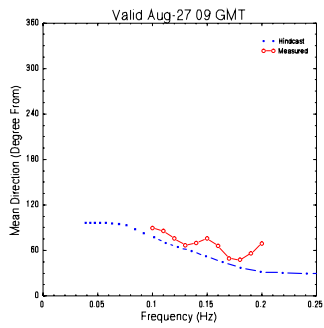
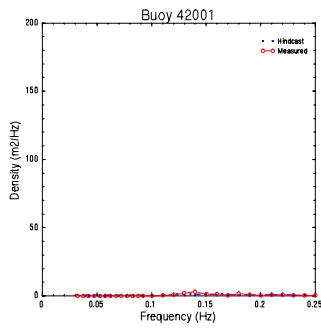
## **APPENDIX C Hindcast Wave Spectra at NDBC Buoys during Katrina**

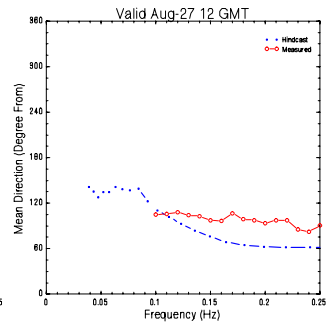
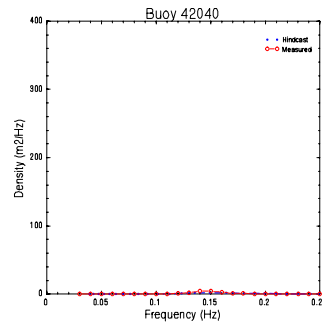
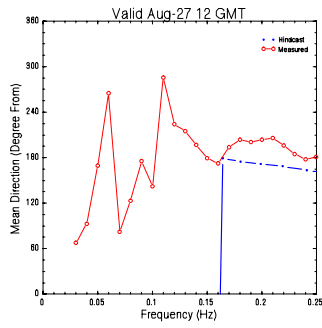
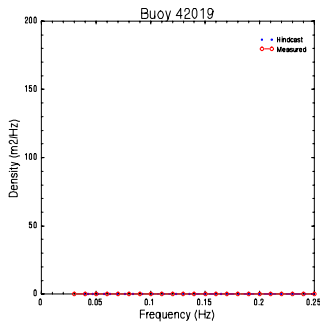
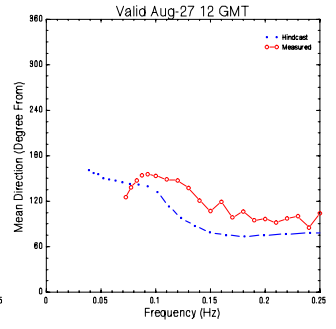
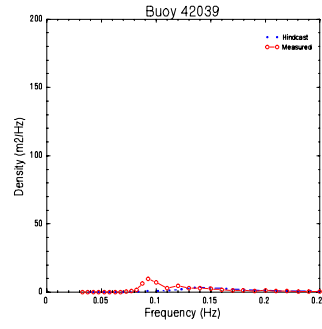
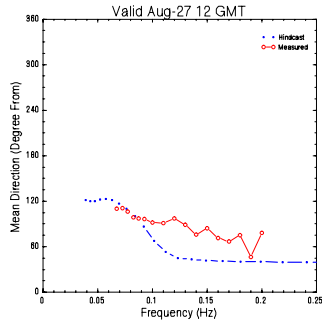
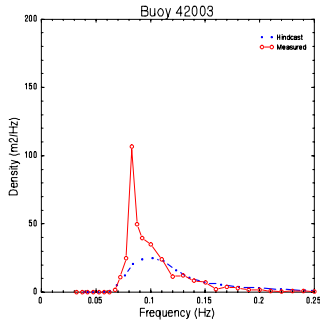
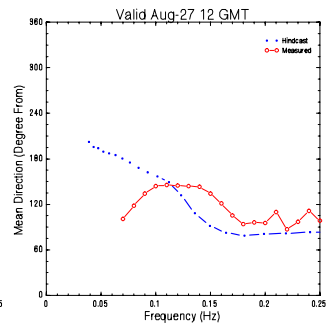
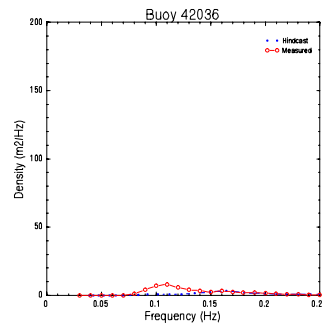
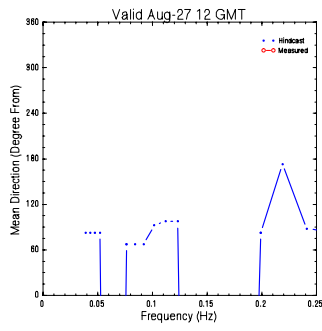
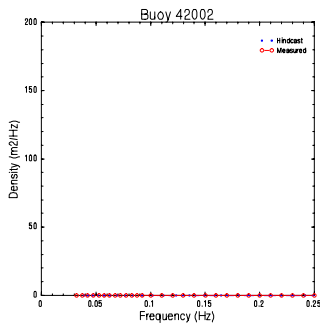
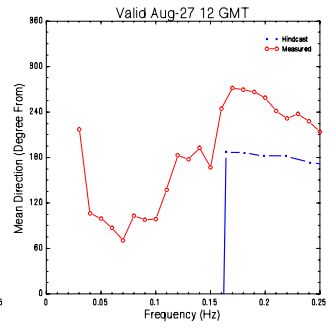
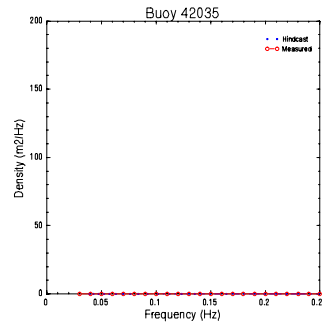
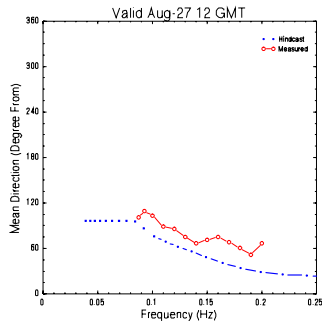
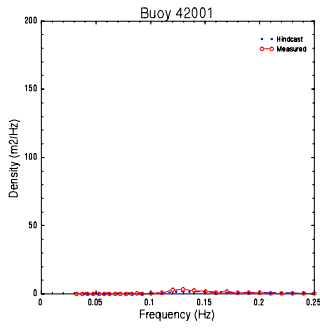


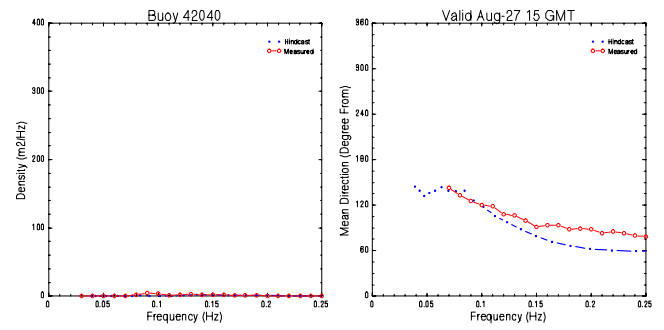
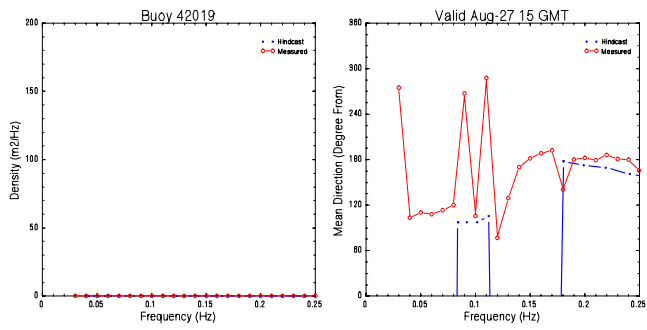
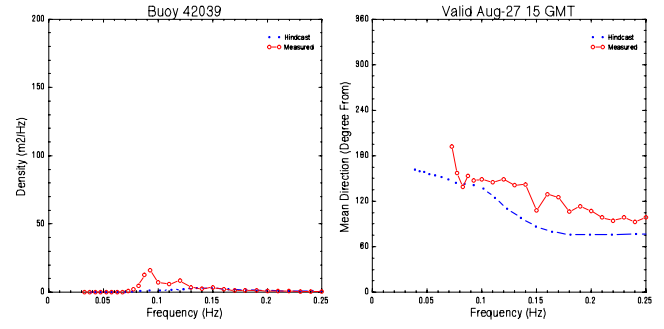
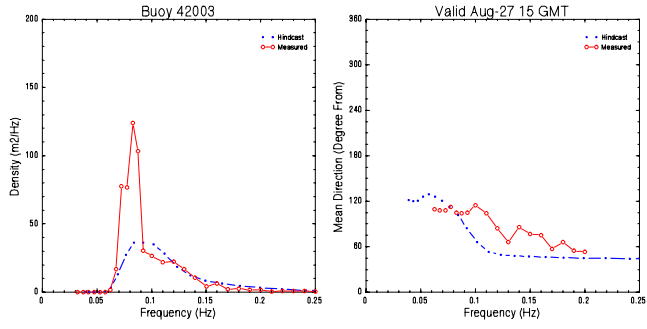
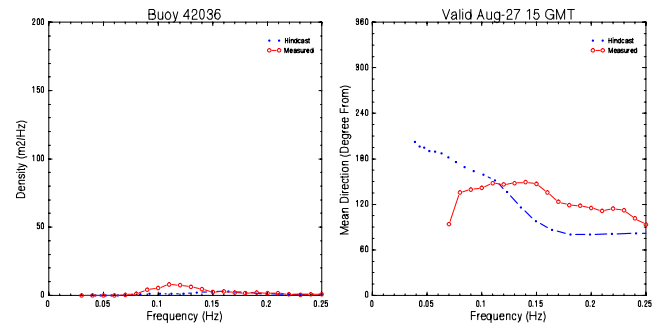
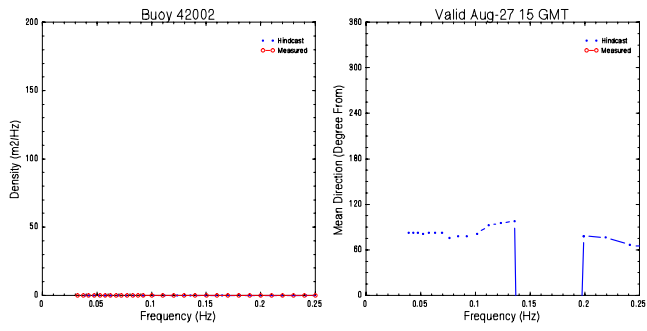
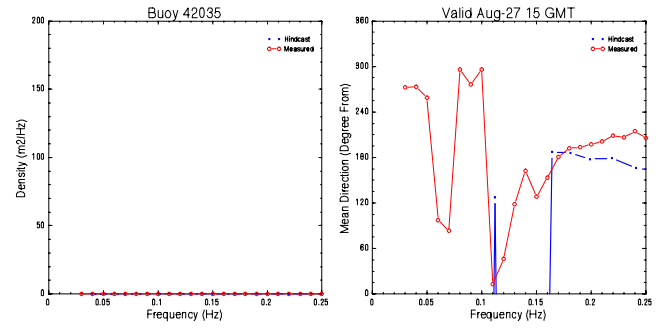
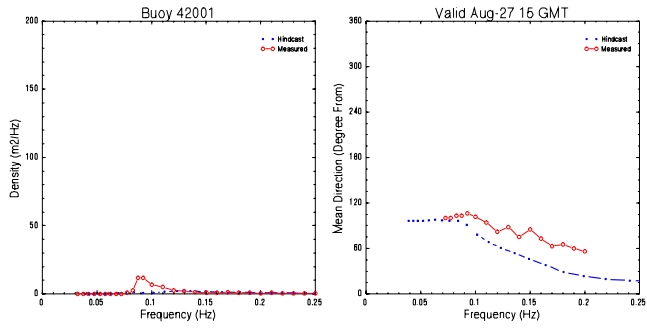


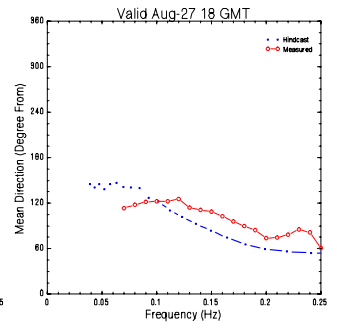
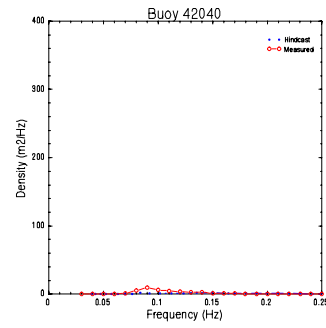
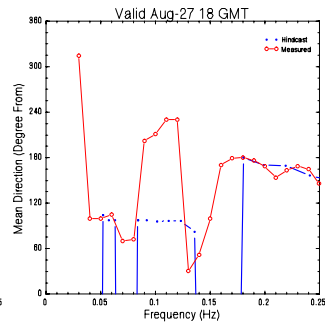
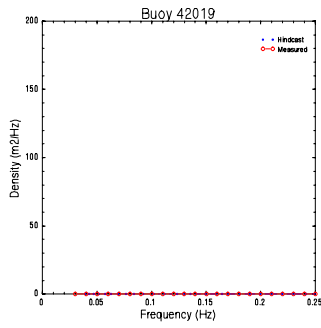
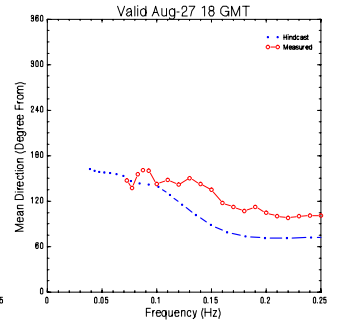
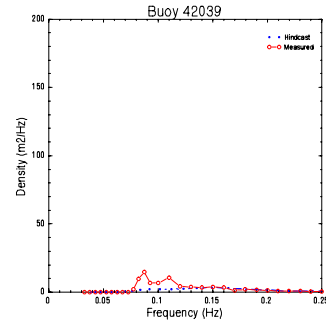
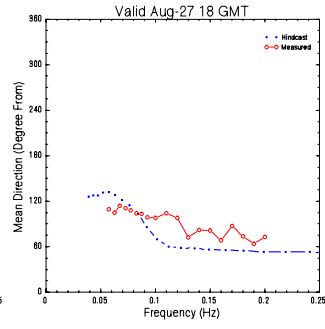
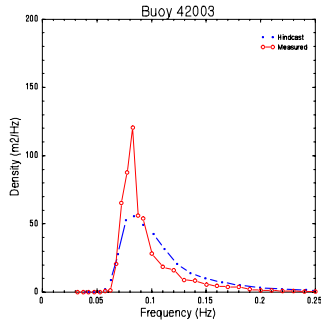
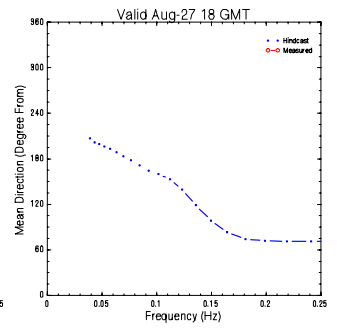
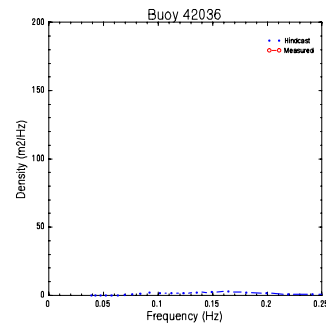
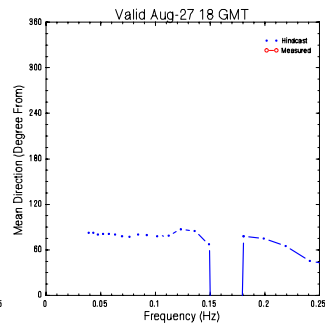
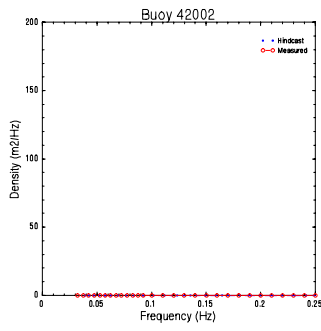
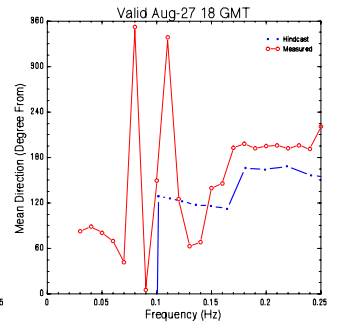
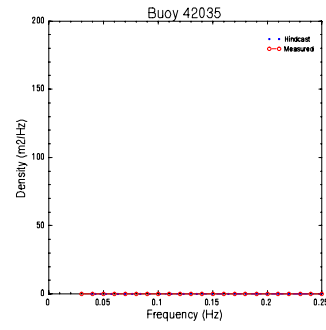
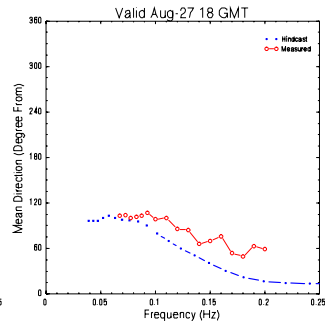
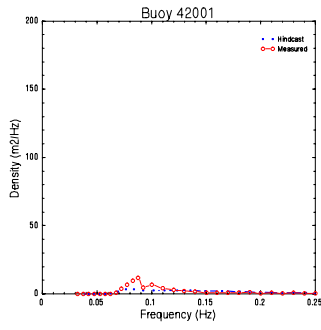


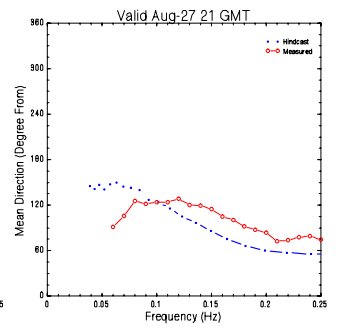
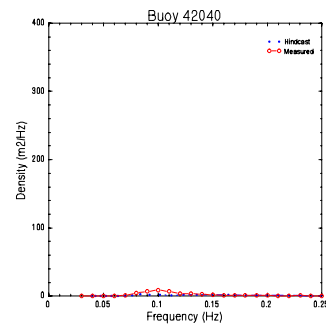
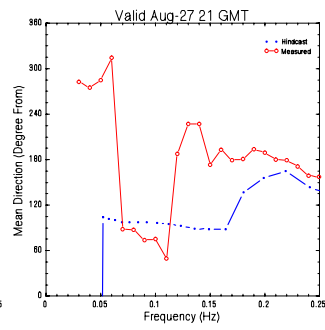
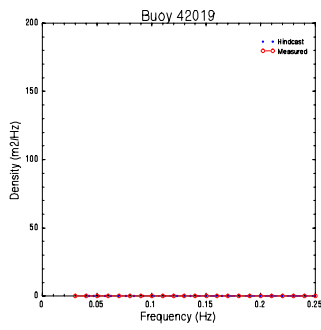
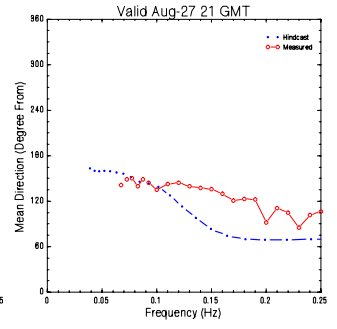
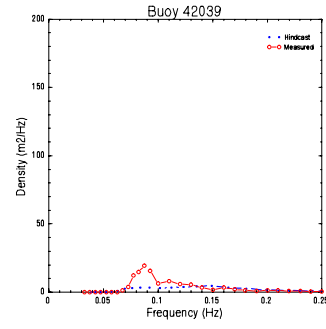
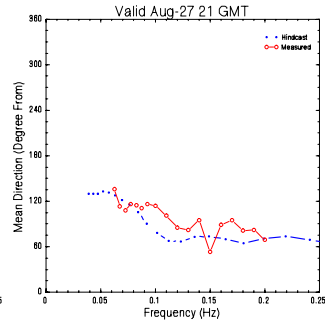
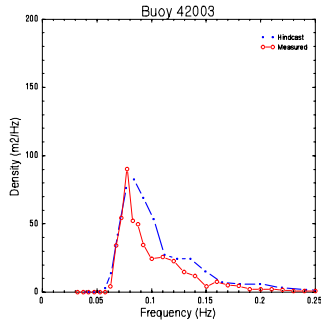
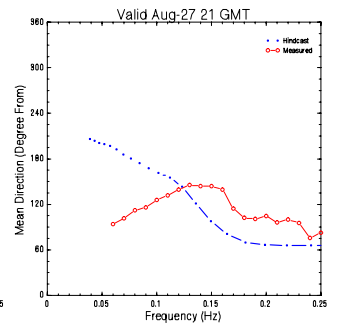
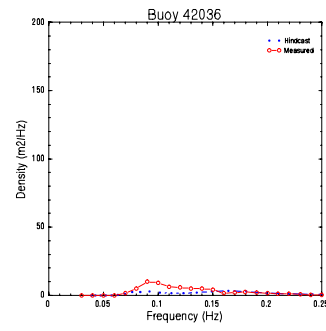
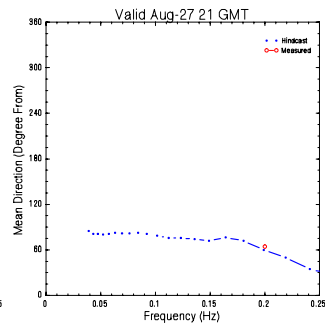
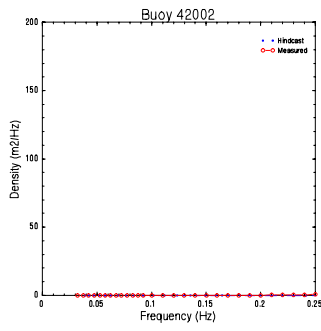
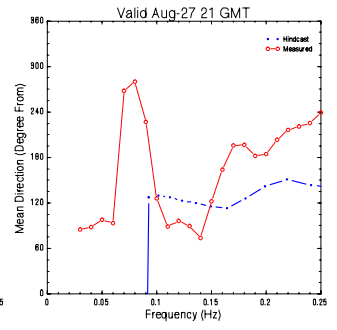
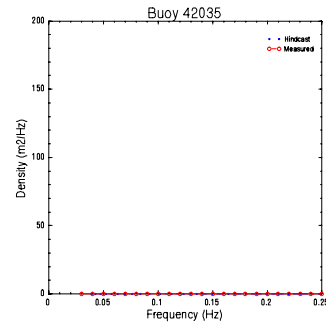
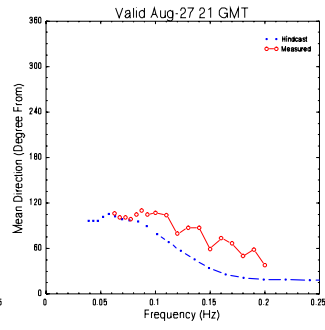
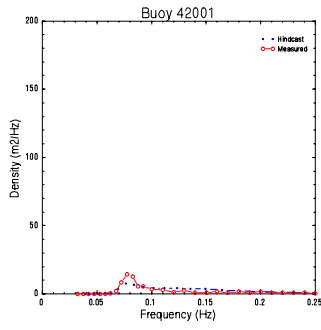


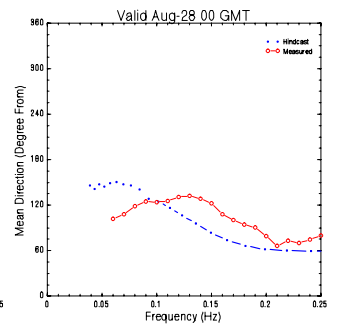
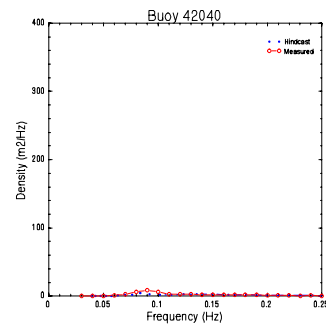
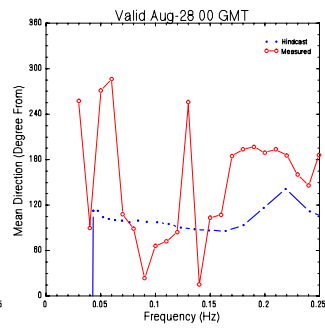
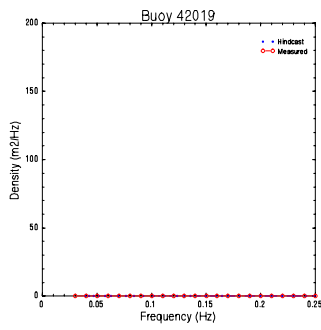
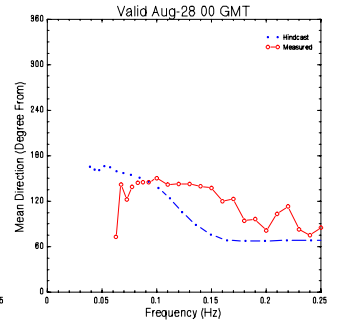
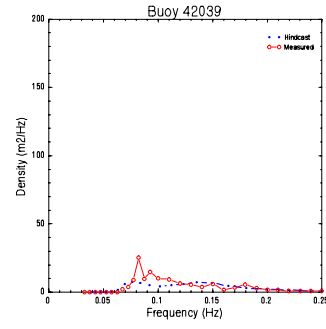
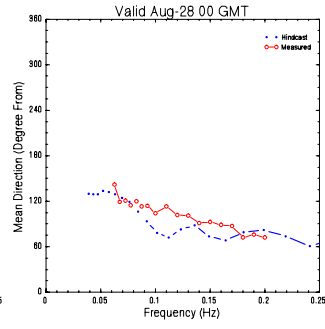
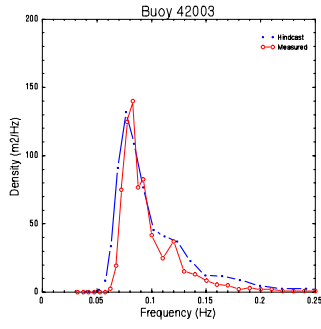
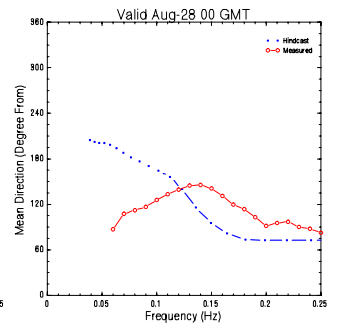
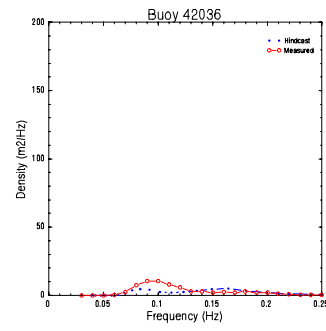
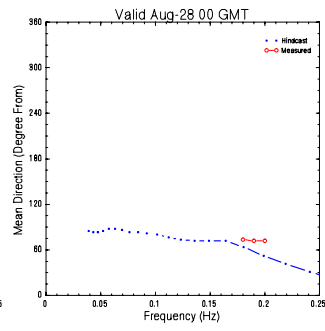
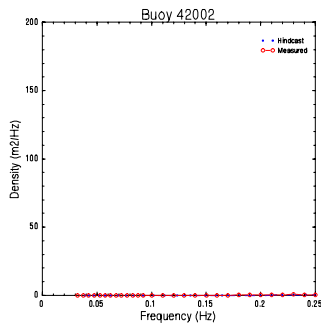
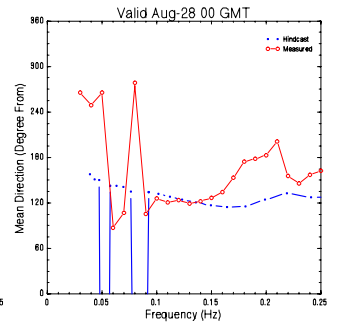
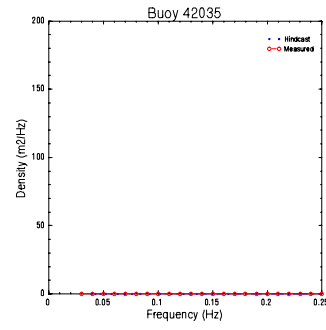
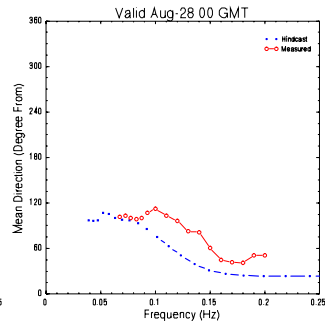
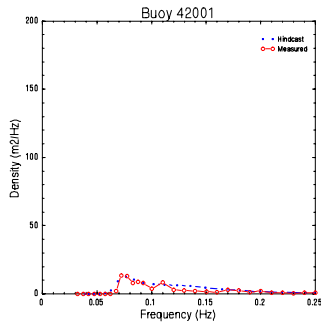


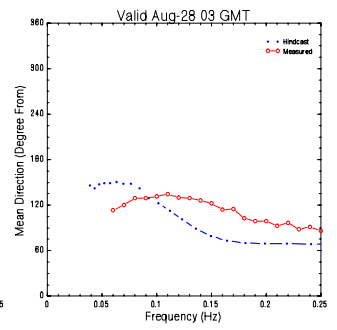
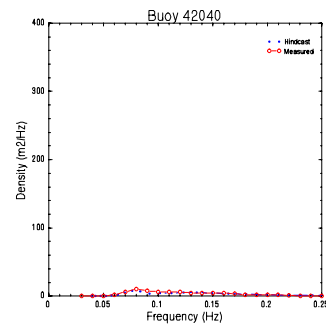
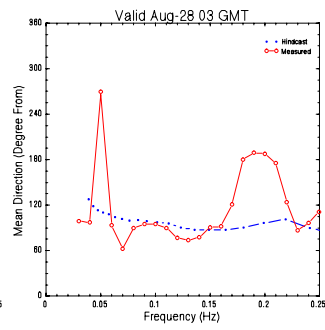
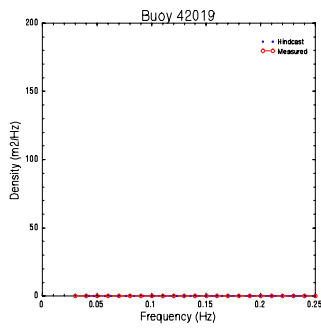
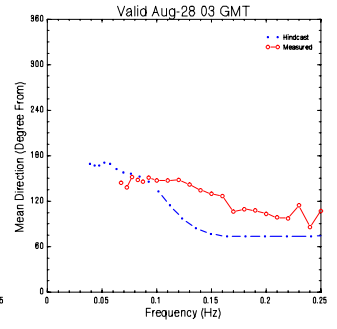
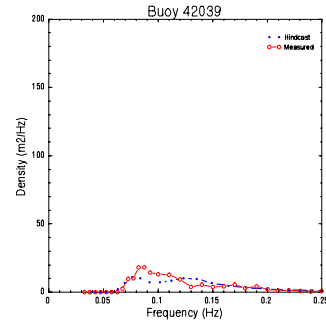
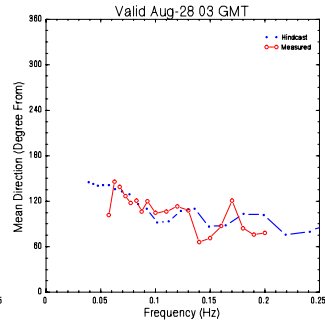
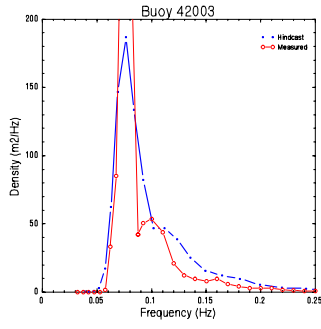
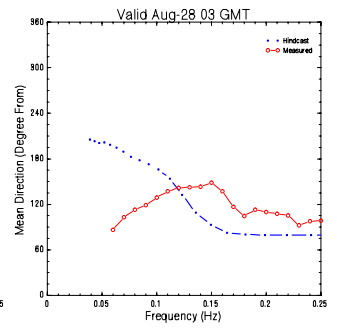
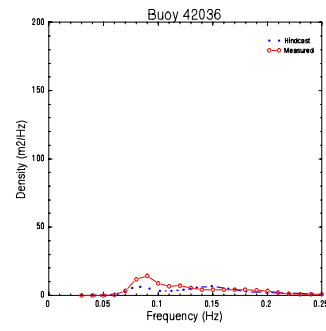
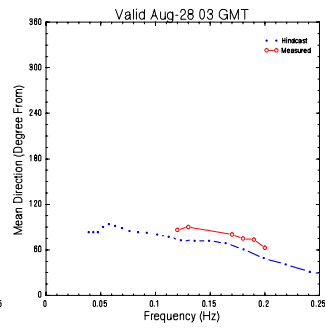
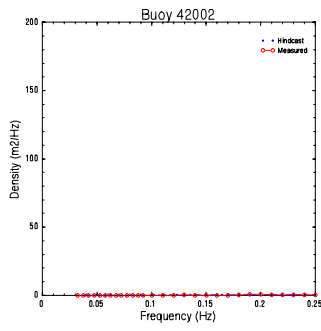
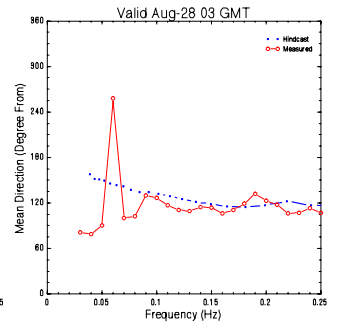
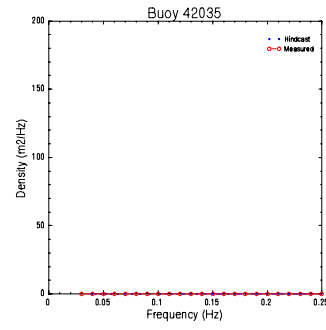
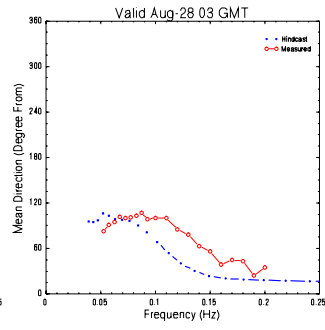
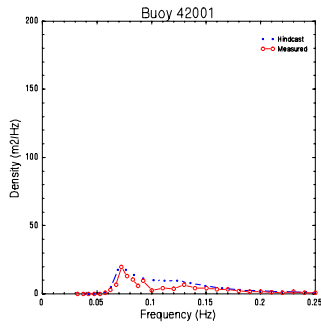


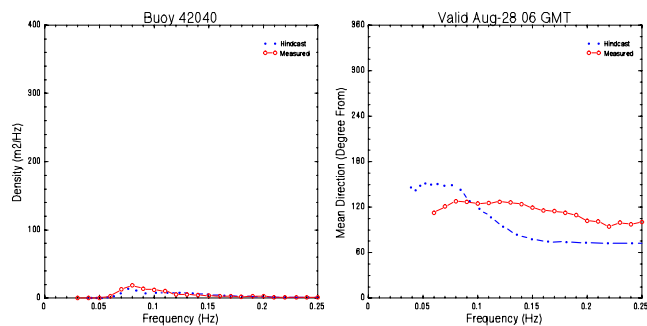
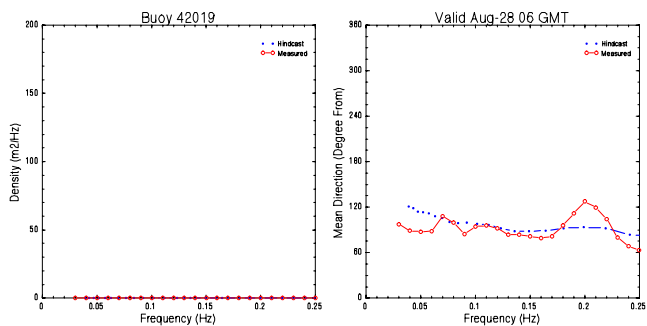
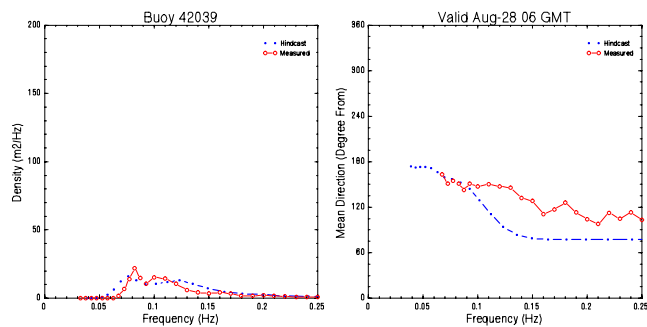
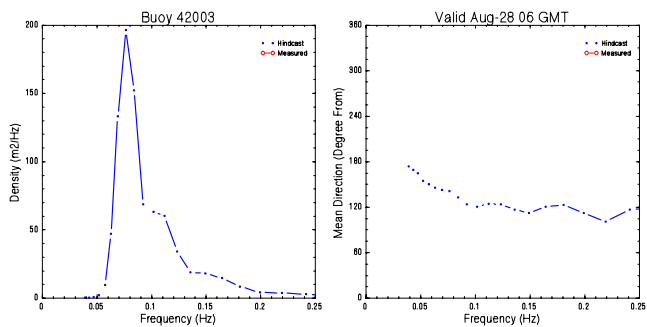
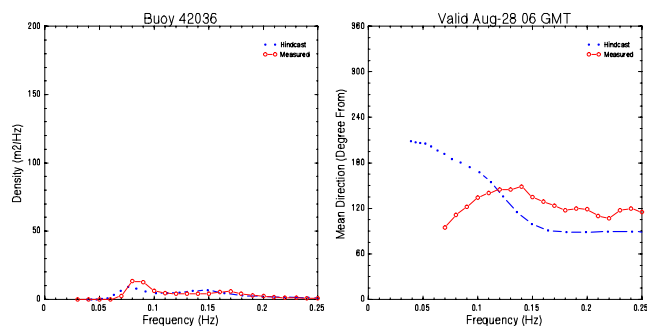
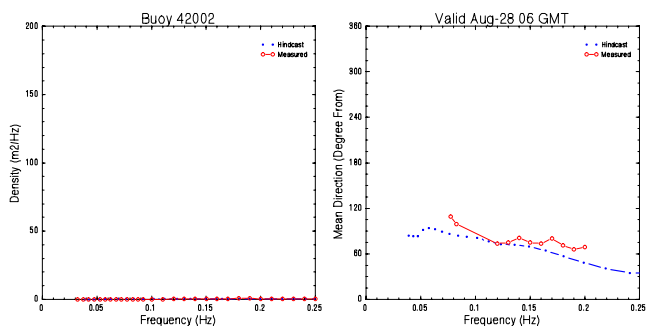
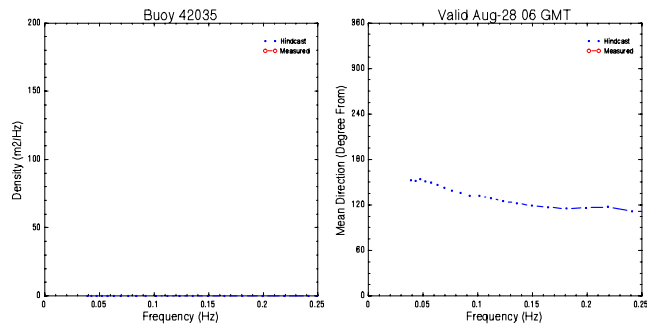
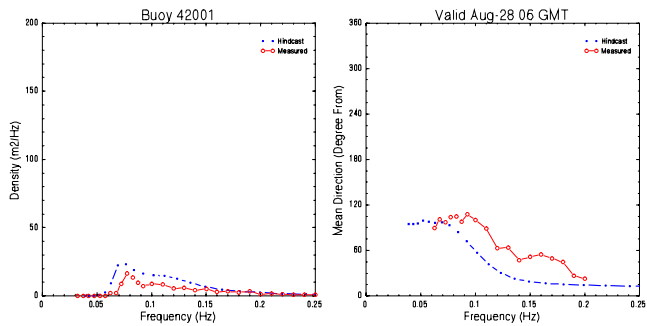


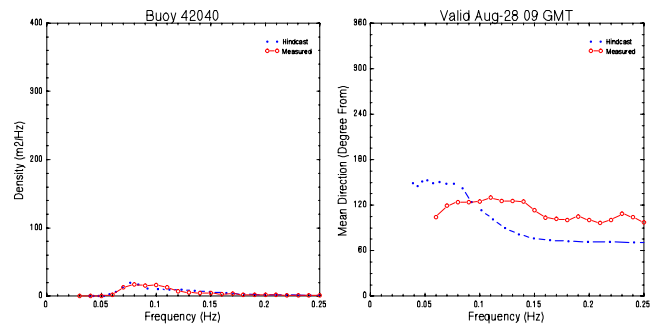
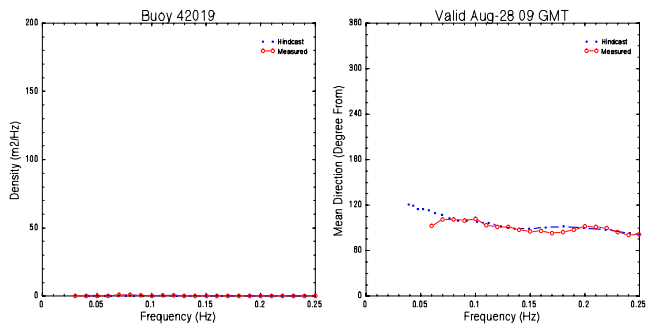
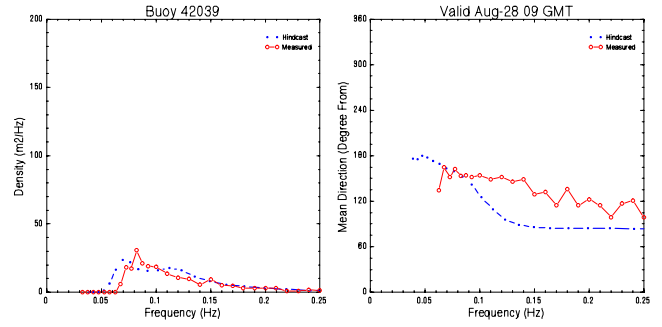
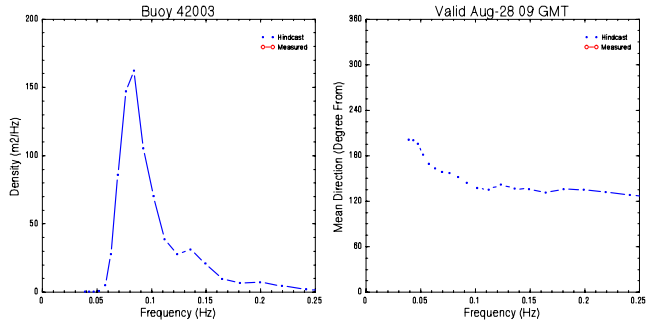
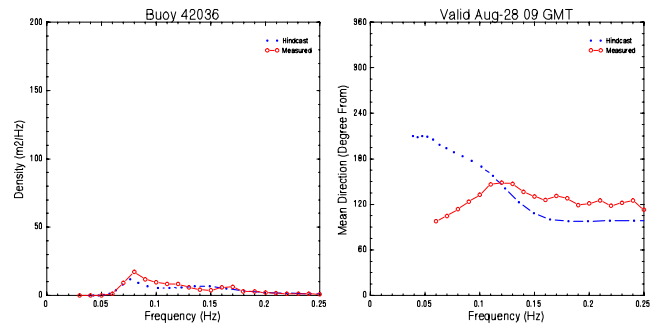
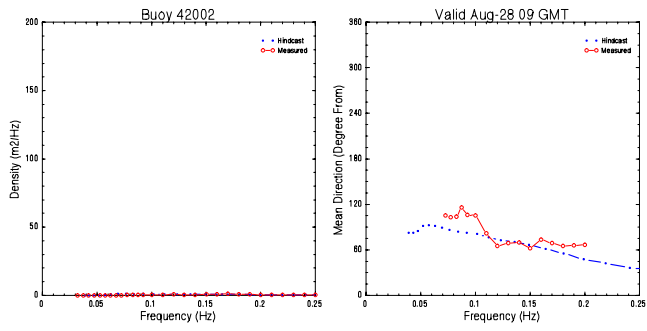
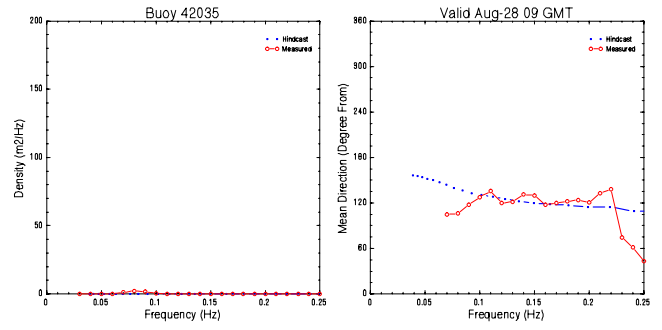
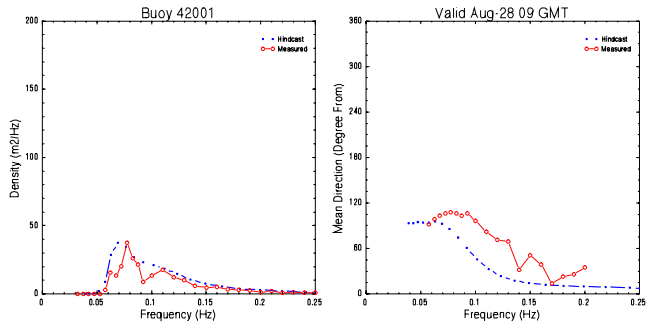


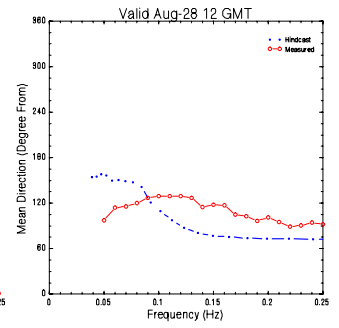
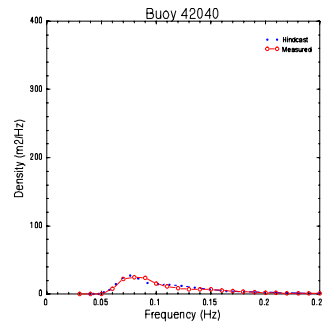
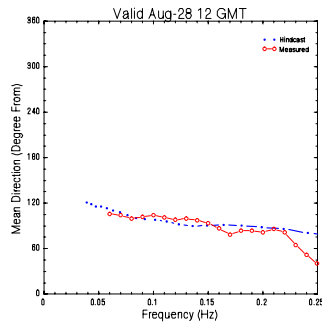
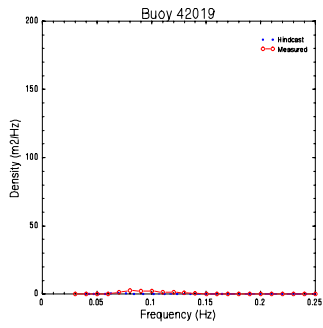
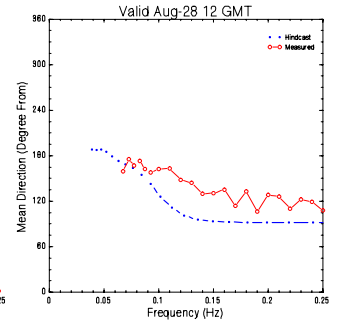
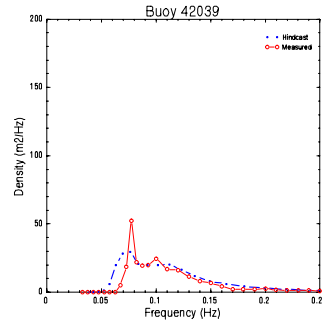
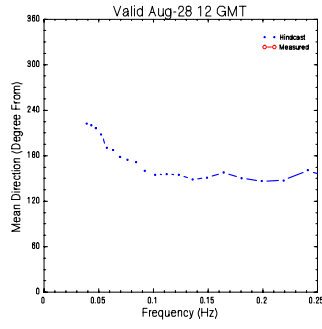
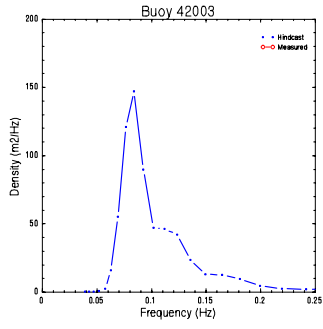
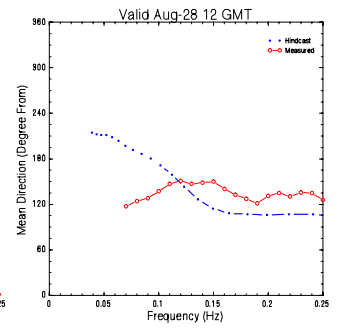
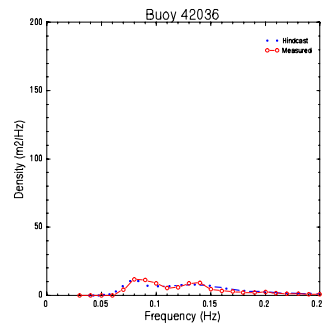
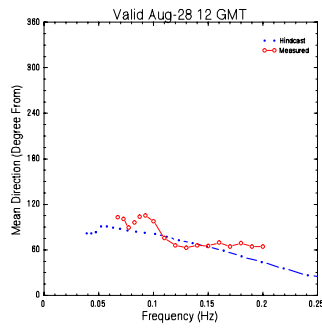
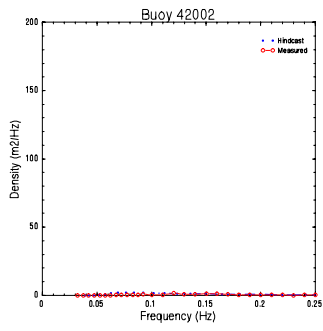
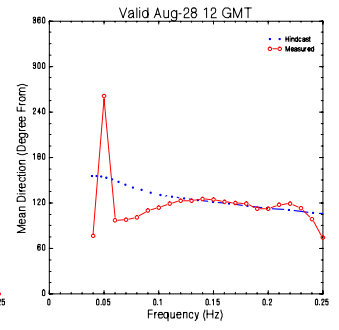
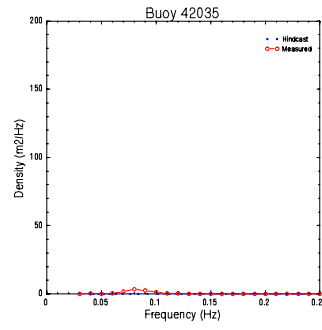
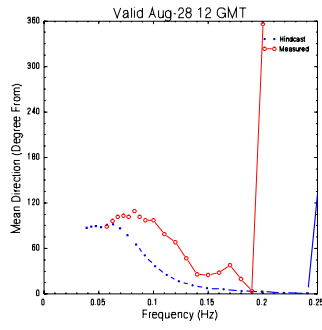
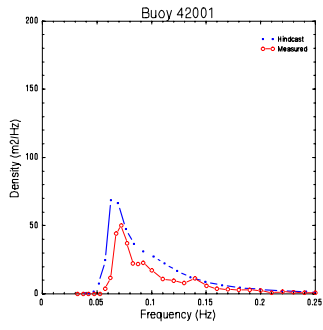


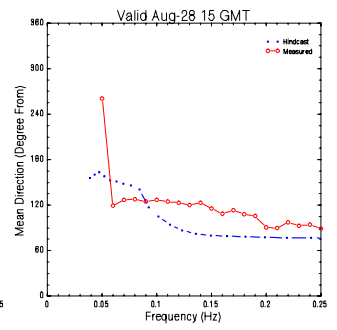
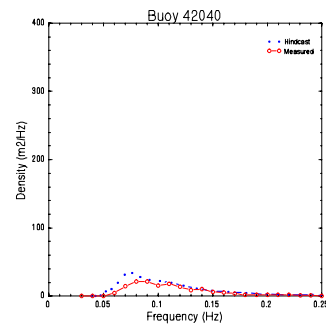
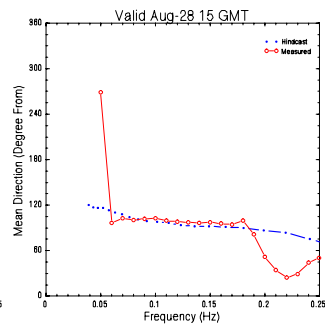
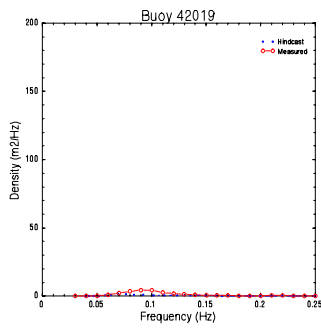
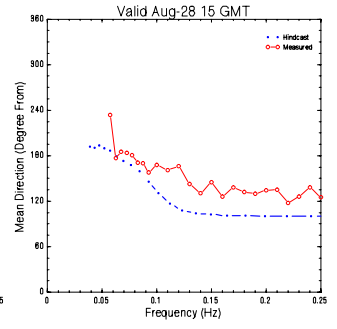
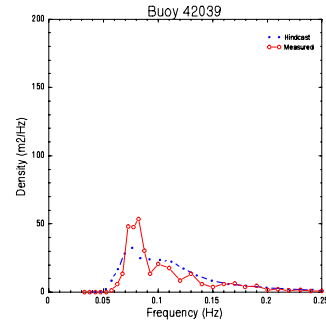
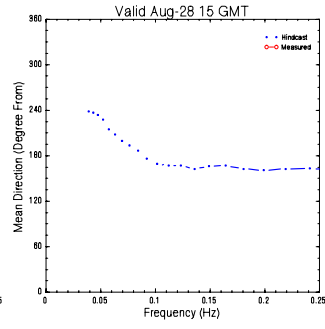
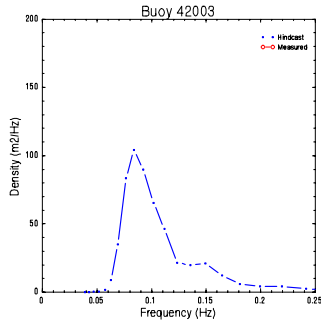
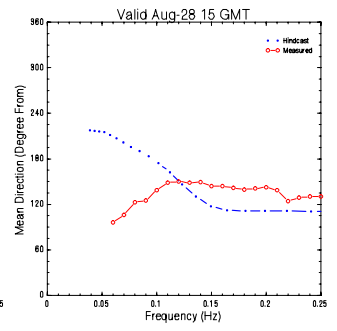
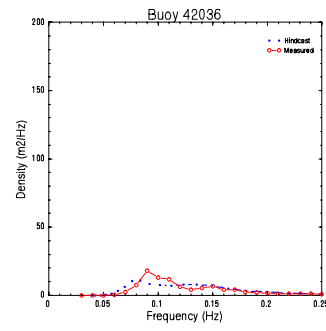
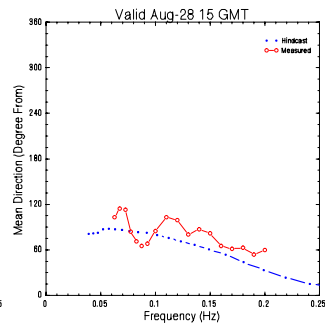
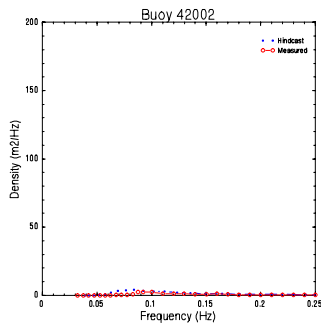
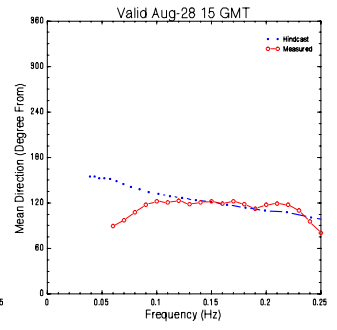
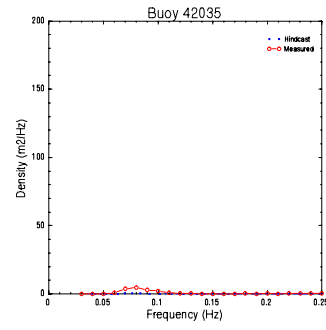
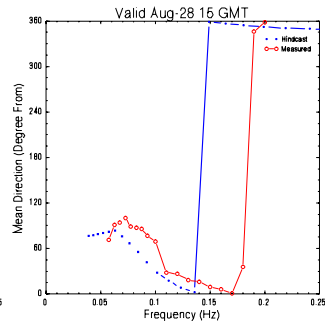
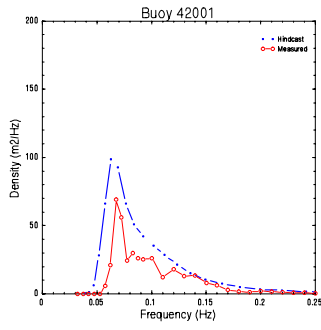


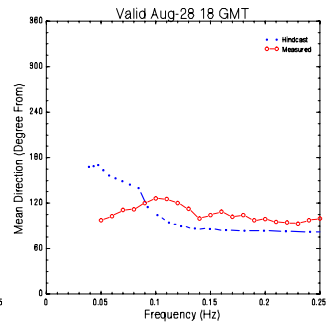
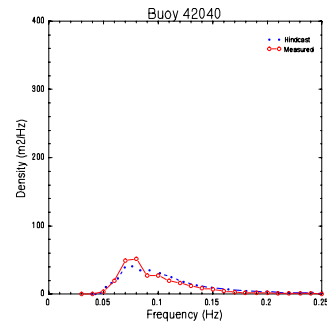
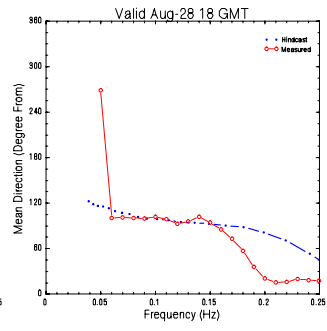
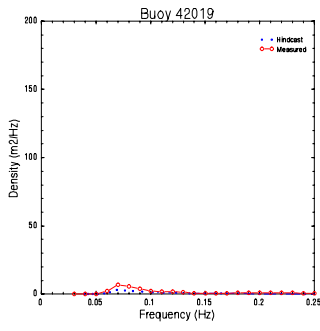
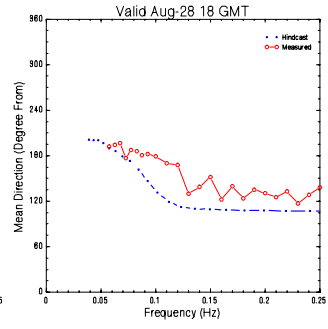
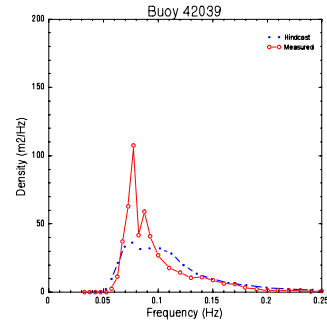
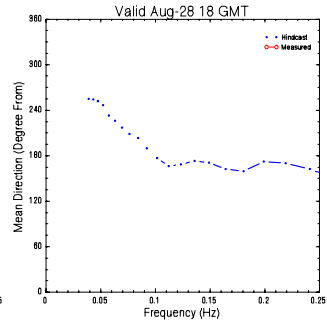
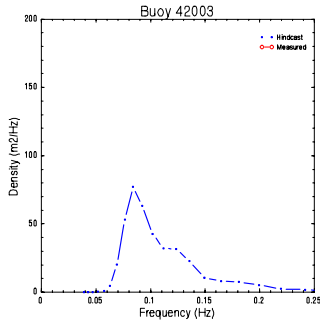
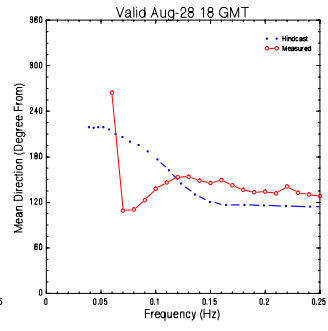
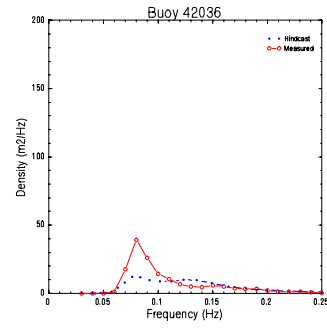
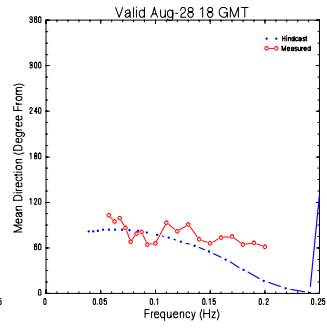
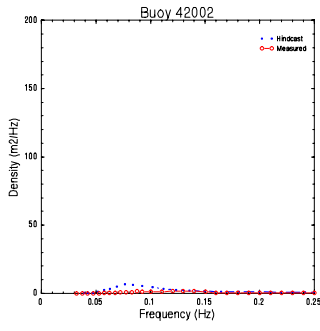
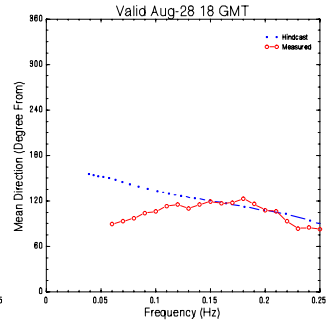
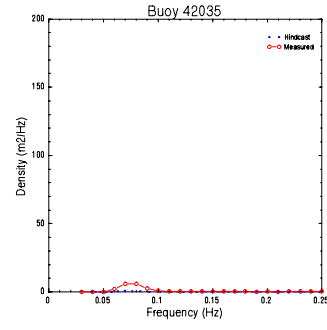
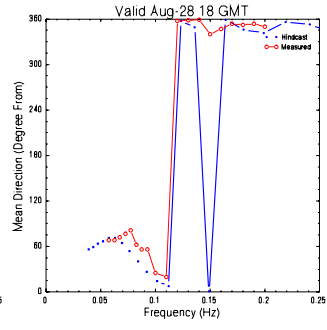
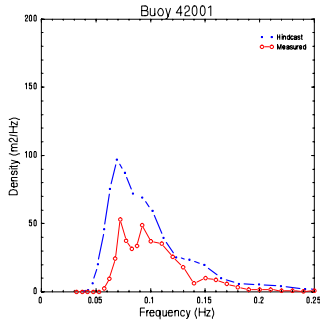


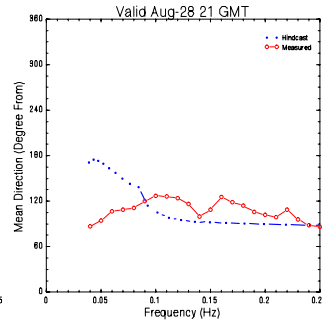
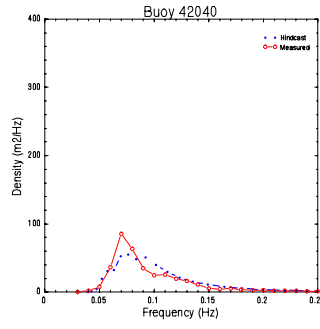
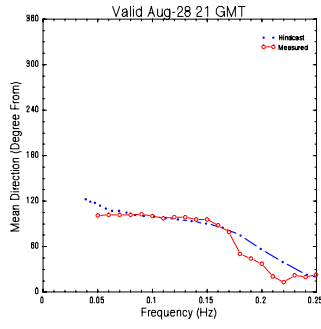
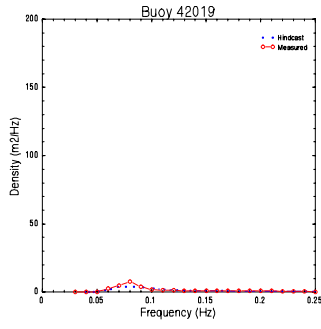
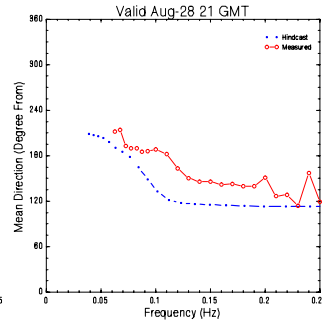
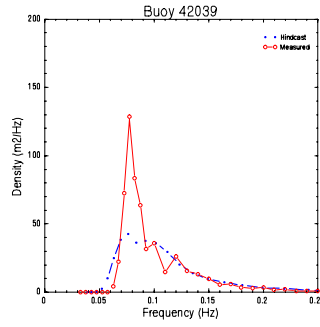
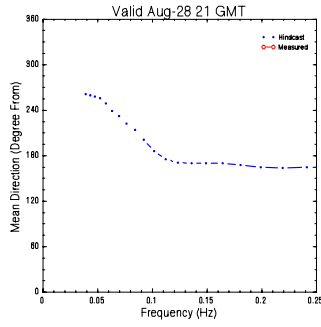
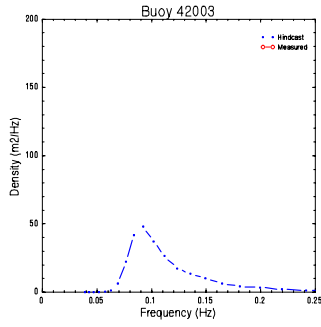
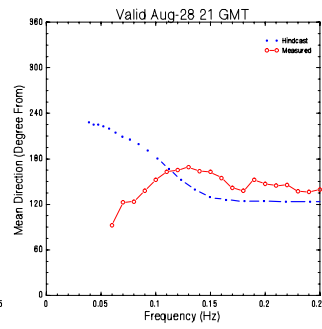
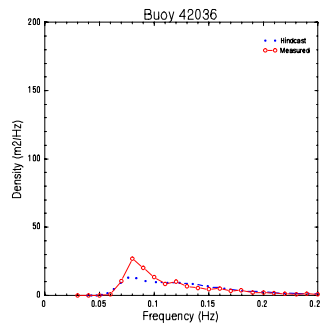
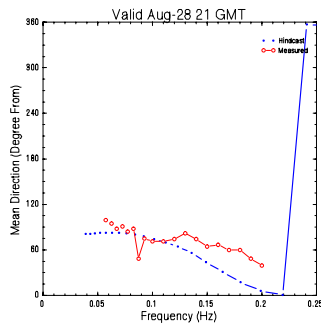
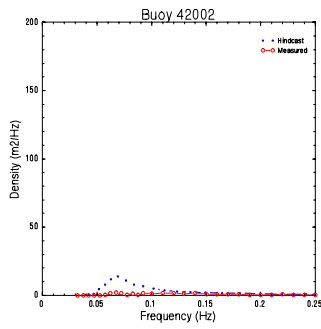
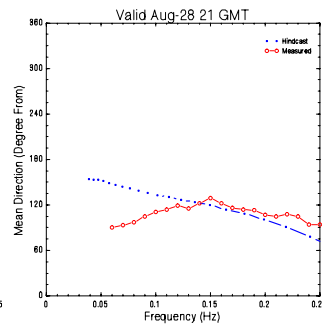
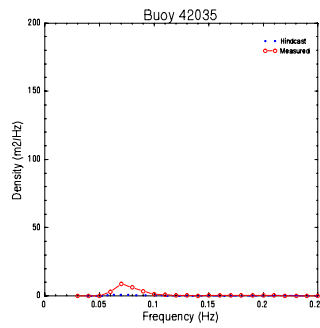
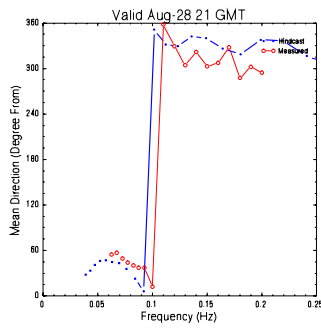
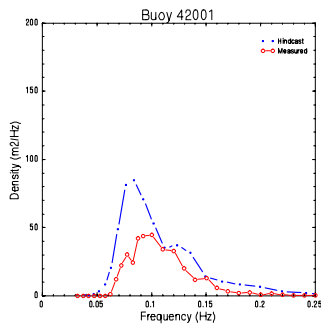


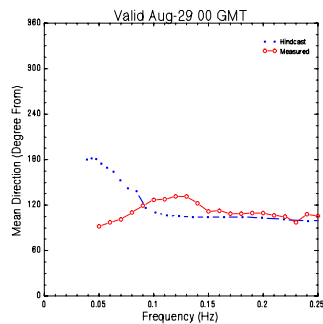
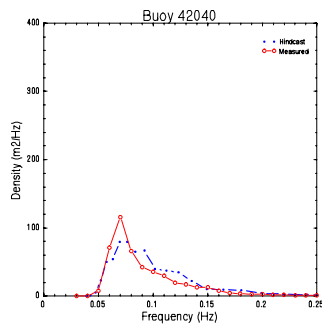
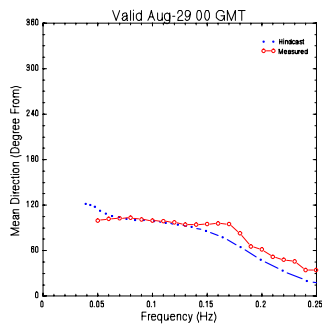
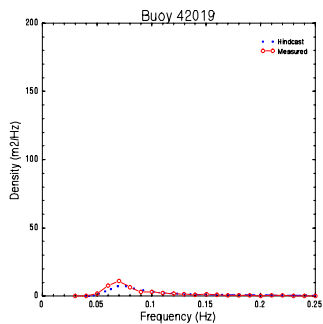
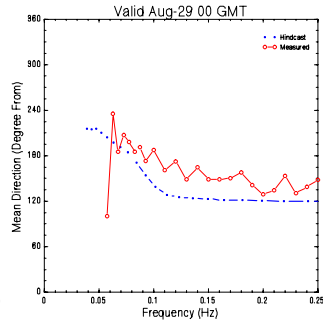
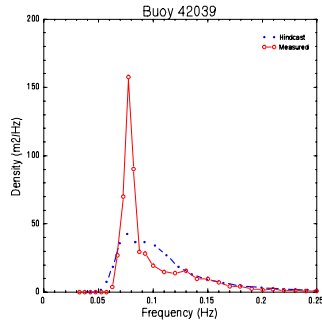
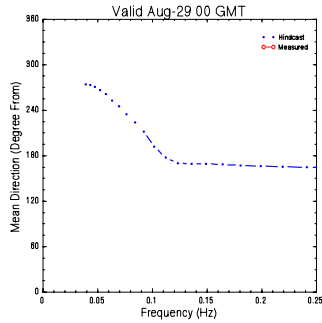
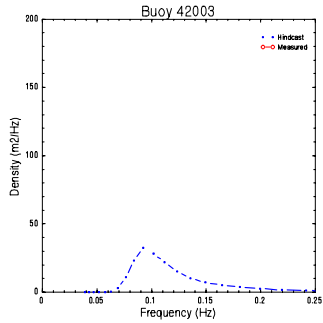
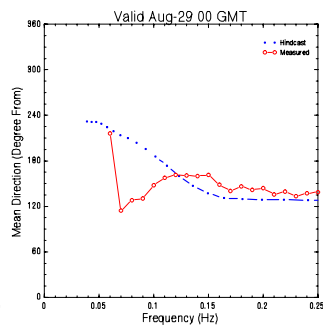
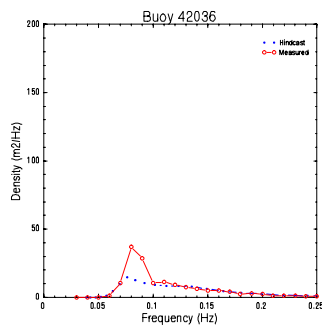
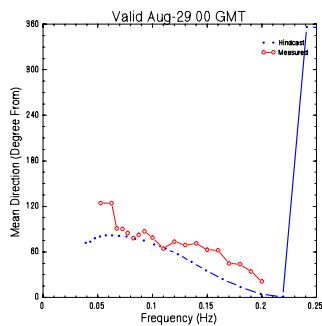
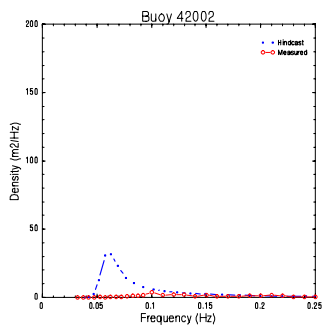
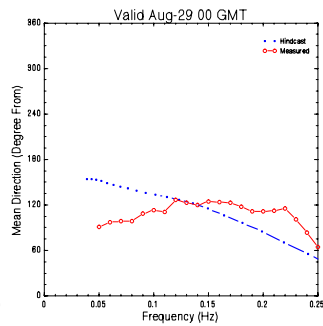
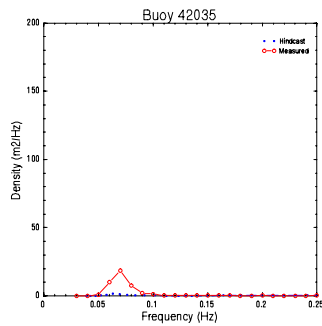
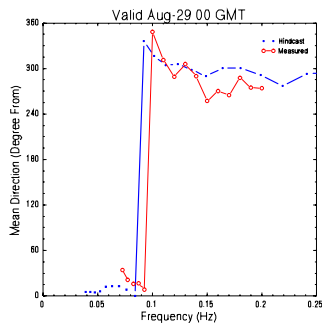
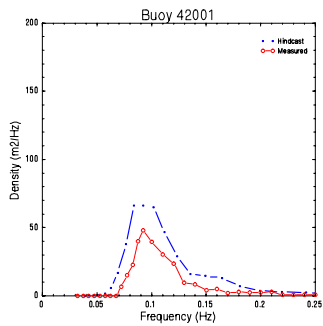


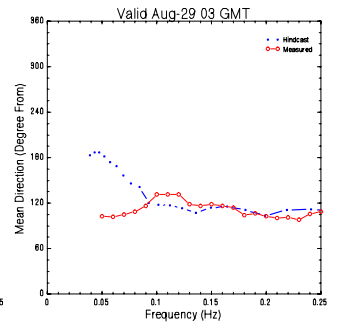
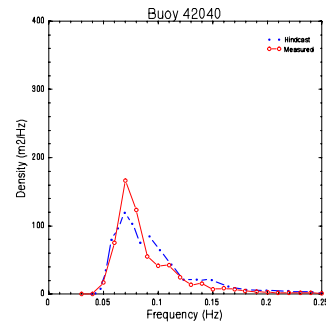
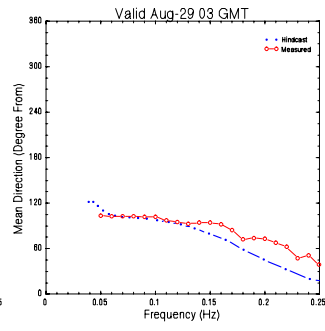
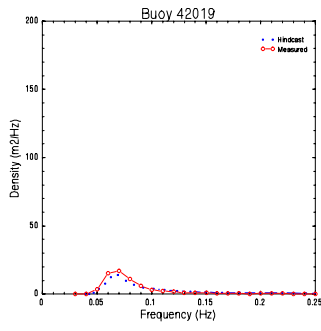
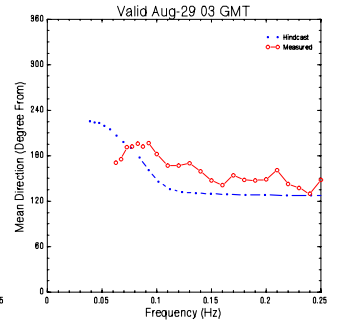
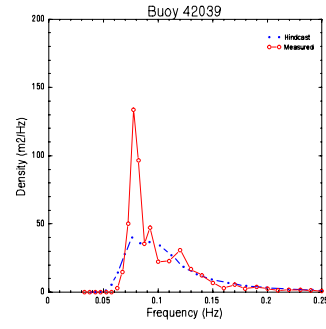
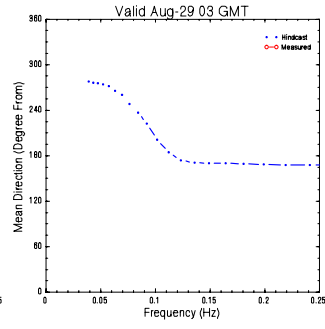
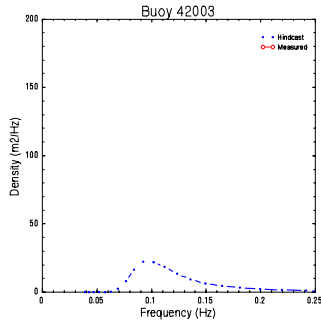
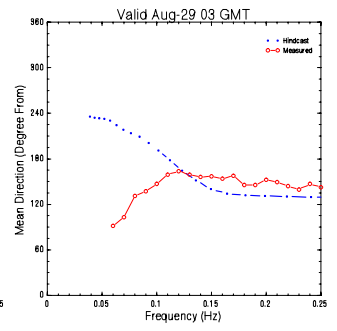
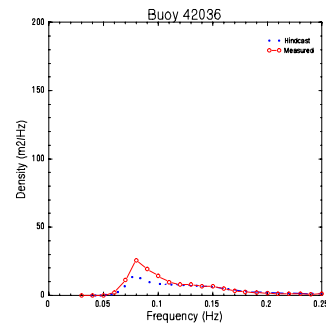
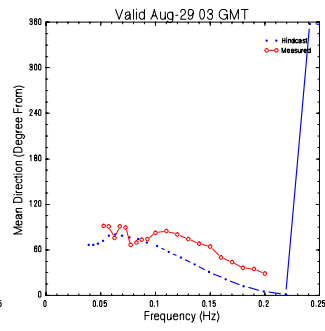
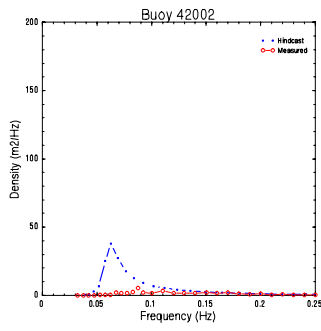
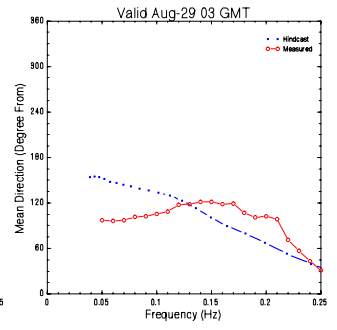
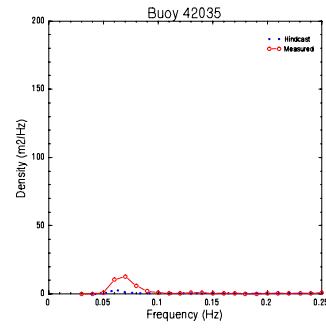
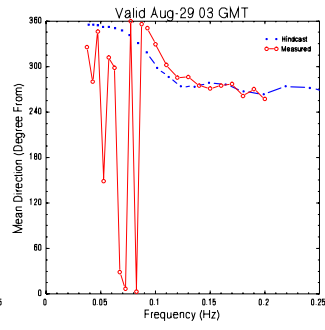
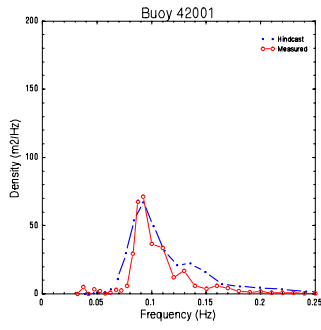


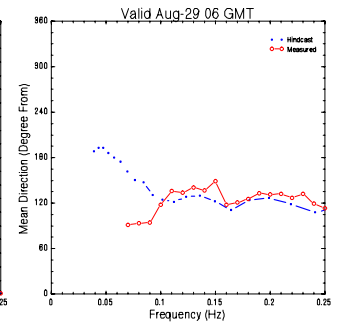
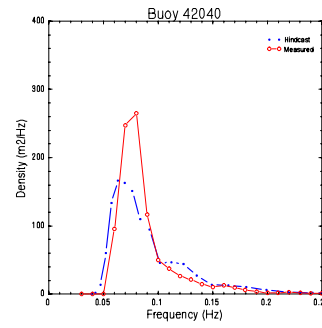
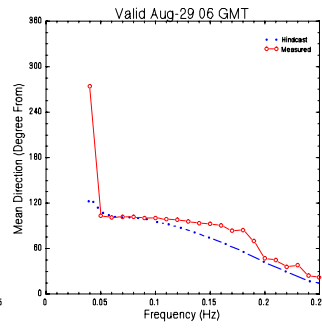
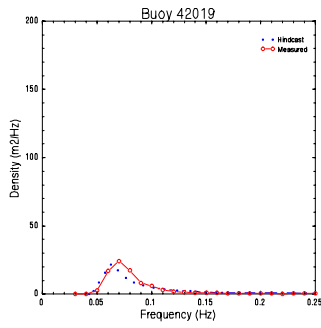
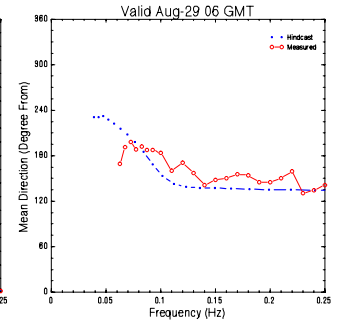
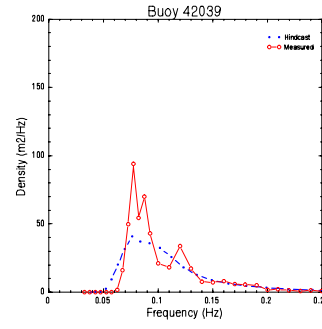
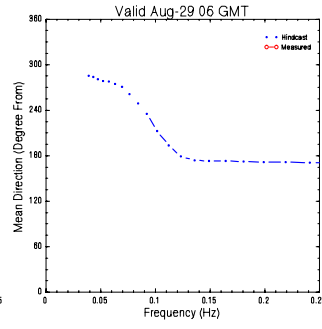
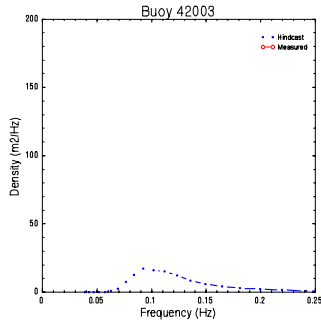
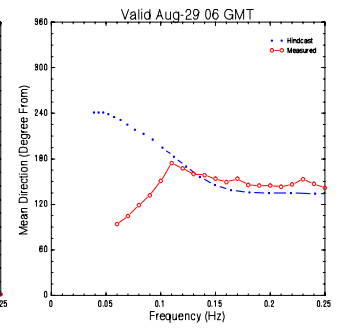
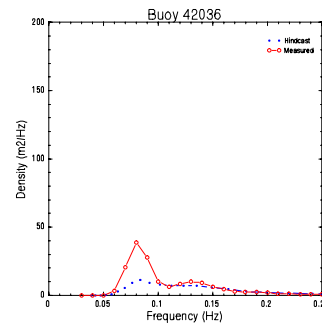
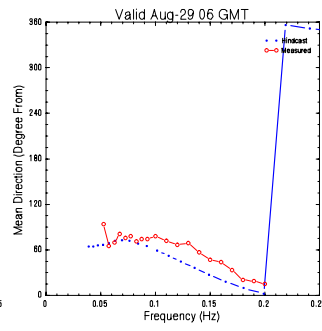
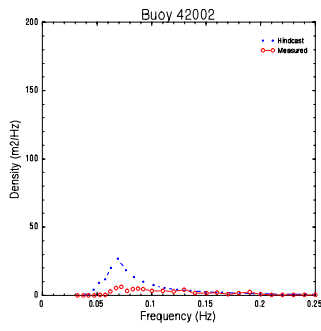
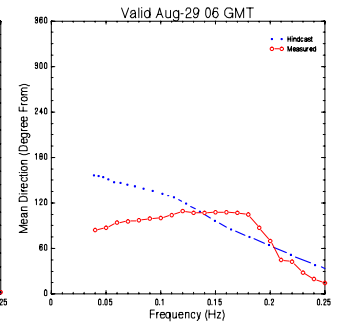
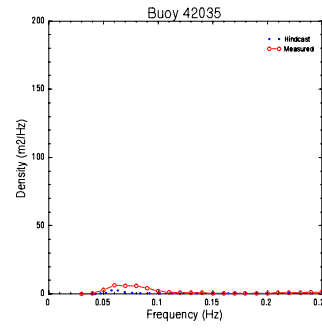
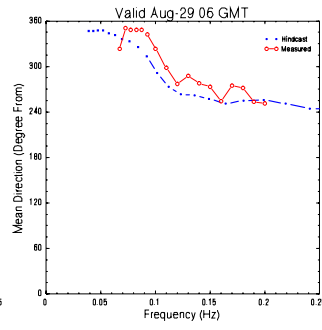
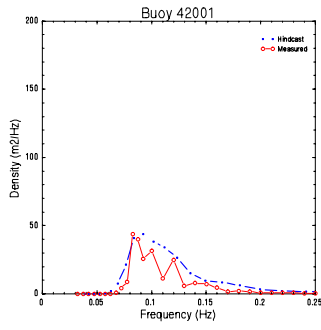


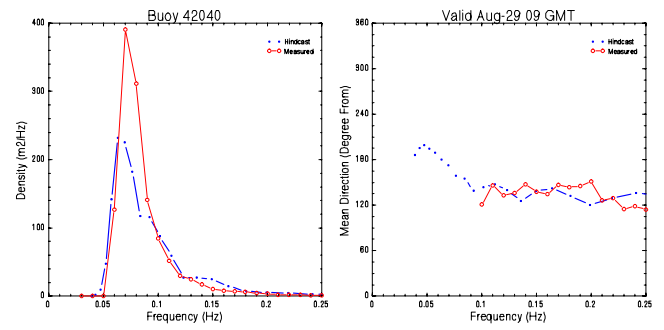
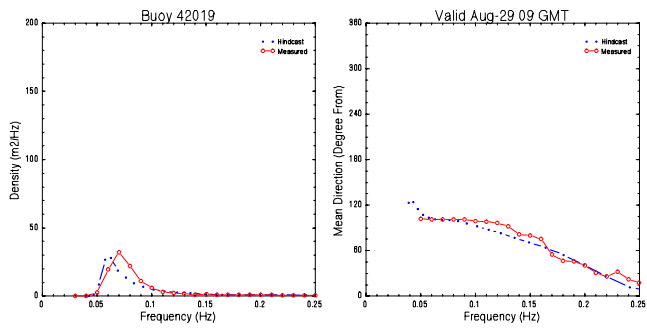
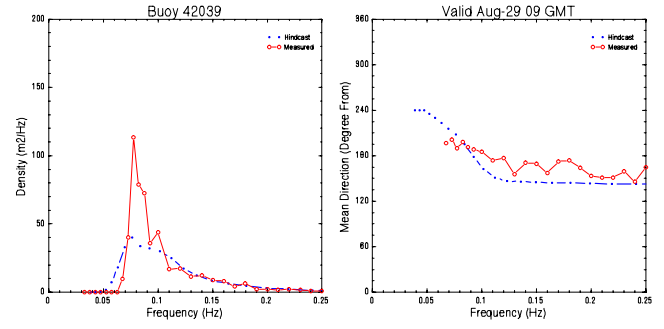
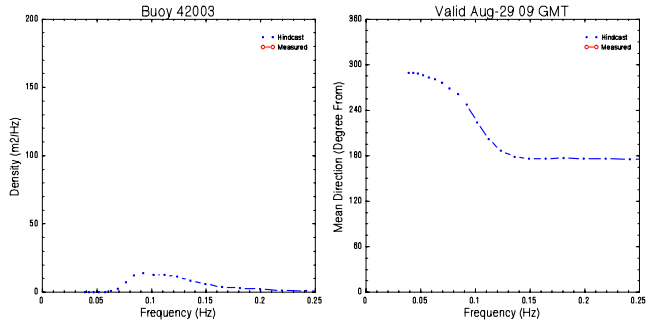
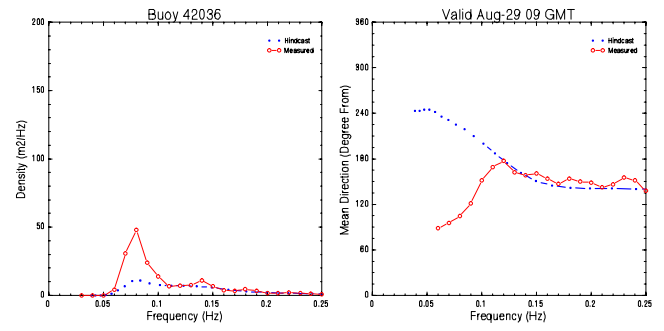
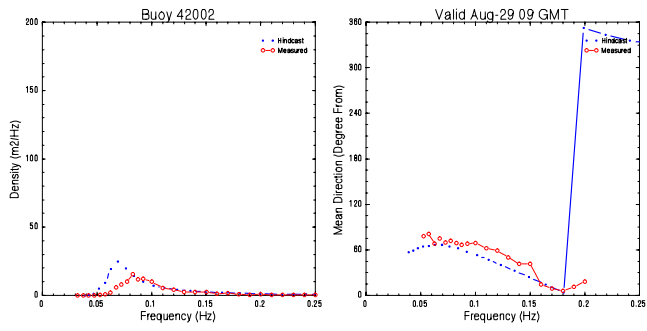
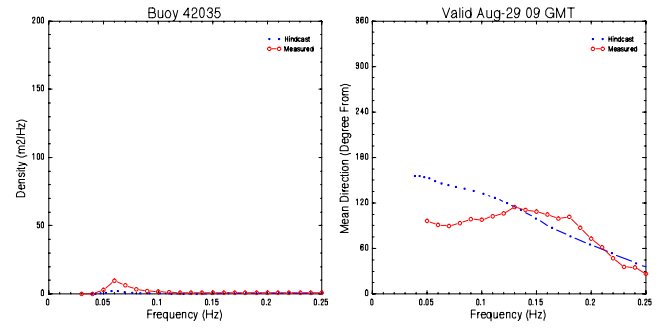
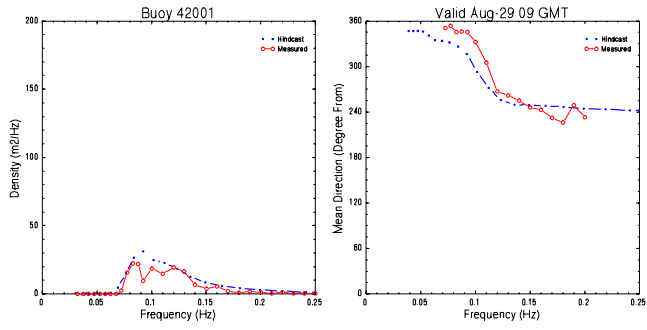


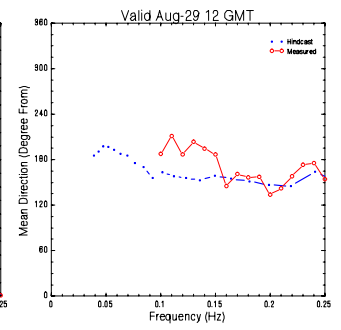
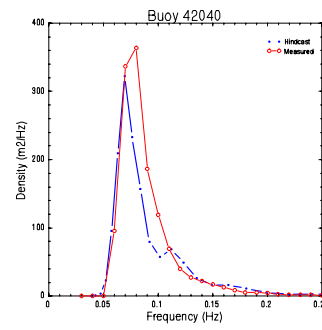
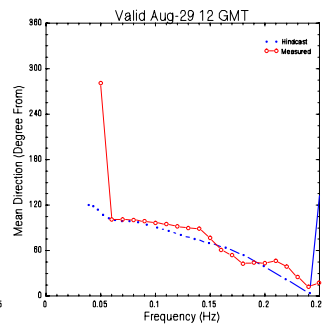
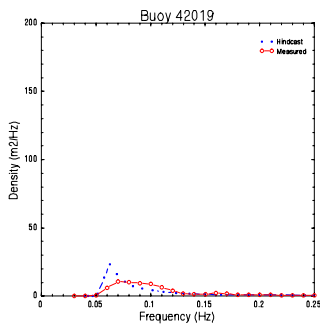
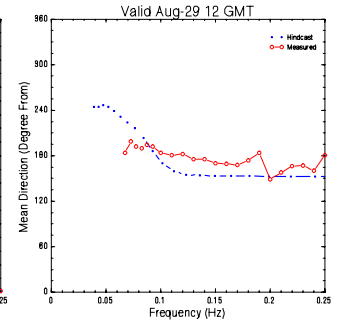
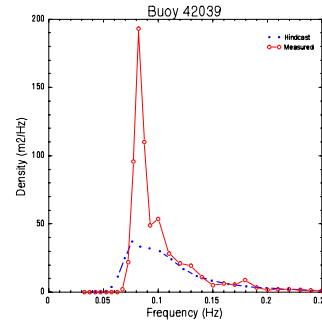
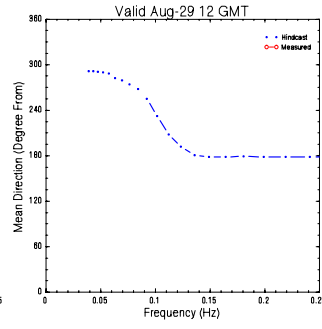
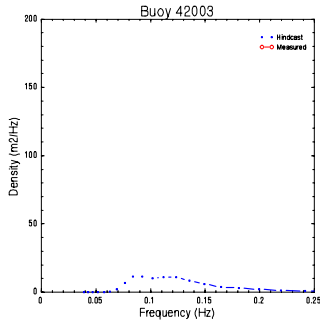
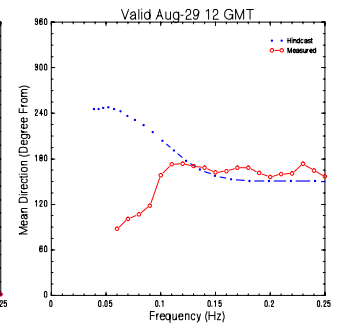
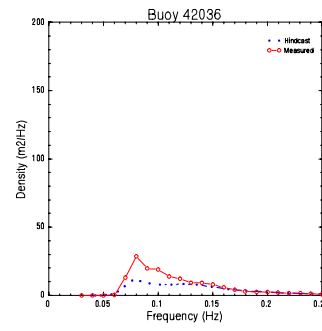
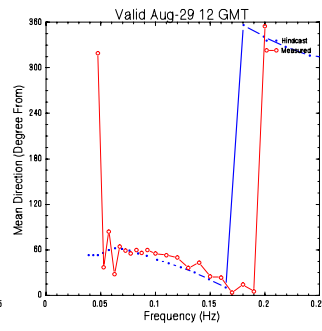
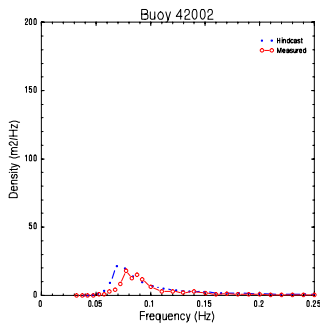
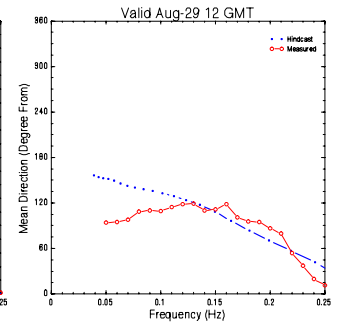
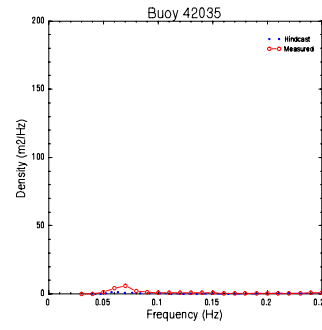
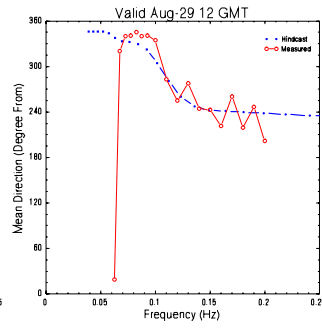
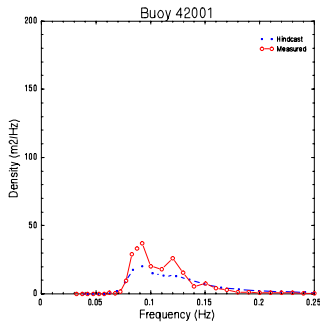


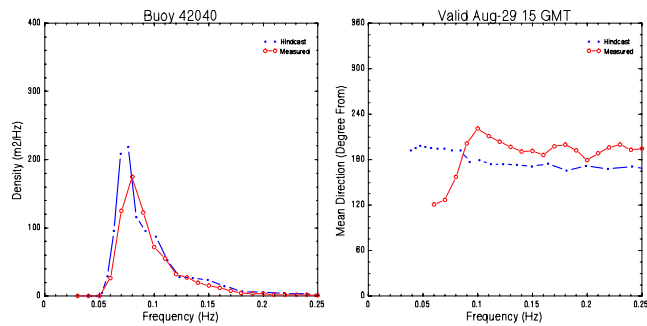
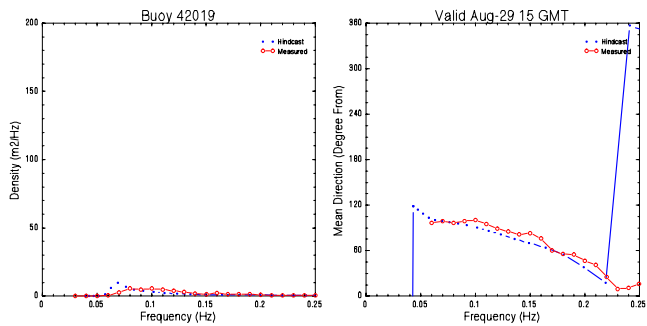
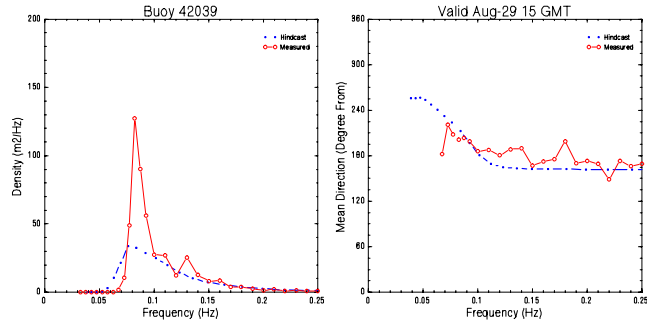
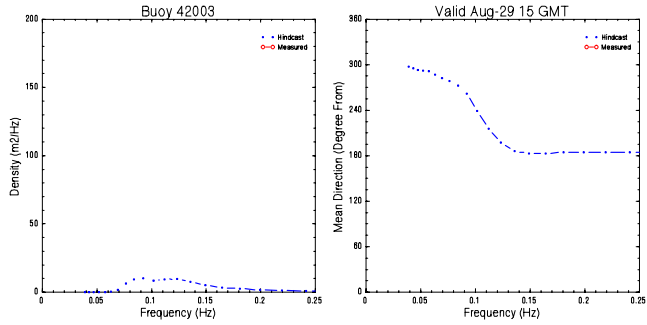
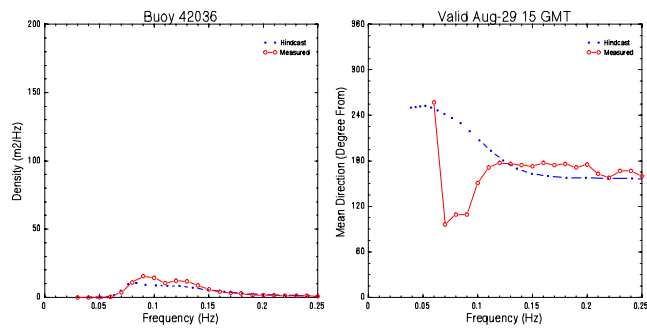
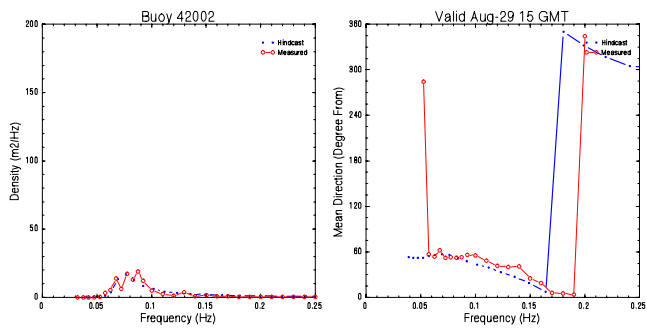
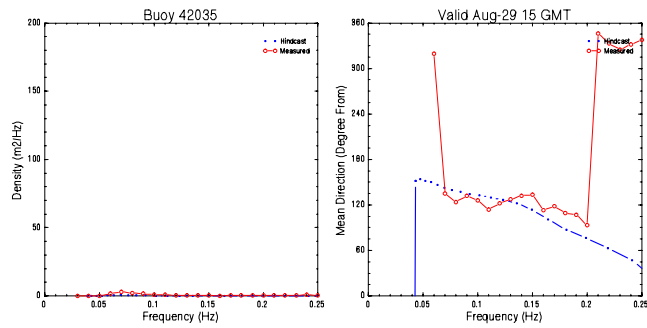
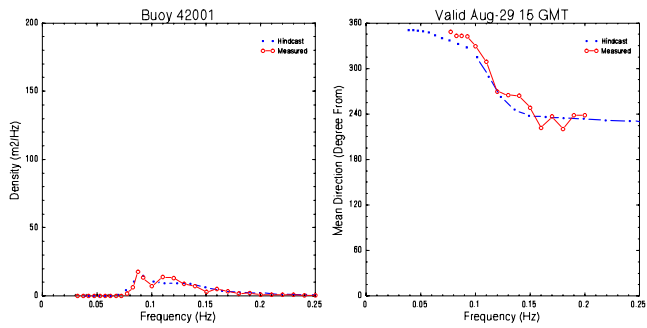


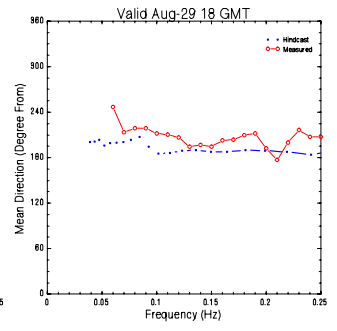
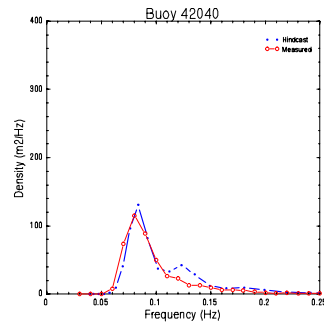
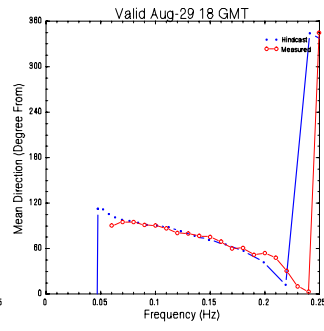
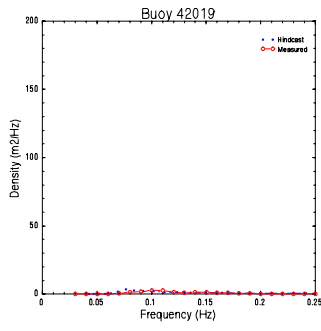
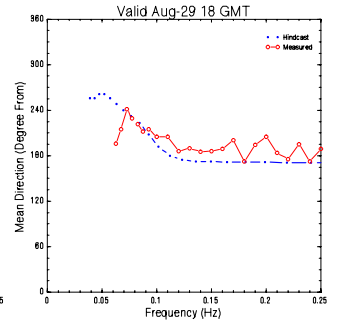
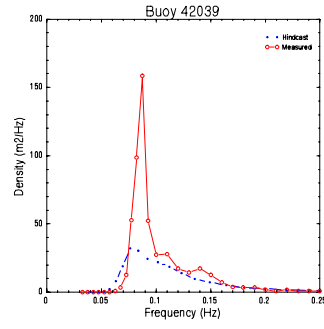
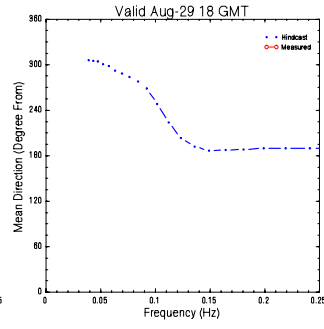
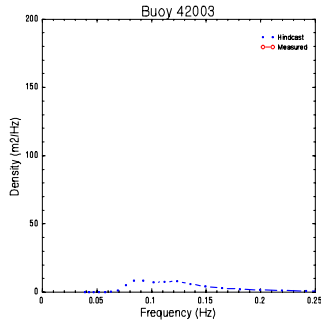
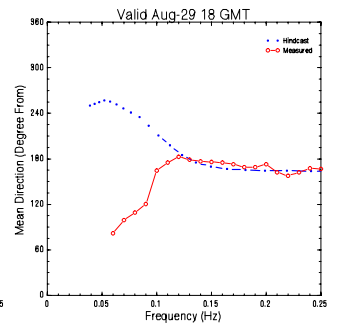
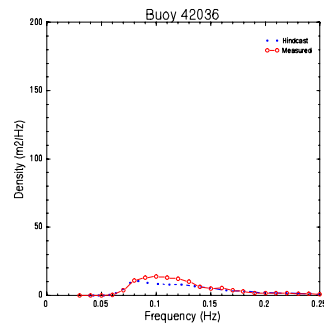
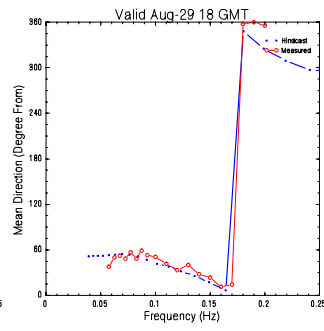
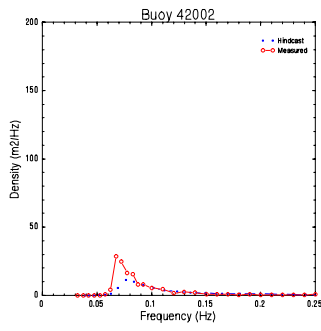
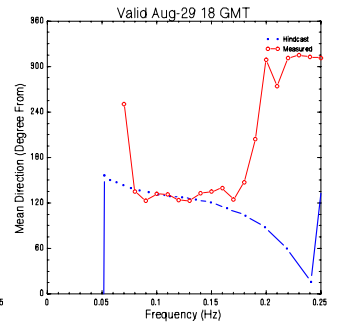
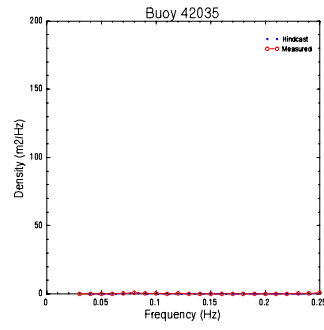
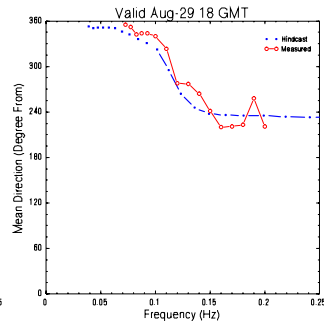
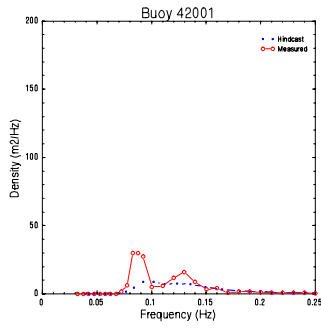


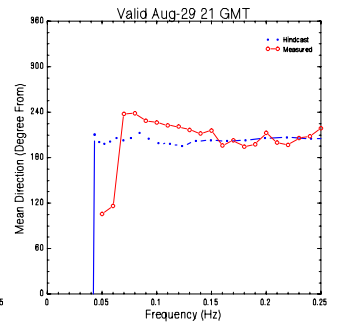
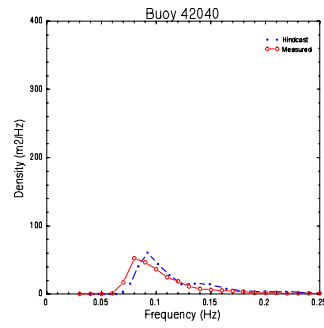
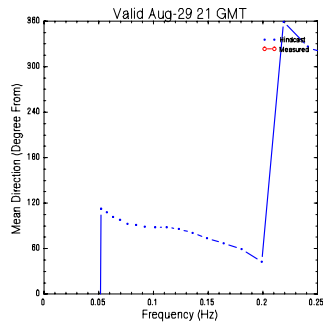
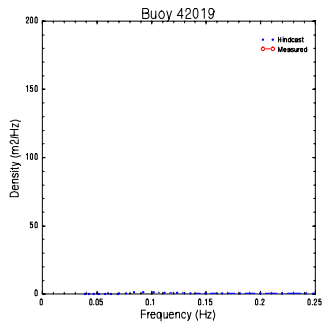
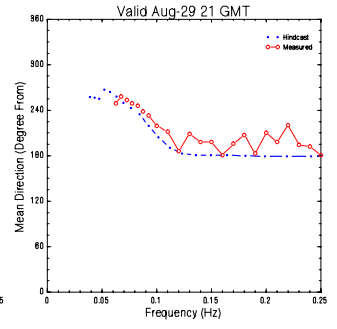
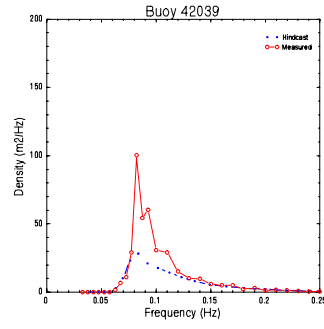
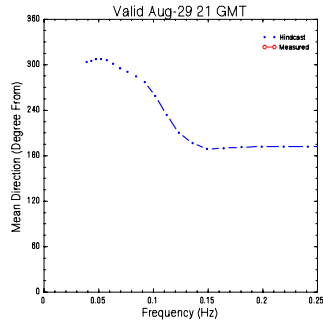
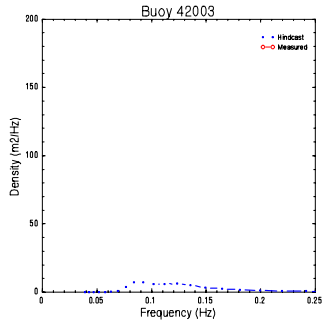
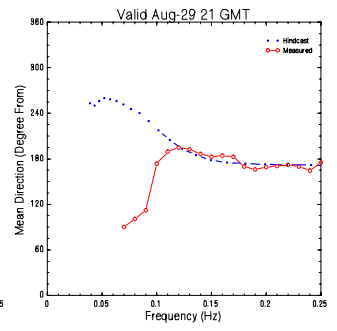
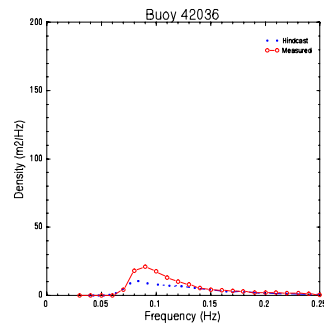
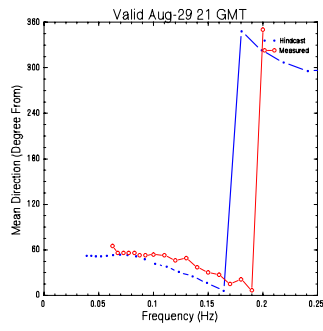
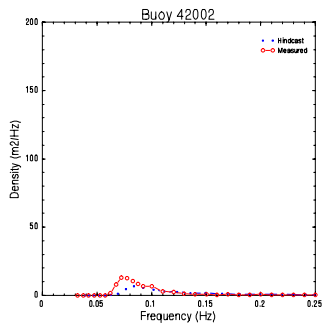
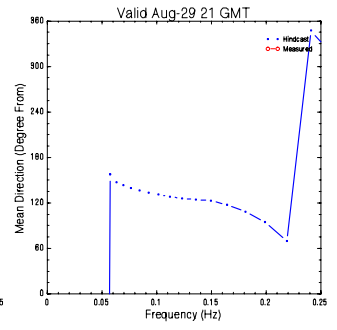
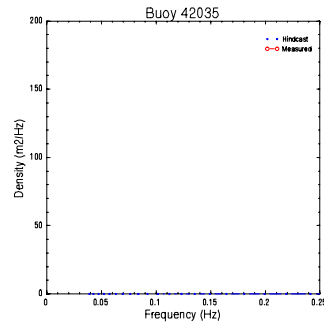
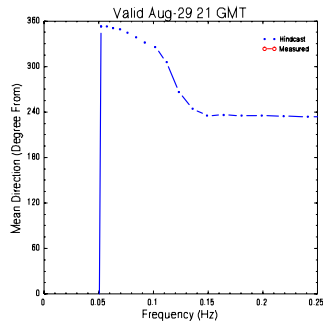
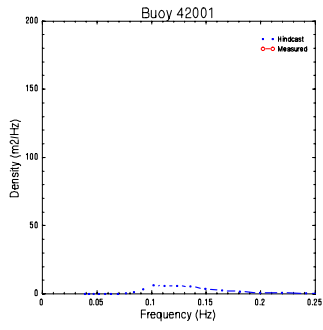






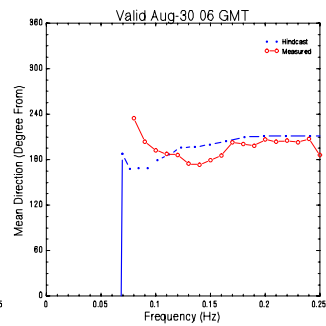
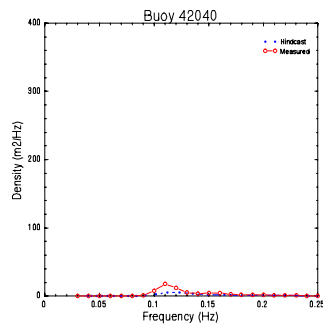
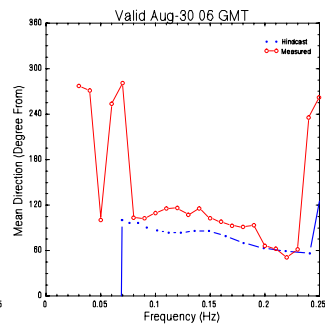
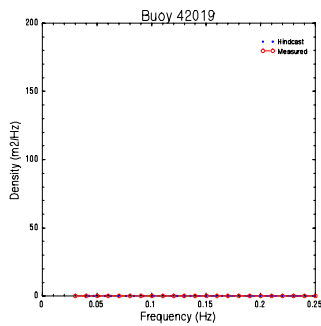
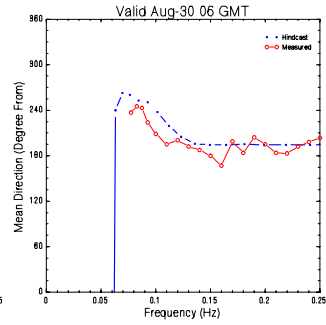
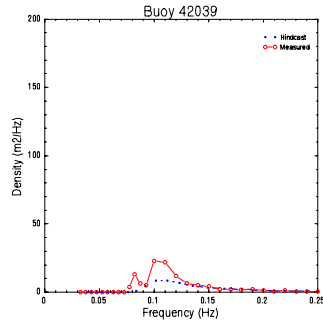
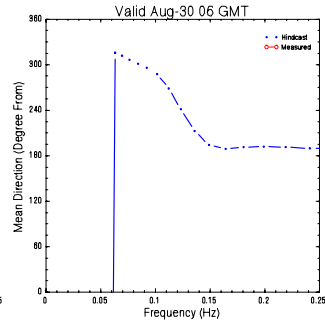
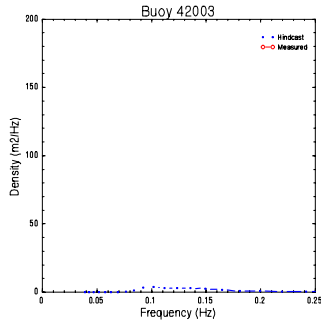
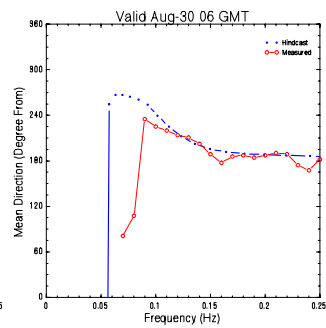
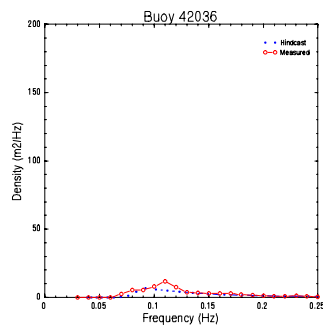
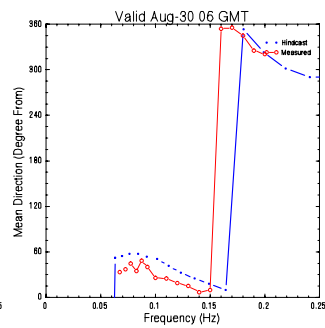
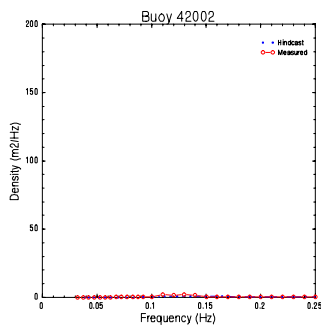
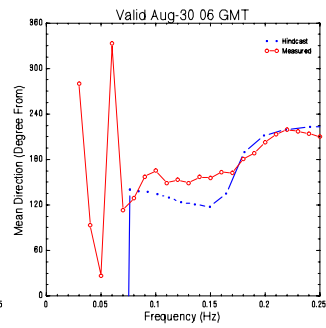
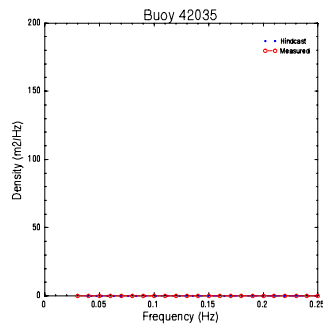
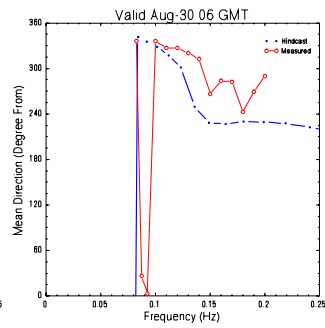
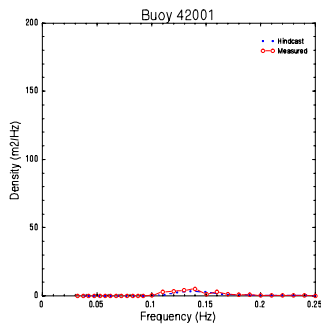


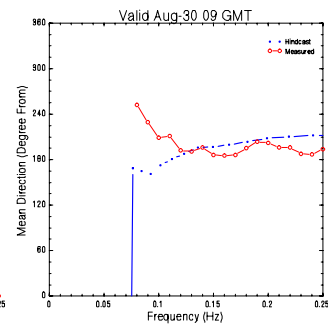
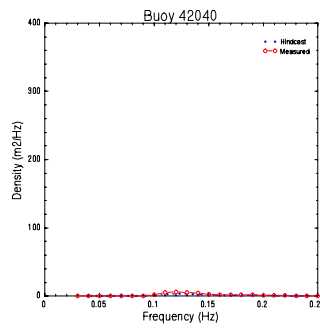
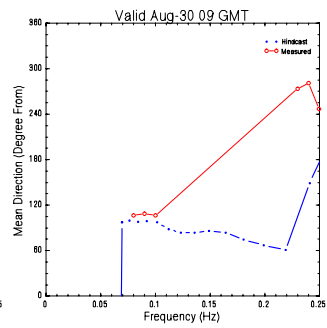
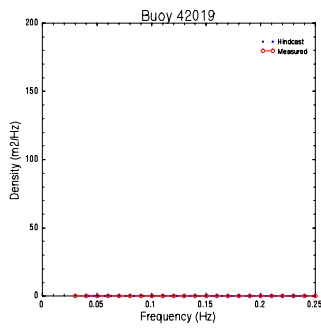
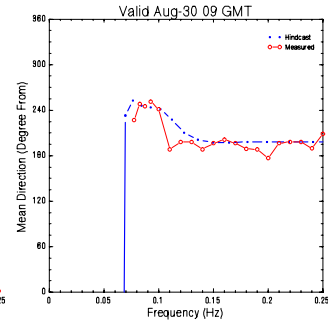
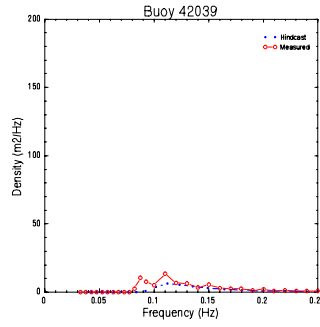
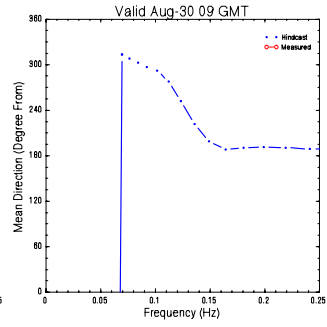
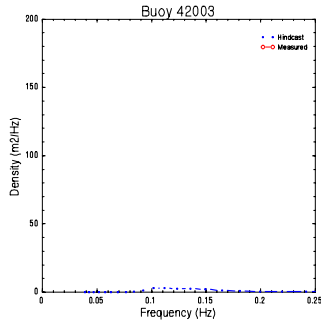
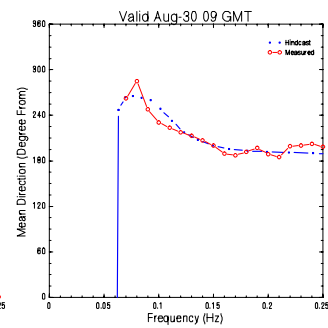
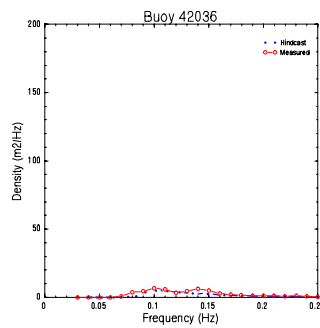
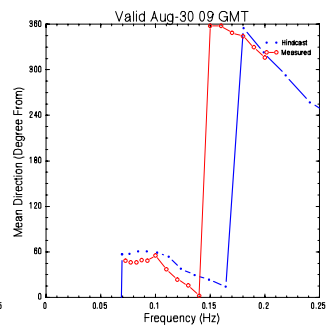
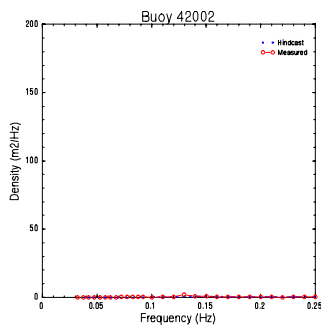
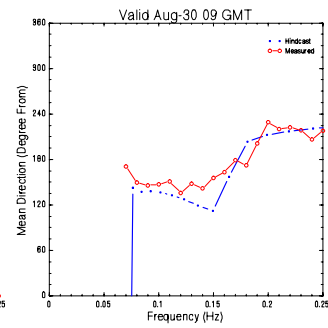
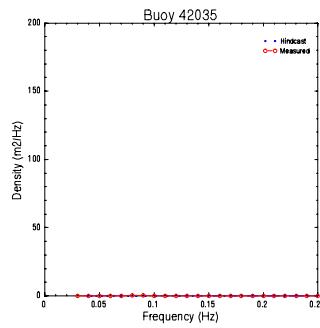
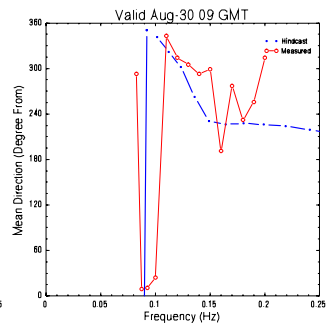
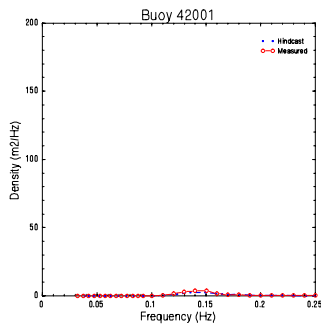






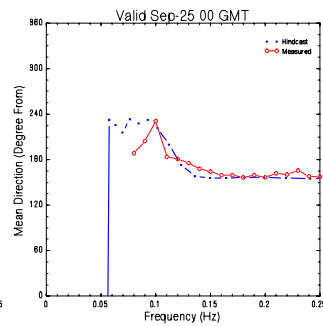
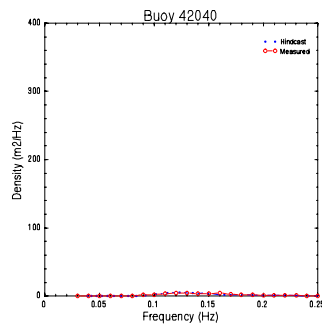
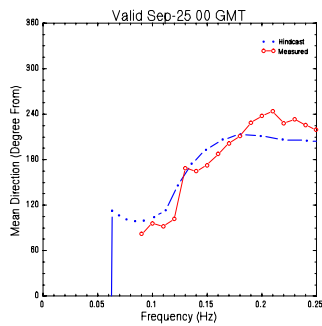
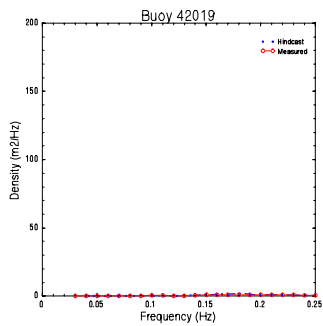
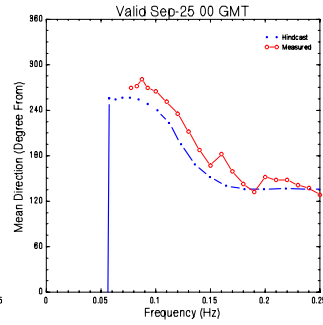
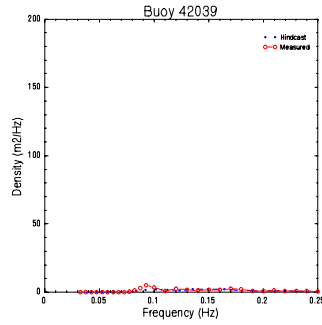
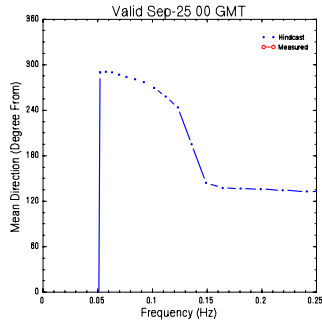
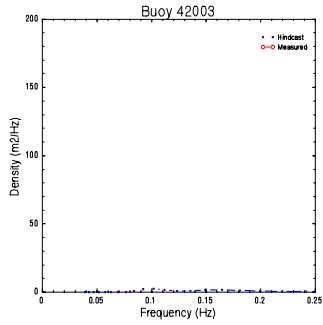
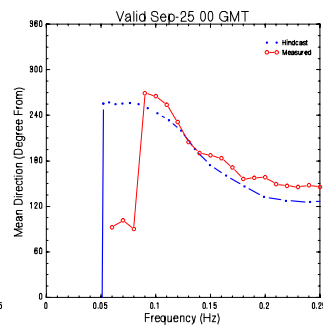
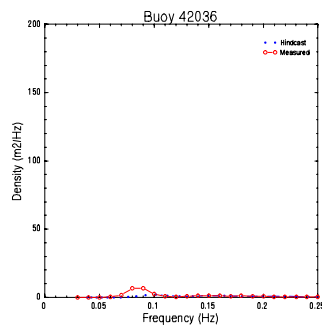
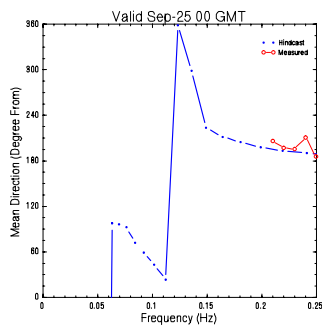
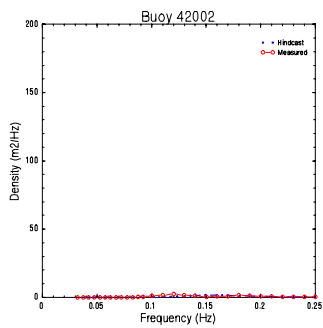
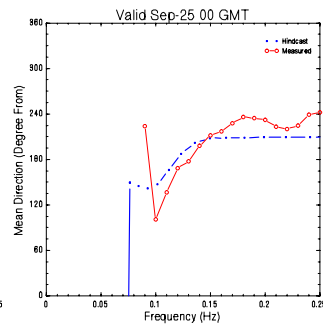
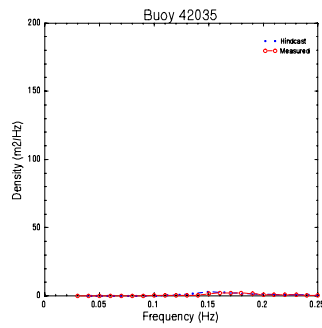
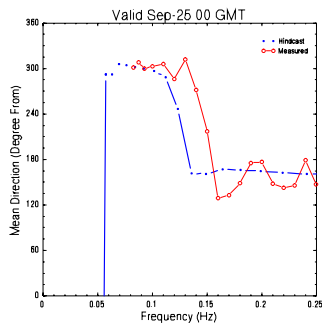
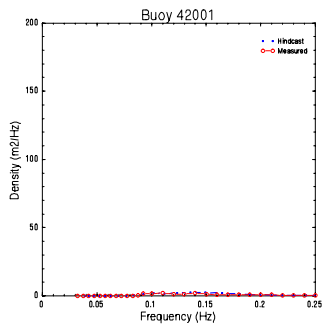


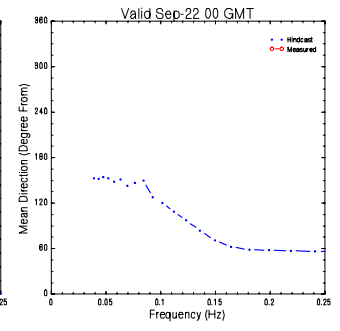
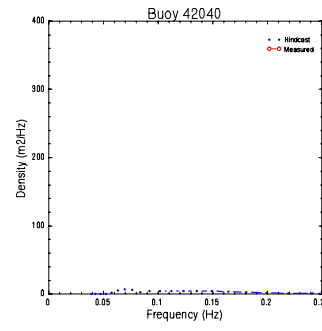
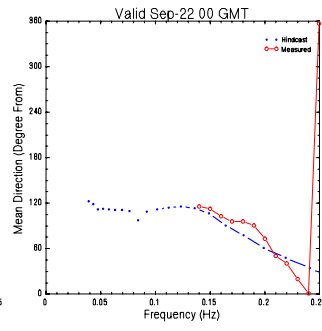
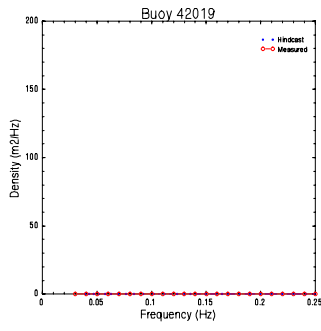
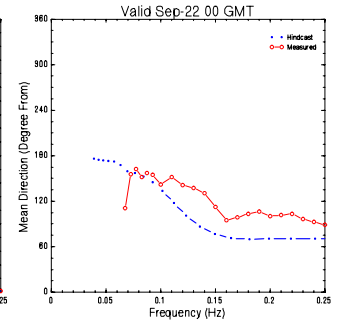
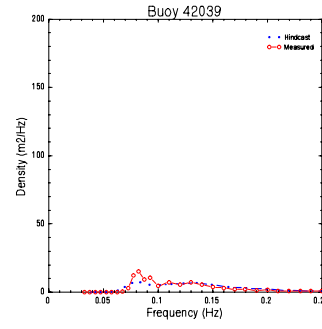
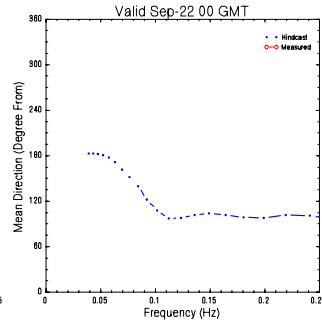
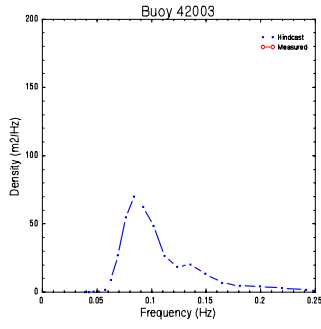
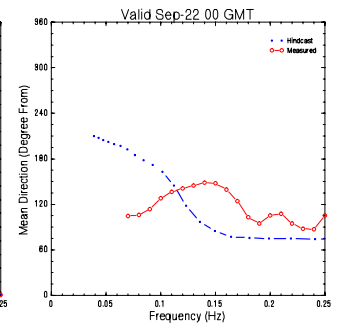
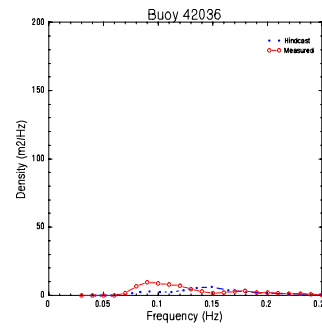
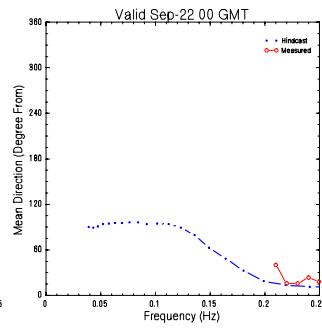
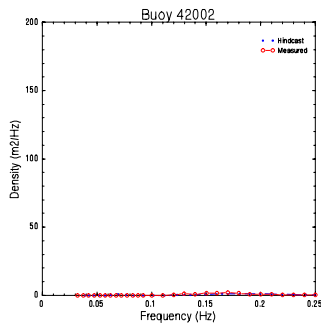
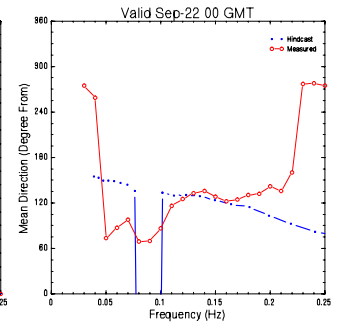
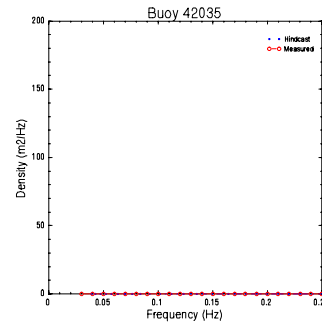
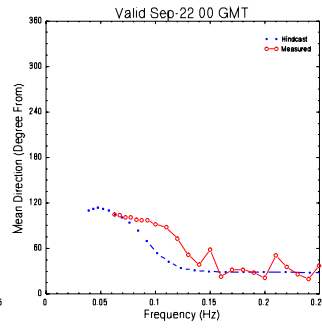
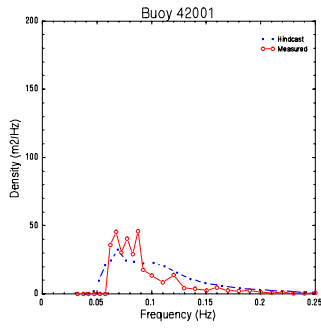


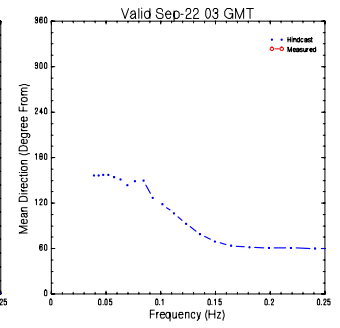
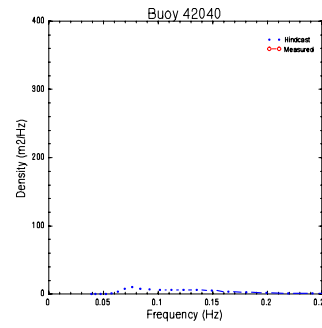
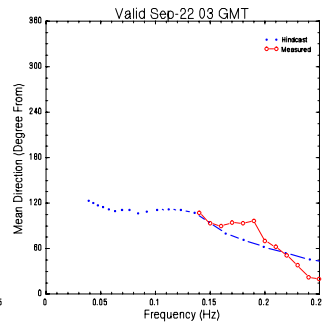
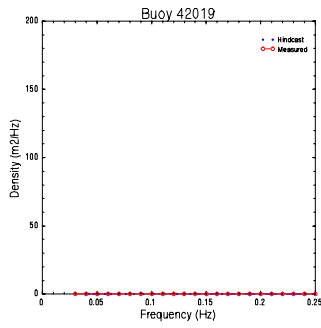
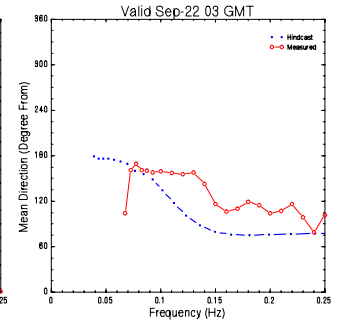
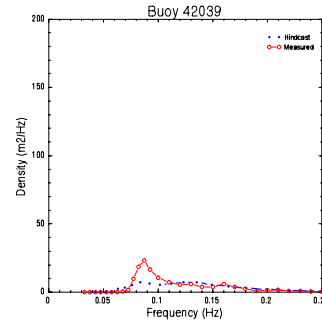
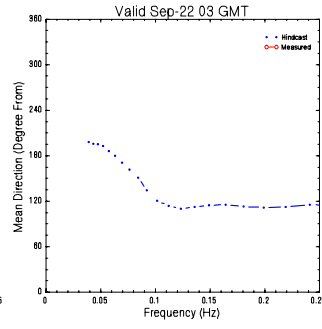
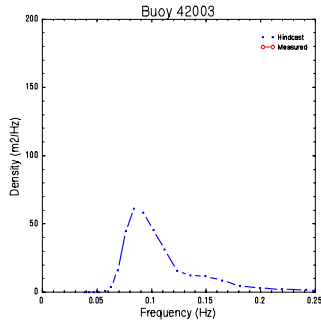
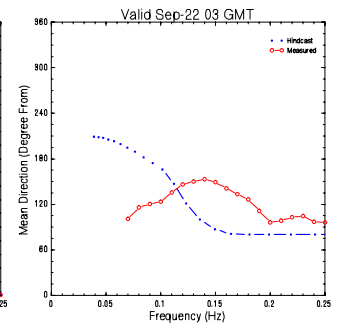
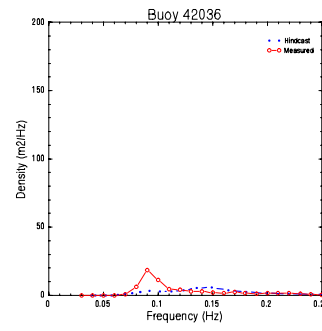
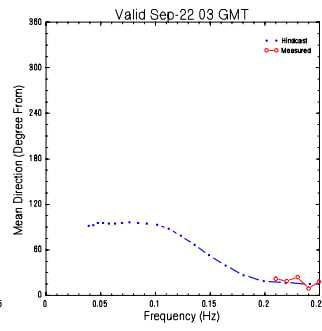
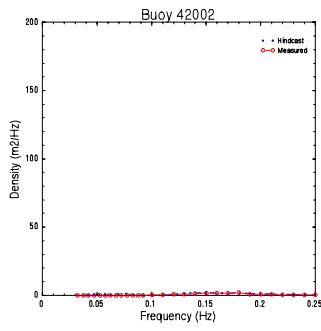
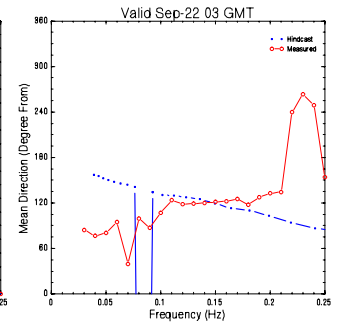
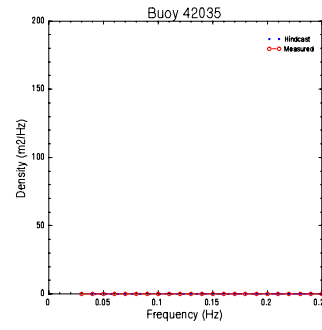
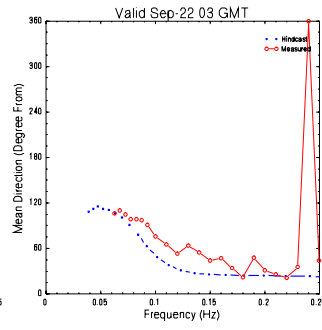
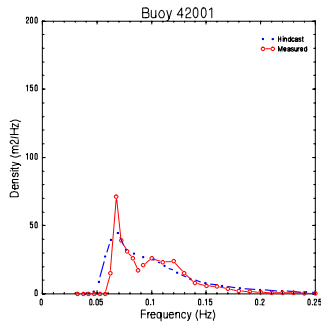


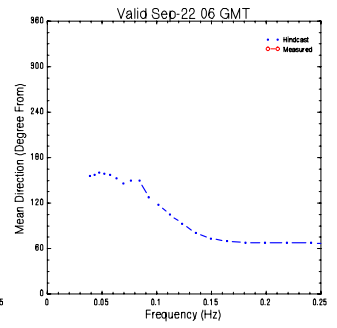
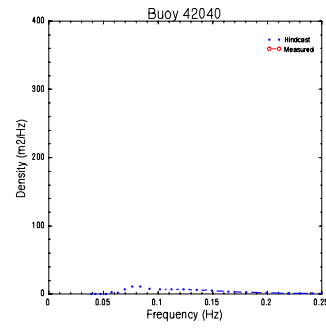
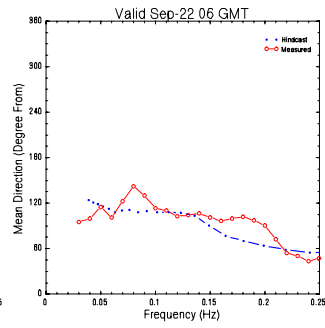
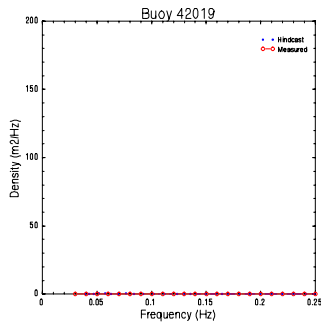
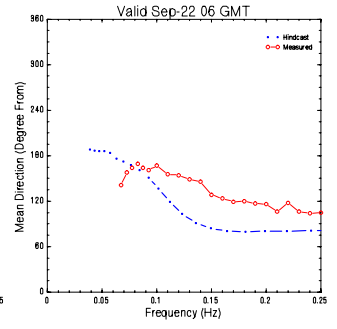
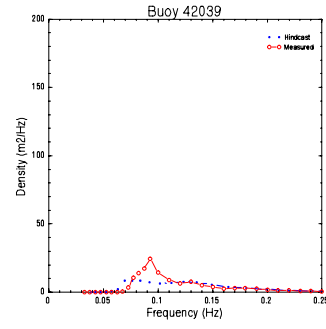
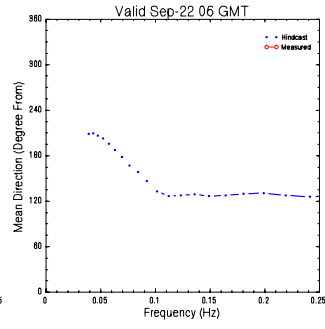
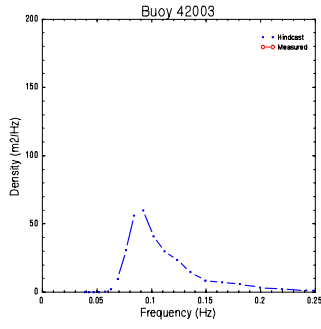
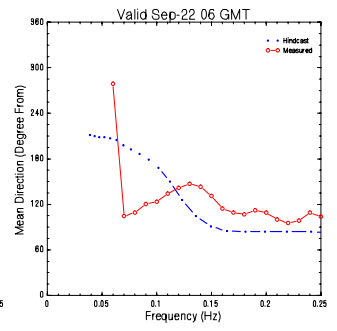
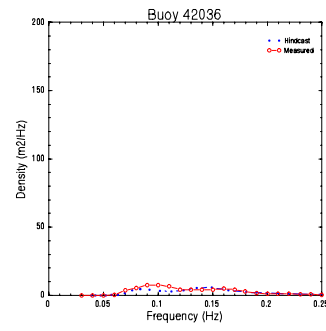
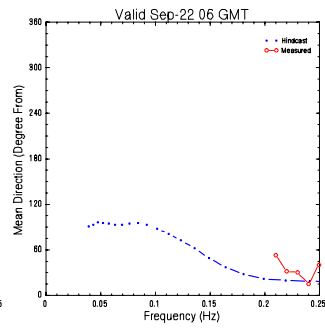
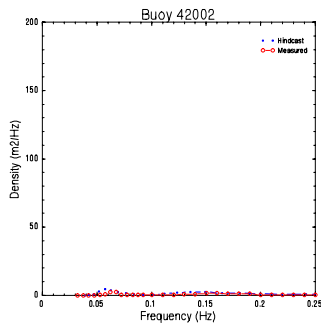
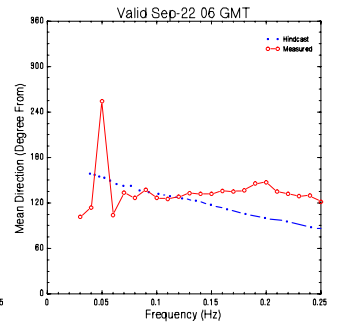
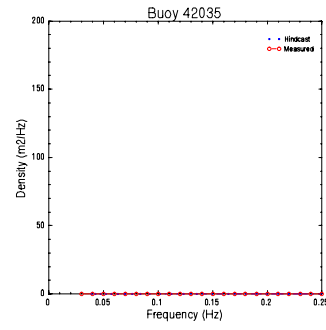
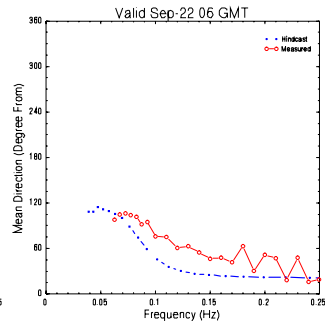
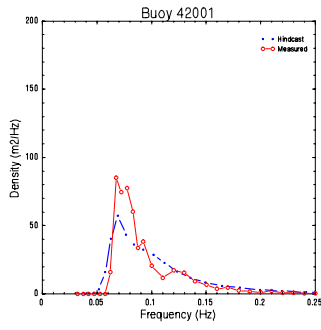


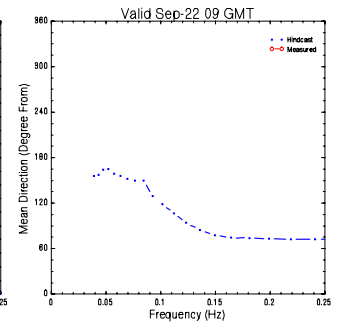
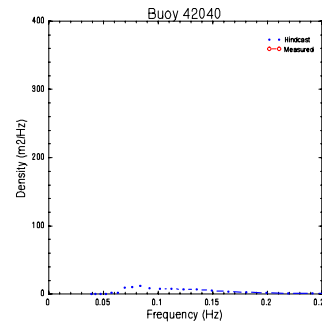
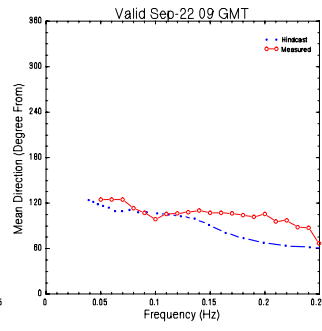
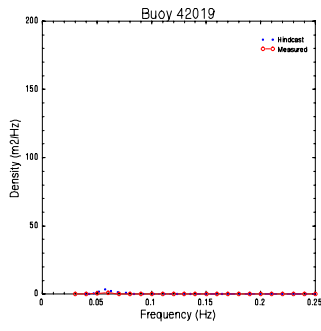
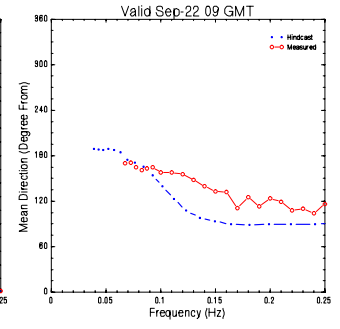
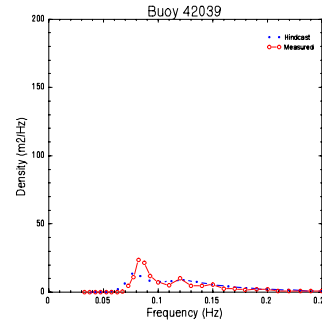
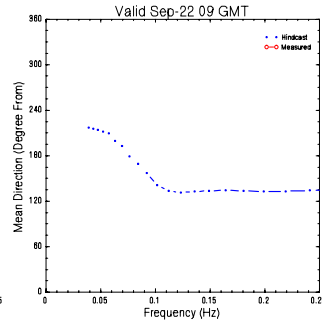
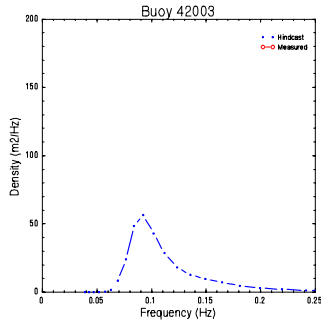
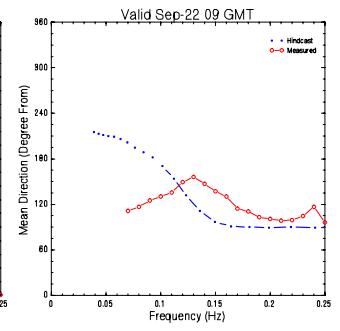
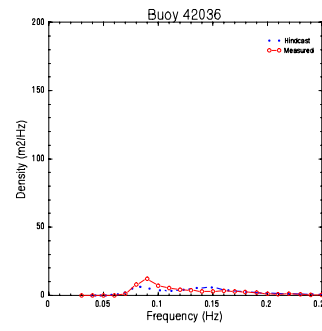
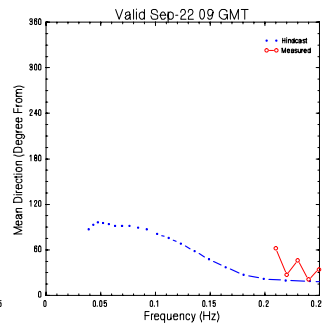
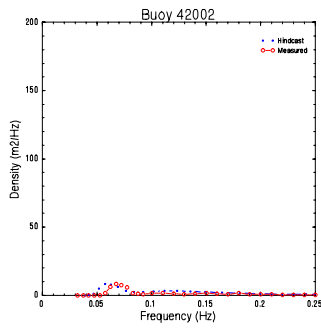
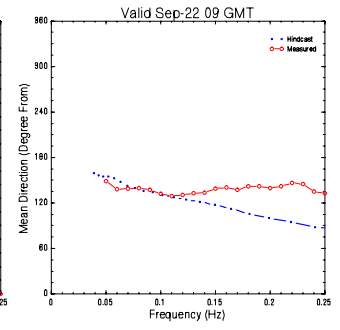
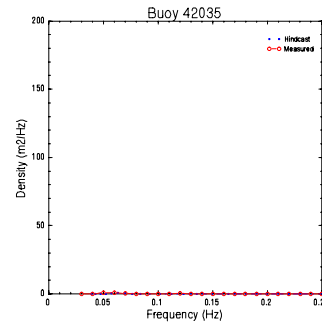
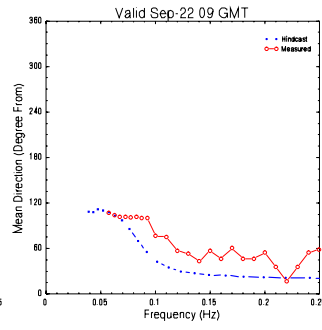
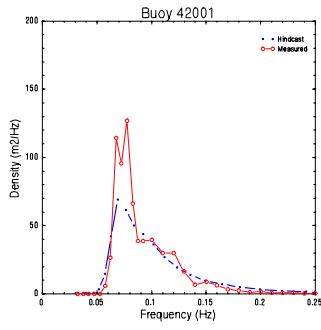
**APPENDIX D Hindcast Wave Spectra at NDBC Buoys during Rita**

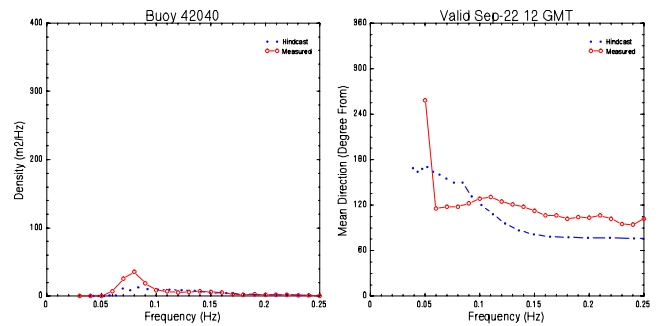
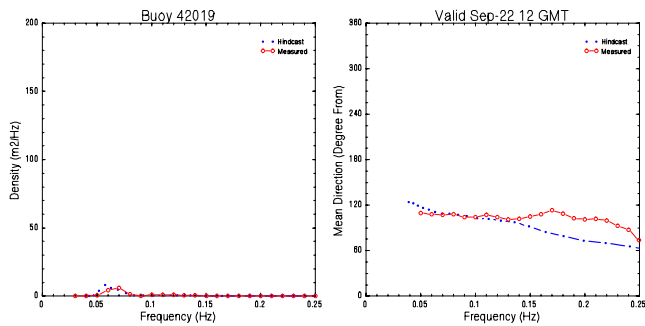
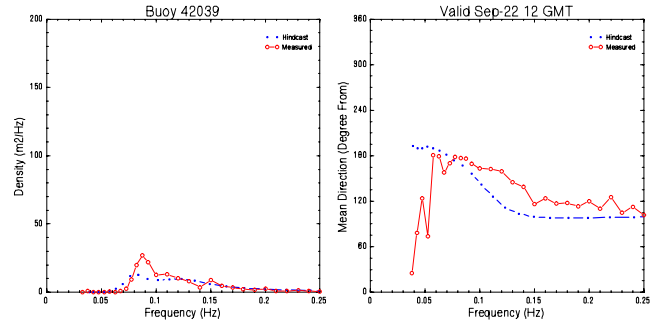
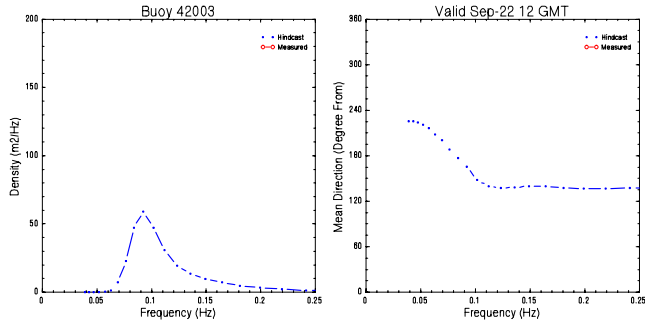
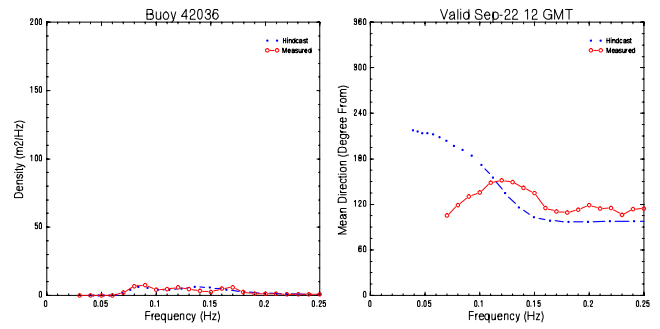
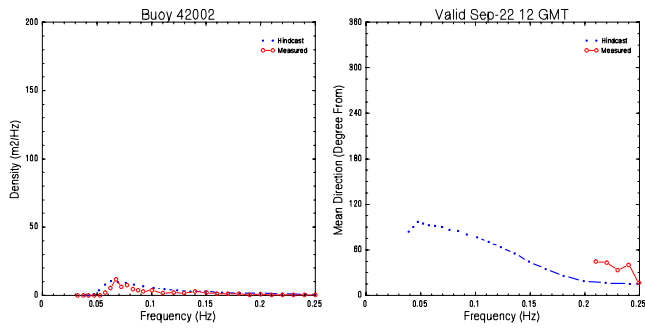
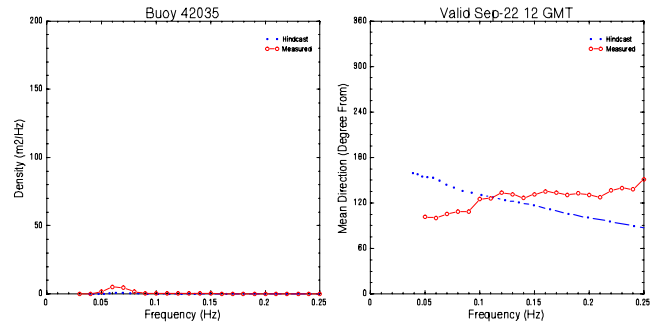
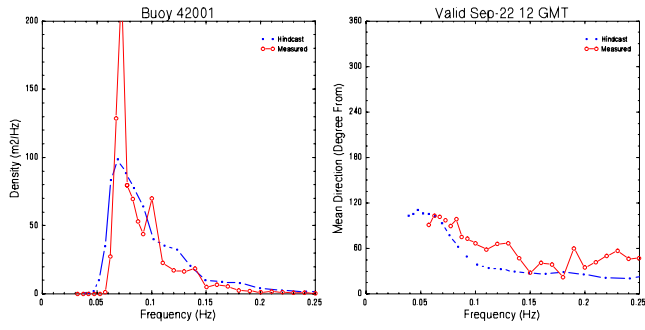


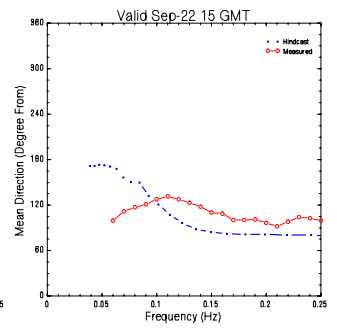
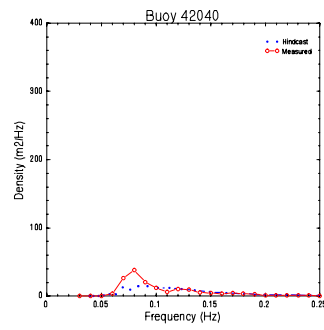
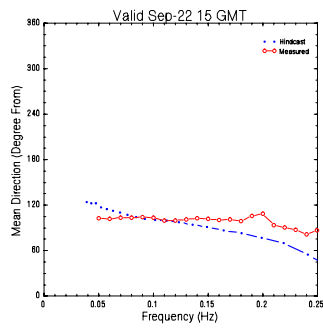
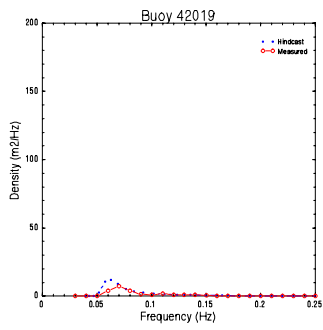
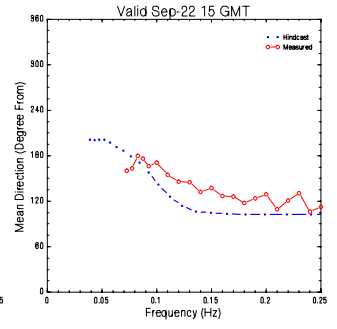
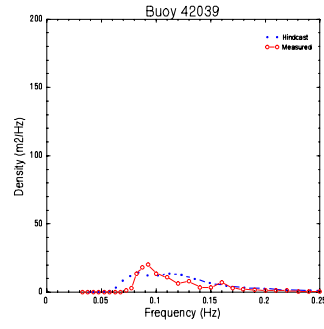
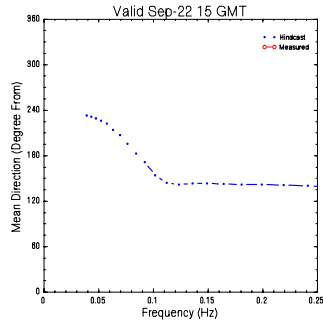
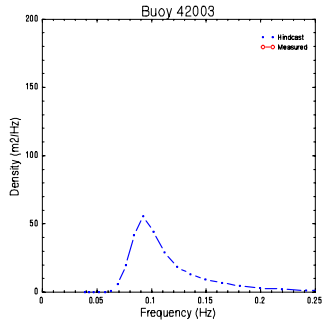
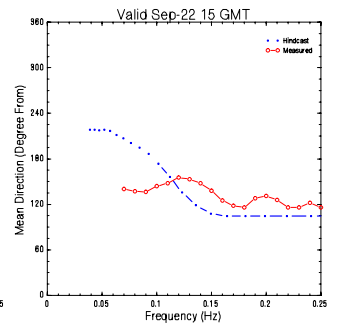
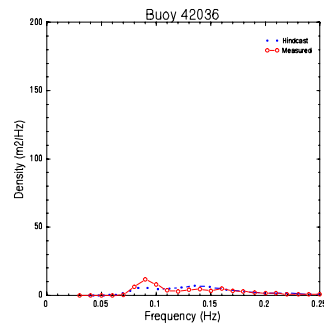
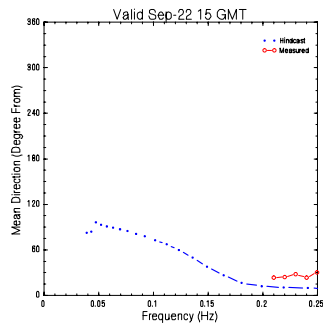
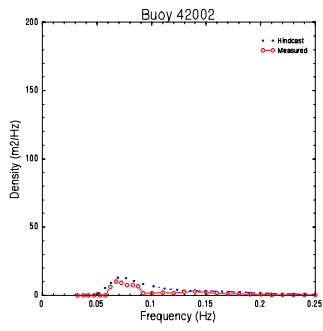
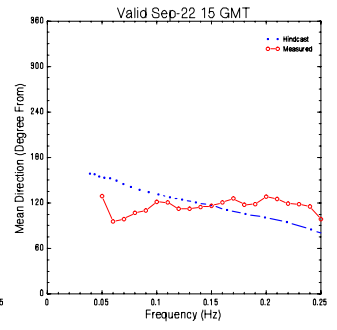
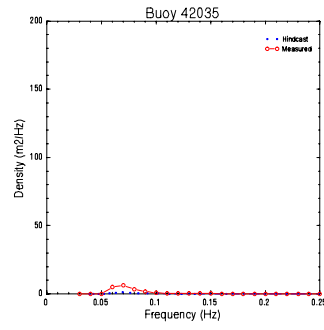
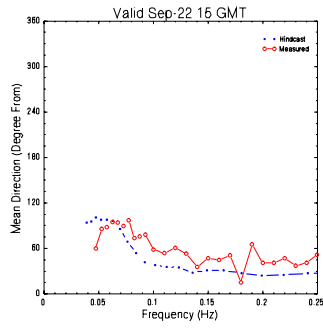
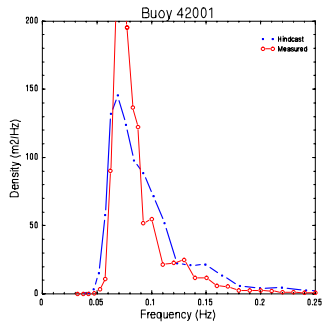


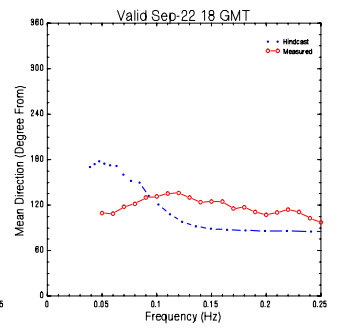
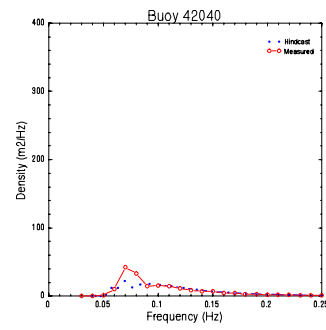
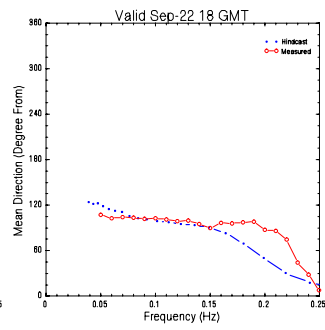
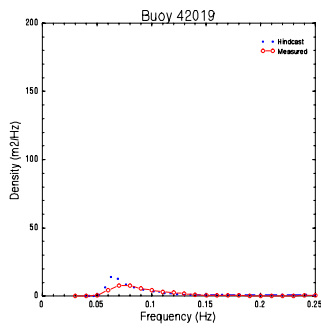
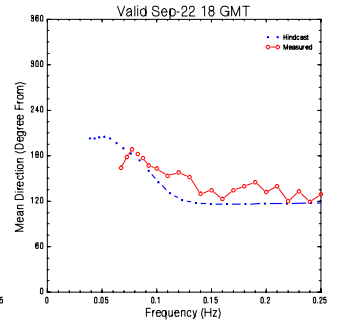
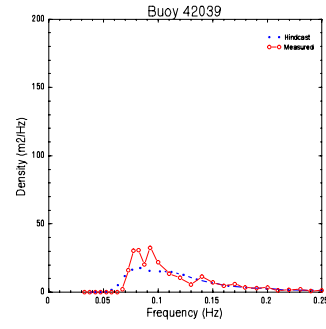
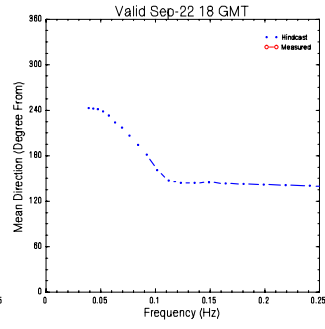
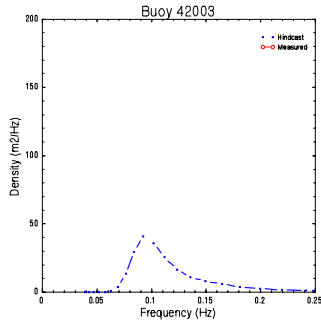
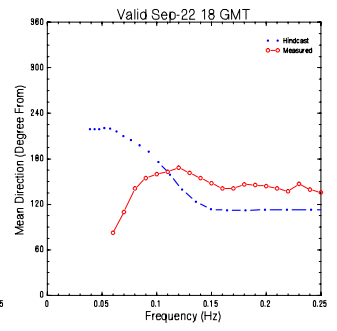
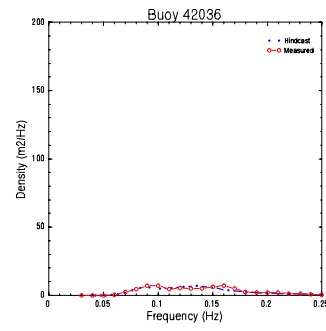
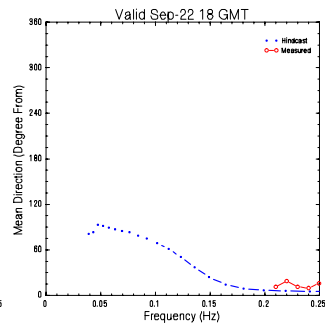
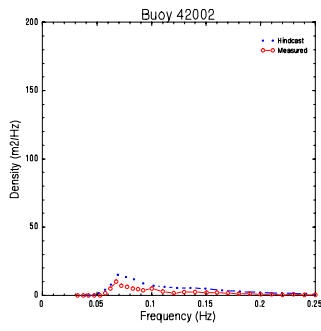
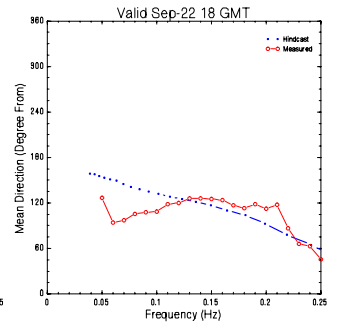
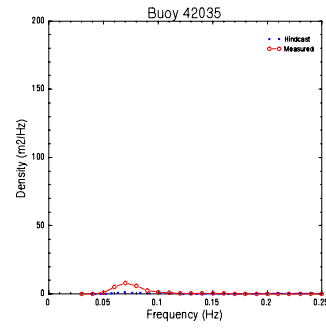
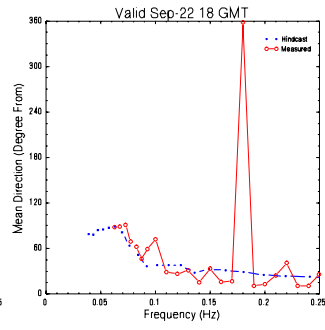
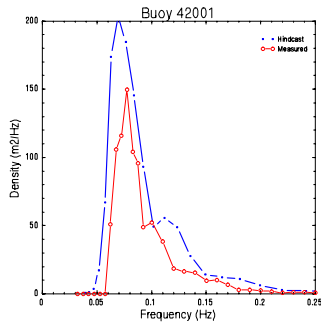


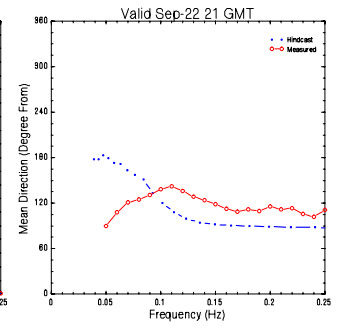
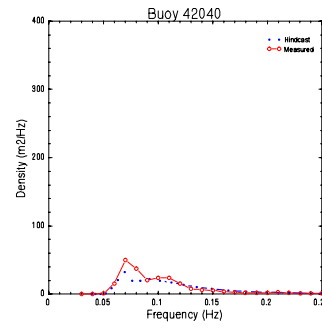
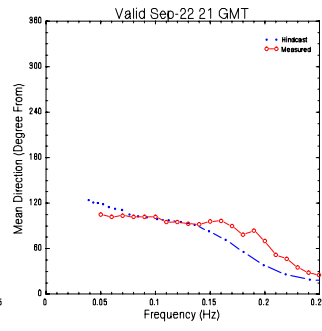
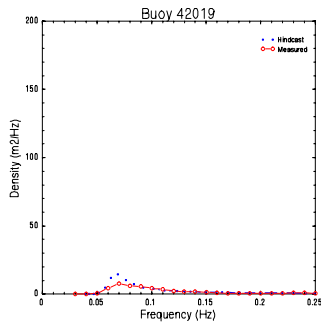
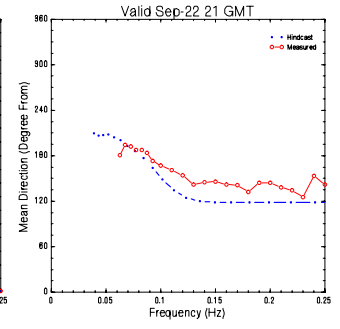
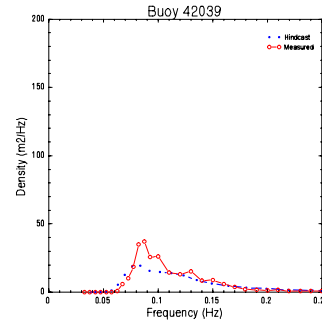
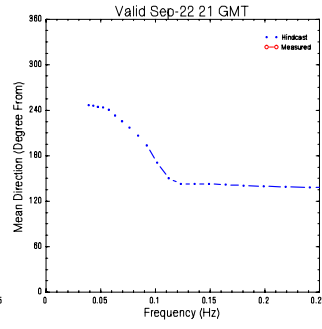
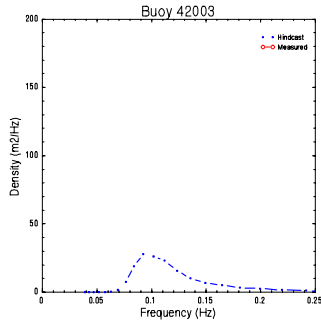
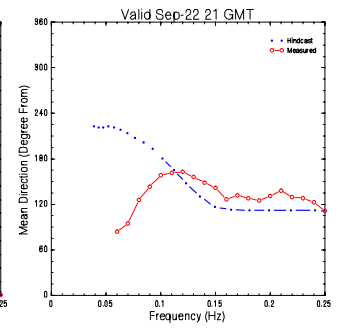
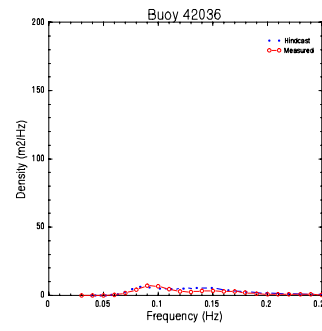
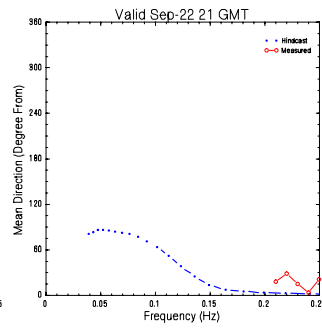
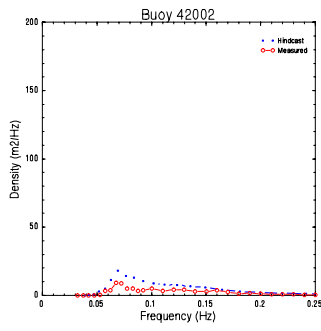
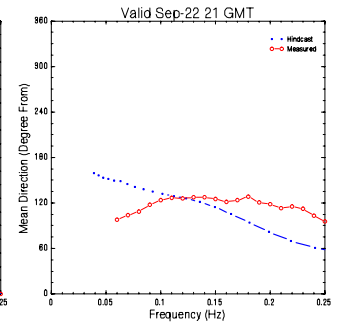
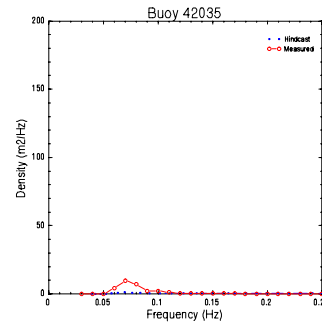
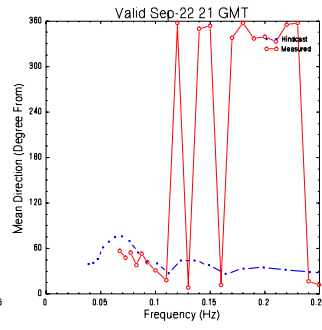
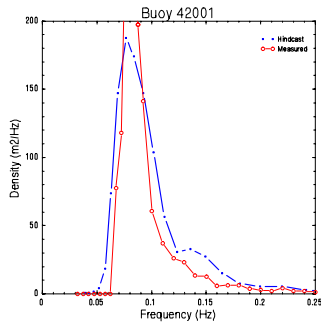


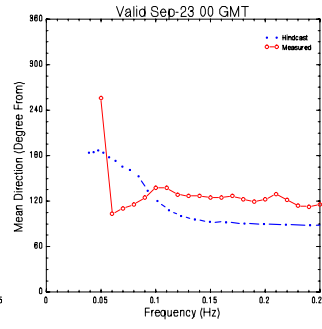
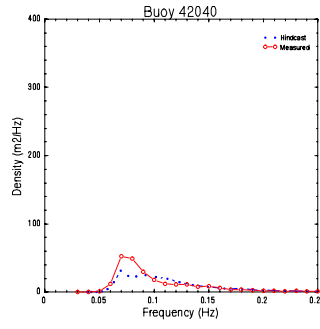
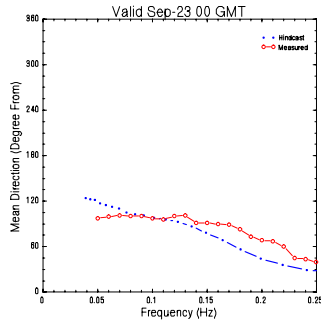
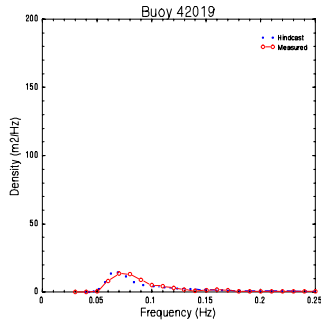
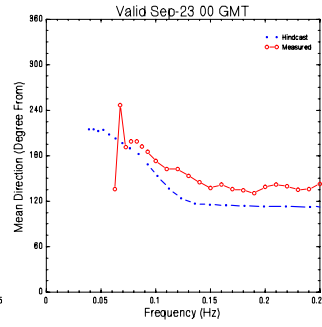
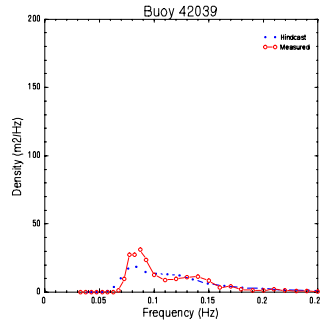
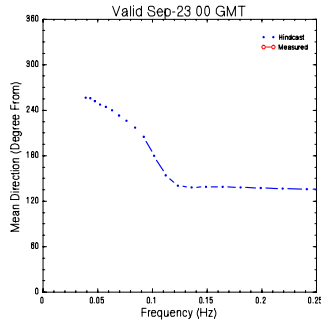
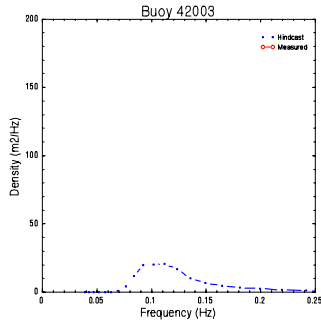
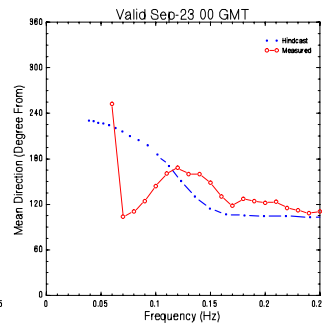
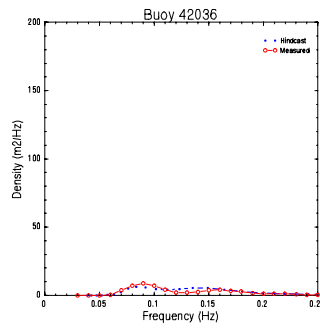
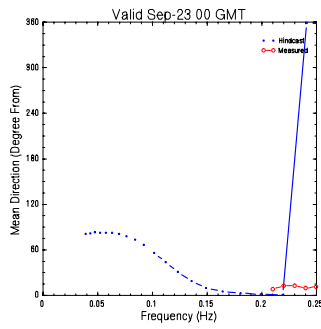
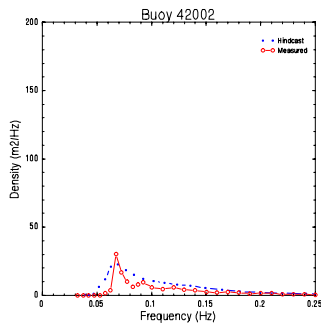
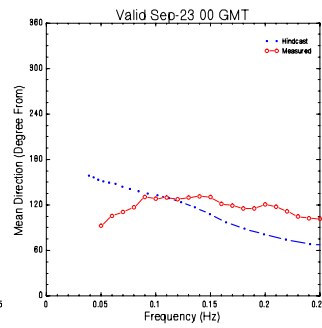
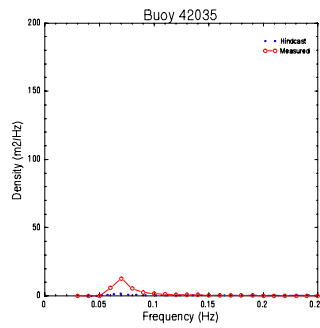
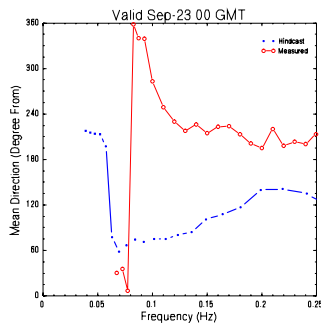
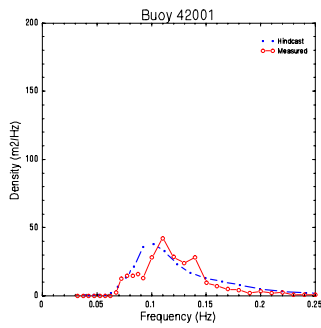


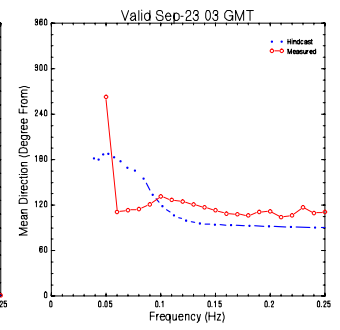
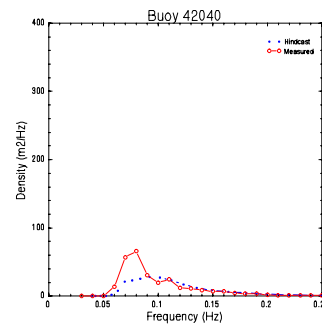
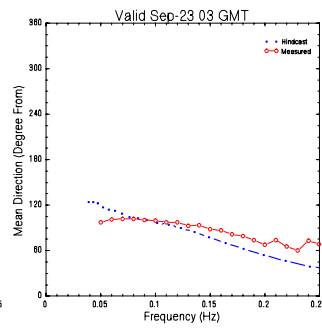
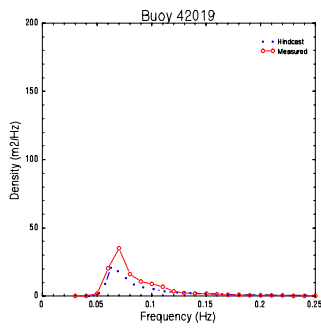
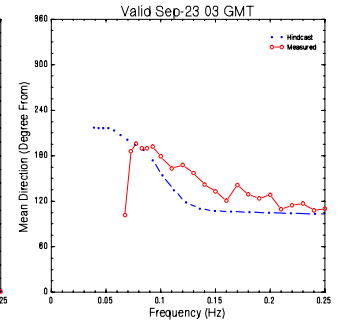
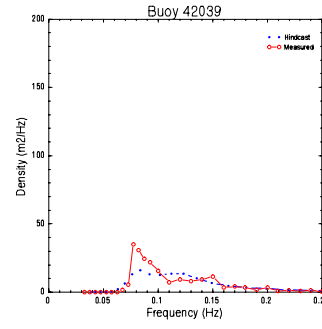
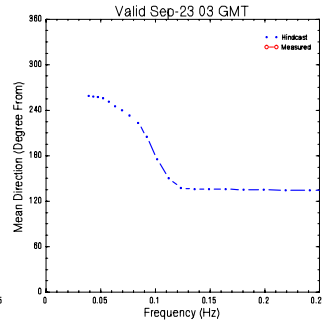
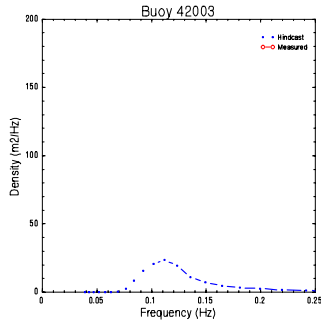
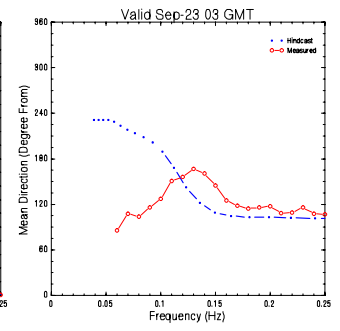
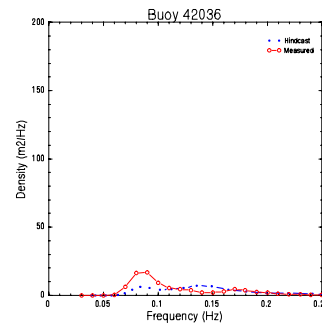
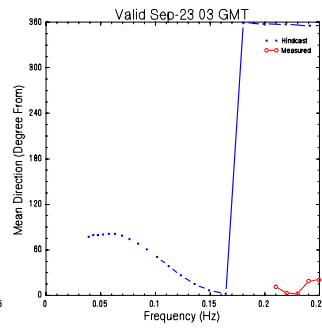
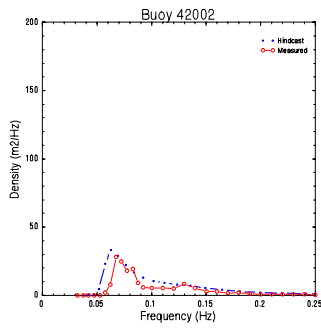
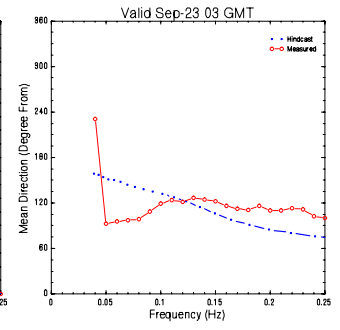
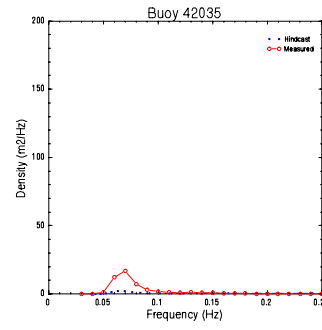
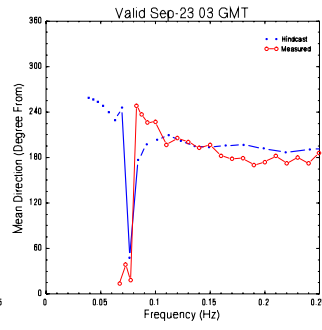
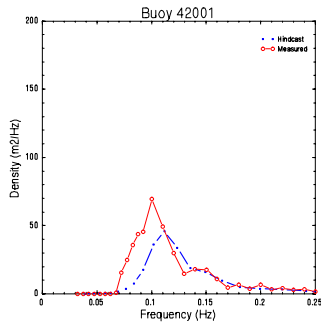


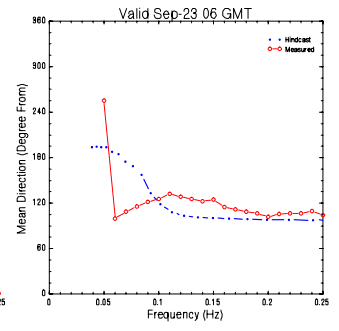
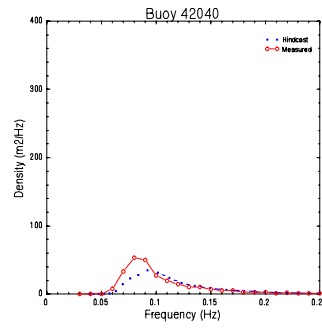
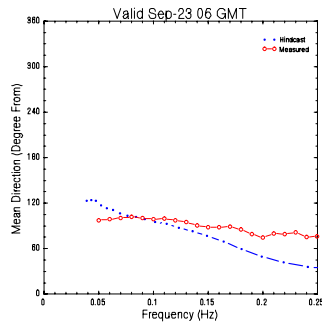
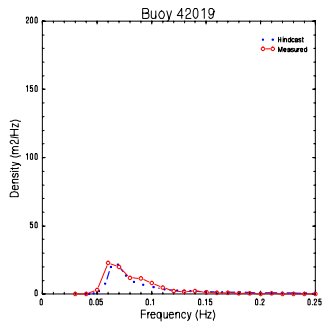
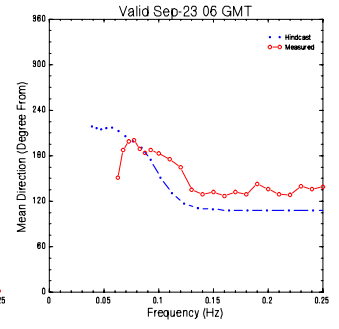
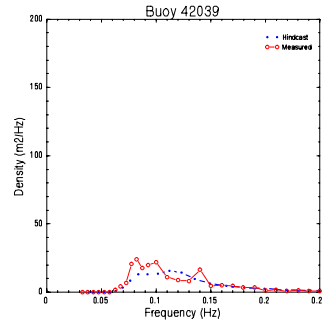
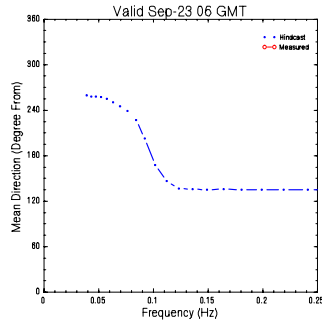
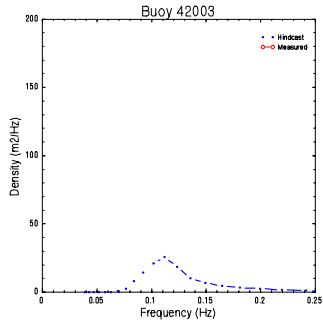
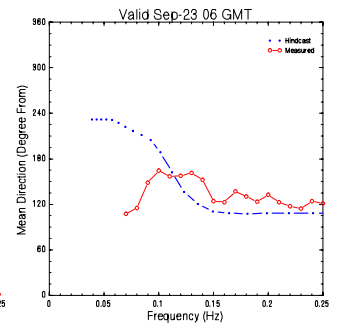
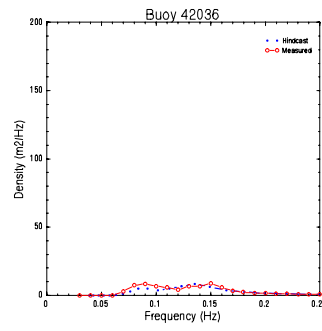
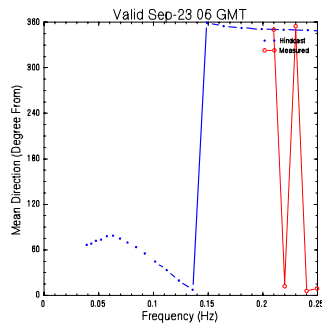
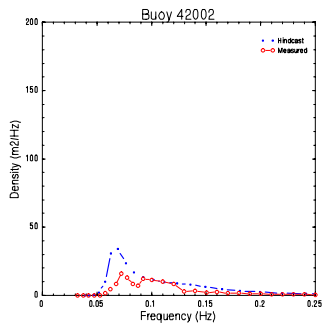
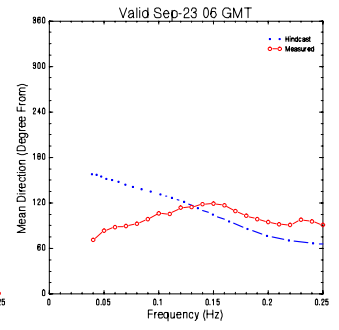
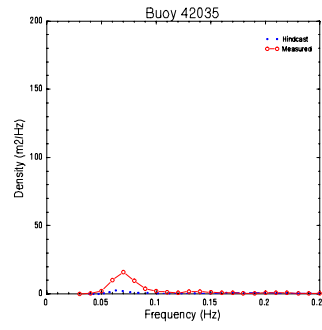
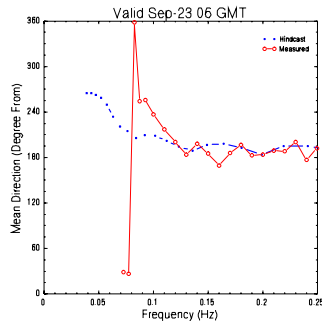
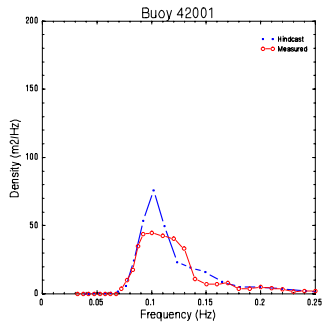


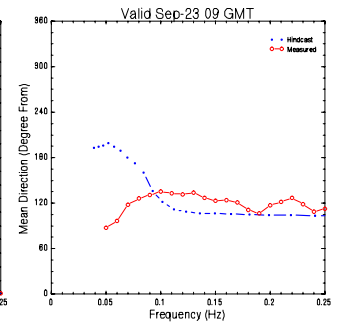
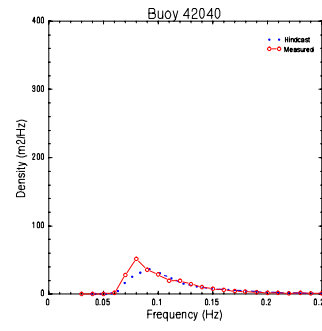
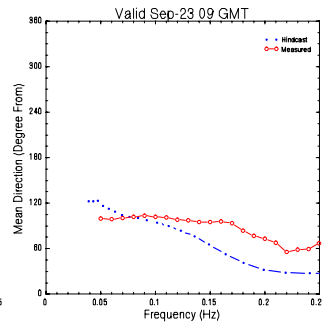
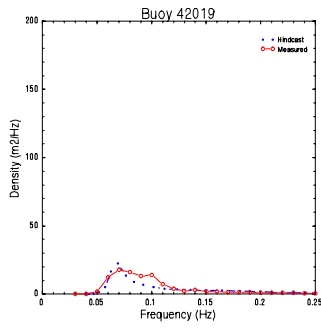
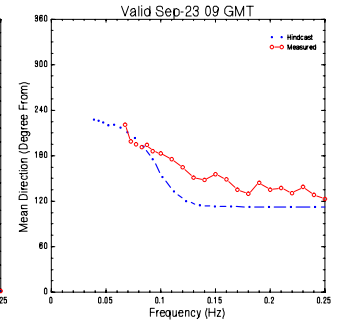
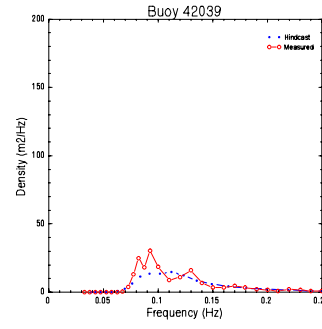
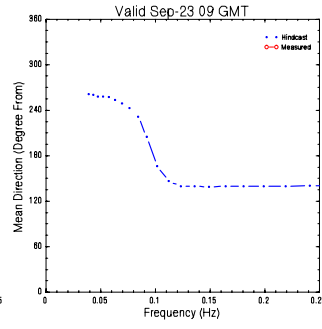
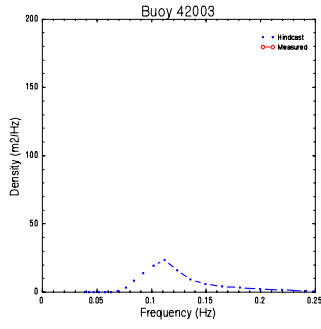
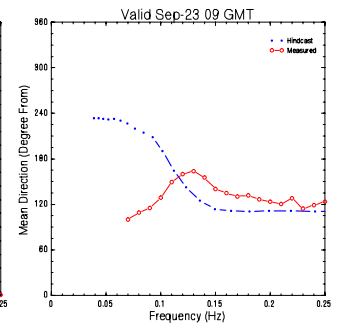
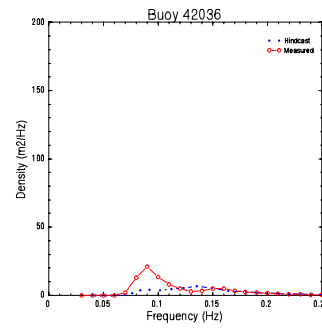
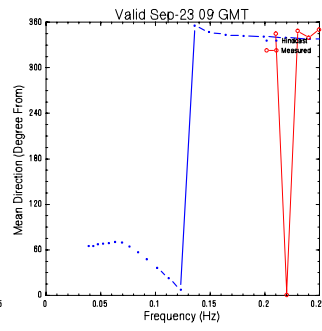
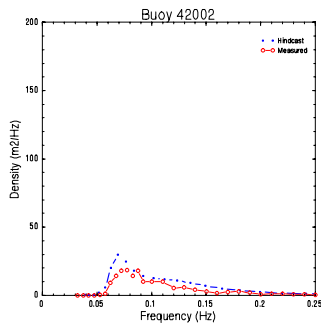
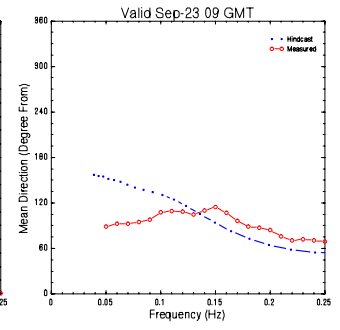
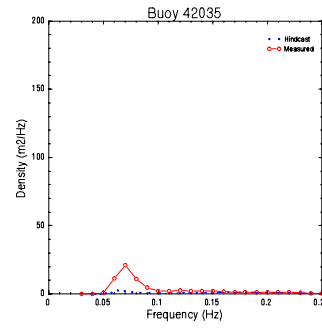
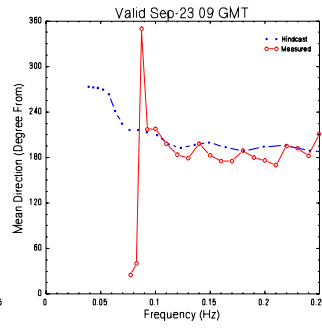
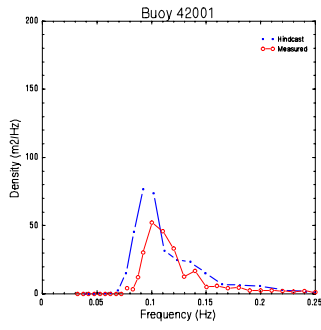


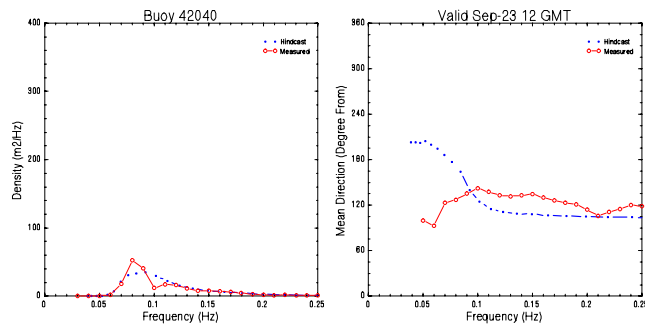
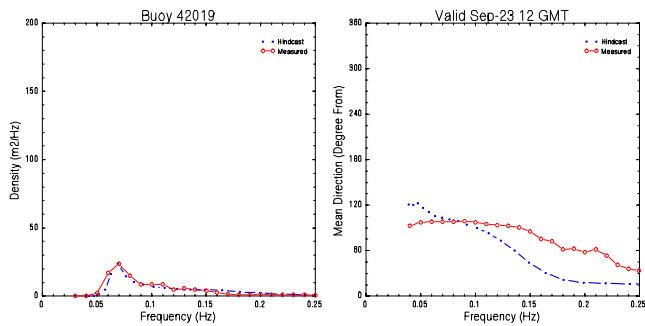
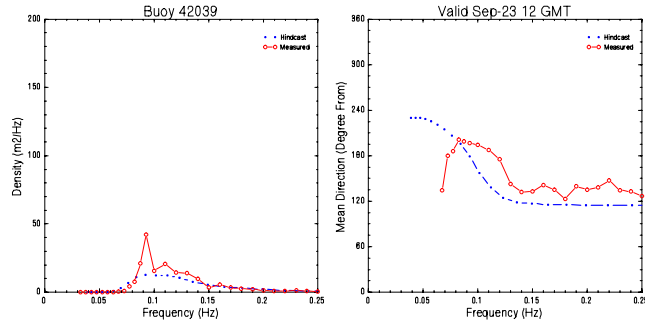
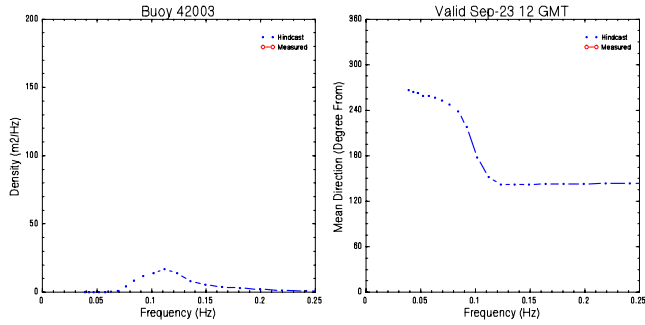
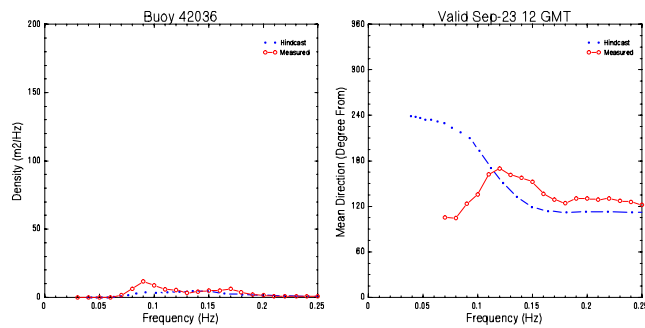
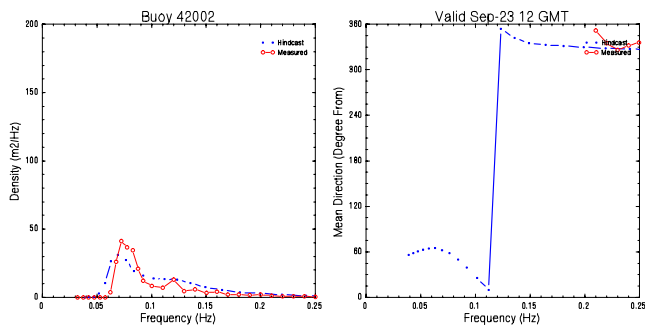
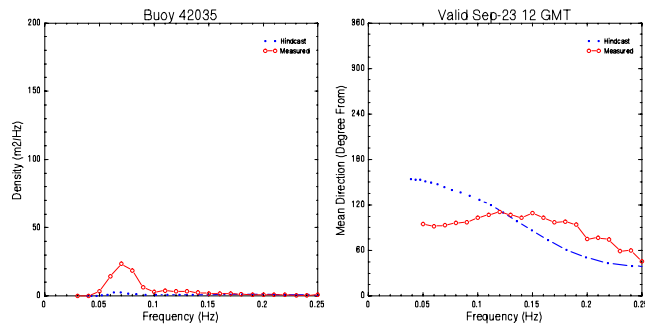
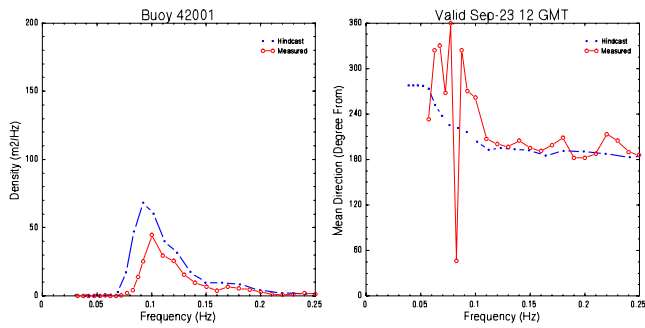


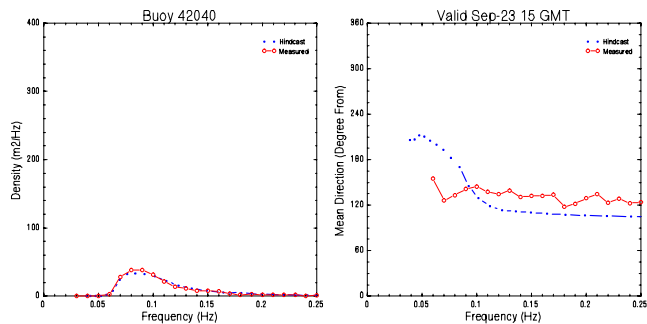
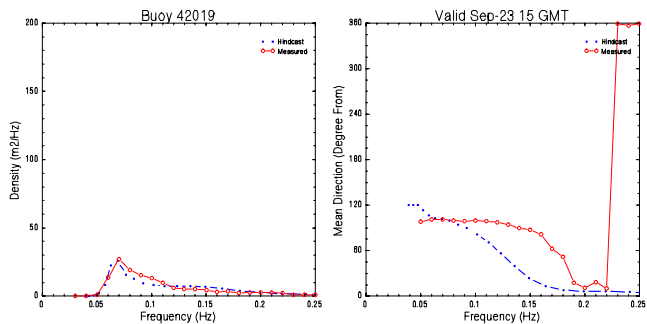
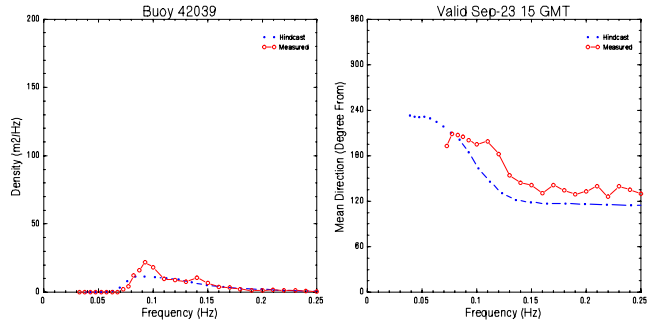
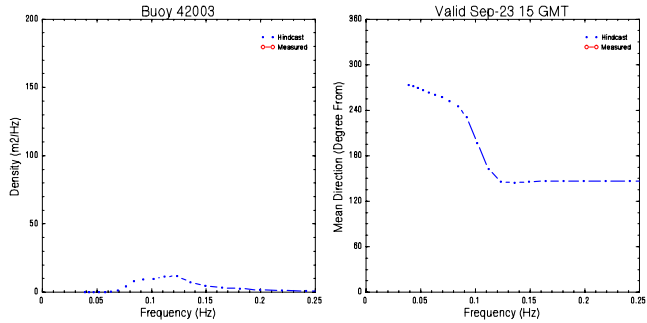
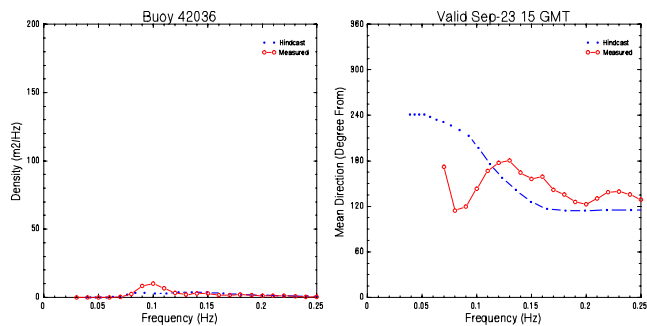
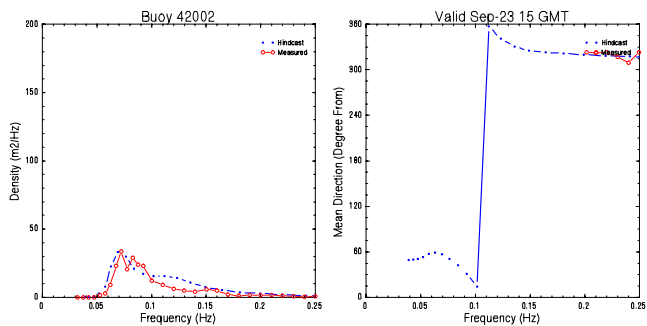
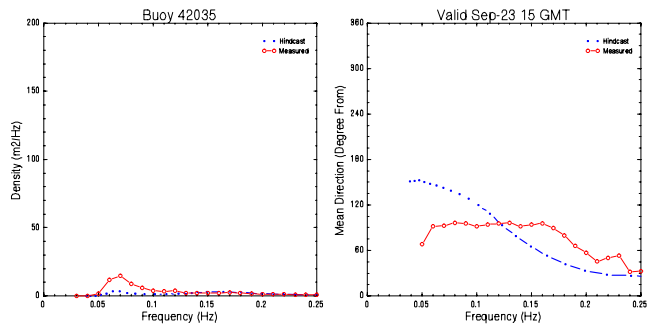
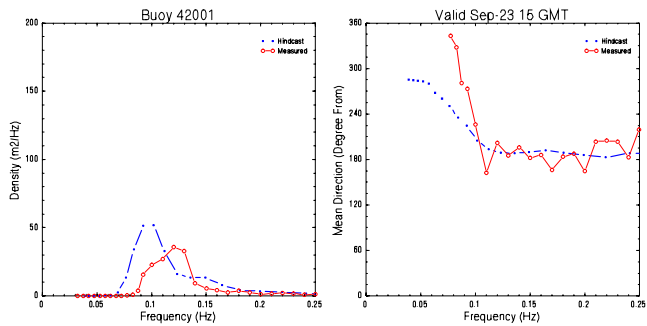






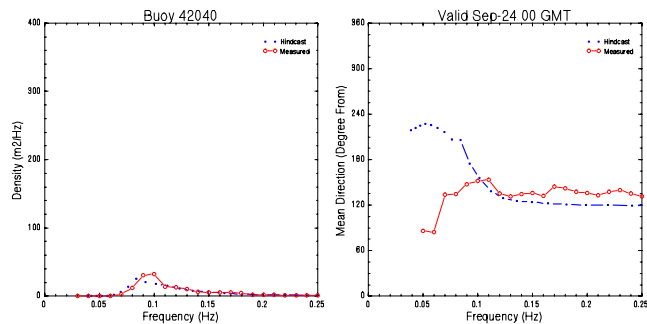
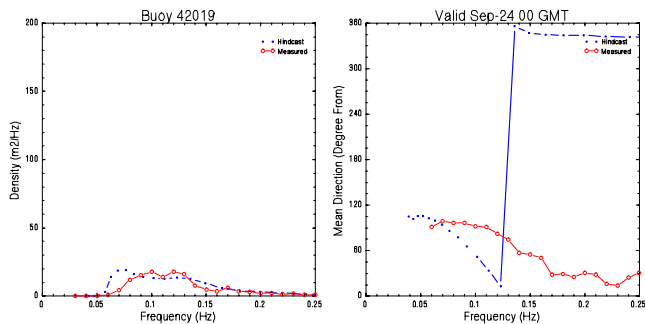
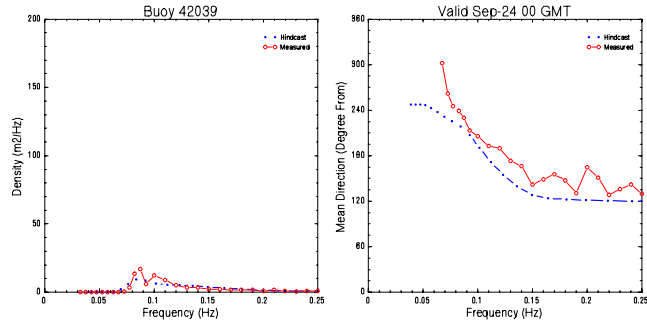
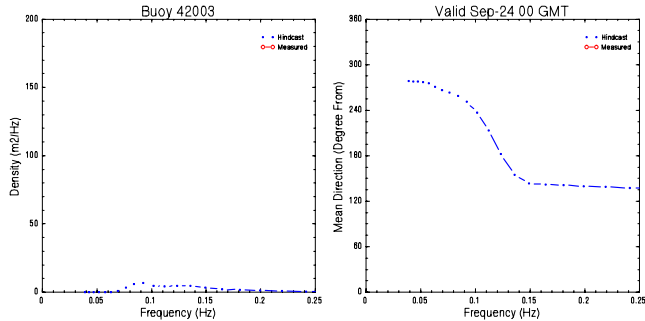
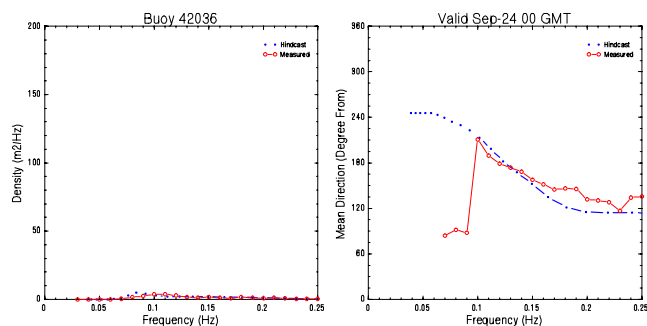
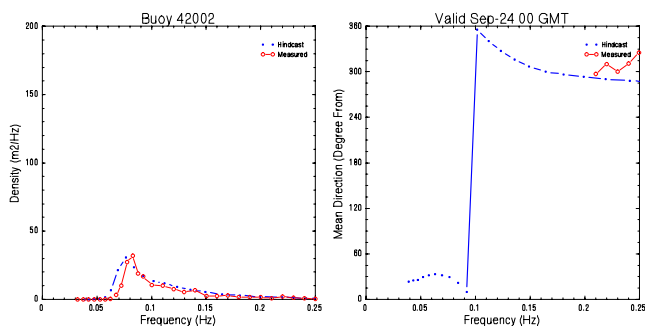
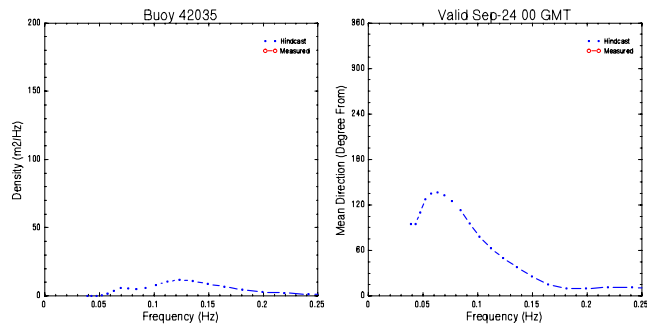
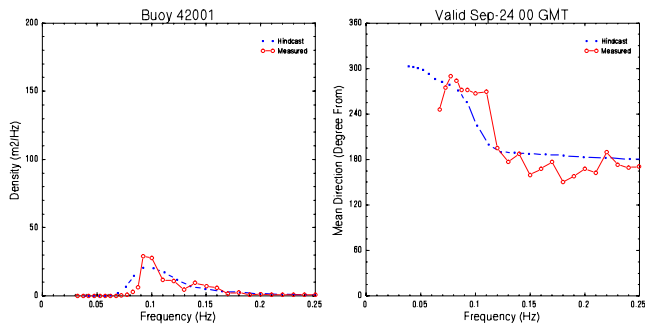


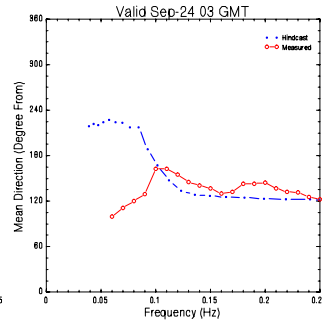
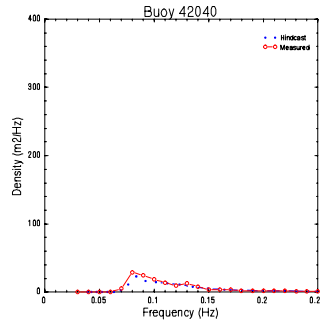
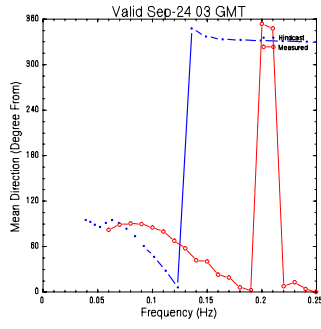
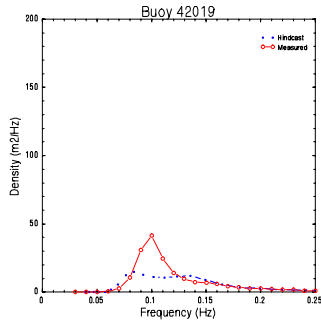
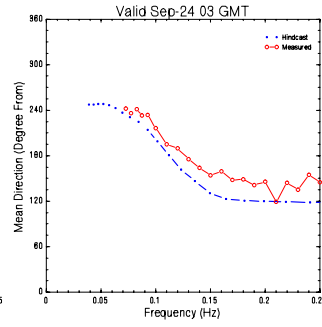
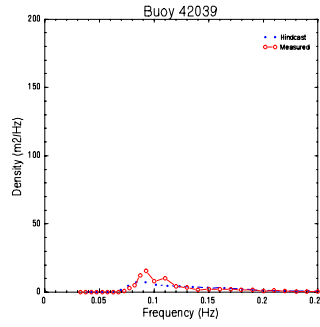
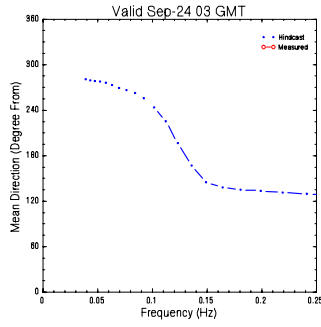
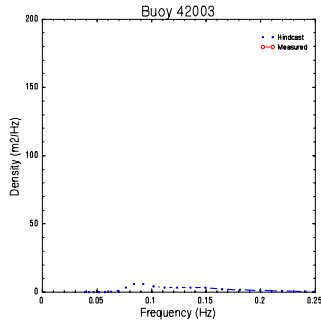
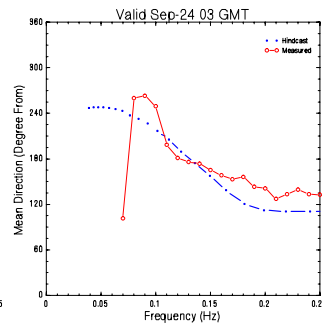
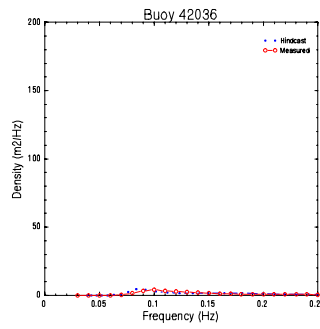
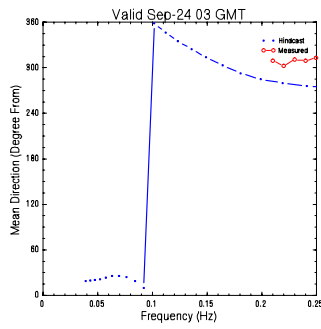
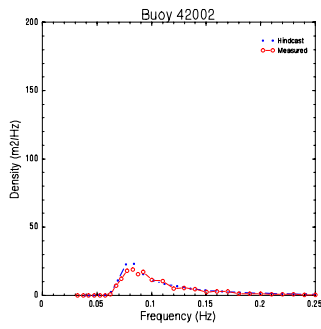
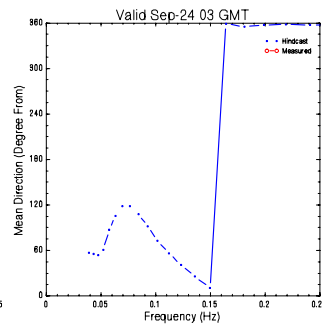
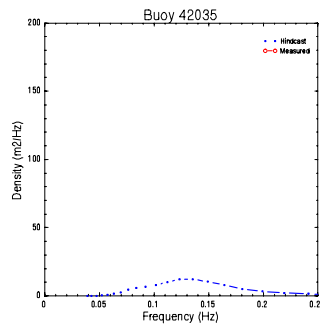
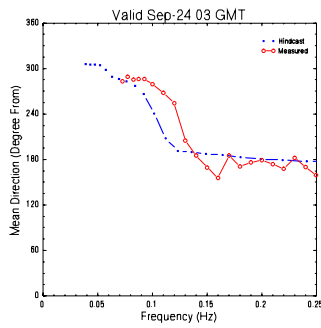
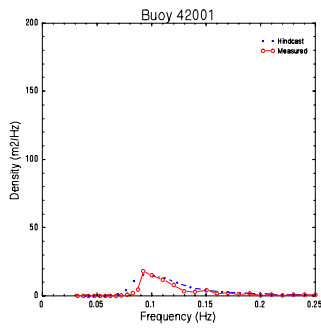


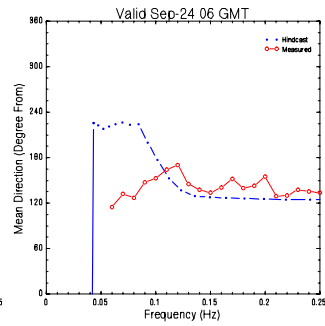
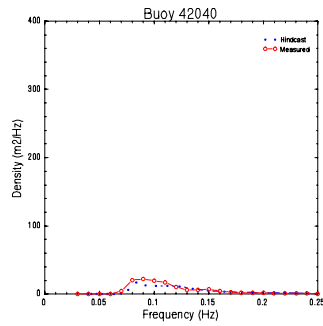
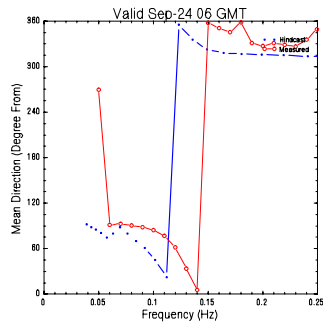
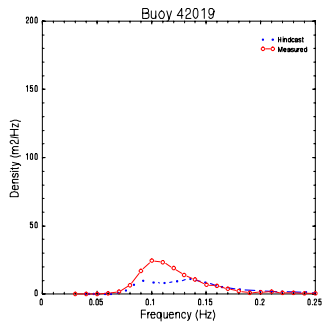
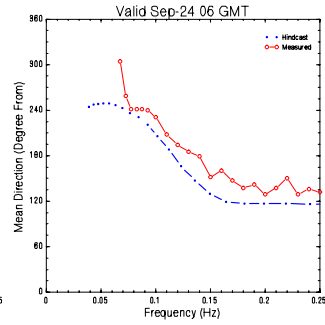
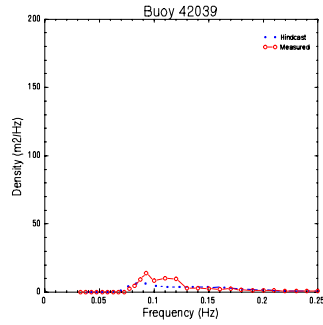
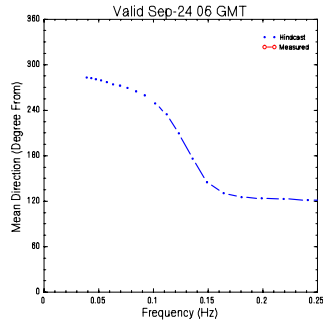
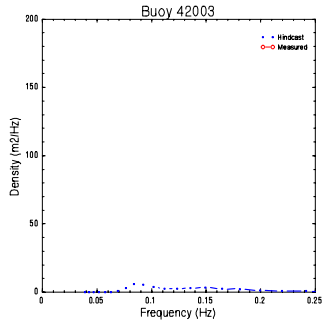
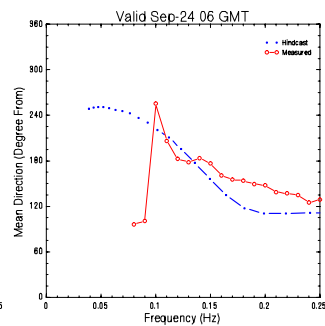
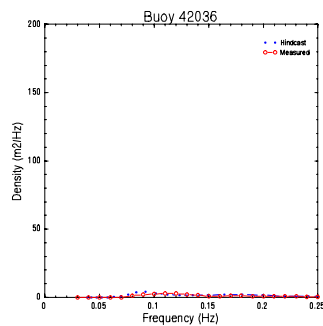
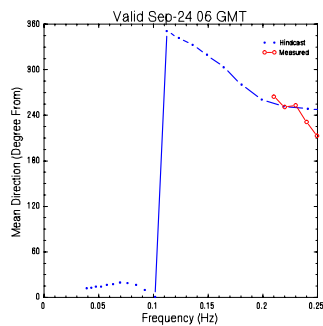
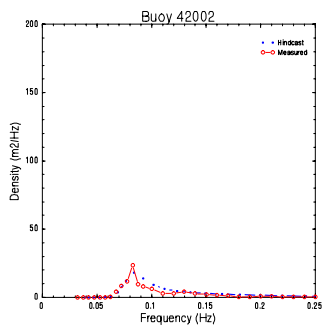
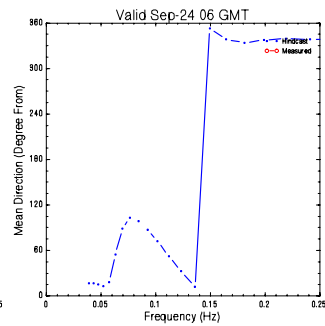
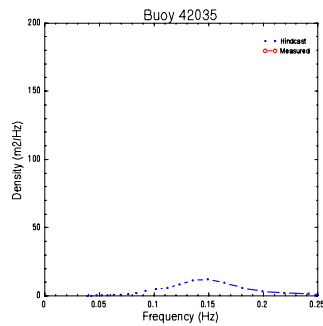
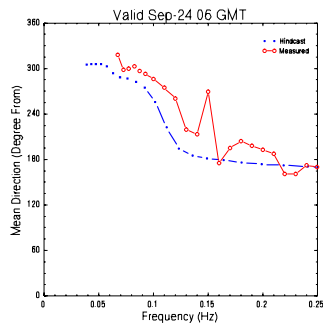
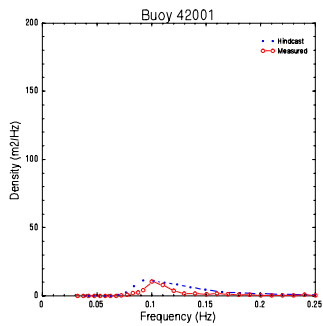


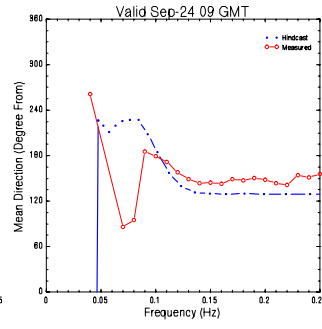
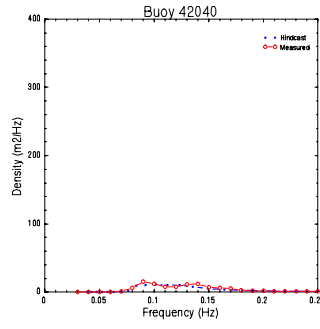
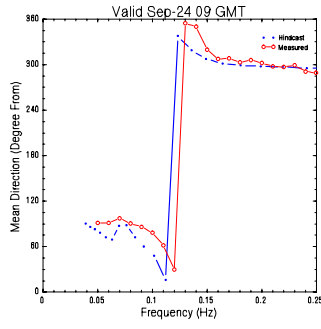
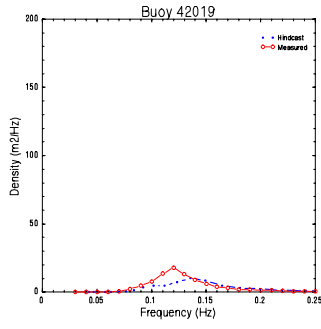
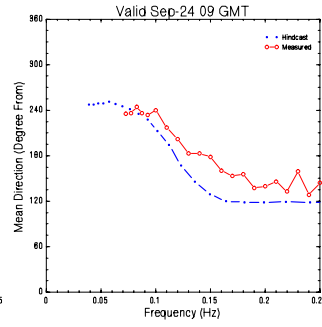
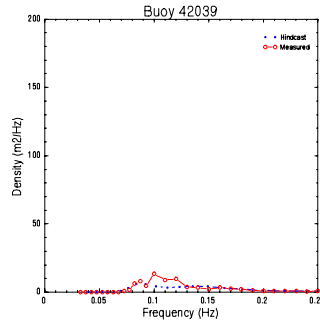
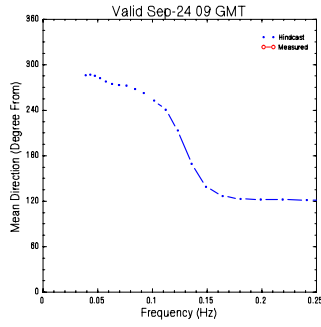
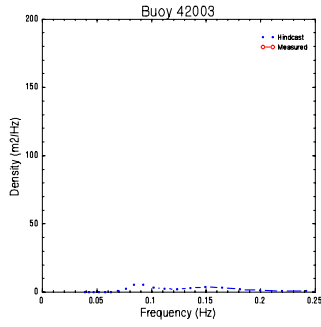
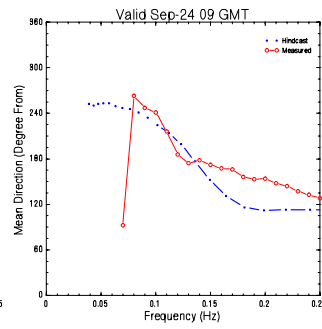
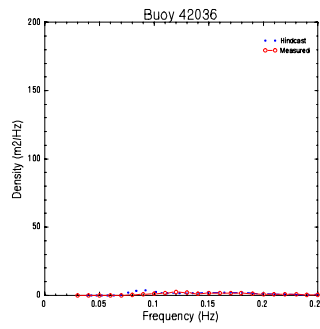
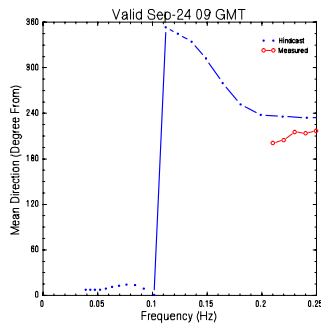
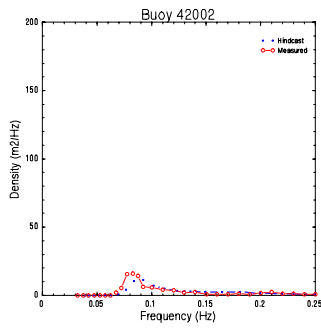
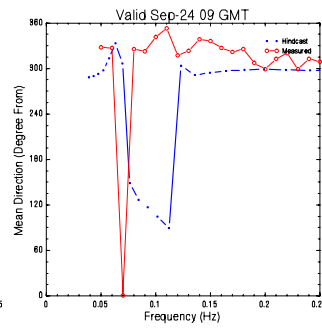
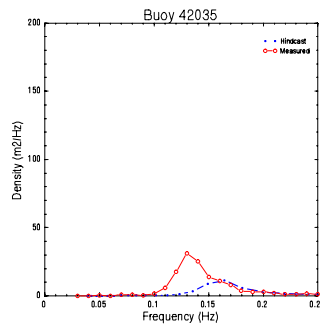
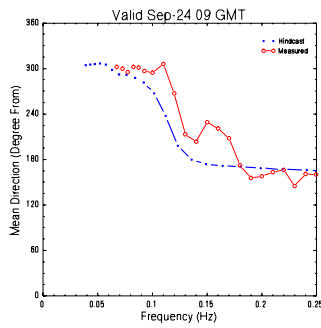
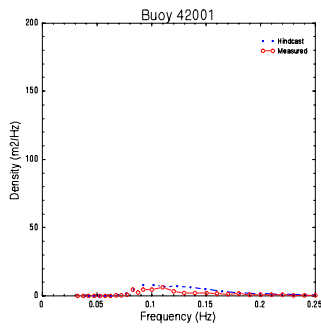




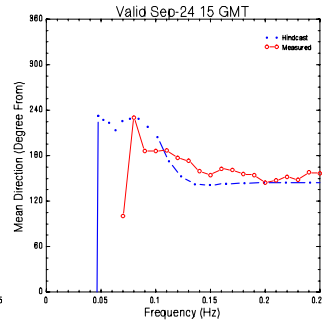
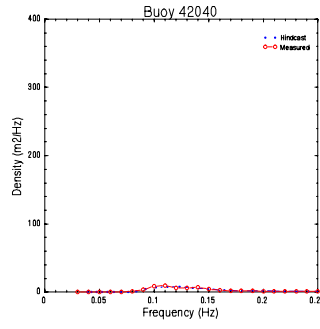
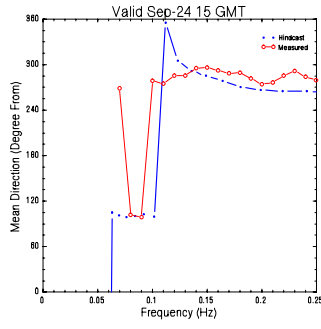
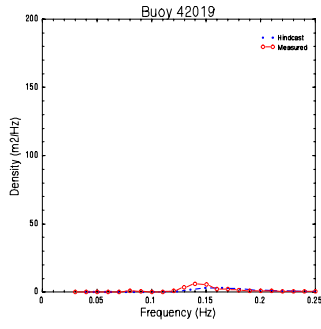
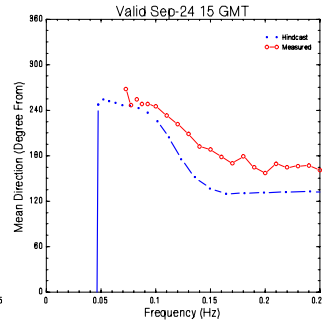
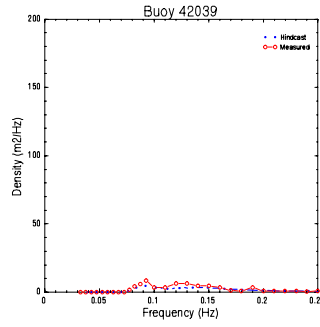
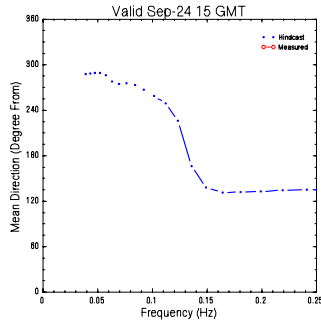
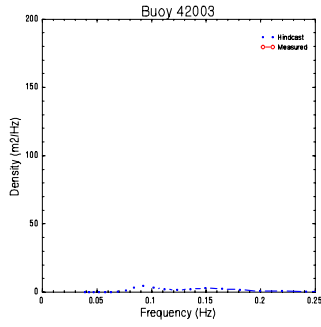
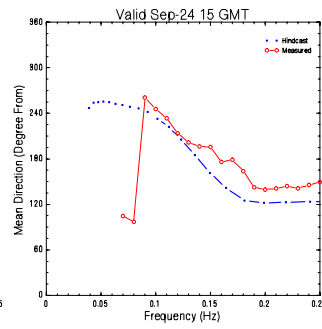
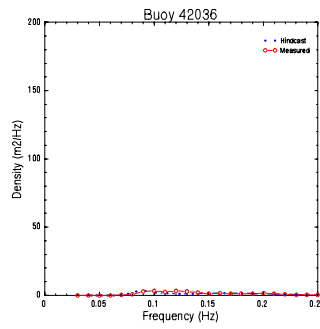
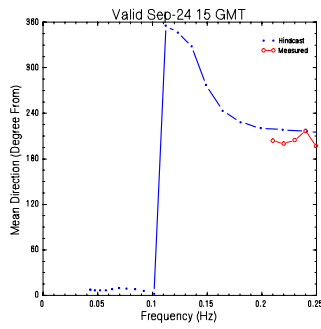
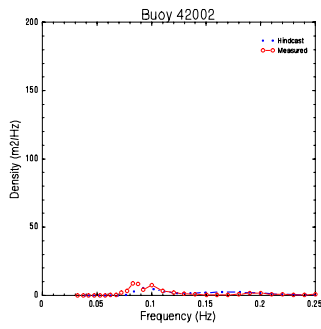
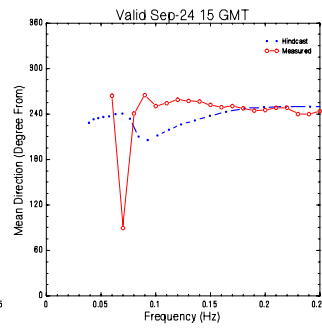
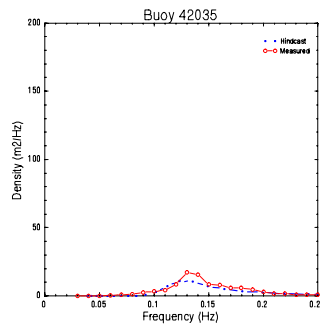
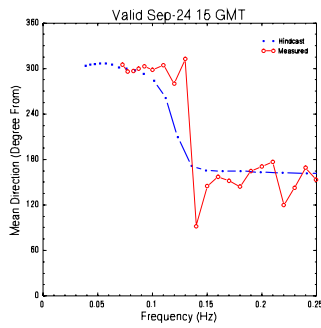
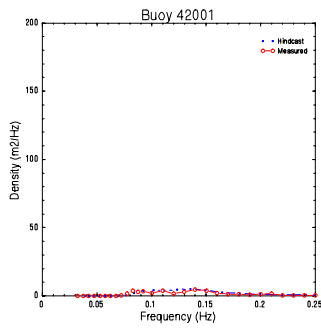


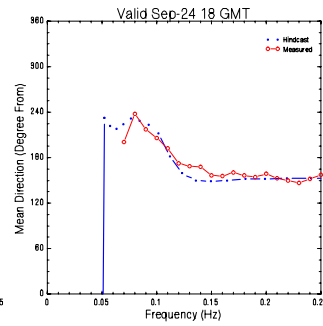
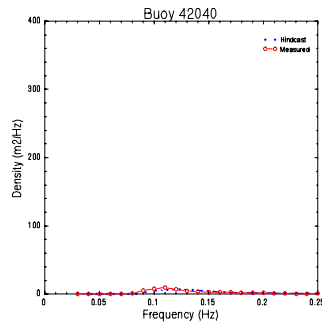
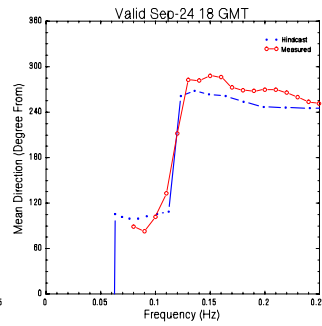
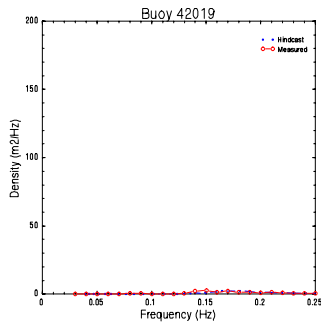
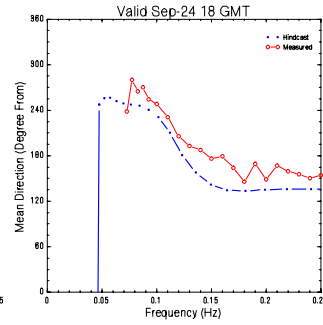
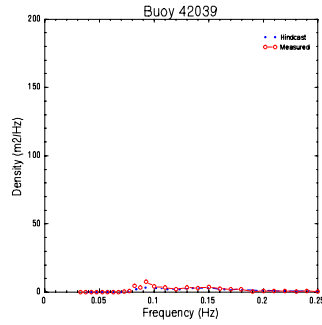
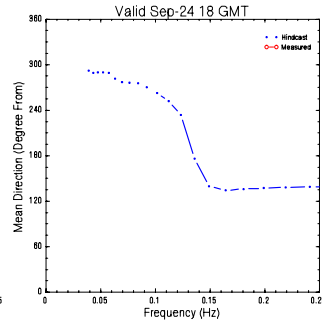
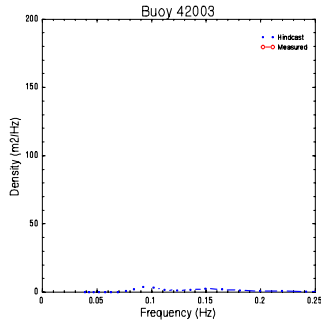
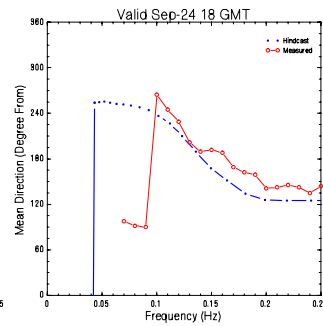
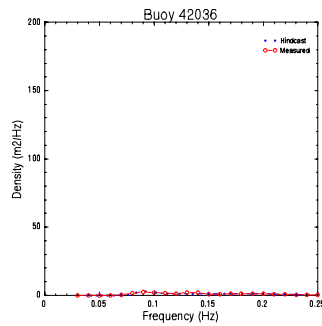
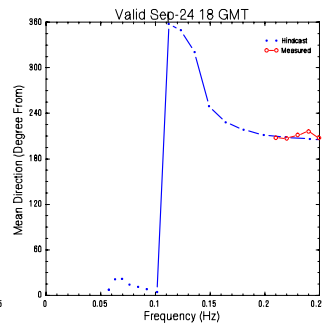
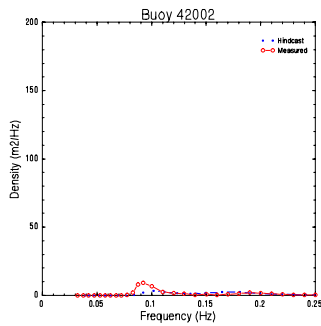
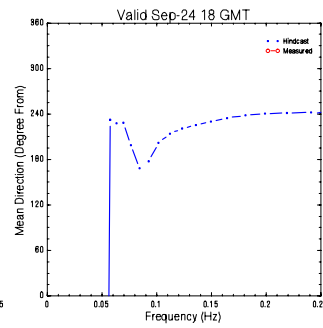
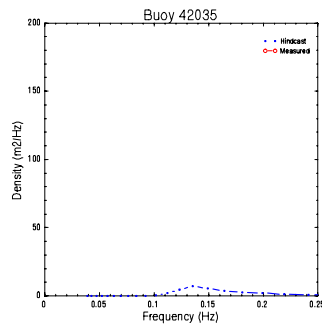
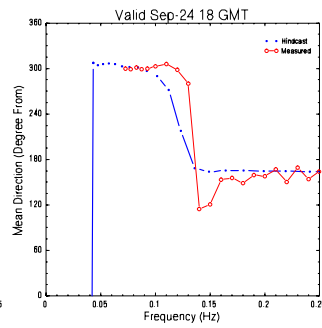
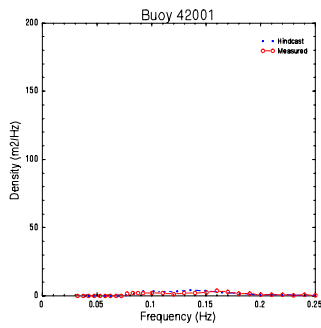


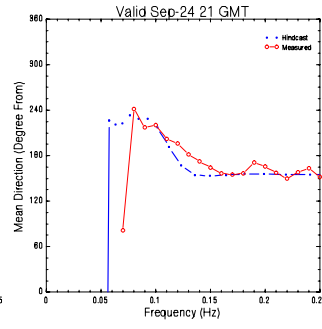
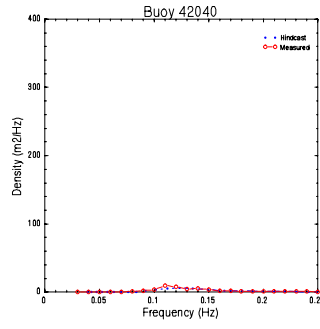
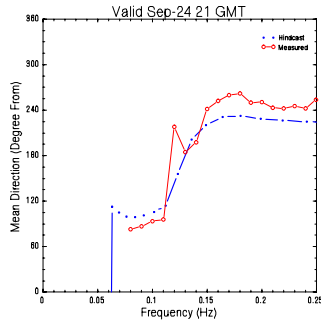
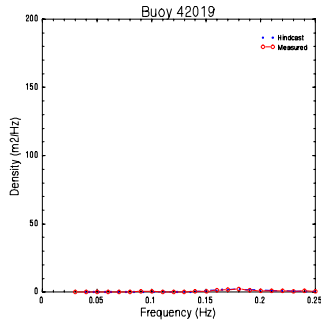
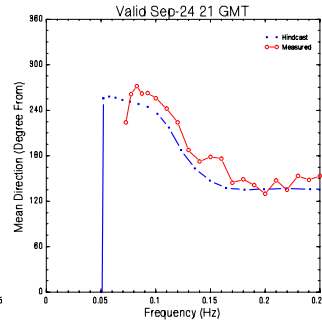
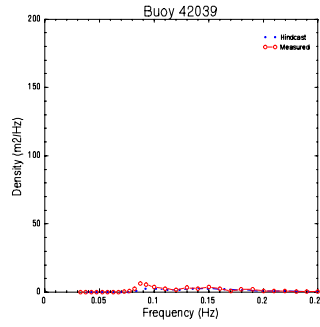
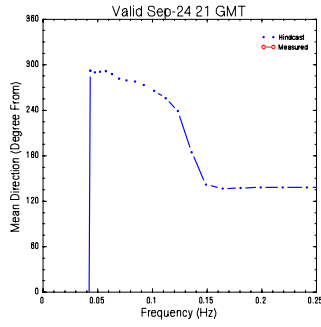
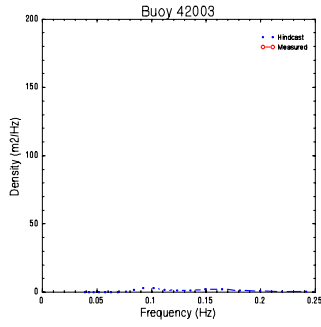
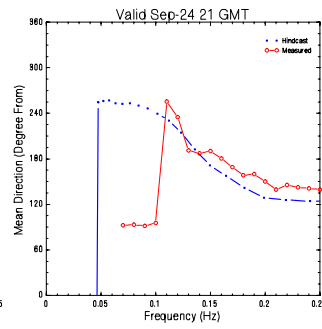
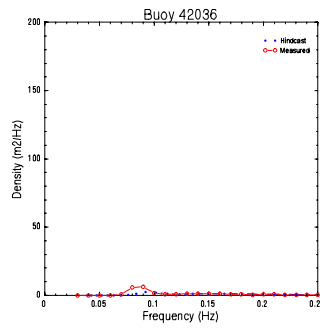
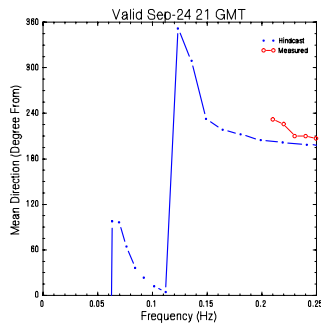
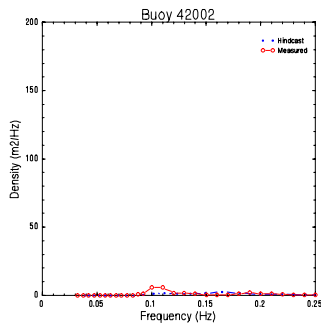
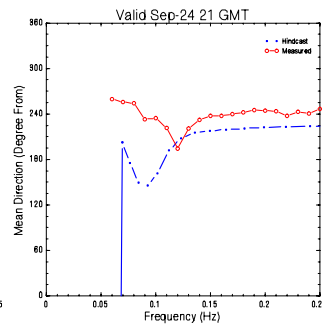
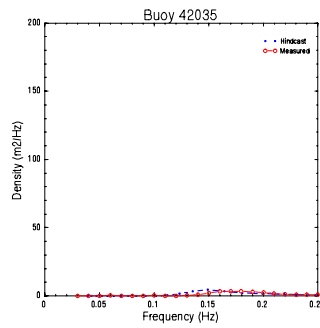
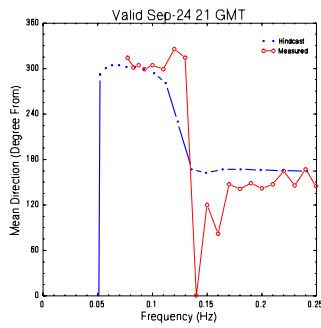
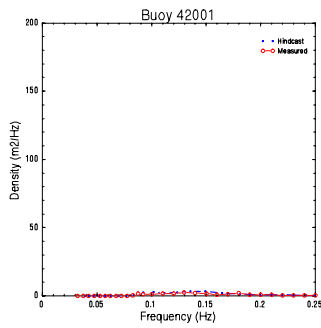












## **APPENDIX E Wind, Wave, and Current Fields Definitions**

<i>Field</i>	<i>Description</i>
Date	Julian format (where Jan 1 1900 = 1, Jan 2 1900 = 2, etc.) All dates GMT
Wind Direction	From which the wind is blowing, clockwise from true north in degrees (meteorological convention).
Wind Speed	30-minute average of the effective neutral wind at a height of 10 meters, units in meters/second.
<b>Total Spectrum Wave Fields:</b>	
Total Variance	The sum of the variance components of the hindcast spectrum, over the 552 bins of the wave model, in meters squared.
Significant Wave Height	4.000 times the square root of the total variance, in meters.
Peak Spectral Period	Peak period is the reciprocal of peak frequency, in seconds. Peak frequency is computed by taking the spectral density in each frequency bin, and fitting a parabola to the highest density and one neighbor on each side. If highest density is in the .32157 Hz bin, the peak period reported is the peak period of a Pierson-Moskowitz spectrum having the same total variance as the hindcast spectrum.
Vector Mean Direction	To which waves are traveling, clockwise from north in degrees (oceanographic convention).
First Spectral Moment	Following Haring and Heideman (OTC 3230, 1978) the first and second moments contain powers of $\omega = 2\pi f$ ; thus: $M_1 = \sum \sum 2\pi f dS$ where $dS$ is a variance component and the double sum extend over 552 bins.
Second Spectral Moment	Following Haring and Heideman (OTC 3230, 1978) the first and second moments contain powers of $\omega = 2\pi f$ ; thus: $M_2 = \sum \sum (2\pi f)^2 dS$ where $dS$ is a variance component and the double sum extend over 552 bins.
Dominant Direction	Following Haring and Heideman, the dominant direction $\psi$ is the solution of the equations $A \cos 2\psi = \sum \sum \cos 2\theta \pi dS$ $A \sin 2\psi = \sum \sum \sin 2\theta \pi dS$ The angle $\psi$ is determined only to within 180 degrees. Haring and Heideman choose from the pair $(\psi, \psi+180)$ the value closer to the peak direction.
Angular Spreading	The angular spreading function (Gumbel, Greenwood & Durand) is the mean value, over the 552 bins, of $\cos(\theta -$



## **APPENDIX F Wave Spectra Description**

## Description of Two-Dimensional Hindcast Spectrum Table

The first line of each spectrum gives date, grid point number, latitude, longitude, water depth, wind speed, wind direction (measured from which) and significant wave height. The next line gives the nominal frequencies of each frequency bin. Directional bands are identified at the left. The 552 element array contains the variance components (NOT spectral densities) for 23 frequencies and 24 directions. The 24 directional bins, each 15 degrees wide, are numbered clockwise from north; the first bin, with a nominal direction 7.5 degrees, extends from 0 to 15 degrees.

Frequency bins are spaced in geometric progression (to facilitate the computation of interactions); the nominal frequency is the geometric mean of the two ends. The frequency ratio is  $.75^{**(-1./3.)}$ , i.e. 1.100642416; this ratio was chosen in preference to the 1.1000 of official WAM to simplify interaction formulas. The first 22 bins are straightforward; the last requires explanation (continued below table).

	nom. freq	left end	right end	bandwidth
1	0.0390000	0.0371742	0.0409155	0.0037413
2	0.0429251	0.0409155	0.0450333	0.0041178
3	0.0472451	0.0450333	0.0495656	0.0045323
4	0.0520000	0.0495656	0.0545540	0.0049884
5	0.0572334	0.0545540	0.0600444	0.0054904
6	0.0629935	0.0600444	0.0660874	0.0060430
7	0.0693333	0.0660874	0.0727386	0.0066512
8	0.0763112	0.0727386	0.0800592	0.0073206
9	0.0839914	0.0800592	0.0881166	0.0080574
10	0.0924444	0.0881166	0.0969849	0.0088683
11	0.1017483	0.0969849	0.1067457	0.0097608
12	0.1119885	0.1067457	0.1174888	0.0107431
13	0.1232593	0.1174888	0.1293131	0.0118244
14	0.1356644	0.1293132	0.1423275	0.0130144
15	0.1493180	0.1423275	0.1566517	0.0143242
16	0.1643457	0.1566517	0.1724175	0.0157658
17	0.1808858	0.1724175	0.1897700	0.0173525
18	0.1990906	0.1897700	0.2088690	0.0190989
19	0.2191276	0.2088690	0.2298900	0.0210211
20	0.2411811	0.2298900	0.2530267	0.0231367
21	0.2654541	0.2530267	0.2784919	0.0254652
22	0.2921701	0.2784919	0.3065200	0.0280281
23	0.3215748	0.3065200	2.5274134	

The 23<sup>rd</sup> frequency band is an integrated band comprising what would be bins 23 through 44 (continuing the geometric progression) of a fully discrete bin system. To model the cascade of wave energy from high to low frequencies endorsed by non-linear interactions, we compute interactions involving bins out to 44. This requires a parametric assumption about the spectral density between 0.30652 and 2.52741 Hz; and the customary assumption is that density is proportional to  $\omega^{**(-x)}$ , where x is a disposable parameter. We are using  $x = 4.5$  for the following reasons:

- (1) There are quasi-physical arguments supporting the exponents 4 & 5. The exponent 5 is germane to a Pierson-Moskowitz spectrum.
- (2) A crude energy balance computation in the tail, with wind input scaled as  $\omega^{**2}$  and interactions scaled as  $\omega^{**11}$ , shows that 4.5 is the only exponent capable of yielding an equilibrium spectrum in the tail.

To compute a "density" at 0.32157 Hz, we compute what fraction of the integrated band belongs to the bin from 0.30652 to 0.33737 Hz. Sparing a few details, the result is:

$$\text{dens} = (\text{variance component}) * \text{rbw}$$

where rbw (dimensions seconds) is a function of the exponent as follows:

x	rbw
4.0	8.11849
4.5	9.24794
5.0	10.32933

Anspec is the variance summed over frequency per direction bin.

Fspec is the variance summed over direction per frequency.

Dens is the frequency spectrum represented as density in units of  $\text{m}^2\text{Hz}$ .